Downloaded from orbit.dtu.dk on: May 06, 2023

DTU Library

Dissolution of Light Hydrocarbons in Drilling Muds, Prediction of the Nature of Reservoir Fluids Based on Gas Shows

Liège, Xavier C.

Publication date:
2006

Document Version
Publisher's PDF, also known as Version of record

Link back to DTU Orbit

Citation (APA):
Liège, X. C. (2006). *Dissolution of Light Hydrocarbons in Drilling Muds, Prediction of the Nature of Reservoir Fluids Based on Gas Shows*. Technical University of Denmark.

General rights
Copyright and moral rights for the publications made accessible in the public portal are retained by the authors and/or other copyright owners and it is a condition of accessing publications that users recognise and abide by the legal requirements associated with these rights.

- Users may download and print one copy of any publication from the public portal for the purpose of private study or research.
- You may not further distribute the material or use it for any profit-making activity or commercial gain
- You may freely distribute the URL identifying the publication in the public portal

If you believe that this document breaches copyright please contact us providing details, and we will remove access to the work immediately and investigate your claim.

Dissolution of Light Hydrocarbons in Drilling Muds, Prediction of the Nature of Reservoir Fluids Based on Gas Shows

Xavier C. Liège

2006

Ph.D. Thesis

DTU

TECHNICAL UNIVERSITY OF DENMARK
DEPARTMENT OF CHEMICAL ENGINEERING

Dissolution of light hydrocarbons in drilling muds, prediction of the nature of a reservoir fluid based on Gas Shows

Xavier C. Liège

PhD. Dissertation, May 2006

Centre for Phase Equilibria and Separation Processes (IVC-SEP)

Department of Chemical Engineering

Technical University of Denmark

DK-2800 Lyngby, Denmark

Copyright © Xavier C. Liège, 2006
ISBN 87-91435-41-2
Printed by Book Partner, Nørhaven Digital, Copenhagen, Denmark

Acknowledgments

This thesis is submitted in partial fulfilment of the requirements for the Ph.D. degree at the Technical University of Denmark (Danmarks Tekniske Universitet). This work was carried out at the IVC-SEP research group at the Department of Chemical Engineering of the Technical University of Denmark under the supervision of Professor Erling H. Stenby and Associate Professor Alexander Shapiro. This work was funded jointly by Total (France) and Eni E&P (Italy). The author gratefully acknowledges their financial support.

I would like to express my gratitude to Pr. Stenby for giving me the opportunity to work at the IVC-SEP. I would like also to thank him and A. Shapiro for supervising my work. I would like to thank all the co-workers at IVC-SEP for the good moments we shared and for creating such a good work environment. I am grateful to Mariana Gonzales Bagnoli for being a patient and helpful office-mate as well as a friend. I would like to thank also Mrs Annelise Kofod and Mrs Anne Louise Biede for their support and their help with the administrative work.

I would like to thank Paola Ceragioli, Carlo Carugo and Gianfranco Bagnoli for making my stays at Eni E&P in Milan very pleasant and for all their help during the project. I am especially thankful to Paola Ceragioli for all the time she dedicated to me and her precious help. I would like to thank also François Montel, Gérard Segalini, Philippe Blanc and Alain Louis for hosting me at Total's Research Centre in Pau as well as their support and their friendly welcome.

Finally, I am grateful to all my friends in Denmark and my family in France for their repeated encouragements and the love and understanding that they showed to me.

Summary

The development of real-time measurement techniques to be used on field while drilling is of major interest for oil companies. Such techniques not only provide more data to assess the potential of a reservoir or well, but are also very cost effective as they do not require stopping the drilling. As such, Gas While Drilling™ enables to measure content of the light hydrocarbon of the drilling on field and then through an analysis procedure, to assess the characteristic of the well or reservoir. The aim of this project is to understand and model the link between the reservoir fluid encountered at the bottom-hole and the related gas show that will appear at the surface. The background of the project is presented in Chapter 1.

Creation of a thermodynamic model has required an advanced study of the phase equilibria between water (as a basis for the widest spread muds) as well as liquid and gas hydrocarbon phases in wide temperature and pressure ranges: from reservoir to atmospheric conditions. A comprehensive collection of experimental data on water-hydrocarbon equilibria was created, and several most widely applied equations of state were tested for this purpose. The results of the analysis of the available experimental data and modelling the hydrocarbon-water equilibria are described in respectively Chapter 2 and Chapter 3.

After initial stage of collecting the information and describing the process in terms of governing physical mechanisms, it has been decided to restrict further modelling with the simplest thermodynamic model, involving different phase equilibria between the mud and hydrocarbon phases under different thermodynamic conditions corresponding to propagation of the fluids from a well bore to a gas trap. Other mechanisms (kinetics of dissolution, adsorption, complex hydrodynamics etc.) were assumed to be of a lesser importance for the "zero-order" description of the process.

The scheme of the GWD process was developed, involving two- and three-phase equilibria, which should have been computed on the basis of the selected thermodynamic models. This scheme was implemented into BEST, the in-house process simulator of Total and is presented in Chapter 4. The model developed contains the three adjustment parameters accounting for our incomplete knowledge of the processes occurring in the well bore (Alpha_1), between the well head and the gas trap (Alpha_2), as well as inside the gas trap (Alpha_3).

In the course of the project, it was uncovered that part of the gas might be transferred in the mud, being not in the dissolved state (as was initially assumed), but as micro-bubbles stabilized by natural surfactants present in the mud. In order to verify presence and importance of such micro-bubbles, an industrial experiment was carried out. Although this experiment indicated possibility and importance of the micro-bubbles, their quantitative inclusion into the model requires a further study. This information was important for proper determination of the coefficient Alpha_2, as shown in Chapter 5.

Analysis of the experiment with the two gas traps carried out in the Eni E&P (cf. Chapter 6) has provided important information about the value of Alpha_2 responsible for degassing in the gas trap.

The created software was tested by comparison with available industrial GWD data. The process of testing was highly interactive, since in the course of the comparison necessity for more data had become necessary, and simultaneously the model was changed and adjusted. Due to roughness of both the data and the model, only the qualitative agreement between them was possible to be achieved for some most well documented cases.

In sum, the project has resulted in an important advance in understanding and modelling of the GWD process. For more detailed and more precise modelling, further work is required.

Resumé på dansk

Udviklingen af real-time målingsteknikker til brug på feltet under boring er af stor interesse for olieselskaberne. Sådanne teknikker giver ikke blot flere data til at vurdee et reservoirs eller en brønds potentiale, men er også meget kosteffektive, da de ikke kræver, at boringen stoppes. Som sådan gør Gas While DrillingTM det muligt at måle indholdet af den lette kulbrinte i boringen på feltet og så ved en analyseprocedure at vurdere de særlige kendetegn ved brønden eller reservoiret. Formålet med dette projekt er at forstå og modellere leddet mellem den resoirvæske, der stødes på ved bundhullet og den dermed forbundne gasforekomst, som vil fremkomme ved overfladen. Baggrunden for projektet fremlægges i kapitel 1.

Udarbejdelsen af en termodynamisk model har krævet et avanceret studie af faseligevægtene mellem vand (som grundlag for de mest spredte typer af mudder) så vel som væske og gas kulbrinte faser i vide temperatur- og trykområder: fra reservoir til atmosfæriske betingelser. Der blev iværksat en omfattende indsamling af eksperimentelle data om vand-kulbrinte ligevægte, og adskillige hyppigt anvendte tilstandsligninger blev testet med dette formål. Resultaterne af analysen af de foreliggende eksperimentelle data og modelleringen af kulbrinte-vand ligevægtene beskrives i henholdsvis kapitel 2 og kapitel 3.

Efter det indledende eksperimentelle stadium med at indsamle oplysninger og beskrive processen i form af styrende fysiske mekanismer, blev det besluttet at begrænse yderligere modellering med den enkleste termodynamiske model, som inddrager forskellige faseligevægte mellem mudder- og kulbrintefaserne under forskellige termodynamiske forhold, som svarer til udbredelsen af væskerne fra et brøndborehul til en gasfælde. Andre mekanismer (opløsningskinetik, adsorption, kompleks hydrodynamik etc.) blev anset for at være mindre betydningsfulde for "zero-order" beskrivelsen af processen.

Planen for GWD processen blev udviklet ved at inddrage to- og trefaseligevægte, som skulle have været beregnet på grundlag af de udvalgte termodynamiske modeller. Denne plan blev implementeret i BEST, Totals interne processimulator, og præsenteres i kapitel 4. Den udviklede model indeholder de tre tilpasningsparametre, som gør rede for vores ufuldstændige viden om de processer, der finder sted i brøndborehullet (Alpha_1), mellem brøndhovedet og gasfælden (Alpha_2) så vel som inden i gasfælden (Alpha_3).

I løbet af projektet blev det afsløret, at en del af gassen kunne overføres til mudderet, som ikke var i opløst tilstand (som det blev antaget til at begynde med), men i en tilstand som mikrobobler, der var stabiliseret af naturlige tensider i mudderet. For at verificere tilstedeværelsen og vigtigheden af sådanne mikrobobler blev et industrielt eksperiment udført. Skønt dette eksperiment påpegede muligheden for og vigtigheden af mikroboblerne, kræver en kvantitativ indbefatning af disse i modellen et videre studie. Disse oplysninger var af betydning for den rette bestemmelse af Alpha_2 -koefficienten, som vist i kapitel 5.

En analyse af eksperimentet med de to gasfælder, som blev udført i Eni E&P (jf. kapitel 6) har givet vigtige oplysninger om Alpha_2-værdien, som er ansvarlig for afgasning i gasfælden.

Det udviklede software blev testet ved sammenligning med foreliggende industrielle GWD data. Testprocessen var i høj grad interaktiv, da der i løbet af sammenligningen opstod behov for flere data, og modellen samtidig blev ændret og tilpasset.

På grund af grovheden af både data og modellen, kunne kun kvalitativ overensstemmelse mellem dem opnås for nogle særdeles veldokumenterede tilfælde.

Alt i alt har projektet resulteret i et vigtigt skridt frem mod forståelse og modellering af GWD processen. For at få en mere detaljeret og præcis modellering kræves der yderligere arbejde.

Table of Contents

1 Introduction to Gas While Drilling

1.1 Drilling

Drilling has an important role in the oil production industry. Whether used for exploratory wells or production wells, it consists in entering physically the reservoir. It enables thus to give valuable information about the nature of the rock and the fluids contained in it.

The basic purpose of drilling is to reach the reservoir. More precisely any drilling operation must penetrate the subsurface strata and penetrate deep enough to reach the target reservoir. It must also prevent the caving of the penetrated strata and excavate the drill cuttings. Finally, it must drill a hole large enough to produce efficiently the reservoir fluids, keep the hole oriented in the desired direction and prevent the intrusive fluids from entering the hole.

While the drilling bit is attacking the reservoir rock at the bottom-hole of the well, the circulating mud cleans the hole from the drilling cuttings and maintains the stability of the drilled hole. The drilling fluid is circulating continuously: it is first injected inside the drill-pipe where it travels down-hole, then is released into the well through the injectors of the drilling bit, before travelling back upwards in the annular space formed by the walls of the well and the drill-pipe (cf Fig. 1.1). At the well-head, the mud is evacuated through the flow-line. The flow-line can either be an opened pipe or a closed one. The mud reaches then a first mud pit before passing through a series of shakers and desilters, where the drilling cuttings are separated from the mud. The mud sojourns then in the recycling pits until it is pumped back into the well. The characteristic of drilling muds and their hydrodynamics are presented in Appendix 1.

Several parameters are registered and monitored while drilling in order to control the operation and keep it safe. The most commonly operative data are the weight on bit (WOB), the drilling rate, the mud flow-rate measured at the entrance and at the exit of the well, the density of the mud measured at the entrance and exit of the well. Much information is retrieved during a well drilling: first any change of the operative parameters tells about changes in the rock currently drilled. Besides, the analysis of the drilling cuttings gives information about the reservoir and the reservoir fluid by fluorescence test.

Tests can be performed in order to retrieve information about the reservoir or the fluids contained in it. Most of these tests require to stop drilling and to send into the well specific tools. These tests are very carefully and parsimoniously planed as they have a high cost in money and time. As an alternative, tools and techniques are being developed to retrieve information while drilling. Gas While Drilling™ is one of these techniques.

Fig 1.1. Rotary rig fluid circulation and mud treating system (Austin, 1983)

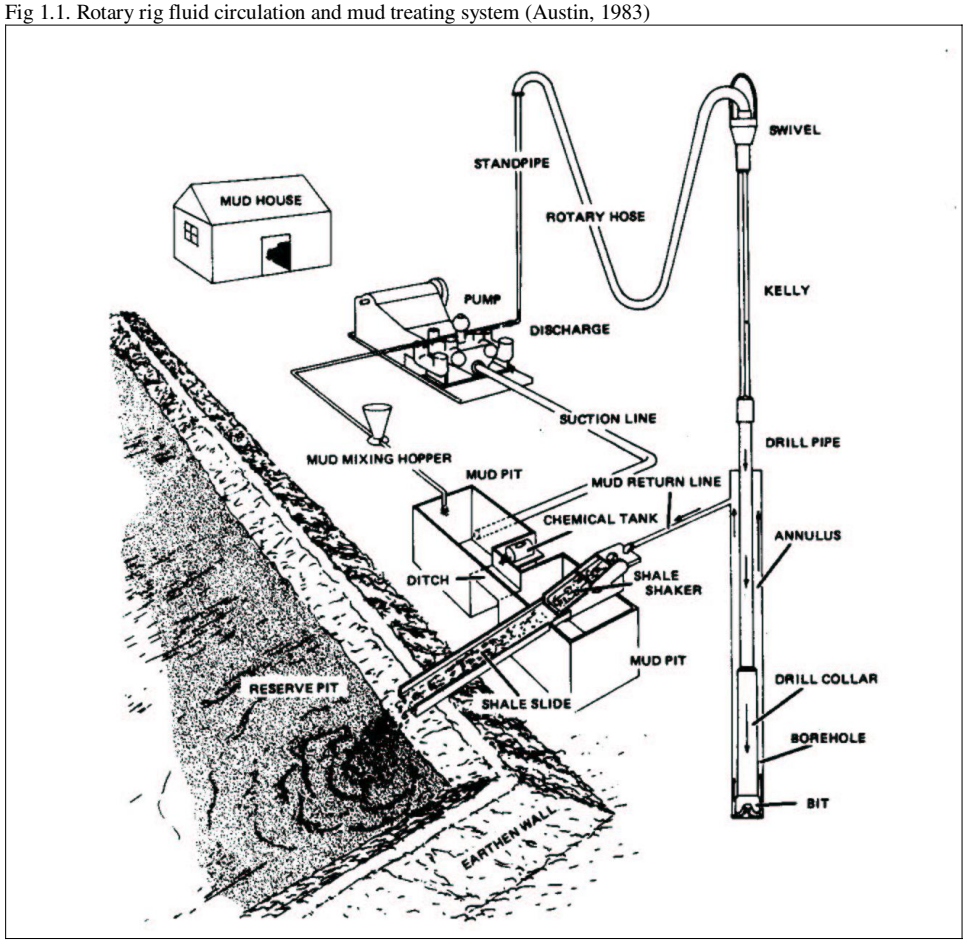

1.2 Gas While Drilling™

1.2.1 Introduction

The key idea behind Gas While Drilling™ (GWD) lays in the fact that the drilling mud gets in contact with the reservoir rock and any fluid that it may contain before travelling back to the surface. Thus traces of hydrocarbons could be available at the surface in the drilling mud.

Indeed, monitoring the gas detected in the drilling mud is an old practice. The technique was initially implemented for safety reasons in order to prevent blow-outs -when reservoir fluid invades the drilling mud and burst out on the drilling platform due to violent gas expansion. The mere presence of gas bubbles in the drilling mud could visually warn in case of such an invasion.

The reservoir fluid is first released into the drilling mud at the instant the section is drilled. Besides, the remaining gas in the cuttings is released by gas expansion as the pressure decreases while the cuttings are carried to the surface. Moreover, some of the oil from the cuttings can be flushed by the mud while ascending.

The gas detection technique was improved over the years and started to be used to indicate hydrocarbon bearing zones. The main improvements were achieved when mechanical separators (also referred as gas-traps) were coupled to gas detection instruments. The gas-traps became more sophisticated, until they were not affected anymore by external conditions. In parallel, high resolution gas chromatographs (GC) -more rapid and reliable- became widely used.

Especially, the use of closed gas-traps, thermo-isolated gas-lines, constant aspiration conditions from the gas-trap and high resolution gas chromatographs made it possible to obtain comparable gas reading for identical formation from well to well (Beda, 1999). The typical gas data available on field are the composition of the gas from C1 to C5 and the Total Gas (TG), obtained from the combustion of the gas through a catalytic filament giving an indication of the number of carbon atoms present in the gas.

GWD is under constant development as it integrates new technologies. The latest improvement to GWD is the addition of a mass spectrometer to the analytical part of the system in order to detect hydrocarbons up to C8 and CO_2.

1.2.2 Gas-traps and analytical unit

Different gas traps are used in GWD. All of them work on the same principle: a small amount of drilling mud is mixed with air in order to release the light hydrocarbons into the gas phase. The air is then sent to the analytical part where the hydrocarbons are detected.

- Quantitative Gas Measurement™

One of the first gas-traps to be fully efficient was the Quantitative Gas Measurement™ (QGM) developed by Texaco and the Gas Research Institute in the 90's (QGM User's Guide, 1998). The trap works as a centrifugal pump (Fig. 1.2): the drilling mud is drawn up to the trap from the bottom and exits through a side pipe. The air flow is pumped in and out of the top of the trap. A ring and a baffle stabilize the mud circulation and also increase mud residence time. The agitation is kept constant at 1750 rpm. The air flow is kept constant at 3 l/min. The trap is fixed in a mud pit located right after the flow-line at a fixed immersion level. The pressure in the trap is slightly under 1 atm, due to the air aspiration. The temperature in the trap is set by the mud temperature.

Provided that the mud level in the pit is constant, then the volume of mud degassed in the trap is constant. However, as the mud flow-rate fluctuates almost constantly on field, the mud level in the pit does as well. In this case, it is difficult to decide if a high reading in gas is due to a high level of the gas content of the mud or an increase of the volume of mud degassed.

Fig. 1.2. QGM gas-trap (Hanson, 1999)

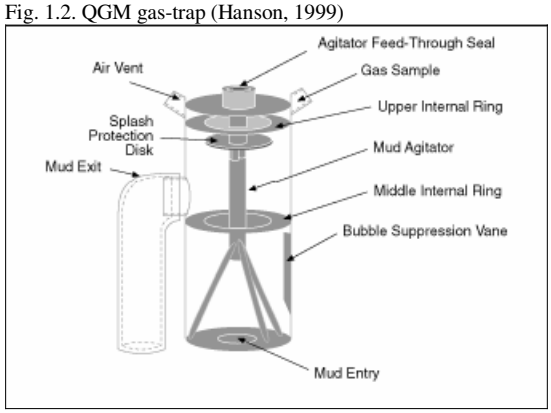

- GZG

The GZG gas-trap was developed by Geoservices. It is a constant volume trap. The mud is drawn up by a pump at constant rate into the trap, where it is agitated. The mud flow is kept at 1.5 l/min. Air is injected into the trap at controlled rate of 0.5 l/min. The pressure is kept constant in the trap at 0.8 atm, while the temperature is set but the mud temperature.

Contrary to the QGM gas-trap, the GZG is not placed in the mud pit: a line-probe is immersed into the mud and carries the mud into the trap body. The probe is immersed in the pit next to the flow-line most of times, but the probe can also be placed directly in the flow-line.

- Extractor

The extractor gas-trap is an improved version of the GZG. It is as well a constant volume gas-trap with probe-line. The difference lies in the fact that the release of hydrocarbon into air is operated at a high temperature, 90°C. The mud flow-rate is also reduced to 0.5 l/min, the air flow-rate remaining the same as for the GZG gas-trap. The pressure in the trap is 0.8 atm.

For all the three gas-traps, a gas-line carries the air out of the gas-trap to the gas chromatograph. The line equipped with a cold trap for water removal as well as a water drop out filter and an oil/particle filter.

- Analytical unit

Two kinds of analysis are carried out. The first one uses a flame ionization detector to measure the Total Gas (TG). It consists in burning all the gas extracted from the mud using a catalytic filament. It gives the amount of gas “in equivalent C1”.

The second apparatus is a gas chromatograph, which gives the concentration of light hydrocarbons (C1 to C5) in the sample, expressed in volume ppm.

Sometimes, a mud sample is analyzed directly using a micro-oven steam still, a steam still (QGM User’s Guide, 1998) to separate the gas form the mud sample. After analyzed by gas chromatography, the concentrations of hydrocarbons are expressed in volume of gas

contained in the mud volume in ppm. Such an analysis is carried out once per day to check the calibration of the chromatograph, or to for special measurement campaigns. It requires that an operator samples manually the mud in the mud pit next to the gas-trap entry.

1.2.3 GWD™ procedure

With more reliable data at hand from light hydrocarbon shows, some mud-logging interpretation procedure appeared. The aim of these procedures was to predict the nature of the reservoir fluid. Several indexes and charts were created (Pixler (1968), Hayworth (1984)). In the 90's, ENI E&P and Total (at the time, Elf E&P) started to develop their own interpretation method, called Gas While Drilling™.

The reservoir evaluation is performed by mean of gas ratios. The first steps of the procedure are to ensure that the signal is not an artefact from the drilling operation and reflects the presence a hydrocarbon layer. The quality of the data is first checked by comparing the TG to the summed concentrations of C1 to C5. This enables to discard all unreliable data from the set. Then, concentration ratios are calculated with the remaining data. Fig 1.3 shows examples of ratio and their use. For instance, the ratio C1/(C1-C5) is used to identify lithology changes (Beda, 1999).

Fig. 1.3. Examples of gas ratios (Beda, 1999); QC stands for Quality Control

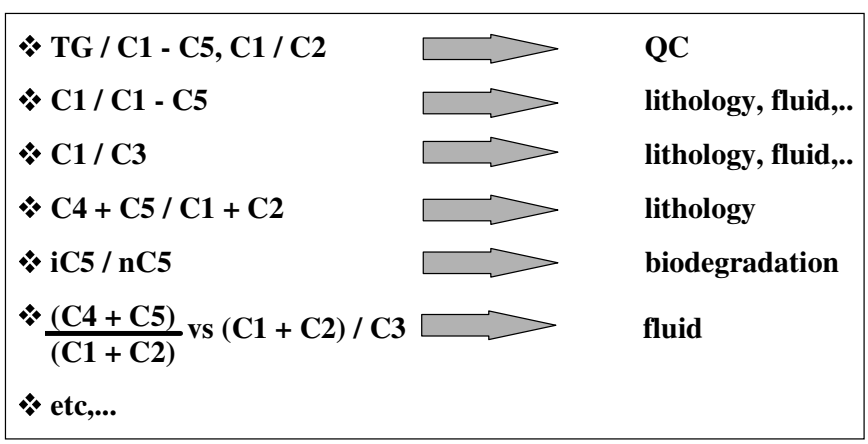

The ratios are then plotted versus depth in order to identify any trend or breaks. In the example below (Fig. 1.4), the ratio is C1/(C1-C5) is used to identify a gradual fluid change within a reservoir. The ratio is high at the top of the reservoir as the fluid is richer in methane

and decreases when approaching the oil water contact (OWC) as the fluid is richer in heavy compounds.

Fig. 1.4. Example ratio platted vs. depth (Beda, 1999)

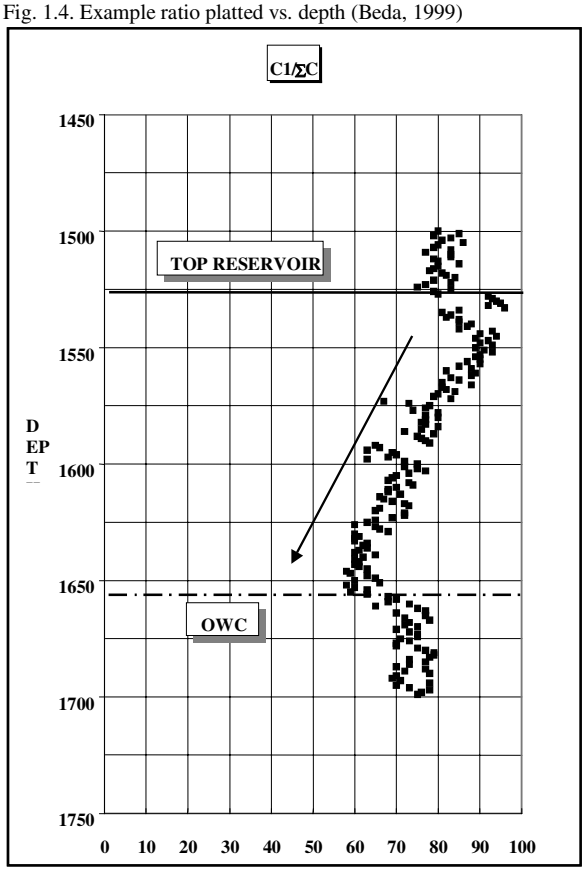

The GWD interpretation relies on many ratios and on the cross-checking of all of them. For instance, the ratio on Fig 1.4 shows that there is something to investigate at 1575 m and around 1650 m. The reservoir top and the OWC were then identified with help of other ratios.

2 Solubility of light hydrocarbons in water

2.1 Introduction

In the scope of the project, some thermodynamic models were selected and investigated for their ability to calculate the thermodynamic equilibrium between water and light hydrocarbons.

The objective of this study was to find experimental values of the solubility of the binary systems composed of a light hydrocarbon and water in order to check the accuracy of these thermodynamic models. The systems which were investigated were methane/water, ethane/water, propane/water, i-butane/water, n-butane/water, i-pentane/water and n-pentane/water. The systems were first supposed to be studied for pressures ranging from atmospheric pressure to high pressures such as 700 bars and for temperatures ranging from 273.15 K to 373.15 K.

The effects induced by the multicomponent nature of the system drilling mud/reservoir fluid as well as the those induced by the mud additives are not covered by the present collection of experimental data points. They will be considered in Chapter 3.

2.2 Overview

The tables 2.1 to 2.4 present an overview of all the experimental data points collected during the project for the systems methane/water, ethane/water, propane/water and n-butane/water. Each line corresponds to a reference, where the three first columns show the number of data points for each of the following type of solubility: the first column corresponds to the solubility of the hydrocarbon in the water phase, the second column to the solubility of the hydrocarbon in the hydrocarbon liquid phase (when existing) and the third column presents the hydrocarbon solubility in the vapour hydrocarbon phase. Columns four and five show respectively the pressure range and the temperature range of the data-set. Finally the last column gives the article or book reference (the full reference can be found in the section References).

Table 2.1. Methane/water systems; type and number of data points, pressure and temperature range, reference

Number of points			P (bar)	T (K)	Reference
x_{HC} in liq H_2O	x'_{HC} in liq HC	y_{HC} in vap			
8	***	***	41 - 344	310 - 344	Amirijafari, 1972
6	***	***	1	274 - 312	Clausen, 1952
7	***	7	13 - 65	297 - 520	Crovetto, 1982
11	***	***	36 - 667	298	Culberson, 1950
71	***	***	13 - 690	298 - 444	Culberson, 1951
43	***	***	3.5 - 28	310 - 394	Davis, 1960
4	***	***	200 - 1000	344	Dhima, 1998
17	***	***	3 - 52	298 - 303	Duffy 1961
16	***	16	13 - 170	323 - 588	Gillepsy, 1982
60	***	***	1 - 500	273 - 625	Kertes, 1987
***	***	29	0.6 - 106	343 - 481	Joffrion, 1988
3	***	***	1	291 - 310	Lannung, 1960
18	***	***	5.6 - 91	274 - 285	Lekvam, 1997
1	***	***	1	293	Mc Auliffe, 1966
39	***	***	40 - 469	298 - 423	Michels, 1936
***	***	75	13 - 690	310 - 510	Olds, 1942
18	***	***	101 - 616	324 - 398	O'Sullivan, 1970
71	***	***	35 - 1973	427 - 627	Price, 1979
3	***	***	24 - 51	298	Stoessel, 1982a
3	***	***	24 - 51	298	Stoessel, 1982b
71	***	***	49 - 1079	423 - 633	Sultanov, 1972a
***	***	60	98 - 1078	423 - 633	Sultanov, 1972b
3	***	***	1	278 - 318	Wetlaufer, 1964
6	***	***	1	274 - 312	Winkler, 1901
2	***	***	1	298 - 310	Winkler, 1899
***	***	15	25 - 125	298 - 338	Yarym, 1985
19	***	***	23 - 148	273 - 298	Yang, 2001

Table 2.2. Ethane/water systems; type and number of data points, pressure and temperature range, reference

Number of points			P (bar)	T (K)	Reference
x_{HC} in liq H_2O	x'_{HC} in liq HC	y_{HC} in vap			
5	***	4	25 - 281	310 - 377	Anthony, 1967
6	***	***	1	274 - 312	Clausen, 1952
***	***	12	24 - 36	298 - 373	Coan, 1971
30	***	***	4 - 84	310 - 444	Culberson, 1950a
64	***	***	50 - 685	310 - 444	Culberson, 1950b
78	***	78	200 - 3700	473 - 673	Danneil, 1967
4	***	***	20 - 100	344	Dhima, 1998
11	***	***	1	273 - 323	Kertes, 1982
1	***	***	1	293	Mc Auliffe, 1966
***	***	65	22 - 682	310 - 510	Reamer, 1943
3	***	***	1	278 - 318	Wetlaufer, 1964
6	***	***	1	274 - 312	Winkler, 1901

Table 2.3. Propane/water systems; type and number of data points, pressure and temperature range, reference

Number of points			P (bar)	T (K)	Reference
x_{HC} in liq H_2O	x'_{HC} in liq HC	y_{HC} in vap			
71	***	***	1 - 35	288 - 410	Azarnoosh, 1958
2	***	***	1	293 - 303	Clausen, 1952
40	***	***	1 - 34	288 - 410	Kertes, 1989
63	13	13+53	5 - 192	310 - 422	Kobayashi, 1953
1	***	***	1	290	Lebeau, 1905
1	***	***	1	293	Mc Auliffe, 1966
8	***	***	5 - 12	344	Wehe, 1961a
3	***	***	1	278 - 318	Wetlaufer, 1964
100	***	***	1 - 5	256 - 284	Blanco, 1999

Table 2.4. N-butane/water systems; type and number of data points, pressure and temperature range, reference

Number of points			P (bar)	T (K)	Reference
x_{HC} in liq H_2O	x'_{HC} in liq HC	y_{HC} in vap			
26	***	***	1 - 41	298 - 423	Carroll, 1997
2	***	***	1	293 - 303	Clausen, 1952
8	***	8	255 - 1125	628 - 637	Danneil, 1967
5	***	***	100 - 1000	344	Dhima, 1998
10	***	***	1.4 - 8	310 - 377	Kertes, 1989
65	***	***	1.4 - 33	310 - 410	Le Breton, 1964
1	***	***	1	290	Lebeau, 1908
1	***	***	1	293	Mc Auliffe, 1966
***	26	26	3.6 - 43	310 - 425	Reamer, 1944
148	4	148	1.4 - 690	310 - 510	Reamer, 1952
6	6	6	3.6 - 34	310 - 410	Wehe, 1961b
3	***	***	1	278 - 318	Wetlaufer, 1964
7	***	80	90 - 3100	502 - 707	Yiling, 1991

All the corresponding data points are presented in Appendix 2 to 5.

2.3 Presentation of the binary systems water-light hydrocarbon

2.3.1 Generalities

Based on the data available, most of the hydrocarbon/water mixtures are classified as type III systems according to the classification of Van Konynenburg (1980). In type III mixtures, a vapour-liquid critical locus (or Lower Critical Curve) connects the critical point of the most volatile compound to the VLLE three-phase critical end point (also called the Upper Critical End Point). A separate fluid-fluid critical line originating from the other pure-component critical point rises to very high pressures, sometimes passing through maxima and minima in pressure or temperature. In many cases, the critical line rises to temperatures above the critical point of water, leading to a high-pressure region of gas-gas equilibrium.

Fig. 2.1. PT-projection of Type III of phase equilibrium

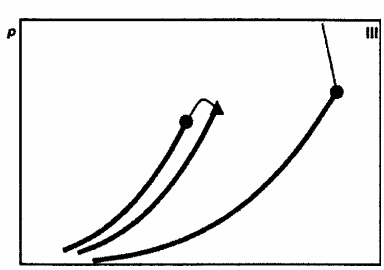

From such P-T diagrams, the P-x and T-x projections can be deduced. The examples below come respectively from the projection of an isotherm plan and an isobar plan intersecting the VLLE three phase equilibrium line in the P-T-x space.

Fig 2.2. P-x and T-x projections for an isotherm and an isobar intersecting the VLLE three-phase equilibrium line

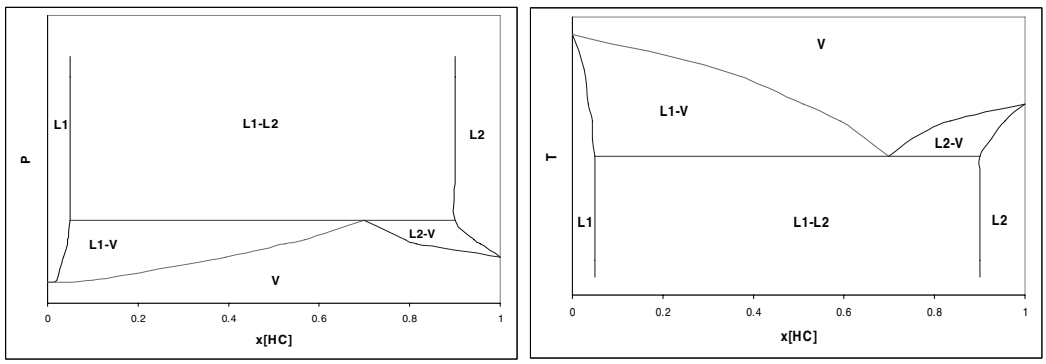

Typically, L1 is an aqueous liquid phase and L2 is a hydrocarbon liquid phase. The presence of a three-phase threshold can be observed. These diagrams can be observed for conditions under the critical point of the hydrocarbon. When the hydrocarbon is over-critical, there is no hydrocarbon liquid phase, but a continuous vapour phase, as seen on the figure below.

Fig. 2.3. P-x and T-x diagrams of a water/light hydrocarbon system at conditions over the critical point of the hydrocarbon and below the critical point of water

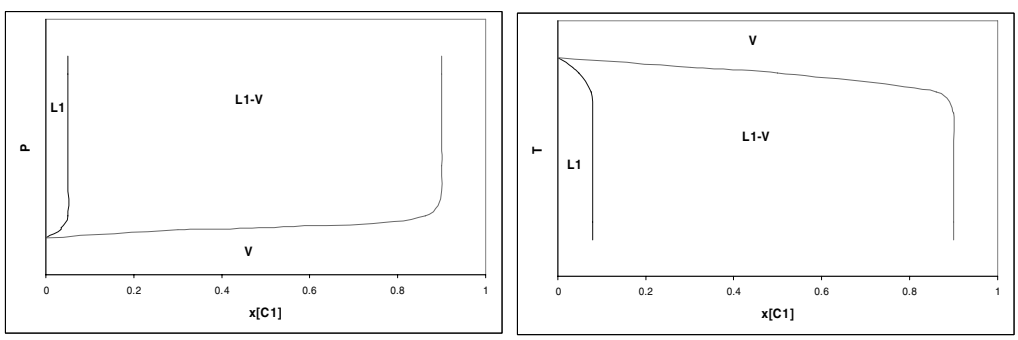

2.3.2 Water-light hydrocarbons

For the water-light hydrocarbon binary systems, the most volatile compounds are the hydrocarbons as seen on Fig. 2.4, thus the VLLE three-phase line is connected to their critical point. The Upper Critical Curve is starting from the critical point of water.

Fig. 2.4. Vapour pressure lines and critical points for methane, ethane, propane, n-butane and water in the PT-space (Data from NIST Chemistry Webbook)

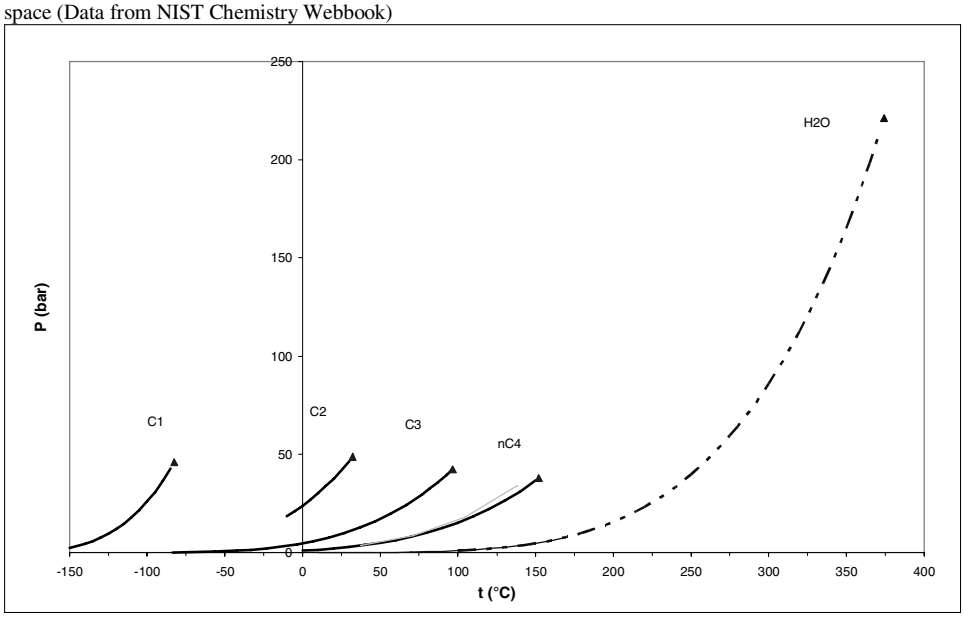

Moreover, we can see that the vapour pressure line of methane is located at temperatures below 0°C. This means that for systems over the freezing point of water, methane is always over-critical, thus cannot be present as liquid in the system. This gives a simplified P-T diagram for this system, as shown on Fig. 2.5 some three-phase lines exist for methane but are located below or around the freezing point of water and involve ice and hydrates.

Fig. 2.5. PT-diagram for methane (Data from NIST Chemistry Webbook; Brunner, 1990)

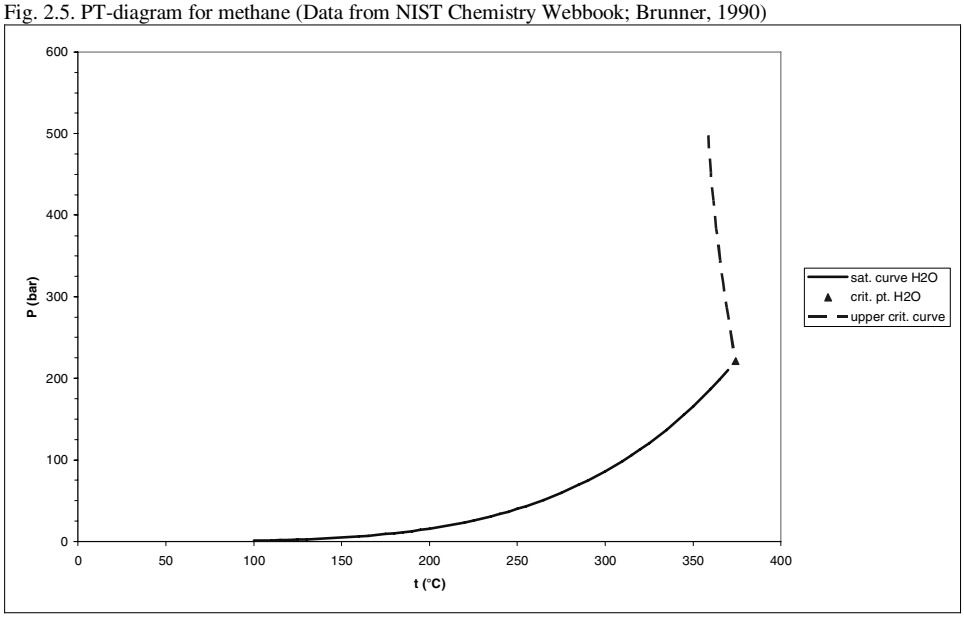

The critical temperature of ethane is 32.25°C, which place this compound at an intermediate position between methane and the other light hydrocarbons. For temperatures above 32.25°C, ethane is over-critical and behaves as methane. But for temperatures lower than its critical temperature, ethane can exist as a separate liquid phase. Unfortunately, this behaviour cannot be described as no data can be found the three phase line and the lower critical line. Fig. 2.6 shows the PT-diagram for water and ethane.

Fig. 2.6. PT-diagram for ethane (Data from NIST Chemistry Webbook; Danneil, 1967)

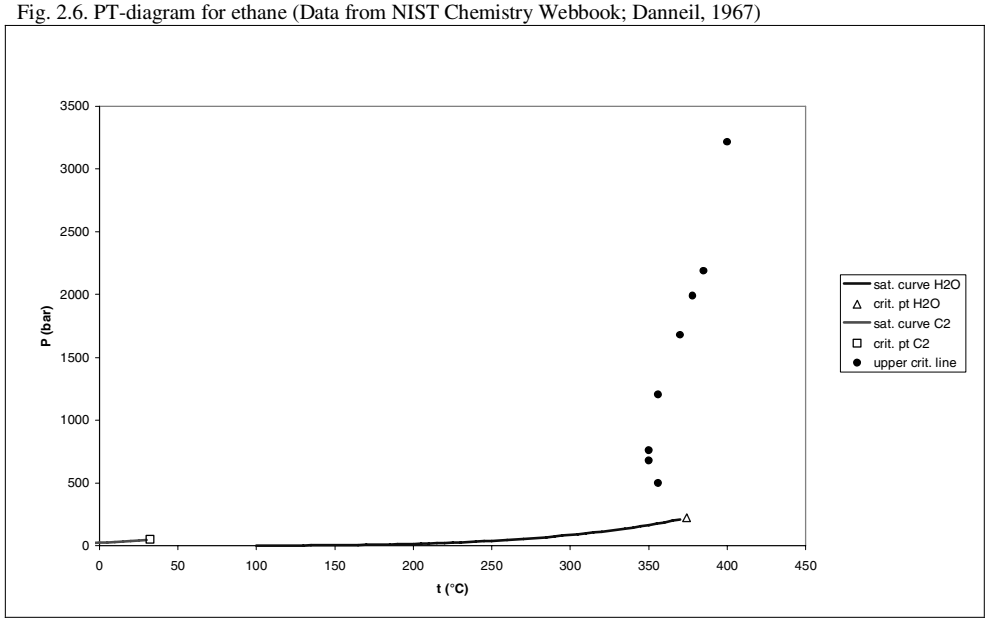

More data could be found for the system water-propane. Fig. 2.7 shows the resulting PT-diagram.

Especially, data are available for the three phase line and the upper critical end point (also called three phase critical end point) as shown on Fig 2.8. The lower critical line connecting the two previous curves is missing however.

Fig. 2.7. PT-diagram for propane (Data from NIST Chemistry Webbook; Kobayashi, 1953; De Loos, 1980)

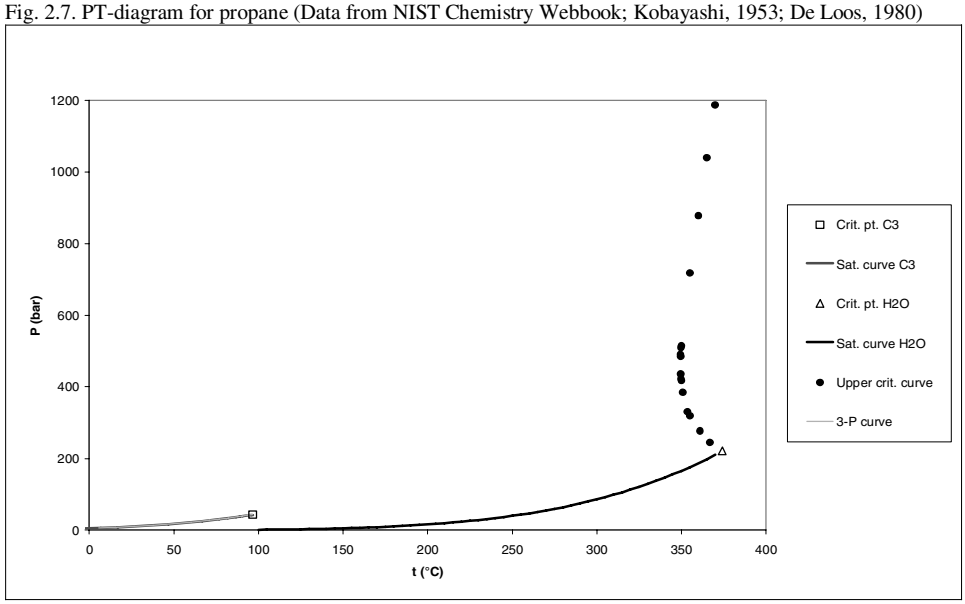

Fig. 2.8. PT-diagram for propane; close-up on the three phase line (Data from NIST Chemistry Webbook; Kobayashi, 1953)

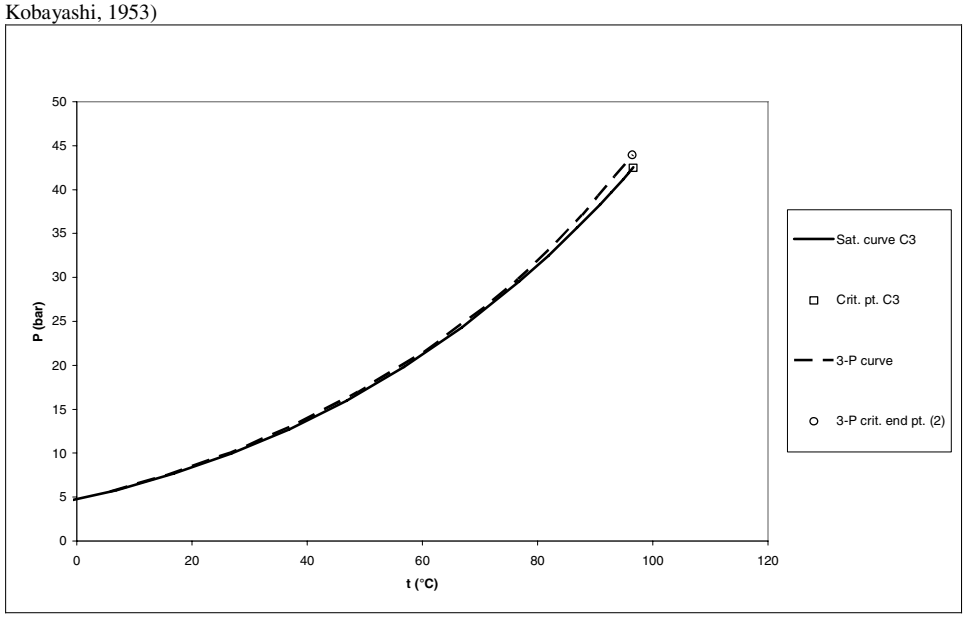

The same kind of data is available for water/n-butane and is displayed on Fig. 2.9 and 2.10.

Fig. 2.9. PT-diagram for n-butane (Data from NIST Chemistry Webbook; Yiling, 1991; Reamer, 1952)

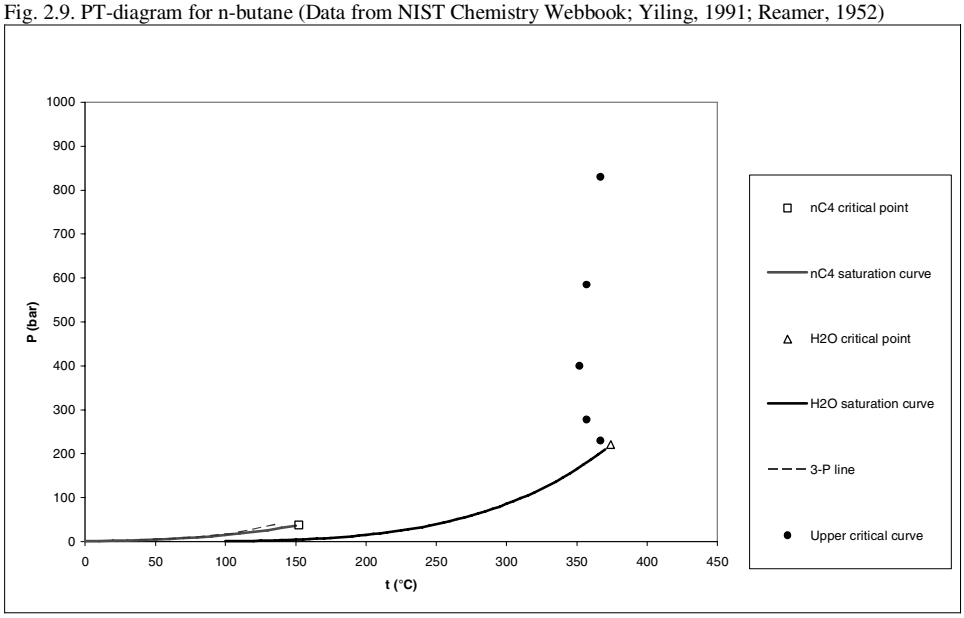

In the case of butane, the location of the upper critical end point differs according to the sources as shown on Fig. 2.8.

Fig. 2.10. PT-diagram for n-butane; close-up on the three phase line (Data from NIST Chemistry Webbook; Reamer, 1952; Roof, 1970; Reamer, 1944; Brunner, 1990)

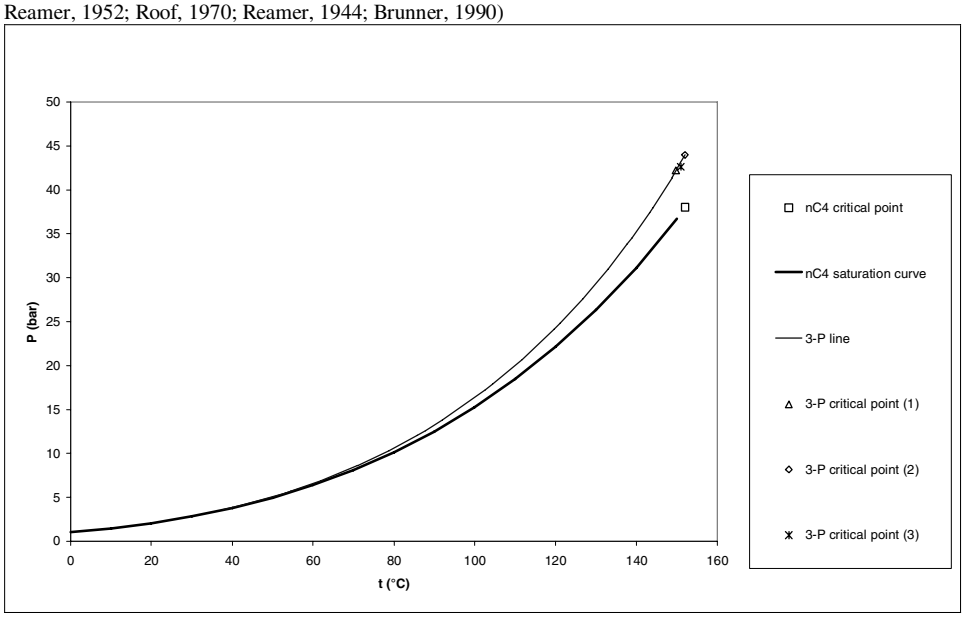

2.4 Study of the minima of solubility

In order to check the consistency of the data, the minima of solubility of the different hydrocarbons in water were studied.

As shown on Fig. 2.11, the minimum of solubility is plotted as a function of pressure for the binary systems methane/water, ethane/water, propane/water and n-butane/water. For each hydrocarbon, the minimum of solubility at a given pressure is found in the corresponding set of solubilities as a function of temperature; all the data used are reported in Appendix 2 to Appendix 5. We can see that the minimum of solubility is an increasing function of the pressure. We can also see that the solubility is decreasing as the hydrocarbon becomes heavier.

Moreover, on Fig. 2.11 is also plotted the minimum of solubility of ethane based on values collected in IUPAC's Solubility Data Series for Ethane (Kertes, 1982): the trend (shown in dashed lines on Fig. 2.9) is very different from those of the other light hydrocarbons. The original articles were found (Culberson (1950a), Anthony (1967)) and the corresponding values corrected, leading then to a more reasonable plot for ethane as shown on Fig. 2.11.

Fig. 2.11. Minimum of solubility of light hydrocarbons in water as a function of pressure. The dashed curve contains data from Kertes (1982).

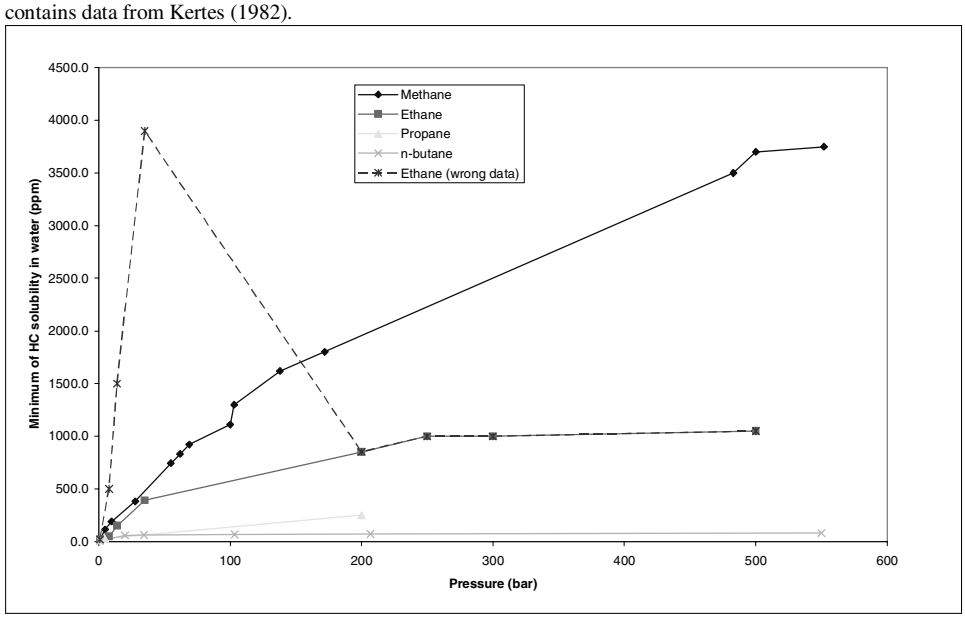

Fig. 2.12 and 2.13 show the plot of the minimum of solubility as a function of temperature for respectively methane in water and n-butane in water.

The minima of solubility as a function of temperature are difficult to identify. Most of times, the minimum is located between two measured points, thus its temperature has to be interpolated, leaving some uncertainties. Fig. 2.12 and 2.13 show the plot of the minimum of solubility as a function of temperature for respectively methane in water and n-butane in water. For each point, the value judged the most accurate is plotted as well as the two closest temperatures where experimental values were reported by authors. It first shows that the interpolation was applied to very different and sometimes wide intervals of temperatures. Besides, no trend can be explicated based on these curves.

Moreover the location of the minimum of solubility as a function of temperature is not as precise as for the solubility as a function of pressure. This comes from the fact that most of the data-sets were measured at isobaric conditions with a varying temperature. Whereas to isolate the minimum of solubility as a function of temperature, the solubility curves have to be re-built as functions of pressure at a given temperature. From each isotherms obtained, the minimum is found. The discrepancy between the different data-sets is then emphasized in such a process as shown by the uncertainty attached to each point on Fig 2.12 and 2.13.

Fig. 2.12. Minimum of solubility of methane in water as a function of temperature (Values extracted from all data sets from Appendix 2)

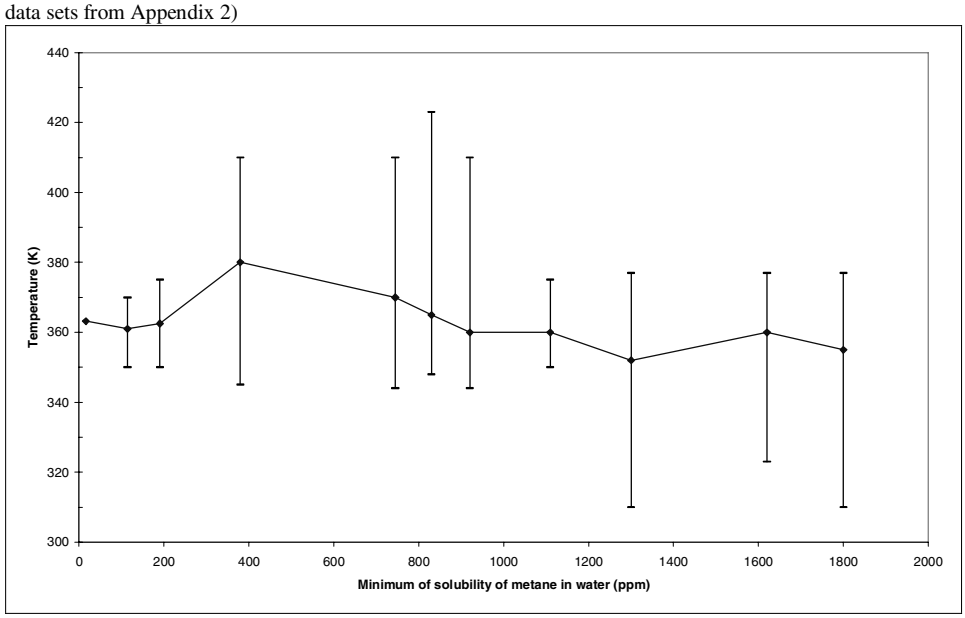

Fig. 2.13. Minimum of solubility of n-butane in water as a function of temperature (Values extracted from all data sets from Appendix 5)

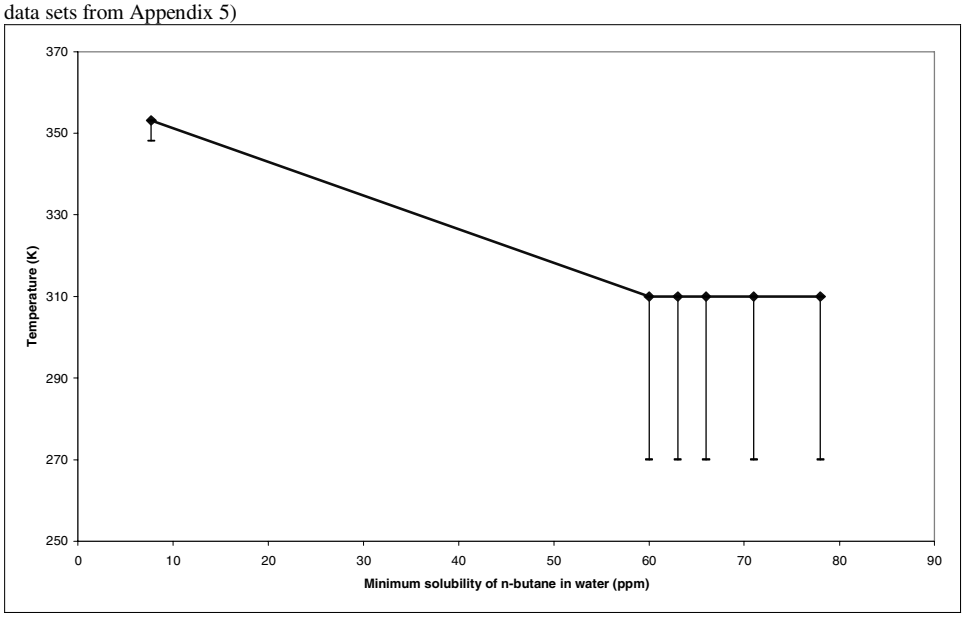

2.5 Px and Tx diagrams

In the previous subsection, the question of the existence of the minima of solubility was raised. In order to study this question more grandly, a more general approach was then chosen, focusing on the study of the P-x and T-x diagrams.

It enabled to enlighten the relation between the solubility of a compound in another and the phase diagram of the mixture of these two compounds, as shown on Fig. 2.14 and 2.15 below. Especially, the solubility curves for methane and ethane correspond to the liquid phase branch of the T-x phase diagram, meaning that when these two compounds are not soluble, they appear as gases. But for compound heavier than ethane, the solubility curve is composed of two boundary lines: for a temperature over the triple point, these hydrocarbons will appear as separate liquids when not soluble.

Fig. 2.14. Relation between a Tx phase diagram and a solubility curve.

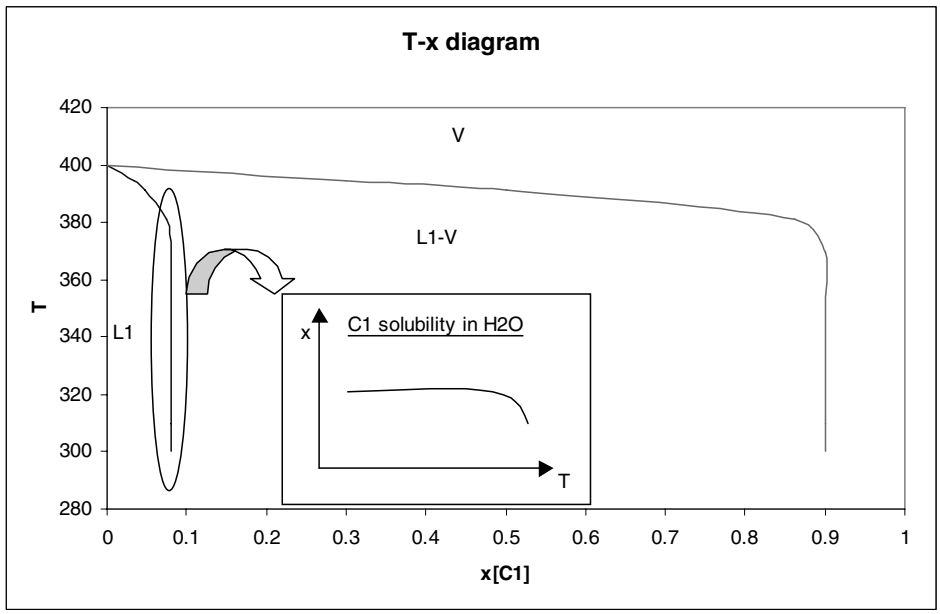

Fig. 2.15. Relation between a Tx phase diagram and a solubility curve

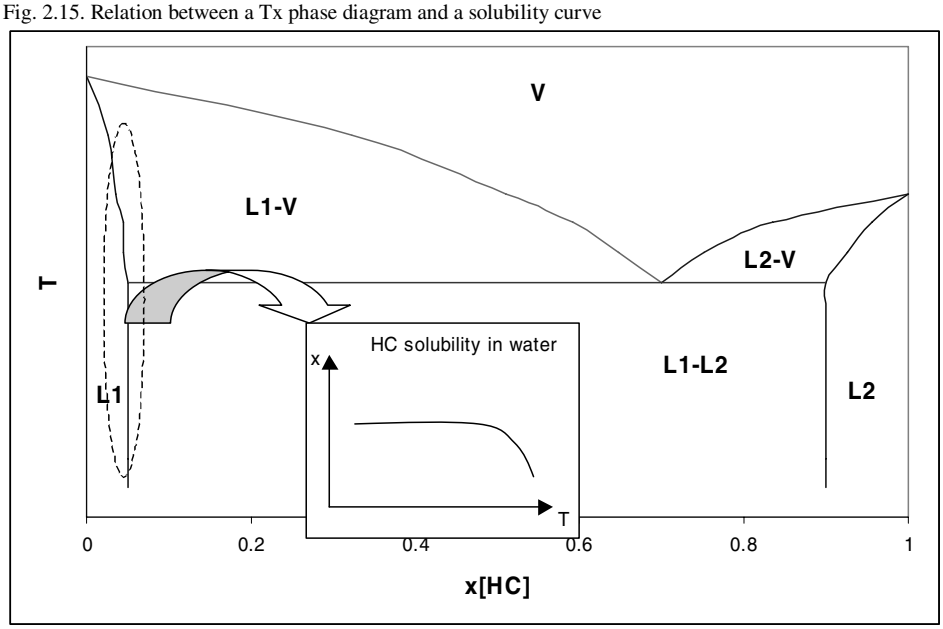

The evolution of the T-x phase diagram of the binary methane/water as a function of increasing pressure is shown on Fig. 2.16 to 2.19. Additional P-x and T-x projections are shown in Appendix 6.

Fig. 2.16. T-x diagram for methane/water at 13.8 b (Data from Davis, 1960; Olds, 1942; Gillepsie, 1982; Culberson, 1951a)

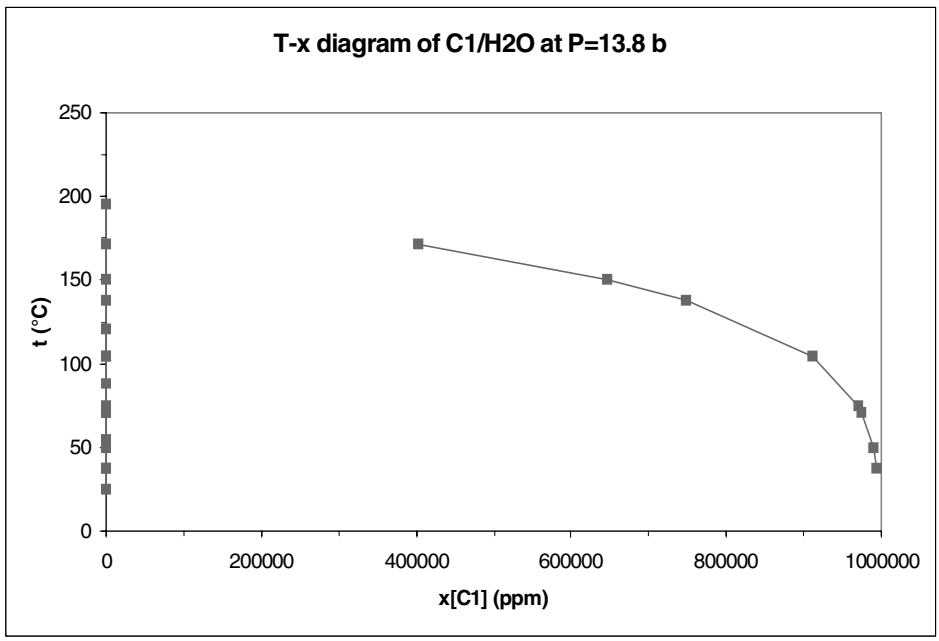

Fig. 2.17. T-x diagram for methane/water at 41.1 (Data from Olds, 1942; Culberson, 1951a; Amirijafari, 1972)

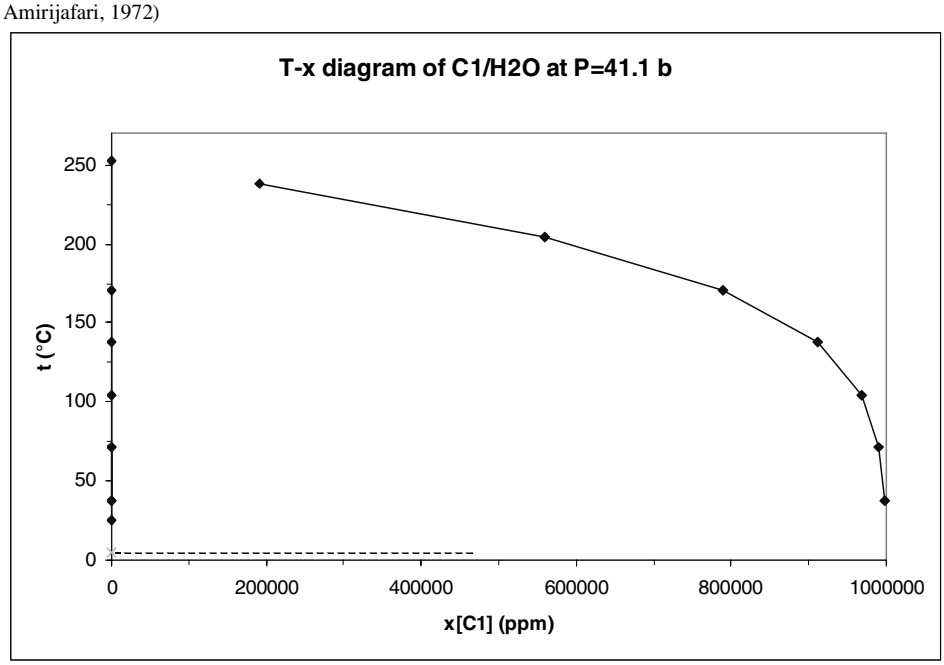

Fig. 2.18. T-x diagram for methane/water at 245 b (over the critical pressure of water) (Data from Olds, 1942; Culberson, 1950, 1951a, 1951b; Sultanov, 1972a, 1972b)

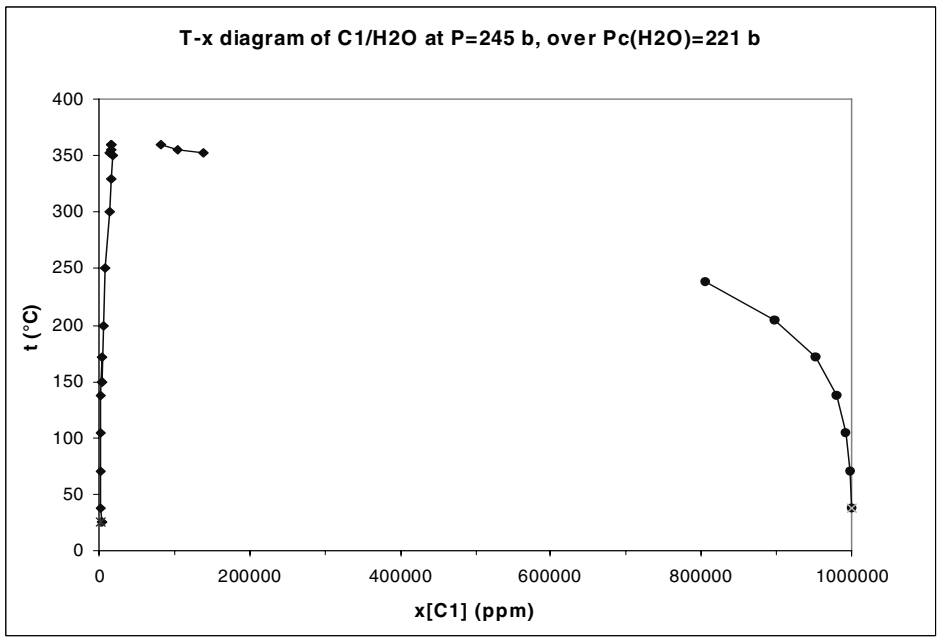

Fig. 2.19. T-x diagram for methane/water at 392.3 b (over the critical pressure of water) (Data from Sultanov, 1972a, 1972b)

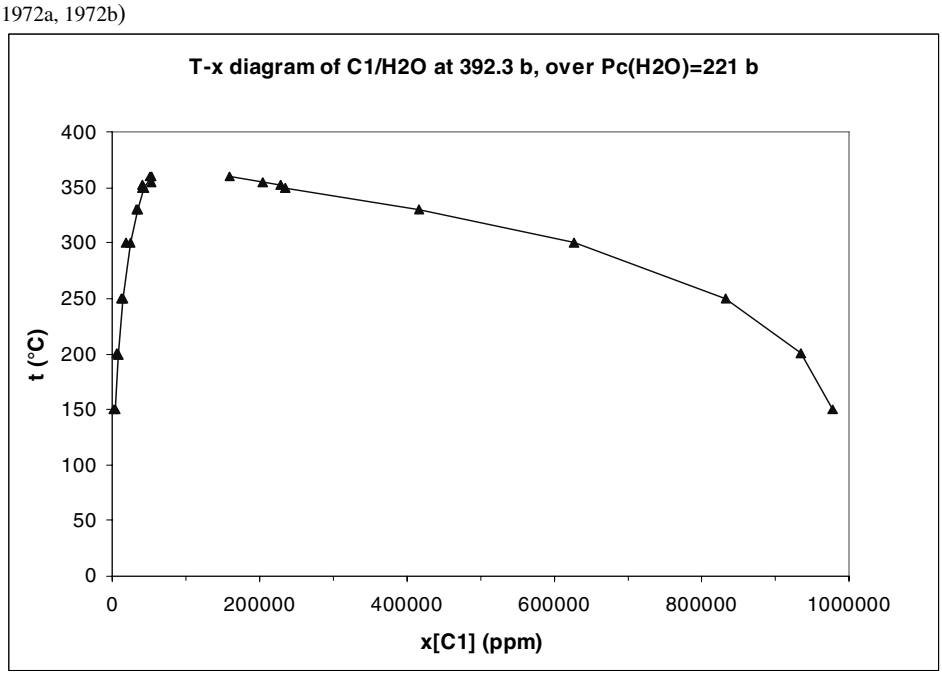

Collecting the left-hand branches of the T-x diagrams above, the right evolution of the solubility of methane in water as a function of temperature at different pressures is obtained as shown on Fig. 2.20 below. We can observe that the minimum of solubility becomes less tangible at lower pressures.

Fig. 2.20. Solubility limit of methane in water at different pressures

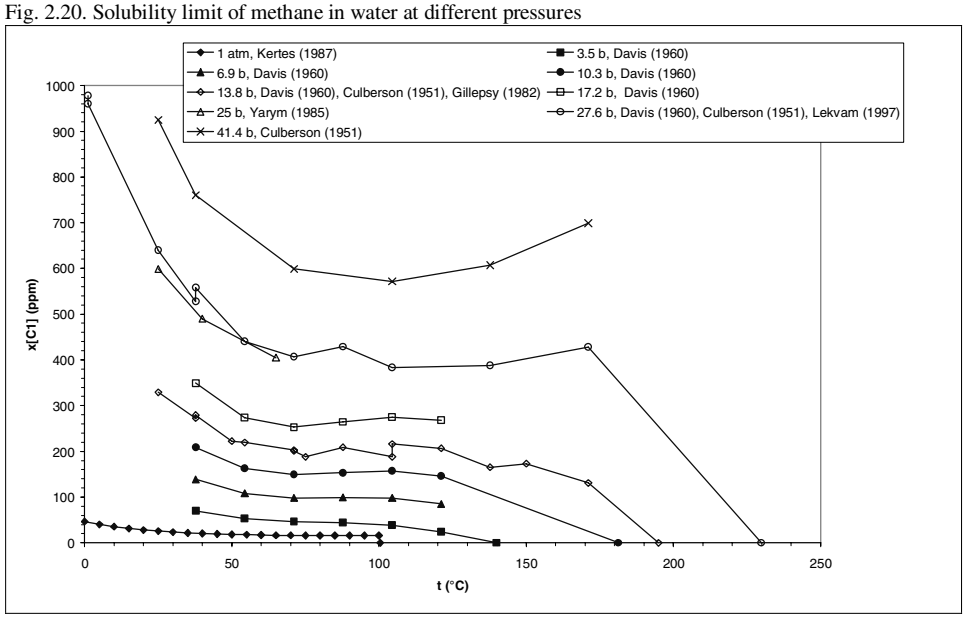

Similarly, the solubility of ethane, propane and n-butane can be obtained.

Fig. 2.21. Solubility limit of ethane in water at different pressures

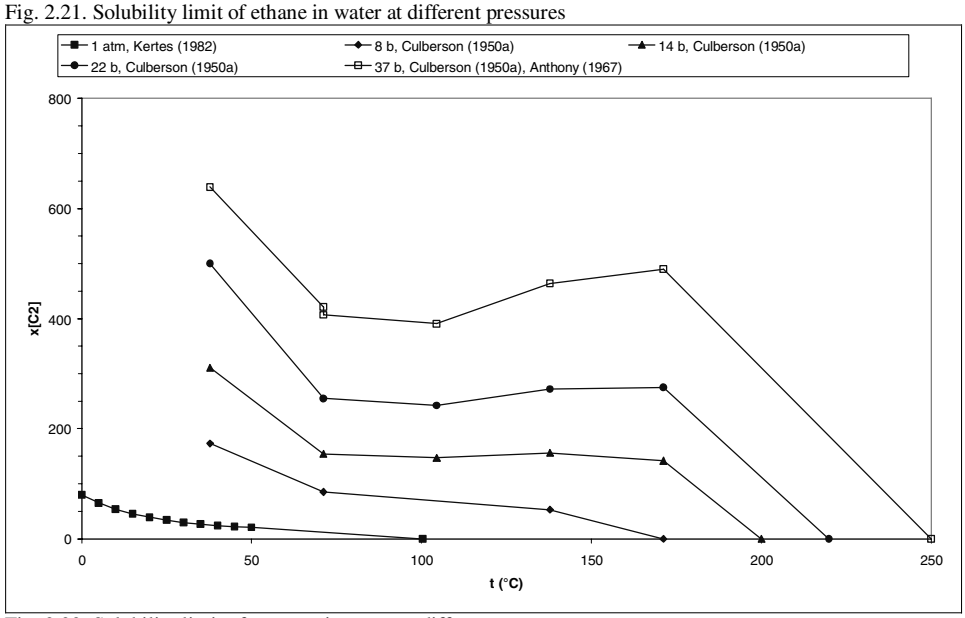

Fig. 2.22. Solubility limit of propane in water at different pressures

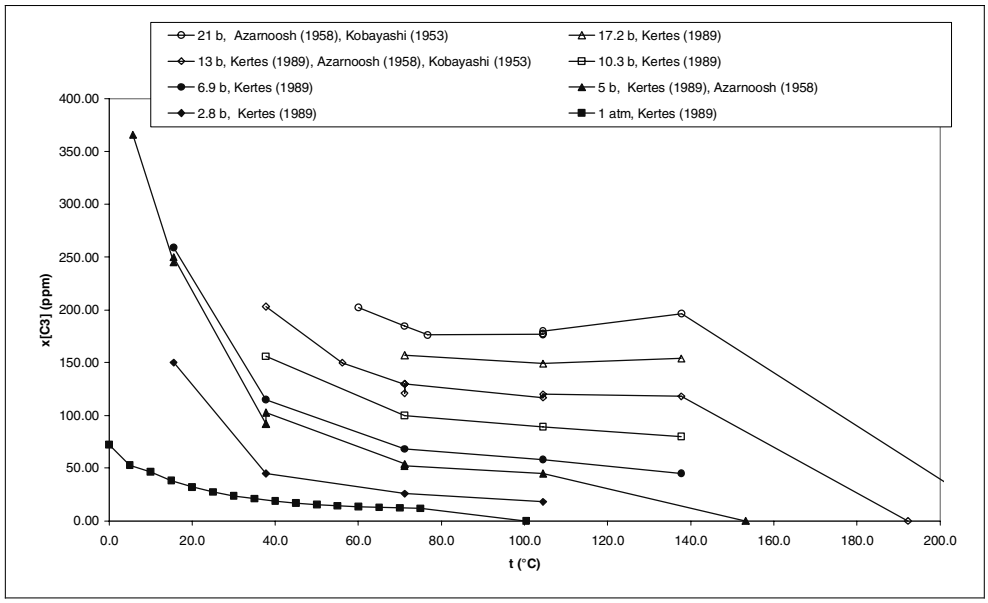

Fig. 2.23. Solubility limit of n-butane in water at different pressures

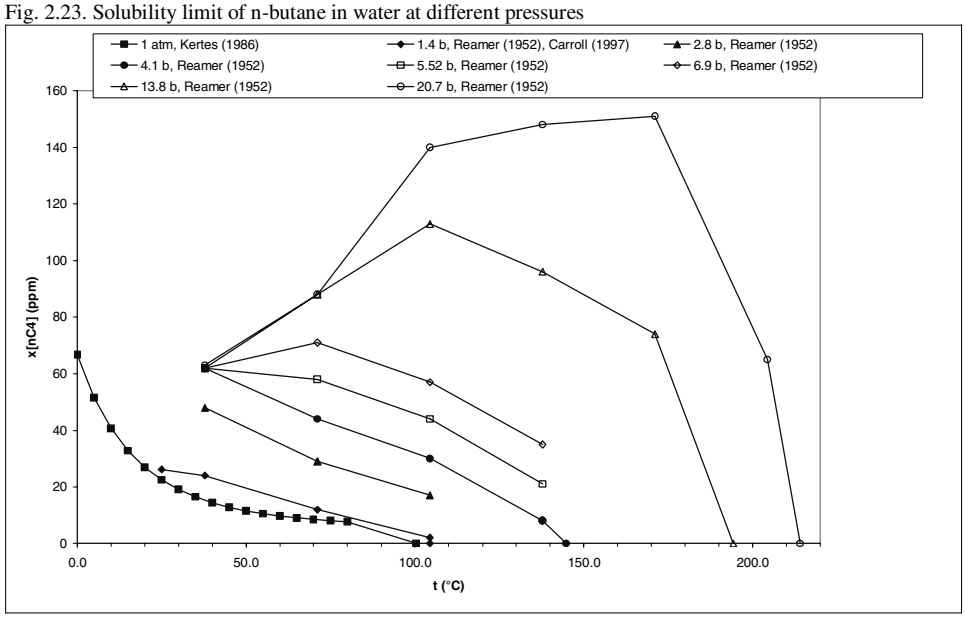

It seems that the concept of minimum of solubility does not apply for lower pressures or for heavier hydrocarbons.

Then, based on the previous results, it appears that the correlations for the solubility of light hydrocarbons in water published in the IUPAC's Solubility Data Series (Kertes, 1987) are wrong for the extrapolated branches, as shown on Fig. 2.24 and 2.25 for methane in water at respectively 100 bars and 1 atm. On both figures, the dashed line represents the solubility as correlated by Kertes et *al*. It fails to reach the vaporizing temperature of pure water located on the temperature axis (i.e. at a zero mole fraction of methane). On Fig 2.24, it clearly contradicts the available experimental data points. On Fig. 2.25 the same contradiction can be observed between the correlation of Kertes et *al.* (pink dashed curve) and the schematic curve which is the right progression (black dashed curve).

Fig. 2.24. Solubility limit for methane in water at 100 b: comparison between the correlation from Kertes (1987) and experimental data.

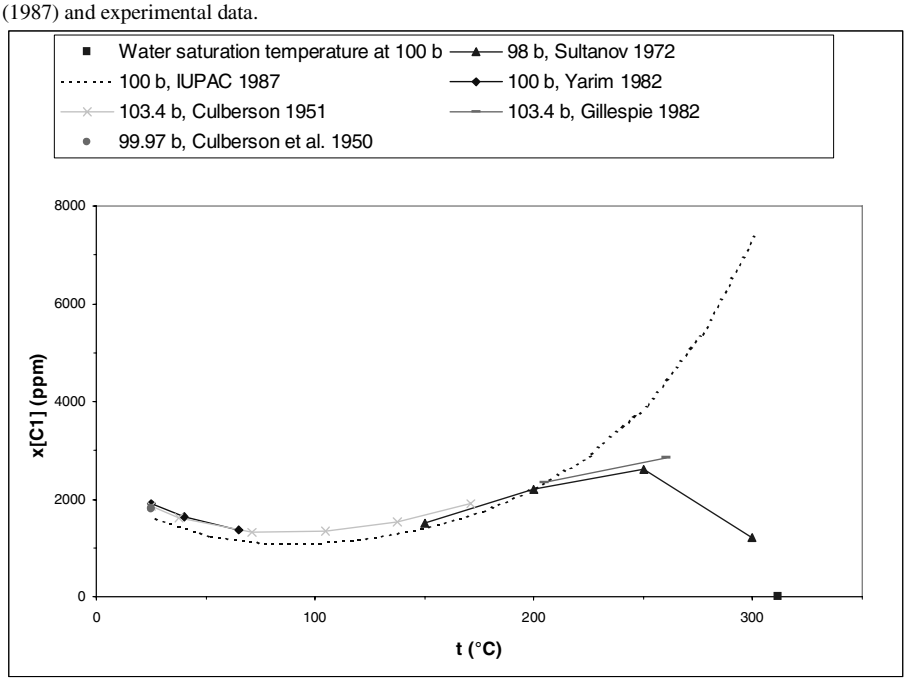

Fig. 2.25. Solubility limit for methane in water at 1 atm: comparison between the correlation from Kertes (1987) and experimental data.

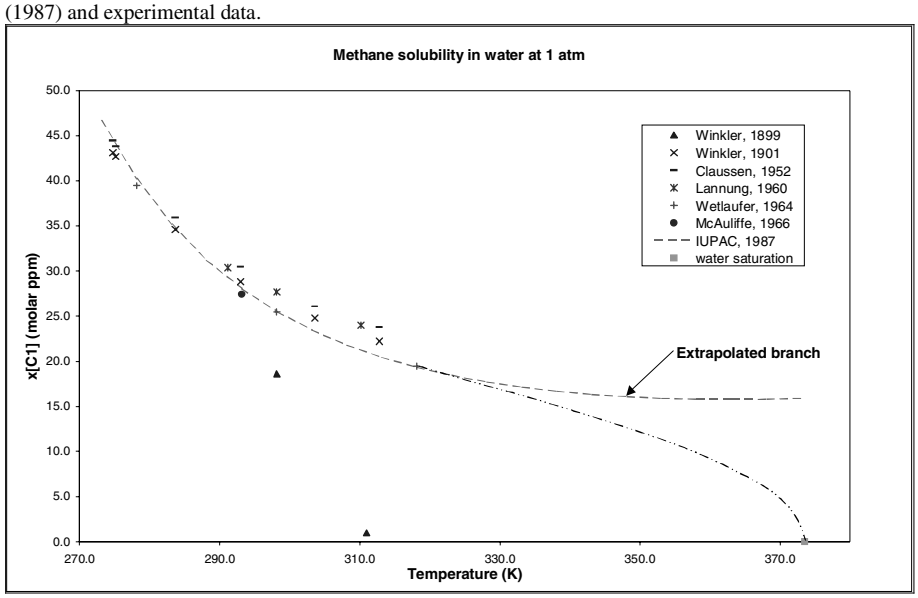

2.6 Conclusions

- Over 1000 data points were collected
- An error was found in Kertes' Solubility Data Series for Ethane (Kertes, 1982), which is the edition available at DTU. The original article was found during the stay at Total from January to May 2002. It has to be noted though that this mistake was corrected in the later edition of the Solubility Data Series for Ethane.
- Another mistake was found in the extrapolated solubilities published by Kertes' Solubility Data Series (Kertes, 1989). The published values of solubility of methane and ethane as a function of temperature do not tend to zero, when the temperature is increasing. Such a behaviour is explained by the shape of phase envelop in the T-x space.
- It appeared also that this compound is not well studied at atmospheric pressure and low temperatures, due to the fact that the critical temperature of ethane is 38.5°C.
- The data for compounds other than methane, ethane, propane are very scarce
- The data collected are a sufficient basis for selection of a model for water/hydrocarbon systems
- The complex behaviour of such systems requires thus advanced models and phase diagram analysis
- The standard IUPAC correlation (1987) is inapplicable when hydrocarbon solubilities at relatively low temperatures are considered (lower than 20°C). In particular, it cannot be applied for description of the drilling mud degassing under certain surface conditions. A more elaborate modelling or direct reference to experimental data is required for this task.

3 Thermodynamic modelling of the equilibrium of light hydrocarbons and water

3.1 Introduction

A thermodynamic model had to be chosen in order to reproduce and predict the behaviour of the system composed of drilling mud and reservoir oil. Especially, the model focuses on the solubility of the light hydrocarbons, as they are the species detected by the GWD™. The solubility of the hydrocarbons dissolved in the oil-phase of an oil-based mud can be described by a classical cubic equation of state (EOS) such as the Soave-Redlich-Kwong equation of state (Soave, 1972) or the Peng-Robinson equation of state (Peng, 1976).

Three models were studied in order to decide which one was the best to reproduce the behaviour of light hydrocarbons in the drilling-mud. They were chosen for their simplicity, as they are all derived or using a cubic EOS, as well as for their wide use in the oil industry. Moreover, each model tackles the interaction between components with specific interaction parameters.

The only mud additives, which are considered in the thermodynamic model, are of two kinds: the specific chemical additives, which may be integrated directly into the mud composition (such as esters, glycols) and the salts which displace the thermodynamic equilibrium. Other additives which may change the mechanical and rheological properties of the mud are assumed to influence marginally the thermodynamic equilibrium.

The studied models are the Peng-Robinson EOS modified by Søreide & Whitson (Søreide, 1992), Henry's law extension by Nghiem (Li, 1986), and the Soave-Redlich-Kwong EOS with the Original Huron-Vidal mixing rule (Huron, 1979).

3.2 Presentation of the models

3.2.1 Peng-Robinson EOS modified by Søreide & Whitson (Søreide, 1992)

This model is based on the Peng-Robinson EOS (Peng, 1976) modified so that the vapour pressure of water is well predicted as well as the solubility of light hydrocarbons in the aqueous phase is calculated.

The first modification consists in a different α parameter for water in the EOS:

$$\alpha^{1/2} = 1 + 0.4530 \cdot \left[1 - T_r \cdot \left(1 - 0.0103 \cdot c_{sw}^{1.1}\right)\right] + 0.0034 \cdot (T_r^{-3} - 1) \qquad (3.1)$$

Besides, two sets of interaction parameters k_{ij} are defined for the water/hydrocarbon pairs and used whether the considered phase is aqueous or not.

In the aqueous phase, the interaction parameter between the hydrocarbon i and water is:

$$k_{i,water}^{AQ} = (1.1120 - 1.7369\ \omega_i^{-0.1}) + (1.1001 + 0.8360\ \omega_i)T_{ri} + (-0.15742 - 1.0988\ \omega_i)T_{ri}^2 \quad (3.2)$$

where ω_i is the acentric factor and T_{ri} is the reduced temperature of hydrocarbon i.

For any hydrocarbon phase (or non-aqueous, NA), the following interaction parameters are used:

$k^{NA}_{H2O, C1} = 0.4850$, $k^{NA}_{H2O, C2} = 0.4920$, $k^{NA}_{H2O, C3} = 0.5525$, $k^{NA}_{H2O, nC4} = 0.5091$, $k^{NA}_{H2O, Cx} = 0.5000$

where C_x represents any hydrocarbon heavier than butane.

3.2.2 Soave-Redlich-Kwong with Original Huron Vidal mixing rule (Huron, 1979)

The classical Soave-Redlich-Kwong EOS is used for all phases, with the mixing rule defined by Huron and Vidal. It uses a classical mixing rule for the b parameter. The relation between the a_{ij}'s and a is the following:

$$a = b \cdot \left[\sum_i x_i \frac{a_{ii}}{b_i} - \frac{G_\infty^{\ E}}{\ln(2)} \right] \quad (3.3)$$

The Gibbs Energy term $G_\infty^{\ E}$ is given by the NRTL model modified by Huron and Vidal:

$$\frac{G_\infty^E}{RT} = \sum_i x_i \frac{\sum_j x_j \cdot b_j \cdot \exp(-\alpha_{ji} \cdot \tau_{ji}) \cdot \tau_{ji}}{\sum_k x_k \cdot b_j \cdot \exp(-\alpha_{ji} \cdot \tau_{ji})} \quad (3.4)$$

with the binary interaction parameters $\tau_{ji} = \tau_{ji}^0 + \tau_{ji}^T \cdot (1 - \frac{298.15}{T})$ (3.5)

and $\alpha_{ji} = \alpha_{ji}^0 + \alpha_{ji}^T \cdot (1 - \frac{298.15}{T})$ (3.6)

3.2.3 Peng-Robinson and Henry's law (Li, 1986)

This model uses the Peng-Robinson EOS to describe the hydrocarbon phases. A Henry's law model is used to describe the fugacity of the aqueous phase. A temperature-dependent Henry constant is used:

$$\ln\left(\frac{H_i^*}{f_{water}^{sat}}\right) = -A + B\cdot\left(\frac{10^3}{T}\right) - C\cdot\left(\frac{10^6}{T}\right) \qquad (3.7)$$

A specific set of interaction parameters k_{ij} for water/hydrocarbons pairs is used in the hydrocarbon phases.

$k_{H2O,\,C1} = 0.4905$, $k_{H2O,\,C2} = 0.4911$, $k_{H2O,\,C3} = 0.5469$, $k_{H2O,\,nC4} = 0.5080$

As for any Henry constant model, it is assumed that the components dissolved in water do not interact with each other.

3.3 Comparisons

The tables below compare the values calculated with the different models with experimental values at different conditions of pressure and temperature.

The tables showing the values are organised as following:

- 1st column: pressure
- 2nd column: temperature
- 3rd column: experimental value of the hydrocarbon solubility in water
- 4th column: data source
- 5th column: solubility calculated with Peng-Robinson EOS (PR)
- 6th column: solubility calculated with PR modified by Søreide and Whitson (PR with SW)
- 7th column: solubility calculated with Soave-Redlich-Kwong EOS with the original Huron-Vidal mixing rule (SRK + HV)
- 8th column: solubility calculated with Peng-Robinson coupled with Henry's law (PR + Henry)

The tables showing the relative errors are organised as following:

- 1st column: pressure
- 2nd column: temperature
- 3rd column: relative error between the experimental values and the values calculated with PR
- 4th column: relative error between the experimental values and the values calculated with PR with SW
- 5th column: relative error between the experimental values and the values calculated with SRK + HV
- 6th column: relative error between the experimental values and the values calculated with PR + Henry

In this series of tables, the boxes emphasised in grey correspond to the lowest relative error between the three models.

3.3.1 Methane in water

Table 3.1.

P (bar)	T (K)	Exp. Data		PR	PR with SW	SRK + HV	PR + Henry
1	325	0.000018	(1)	0.000002	0.00001367	0.000015	0.000016
	350	0.000016	(1)	0.000003	0.00000814	0.000010	0.000009
10	325	0.000220	(1)	0.000020	0.00015169	0.000162	0.000178
	350	0.000200	(1)	0.000039	0.00013080	0.000150	0.000148
	375	0.000200	(1)	0.000065	0.00012133	0.000143	0.000135
	400	0.000210	(1)	0.000094	0.00011202	0.000133	0.000123
100	325	0.001240	(1)	0.000160	0.00121944	0.001319	0.000002
	350	0.001110	(1)	0.000326	0.00111668	0.001289	0.001248
	375	0.001110 0.001400	(1) (2)	0.000603	0.00113522	0.001345	0.001256
	400	0.001220	(1)	0.001032	0.00124741	0.001474	0.001369
	425	0.001420	(1)	0.001646	0.00144785	0.001670	0.001561

Table 3.2.

P (bar)	T (K)	Exp. Data		PR	PR with SW	SRK + HV	PR + Henry
500	325	0.004170	(1)	0.000414	0.00326908	0.003590	0.000004
	350	0.003730	(1)	0.000908	0.00317114	0.003757	0.003495
		0.003720	(3)				
	375	0.003740	(1)	0.001790	0.00341288	0.004145	0.003786
		0.003900	(2)				
	400	0.004090	(1)	0.003250	0.00394979	0.004766	0.004410
	425	0.004770	(1)	0.005527	0.00483497	0.005666	0.005378
1000	325	0.007030	(1)	0.000556	0.00441881	0.004939	0.004748
	350	0.006290	(1)	0.001238	0.00437813	0.005222	0.004736
		0.005090	(3)				
	375	0.006310	(1)	0.002475	0.00475741	0.005804	0.005269
	400	0.006890	(1)	0.004554	0.00555002	0.006705	0.006289
	425	0.008030	(1)	0.007855	0.00683961	0.007985	0.007846

Table 3.3.

P (bar)	T (K)	Rel. Error (%) PR	Rel. Error (%) PR with SW	Rel. Error (%) SRK + HV	Rel. Error (%) PR + Henry
1	325	88.9	24.1	15.9	10.1
	350	81.3	49.1	35.7	41.6
10	325	90.9	31.1	26.3	19.6
	350	80.5	34.6	25.2	26.6
	375	67.5	39.3	28.4	33.1
	400	55.2	46.7	36.8	42.1
100	325	87.1	1.7	-6.4	99.9
	350	70.6	-0.6	-16.1	-11.7
	375	45.7	-2.3	-21.2	-12.1
		56.9	18.9	3.9	11.1
	400	15.4	-2.2	-20.8	-10.7
	425	-15.9	-2.0	-17.6	-8.1

Table 3.4.

P (bar)	T (K)	Rel. Error (%) PR	Rel. Error (%) PR with SW	Rel. Error (%) SRK + HV	Rel. Error (%) PR + Henry
500	325	90.1	21.6	13.9	99.9
	350	75.7	15.0	-0.7	6.9
		75.6	14.8	-1.0	6.7
	375	52.1	8.7	-10.8	-0.2
		54.1	12.5	-6.3	3.9
	400	20.5	3.4	-16.5	-6.4
	425	-15.9	-1.4	-18.8	-10.9
1000	325	92.1	37.1	29.7	32.5
	350	80.3	30.4	17.0	24.7
		75.7	14.0	-2.6	7.0
	375	60.8	24.6	8.0	16.5
	400	33.9	19.4	2.7	8.7
	425	2.2	14.8	0.6	2.3

As seen from Tables 3.3 and 3.4, the model PR with SW is a good fit at high pressures, even if there are problems with this model at lower pressures. This is explained by the fact that the parameters of the model were fitted on high pressure data. The models SRK+HV and PR+Henry work better for methane at low pressures.

3.3.2 Ethane in water

Table 3.5.

P (bar)	T (K)	Exp. Data		PR	PR with SW	SRK + HV	PR + Henry
1	325	0.000021	(1)	0.000002	0.000017	0.000017	0.000057
10	350	0.000118	(1)	0.000046	0.000177	0.000134	0.000412
	375	0.000100	(1)	0.000083	0.000123	0.000118	0.000334
100	375	0.000800	(2)	0.000534	0.000801	0.000786	0.002182
200	344.15	0.000926	(3)	0.000233	0.000874	0.000879	0.002648
500	344.15	0.001146	(3)	0.000281	0.001055	0.001084	0.003197
	350	0.001100	(1)	0.000352	0.001081	0.001105	0.003219
	375	0.001329	(1)	0.000842	0.001262	0.001293	0.003588
		0.001400	(2)				
750	344.15	0.001284	(3)	0.000304	0.001143	0.001181	0.003426
1000	350	0.001398	(1)	0.000401	0.001236	0.001270	0.003594

Table 3.6.

		Rel. Error (%)	Rel. Error (%)	Rel. Error (%)	Rel. Error (%)
P (bar)	T (K)	PR	PR with SW	SRK + HV	PR + Henry
1	325	90.5	20.3	17.7	-171.4
10	350	61.0	-50.0	-13.5	-249.1
	375	17.0	-22.9	-18.3	-234.4
100	375	33.3	-0.2	1.8	-172.8
200	344.15	74.8	5.6	5.1	-185.9
500	344.15	75.5	7.9	5.4	-179.0
	350	68.0	1.7	-0.4	-192.7
	375	36.6	5.1	2.7	-170.0
		39.9	9.9	7.6	100.0
750	344.15	76.3	10.9	8.0	-166.8
1000	350	71.3	11.6	9.1	-157.1

As seen in Table 3.6, there is a problem with the model PR with the Henry constants; it seems that the values of the parameters published by Nghiem et *al*. (Li, 1986) are wrong. In-house values of the parameters for ethane from Total were later used in the project; these values are however confidential. The model SRK+HV is good over all the ranges of pressures and temperatures. The model PR with SW appears nevertheless to be a reasonable fit as well.

3.3.3 Propane in water

Table 3.7.

P (bar)	T (K)	Exp. Data		PR	PR with SW	SRK + HV	PR + Henry
1	325	0.000015	(1)	0.000000	0.000015	0.000014	0.000013
	350	0.000012	(1)	0.000001	0.000007	0.000008	0.000007
10	350	0.000099	(1)	0.000010	0.000109	0.000099	0.000100
	375	0.000110	(1)	0.000024	0.000095	0.000089	0.000089
	400	0.000100	(1)	0.000045	0.000085	0.000085	0.000082
100	375	0.000325	(2)	0.000080	0.000318	0.000324	0.000319
200	344.15	0.000926	(3)	0.000019	0.000261	0.000262	0.000254
500	344.15	0.001146	(3)	0.000021	0.000288	0.000293	0.000277
	375	0.000380	(2)	0.000097	0.000384	0.000403	0.000399
1000	344.15	0.001398	(3)	0.000022	0.000306	0.000311	0.000280

Table 3.8.

		Rel. Error (%)	Rel. Error (%)	Rel. Error (%)	Rel. Error (%)
P (bar)	T (K)	PR	PR with SW	SRK + HV	PR + Henry
1	325	100.0	3.3	9.6	10.9
	350	91.7	37.8	37.4	41.9
10	350	89.9	-10.2	-0.5	-0.5
	375	78.2	13.9	18.8	19.3
	400	55.0	15.3	15.4	17.8
100	375	75.4	2.1	0.2	1.9
200	344.15	97.9	71.8	71.7	72.6
500	344.15	98.2	74.9	74.4	75.8
	375	74.5	-1.0	-6.1	-5.0
1000	344.15	98.4	78.1	77.7	80.0

As seen in Table 3.7, as the data become scarcer with heavier components, the models behave less accurately. The model PR with SW behaves well at low pressures. At higher pressures, all the three models behave alike.

3.3.4 n-butane in water

Table 3.9.

P (bar)	T (K)	Exp. Data		PR	PR with SW	SRK + HV	PR + Henry
1	325	0.000011	(1)	0.000000	0.00001083	0.000012	0.000014
	350	0.000008	(1)	0.000000	0.00000559	0.000007	0.000007
10	375	0.000068	(1)	0.000006	0.00006658	0.000076	0.000079
	400	0.000076	(1)	0.000015	0.00006133	0.000068	0.000071
100	350	0.000095	(3)	0.000002	0.00007019	0.000091	0.000096
	375	0.000150	(2)	0.000009	0.00009813	0.000127	0.000133
500	350	0.000092	(3)	0.000002	0.00007608	0.000100	0.000102
	375	0.000170	(2)	0.000010	0.00010717	0.000140	0.000148
1000	350	0.000098	(3)	0.000002	0.00007656	0.000099	0.000096

Table 3.10.

		Rel. Error (%)	Rel. Error (%)	Rel. Error (%)	Rel. Error (%)
P (bar)	T (K)	PR	PR with SW	SRK + HV	PR + Henry
1	325	100.0	1.5	-13.2	-27.1
	350	100.0	30.1	12.8	13.1
10	375	91.2	2.1	-11.3	-16.6
	400	80.3	19.3	10.1	6.3
100	350	97.9	26.1	4.5	-0.8
	375	94.0	34.6	15.0	11.4
500	350	97.8	17.3	-8.2	-10.9
	375	94.1	37.0	17.4	12.7
1000	350	98.0	21.9	-1.0	1.7

As seen in Table 3.9, the same remarks as for propane apply here. The model PR with Henry appears to be slightly better, especially at high pressures.

3.4 Conclusions

- The models appeared to be accurate only at high pressures, as the parameters they use were fitted with high pressure data
- The model of Søreide and Whitson is less accurate for propane and n-butane than for methane and ethane
- For high pressure ranges, the model of Søreide and Whitson appears to be the best model when looking at all compounds. This model could be a good choice to reproduce the behaviour of the system drilling mud/reservoir fluid in the riser between the bottom-hole and the well-head. The model of Søreide and Whitson was chosen for the first stage of the project for simulation purposes, as it was already implemented in Total's in-house PVT software BEST (Refer to Chapter 4 and 7).
- The model of Nghiem et *al.* (Li, 1986) has a better accuracy than the model of Søreide and Whitson at lower pressures. It means that this model could be used to describe the behaviour of the system drilling mud/reservoir fluid at atmospheric pressure, in the part of the drilling circulating systems which are located on the rig at the surface. The model of Nghiem et *al.* was chosen for developing the final simulation tool.
- No fitting of parameters at low pressure was carried out, even if the needed were collected and are available

4 Modelling the GWD Process

4.1 Introduction

One of the major goals of the project has been to provide a simulation facility for the GWD process. In order to do so the GWD process had to be represented as a series of physical events, each of them allowing for the thermodynamic modelling. This simulation uses a known reservoir fluid and attempts to reproduce the gas shows recorded on field. The thermodynamic models studied in the previous chapter are used to describe the degassing of the drilling mud at the different stages of the process. In the course of such modelling, a system of adjustment parameters reflecting incomplete knowledge of the process and approximations admitted in the model had to be identified.

Total's in-house PVT software BEST was used to describe the process and perform the first simulations. The resulting flow sheet of the GWD process which later has been used for simulations is described in the present chapter.

4.2 Physical assumptions

The following hypotheses about the nature of the GWD process are adopted:

- The flow of mud is piston-like in the riser; this assumption is based on the fact that any gas signal corresponding to a hydrocarbon-bearing layer is not dispersed very much;
- The hole geometry is indicated by the size of the drill bit, supposing that the degradation of the hole occurs over several hours to several days later;
- The reservoir fluid present in a volume of drilling mud comes from the volume of reservoir rock drilled while the reservoir fluid was at the bottom-hole;
- Water-based mud is assimilated as pure water and oil-based mud as a mixture of diesel oil and water;
- Thermodynamic equilibrium is reached at each instant and everywhere in the system (This means that we will use flash calculations to model the different phases);
- The different equilibria reached in the well while the mud is ascending in the well are not described in the model, only the system reaching the surface is taken into account;
- No adsorption of hydrocarbons on the cuttings takes place.

The model described above was constructed based on these hypotheses. The goal was to construct the simplest possible, but still physical, model and to verify whether it is sufficient for reproduction of the industrial GWD data available. This model was supposed to be modified further by inclusion of such mechanisms as adsorption on cuttings and flow dynamics, provided that such modification would later be found to be necessary. Since development and implementation of the basic model has required a lot of effort, such modification was left outside the present project.

4.3 Description of the BEST flow sheet

First, a satisfactory representation of the GWD process has been achieved with Total PVT software BEST. BEST is a simplified process simulator equipped with a thermodynamic simulator and a PVT package. Each unit or box in the simulation corresponds to a single operation, such as mixing fluxes or flashing a flux.

Fig. 4.1 presents basic version of the BEST Worksheet for a water-based mud and a QGM gas trap. Some of the elementary units used in the simulation are detailed below based on Fig. 4.1. Fig. 4.2 shows a flow sheet for a simulation with oil-based mud.

The box "Init" has for input an Excel Worksheet where all the components of the system and their properties are defined. The components describing the reservoir fluid are N_2, H_2S, CO_2, C_1, C_2, and heavier hydrocarbon compounds and cuts, according to the PVT description available for a reservoir fluid. The composition of the reservoir fluid is provided in the input Excel Worksheet. The mud is described by water in case of water-based mud. Oil-based mud is described by water mixed with a diesel cut C_{11}-C_{18}. The properties of the compounds are the molecular weight, the critical properties (temperature, pressure and acentric factor) and the interaction parameters needed by an equation of state.

The first operations in the simulation (boxes "fracN2", "flash_atm3", "fraceau, "flash_atm1", "fracresfl", "flash_res", "flash_atm") prepare all the different fluxes. It especially prepares a flux of pure water to be used as water-based mud. It prepares also a flux of pure nitrogen, which will be used as a close substitute for air in the gas-trap.

The reservoir data obtained from field operation are then used to set the flux of reservoir fluid at the right conditions and calculate the amount of reservoir fluid present. The field data are the following

- the reservoir pressure in bar,
- the reservoir temperature in °C,
- the porosity of the simulated layer,
- the water saturation of the simulated layer,
- the Rate of Penetration (ROP) in m/h,
- the bitsize in m,
- the mud flow-rate in l/min,
- the mud density in kg/m^3, called also mud weight.

The molar flux of mud "Nmud" (in mol/min) calculated with help of the mud flow-rate Vmud" (in m^3/min), the density and the molecular weight of the mud, as following

$$Nmud = Vmud \cdot Mudweight / (mud\ molecular\ weight) \qquad (4.1)$$

Fig. 4.1. BEST flow sheet for a water-based mud system

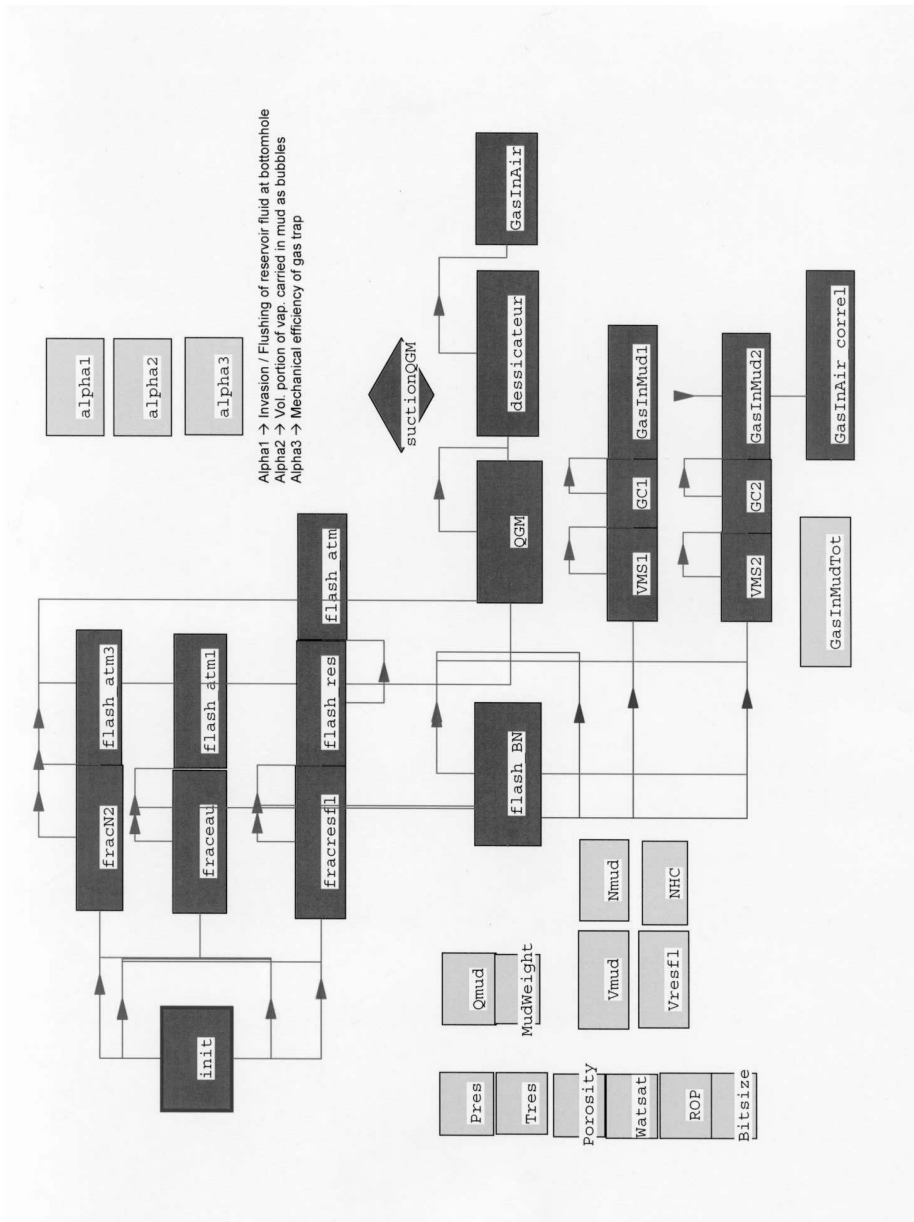

Fig. 4.2. BEST flow sheet for an oil-based mud system

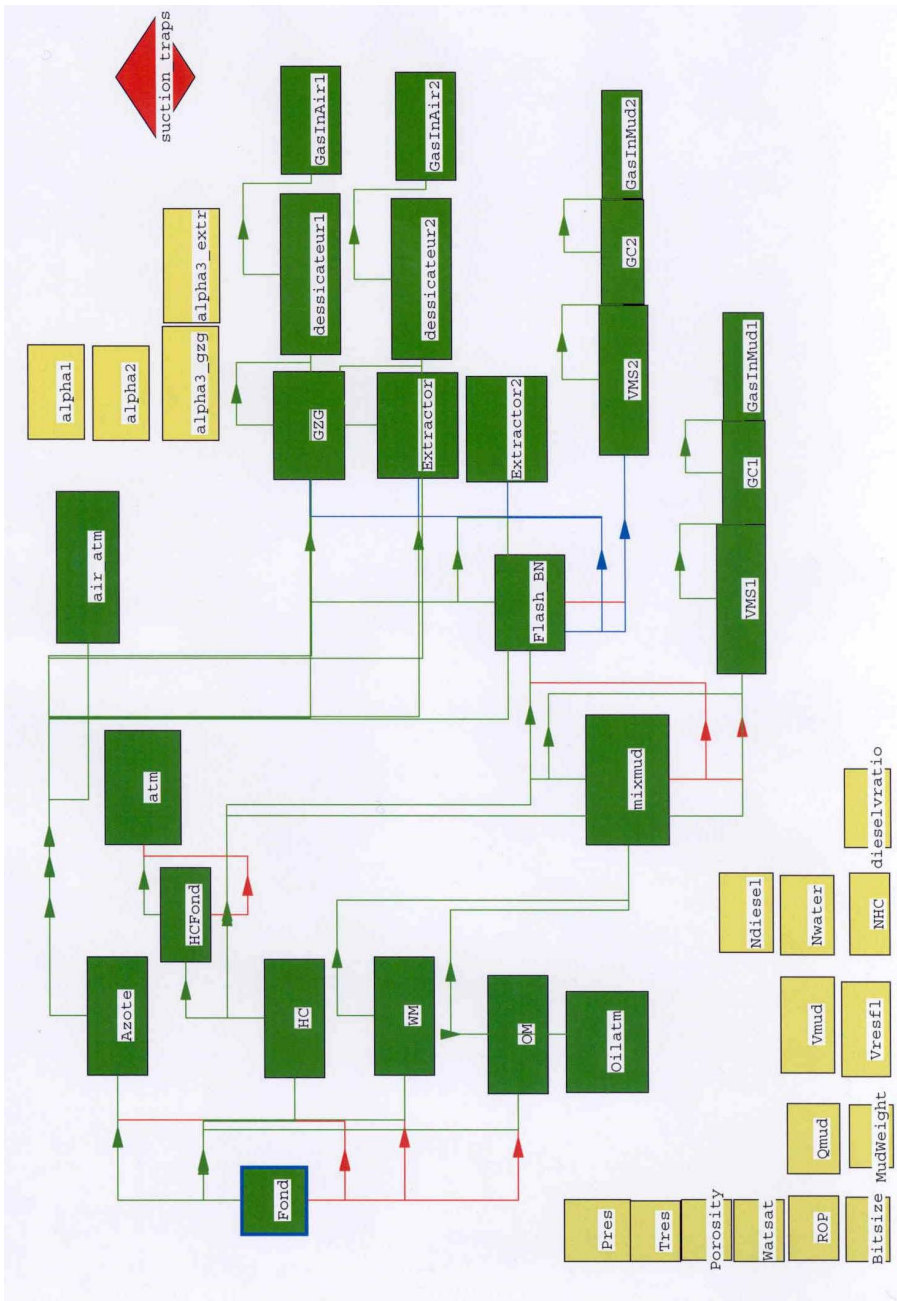

The volume of reservoir fluid (m^3/min) liberated from the drilled rock is calculated with the drilled volume, the porosity and the water saturation as following

$$Vresfl = Alpha\_1 \cdot \pi \cdot (\frac{Bitsize}{2})^2 \cdot \frac{ROP}{60} \cdot porosity \cdot (1 - Watsat) \qquad (4.2)$$

It is possible to modify this volume with the coefficient Alpha_1 as described in the following section.

The number of moles of reservoir fluid (mol/min) liberated from the drilled rock is then calculated with the density and the molecular weight of the reservoir fluid (both calculated in the box "flash_res") as following

$$NHC = \frac{Vresfl \cdot (density\ of\ reservoir\ fluid\ from\ "flash\_res")}{Molecular\ weight\ of\ reservoir\ fluid\ from\ "flash\_res"} \qquad (4.3)$$

Then a flash calculation of the mixture composed by the reservoir fluid and the mud at the conditions found just after the well head is performed in order to describe the system exiting the well at the bell nipple. The reservoir fluid (from the box "fracresfl" which quantity is set by the box "NHC") is mixed with the mud (from the box "fraceau" which quantity is set by the box "Nmud"). The mixture is flashed at 1 atm and at the mud temperature, as measured at the flow-line. This flash calculation enables to see if a gas phase is naturally present right out of the well. A coefficient *Alpha_2* is used to define a partial degassing of the mud and is used to separate a portion of the gas phase.

The group of boxes "VMS1-GC1-GasInMud1" calculates the gas content of the mud (volume ppm) before any degassing. The group of boxes "VMS2-GC2-GasInMud2" calculates the gas content of the mud (volume ppm) after partial degassing; this quantity represents the gas in mud entering the gas trap.

In the unit "QGM", a flash calculation is carried out to represent the degassing of the mud in the gas-trap. The trap contains some reservoir fluid, mud and air at the trap conditions. The input flux are the liquid phases from "flash_BN" (aqueous and hydrocarbon), a fraction Alpha_2 of the vapour phase from "flash_BN" and the air flux from the box "fracN2". The proportion of air depends on the type of gas trap. The gas trap pressure is set at 0.8 atm for the QGM. The gas trap temperature is set at the mud temperature, as measured at the flow-line. This flash enables to calculate the gas content of the air as if the degassing was ideal. A parameter *Alpha_3* is used to correct the quantities of light gases found in air out of the gas trap.

The gas flux from the gas-trap is "cleaned" from heavy traces and water in the boxes "dessicateur" and "GasInAir". The gas compositions in methane to pentane (in volume ppm) are then calculated in the last unit "GasInAir".

The worksheet for the oil-based mud is similar to the worksheet for the water-based mud. It is presented on Fig. 4.2. The main differences are:

- a flux of pure water is fractionated in the box “WM”
- a flux of diesel-oil C11-C18 is fractionated in the box “OM”
- these two fluxes are mixed in the box “mixmud”, according to the value of the volume ratio diesel-water stored in the box “dieselvratio”.

4.4 Description of the adjustment parameters

The scheme described above contains three adjustment parameters. These parameters are introduced in order to take into account incompleteness of the proposed GWD model, which does not take into account many natural phenomena such as dissolution dynamics, adsorption, bubble formation etc.

Alpha_1 (See equation 4.2)

At the bottom-hole, where the reservoir fluid gets into contact with the drilling-mud, the relative amounts of mud and hydrocarbon can be modified in case of under-pressure or over-pressure of the drilling mud compared to the reservoir pressure.

When Alpha_1 is equal to 1, all the reservoir fluid present in the drilled rock is going into the mud. If the pressure exerted by the mud is too high, then the drilled area was previously washed out by the mud and the amount of hydrocarbon entering the system is less than expected. In this case, Alpha_1 is set to value lower than 1. In the opposite case, reservoir fluid invades the drilling-hole and Alpha_1 may be greater than 1.

Alpha_2 (box Flash BN)

In order to take into account any degassing of the drilling-mud occurring before the gas-trap and thus affecting the gas-shows, the part of the circulating system including the bell-nipple, the flow-line and the tank of the shale-shaker was taken into account. A coefficient Alpha_2 is thus used to define a partial degassing of the mud. This parameter corresponds to the fraction of vapour from “flash_BN” that is separated from the mud; the rest of the vapour corresponding to the volume fraction (1- Alpha_2) remains in the mud as small bubbles and thus enters the gas-trap.

Alpha_3 (box QGM for the water-based mud, GZG/Extractor for the oil-based mud)

In the gas-trap, the degassing process from which the gas-shows are obtained is undertaken by agitating and contacting the mud with fresh air. This is simulated by a flash calculation which calculates the gas content of the air as if the degassing was ideal. A coefficient Alpha_3 is then used to correct this amount and represents thus the global mechanical efficiency of the trap.

Moreover, three different gas-traps are simulated: the degassing process is well controlled in the case of the GZG and the Extractor from Geoservices, but it is not the case for the QGM from Texaco. This leads to using a different degassing efficiency Alpha_3 for each trap.

4.5 Conclusions

A thermodynamic model for the GWD process has been developed. In a first time it enabled to conceptualise what is happening to the drilling mud and the reservoir fluid between the bottom-hole and the gas-trap. Then, simulations of selected field-cases could be obtained.

Three adjustment parameters were identified in this conceptualisation phase. Each of them corresponds to a key part of the GWD process where further work had to be undertaken in order to fully understand the impact and functioning of these parameters. Based on field data and experimental results, numerical evaluation of these adjustments parameters was attempted (cf Chapter 5, 6 and 7).

This model was implemented into BEST software (Total) and into a FORTRAN program by M. L. Michelsen, resulting in the final GWD simulation program.

5 Degassing of the drilling mud before the gas trap

5.1 Introduction

The three parameters of the model, described in the previous chapter, contain a lot of indefiniteness. Their simultaneous fitting is a tedious task, which, additionally, provides very little information about the process, especially, taking into account that not all the governing physical mechanisms are included into the model. In particular, the parameter Alpha_2 responsible for degassing of the mud between the well head and the gas trap remains largely unknown.

The gas show may be transferred in the mud in the two states. First, it may be dissolved in the mud, and second, it may exist as micro bubbles, which are kept inside the mud by the surface forces. The second possibility has not been thoroughly studied previously. Meanwhile, if it would be realised, the amount of gas travelled with the mud could be much higher than it is taken in the model. At the present level of knowledge about micro bubbles, it is very difficult to quantify the gas show associated with them. Such quantification would require a separate study.

Thus, the goal of the present research was to establish whether the gas may travel in the mud in the form of micro bubbles, and what could be the amount of gas transferred in this way compared to the amount of the dissolved gas. This study was also connected to determination of the parameter Alpha_2.

In order to examine whether the gas bubbles may occur in the mud, an experiment has carried out in the laboratories of Eni Tecnologie. The “mud” was simulated by the liquid component of a realistic water-based mud, without solid particles. The dissolution gas was taken to be argon. The results of the experiment were analysed qualitatively, in order to obtain the answer of the type of “yes” (the bubbles are present) or “no” (there is no bubbles). Unfortunately, quasi-industrial conditions and inaccuracies that occurred in the course of the experiment did not make it possible a more detailed quantitative analysis of its results. The experiment and the results are presented below. The experiment is presented in Appendix 7 and the results showed and discussed below.

5.2 Presentation of the experiment

The phenomenon of mud degassing between the wellhead and the gas-trap has been highlighted by several field tests by Total and by ENI E&P.

These tests clearly showed that some degassing was occurring but it appeared also rather difficult to quantify it. From one test to another, the amount of lost gas could vary a lot due to reasons that could not be clearly identified. These reasons were anyway linked to either experimental errors or changes in the degassing conditions.

The aim of the experiment is to study the degassing of the drilling mud occurring between the well-head and the gas trap.

In order to study this degassing, drilling mud is first saturated with Argon in an autoclave and pressurized to 5 bar g. The mud is then degassed by decreasing the pressure down to atmospheric pressure and mud samples are taken in order to measure the swelling of the mud and the residual amount of Argon dissolved in the mud.

An inert gas like Argon was chosen to saturate the drilling mud as light hydrocarbons could not be used for safety reasons. The experiment is presented in Appendix 7 with more details..

5.3 Results

Several series of tests were carried out. The preliminary series was for the purpose of adjusting the experimental conditions and overcoming technical problems. For example, the temperature and pressure transductors were added to better control these parameters and it was shown that muds with solid particles could not be included in the experiment, since sampling with the syringes proved to be impossible.

After the preliminary test, a series of 6 main tests was carried out. Table 5.1. shows different characteristics of these tests: they were carried with different muds and at different temperatures. Moreover, table 5.1 shows an overview of the data available from each test. Some data were not measured by technicians of EniTecnologie. In Table 5.2. the composition of each mud is given.

Table 5.1. Test performed, their characteristics and the type of results available for each of them

Test No	**Mud type**	**Test temperature**	**Available measurement**		
			Interfacial tension	**Density**	**Composition gas**
Test 11	Mud High Viscosity	18°C	*Available*	*Non available*	*Available*
Test 12	Mud High Viscosity	40°C	*Available*	*Available*	*Available*
Test 13	Mud Low Viscosity	40°C	*Available*	*Available*	*Available*
Test 14	Mud High Viscosity with glycols	40°C	*Available*	*Available*	*Available*
Test 15	Mud High Viscosity with glycols and defoamer	40°C	*Available*	*Available*	*Available*
Test 16	Mud High Viscosity with glycols and defoamer	20°C	*Available*	*Available*	*Non available*

In Table 5.2., the different components are (World Oil's Fluids '97, 1997):

- Barazan-D is a xanthan gum viscosifier – i.e., an additive used to increase the drilling mud viscosity ;
- PAC-R is a regular grade polyanionic cellulose viscosifier ;
- Dextrid is a fermentation resistant starch, used as a filtration reducer - meant to decrease the loss of drilling fluid into formation rock ;
- Avaglyco is a polyalkylene glycol - used as a shale control agent, i.e. to stabilize shales whiles drilled through, and thus to stabilize the drilled hole, by hindering the water absorption on shale (hydration) ;
- And Defoamex is a general purpose defoamer - i.e., to reduce foaming.

Table 5.2. Composition of the different muds used in the tests

Mud	**Used in Test**	**Components**				
		Barazan-D	**PAC-R**	**Dextrid**	**Avaglyco**	**Defoamex**
Mud Low Viscosity	13	0.3%	0.1%	1.2%	*none*	*none*
Mud High Viscosity	11, 12	0.35%	0.5%	1.5%	*none*	*none*
Mud High Viscosity with glycols	14	0.35%	0.5%	1.5%	0.3%	*none*
Mud High Viscosity with glycols and defoamer	15, 16	0.35%	0.5%	1.5%	0.3%	0.01%

Table 5.3. shows the first results obtained: these are the interfacial tensions between each mud and Argon. The interfacial tension of water is put in this table for comparison.

Table 5.3. Interfacial tension (in mN/m) between Argon and the different muds used in the tests.

Mud	**Used in Test**	**Interfacial tension γ (mN/m)**
Mud Low Viscosity	13	69.0
Mud High Viscosity	11, 12	69.0
Mud High Viscosity with glycols	14	40.5
Mud High Viscosity with glycols and defoamer	15, 16	43.1
Water		72.3

Table 5.4. shows the different masses measured for the mud samples in order to calculate their density. The corresponding volumes are reported as well. These masses are not available for Tests 11 and 12, but the densities for Test 12 were given directly by the laboratory and shown in Table 5.5.

Table 5.4. Masses and volumes of samples according to the different Tests and the different sampling times. (*n.a. means Non Available measurement*)

Definition of the sampling time	**Sample No.**	**Time (s)**	**Volume (ml)**	**mass (g)**					
				Test 11	**Test 12**	**Test 13**	**Test 14**	**Test 15**	**Test 16**
Before argon injection	-1	-10	2	*n.a.*	*n.a.*	2.288	2.169	2.047	*n.a.*
Just before starting degassing	0	0	2.4	*n.a.*	*n.a.*	1.924	1.482	1.605	1.585
10 sec after starting degassing	1	10	2	*n.a.*	*n.a.*	2.022	1.316	1.596	1.484
1 min after starting degassing	2	60	2	*n.a.*	*n.a.*	2.148	1.306	1.660	1.531
2 min after starting degassing	3	120	2	*n.a.*	*n.a.*	2.156	1.492	1.702	*n.a.*
3 min after starting degassing	4	180	2	*n.a.*	*n.a.*	2.161	1.679	1.793	*n.a.*
5 min after starting degassing	5	300	2	*n.a.*	*n.a.*	2.133	1.790	1.792	1.595
1,5 hour after starting degassing	6	5400	2	*n.a.*	*n.a.*	2.283	2.070	*n.a.*	*n.a.*
2,5 hours after starting degassing	7	9000	2	*n.a.*	*n.a.*	*n.a.*	*n.a.*	2.006	*n.a.*
18,5 hour after starting degassing	8	66600	2	*n.a.*	*n.a.*	*n.a.*	2.189	*n.a.*	*n.a.*

Table 5.5. Density results for Test 12

Sample No.	**Time (s)**	**Density (g/ml) of Test 12**
-1	-10	1.046
0	0	0.864
1	10	0.998
2	60	1.036
3	120	1.048
4	180	1.063

The results of analyses performed with the gas chromatograph are shown in Table 5.6 and represented on Figure 5.1. They correspond to the Argon concentration in the gas phase present in the 20cc vials where the syringe samples were transferred.

Table 5.6. Analysis results of the gas phase from the 20cc vials

Sample No.	Time (s)	Moles Argon in 1cc sample				
		Test 11	Test 12	Test 13	Test 14	Test 15
sample -1	-10	*n.a.*	6.798E-05	6.576E-05	6.304E-06	5.402E-05
sample 0	0	6.814E-05	6.694E-05	1.320E-04	8.067E-05	5.395E-05
sample 1	10	6.689E-05	6.672E-05	6.644E-05	6.680E-05	5.771E-05
sample 2	60	6.697E-05	6.628E-05	2.020E-04	6.656E-05	5.721E-05
sample 3	120	*n.a.*	6.682E-05	*n.a.*	1.760E-05	5.672E-05
sample 4	180	*n.a.*	6.752E-05	1.720E-04	5.385E-05	5.825E-05
sample 5	300	*n.a.*	n.a.	1.652E-04	1.835E-05	*n.a.*
sample 6	5400	*n.a.*	n.a.	1.162E-04	1.435E-05	7.192E-05
sample 7	9000	*n.a.*	n.a.	*n.a.*	1.034E-05	*n.a.*

Fig 5.1. Measured Argon concentrations for tests 11 to 15, the measurements are displayed in chronologically

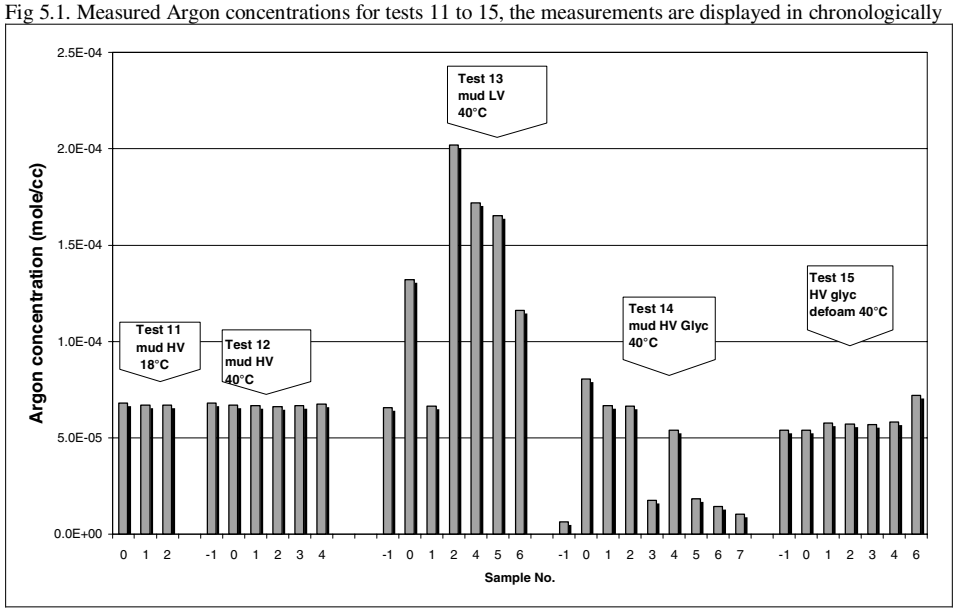

Finally, Table 5.7. shows the volumes of the vials which were used to carry the GC analyses.

Table 5.7. Exact volumes of the 20 cc vials used for each Test for the GC analysis

Sample No	Time (s)	Exact volumes of 20 cc vials					
		Test 11	Test 12	Test 13	Test 14	Test 15	Test 16
sample -1	-10	n.a.	n.a.	21.306	n.a.	21.670	n.a.
sample 0	0	n.a.	n.a.	21.570	21.368	21.791	21.576
sample 1	10	n.a.	n.a.	21.395	21.242	21.817	21.461
sample 2	60	n.a.	n.a.	21.599	21.548	21.509	21.543
sample 3	120	n.a.	n.a.	Broken	21.684	21.420	21.727
sample 4	180	n.a.	n.a.	21.530	21.692	21.519	n.a.
sample 5	300	n.a.	n.a.	21.501	21.693	21.571	n.a.
sample 6	5400	n.a.	n.a.	21.902	21.818	21.752	n.a.
sample 7	9000	n.a.	n.a.	n.a.	21.510	n.a.	n.a.

As an indication, the calibration index calculated after a calibration test is reported in the table below.

Table 5.8. Additional values: calibration index of the gas chromatograph.

Calibration of the gas chromatograph	4.8577e-12 (mol Ar/cc)/(GC Peak Area)

5.4 Analysis of the results

It follows from Table 5.6 that the only consistent test was Test 14. In this test, there was a clear indication that it was possible to saturate the sample with Argon (cf. the Argon concentrations at -10 s and 0 s). Moreover, subsequent measurements show monotonous and reasonable variation of the argon concentration –except sample 3-, indicating that the measurements were taken accurately.

For other tests, either there was no indication that the sample was saturated (Tests 11, 12, 15), or the subsequent measurements of the argon concentration were rather inaccurate, providing random variation of the Argon concentration (like Test 13). That is why in the present analysis we restrict ourselves with Test 14.

First, the density of the mud samples was calculated. The masses and volumes from Table 5.4 were used for the calculation. The results are displayed in Table 5.9. The density of the test series 12 are reported again as previously in Table 5.5. The variation of the density of the different muds as a function of time is shown on Fig 5.2 below.

Table 5.9. Results of the density calculation based on the measured masses and volumes for the Test 13 to 16. Densities for Test 12 were directly available and are reported again here.

Sample N.°	Time (s)	Density (g/ml)				
		Test 12	Test 13	Test 14	Test 15	Test 16
-1	-10	1.046	1.144	1.085	1.024	
0	0	0.864	0.802	0.618	0.669	0.660
1	10	0.998	1.011	0.658	0.798	0.742
2	60	1.036	1.074	0.653	0.830	0.766
3	120	1.048	1.078	0.746	0.851	
4	180	1.063	1.081	0.840	0.897	
5	300		1.067	0.895	0.896	0.798
6	5400		1.142	1.035		
7	9000				1.003	
8	66600			1.095		

Fig. 5.2. Density of the different muds from the test as a function of time

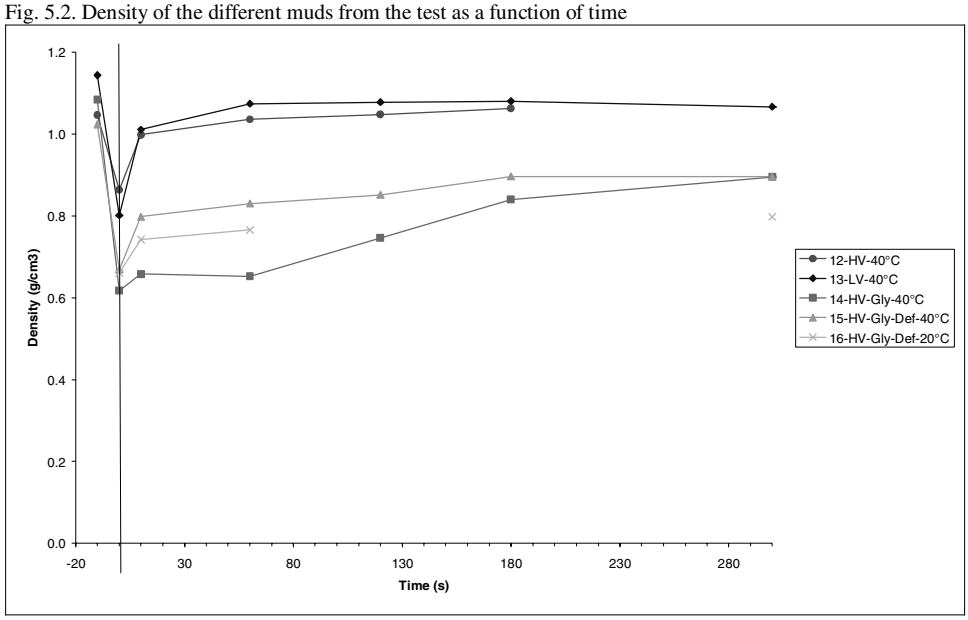

As seen from Table 5.6, the amount of Argon measured does not vary significantly for tests 11, 12 and 15. In order to check if there was any leak, some preliminary controls were carried out.

First, knowing that the natural volume fraction of Argon in air is 0.943% (Perry, 1990) a sample of air has an argon concentration of 4.10^{-7} mol/cc at 40°C.

Let's now calculate the level of saturation that a sample of water in equilibrium with the atmosphere would reach. First, the Henry constant for Argon in water at 40°C is H_{Ar}=4110 MPa (Schultz, 1981). Using Henry's law, we get the amount of Argon dissolved in water as

$$x_{ar} = y_{Ar} \cdot P / H_{Ar} = 0.943 \cdot 10^{-2} \cdot 1.01325 / 41100 = 2.3 \cdot 10^{-7} \quad (5.1)$$

In 2cc of water at 40°C, the number of moles of water is 0.11 mole. This leads to a number of moles of Argon in the 2cc:

$$N_{ar} = \frac{x_{Ar} \cdot N_{H_2O}}{1 - x_{Ar}} = 2.5 \cdot 10^{-8}\ mole\ Ar \qquad (5.2)$$

This means that if such a sample was put in 20cc vial where all the Argon was degassed in the empty space, then the concentration of Argon measured would be of the order of 10^{-8} mol/cc.

In order to use the GC analysis to monitor the amount of Argon present in the samples, a procedure was derived based on certain assumptions.

First, the number of moles of Argon present in the gas phase of the 20 cc vial is calculated knowing the concentration of Argon C_{Ar} (in mol/cc) and the volume of the gas phase. At first approximation, the volume of the gas phase is taken as being the volume of the vial minus the volume of the sample, taken to be 2 cc:

$$V_{gas\ vial} = V_{vial\ total} - V_{sample} = V_{vial\ total} - 2cc \qquad (5.3)$$

Then, $N_{Ar}^{gas\ phase\ vial} = C_{Ar} \cdot V_{gas\ vial}$ (5.4)

Under these conditions, we can calculate the partial pressure of Argon in the vial using the Ideal Gas Law. If we calculate the amount of Argon still dissolved in the liquid phase using Henry's Law, we find amounts of Argon which are 3 orders of magnitude lower than the amount of Argon present in the gas phase. Thus, the Argon from the sample may be considered to be entirely present in the gas phase of the 20 cc vial.

This procedure was applied to Test 14, since it is the only test where a significant amount of gas could be detected after saturation. The *Differential Liberation* in mole is calculated as the difference of Argon between two consecutive measurements. The *Differential Liberation* in % is the previous value reported to the first of the two measurements in consideration. Finally, *Liberation* refers to the % of Argon lost compared to the saturated state (Time = 0s).

Table 5.10. Results of Test 14

Time (s)	Measured concentration (mol Ar/cc)	Total volume vial (cc)	Number mole Argon in gas phase (mole)	Differential liberation (mole)	Differential liberation (%)	Accumulated liberation (%)
-10	6.304E-06					
0	8.067E-05	21.368	1.562E-03			
10	*6.680E-05*	*21.2421*	*1.285E-03*	*2.771E-04*	*17.74*	*17.74*
60	6.656E-05	21.5481	1.301E-03	*-1.587E-05*	*-1.23*	16.72
120	*1.760E-05*	*21.684*	*3.465E-04*			
180	5.385E-05	21.6917	1.060E-03	*2.408E-04*	*69.51*	32.14
300	*1.835E-05*	*21.6931*	*3.613E-04*	*6.991E-04*	*65.93*	71.89
5400	1.43505E-05	21.8181	2.844E-04	*7.690E-05*	*21.28*	81.80
9000	1.0335E-05	21.5097	2.016E-04	*8.277E-05*	*29.10*	87.10

On Fig. 5.3 and 5.4 are shown the accumulated and differential liberation in % as a function of time.

Fig. 5.3. Accumulated percentage of lost gas as a function of time

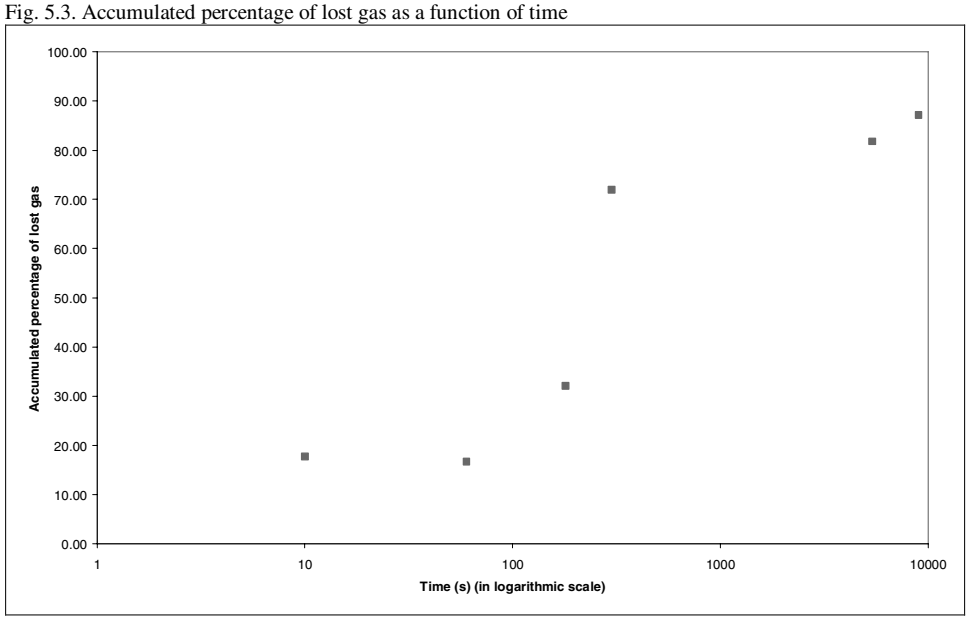

Fig. 5.4. Percentage of lost gas between two consecutive measurements as a function of time

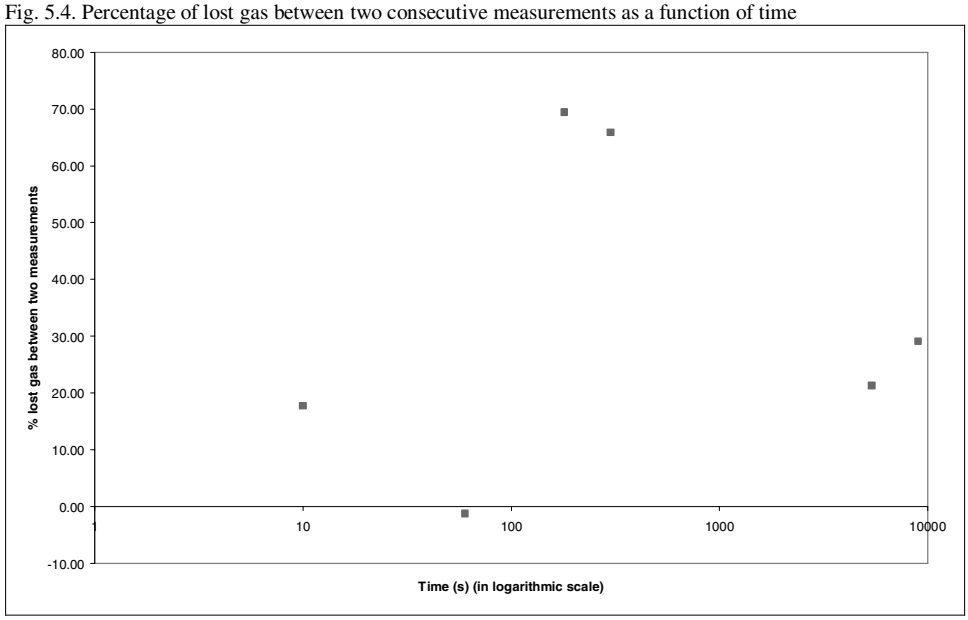

5.5 Discussion

It can definitely be seen that for the mud from Test 14 there is argon in the state different than solution. The initial amount of argon is $1.28 \cdot 10^{-3}$ moles in the sample compared to the order-of-magnitude estimate of 10^{-8}, which would be valid if argon would be just dissolved. Moreover, we can see that after 9000 seconds (2.5 hours), the amount of Argon in the sample is $2 \cdot 10^{-4}$ mole, so that Argon still exists in non-dissolved state after such a time.

Based on the density measurements, we can see that all the muds swell to a certain extent after being saturated with Argon and released at 1 bar. Nevertheless a difference can be seen between muds from tests 12 and 13 and the muds from tests 14, 15 and 16. In the case of the latter, the release mechanism seems to be much slower. As these three muds correspond to low values of the surface tension (See Table 5.3.), we can see that it plays a role in the release mechanism and thus has an influence on Alpha_2.

We can also see by comparing tests 15 and 16 on Fig 5.2 that the temperature plays a role. The mud is more swollen at 40°C than at 20°C, certainly as the amount of dissolved Argon increases with temperature.

Finally, as seen on Fig 5.3, the liberation is dependent on time. It can be seen that after a time of 10 minutes the mud has lost around 80% of the original Argon. Reported to the flow-line conditions, this value could be used to estimate a value of Alpha_2. However, further measurements are required in order to confirm or to disprove this conclusion and to make a more reliable estimate of Alpha_2, including average values and possible deviations. In the future simulations, the value of Alpha_2 = 0.8 was used in many cases, unless it was treated as an adjustment parameter.

On the basis of this experiment, it may be suggested to continue study of micro bubbles in mud or other types of petroleum-related fluids. More detailed and refined experiments, both with specially selected and industrial fluids are required to really evaluate the impact of micro bubbles. The effects of thermodynamic conditions (pressure, temperature), of the gas composition and its multicomponent nature, of the surface tension and presence of the natural surfactants in the solution should be studied. A modelling tool for evaluation of this impact should also be developed. However, this task is outside of the scope of the present work.

5.6 Conclusions

A model experiment has been carried out in order to determine whether the hydrocarbons are present in the mud in the form of solution, or may be contained in the form of micro bubbles.

The experiment indicated that, given the conditions between the well head and the gas trap, there will definitely be gas in mud in the form of micro bubbles, which amount largely exceeds the amount of the dissolved gas. The full degassing, if possible at all, will proceed over much larger times than the travel time between the well head and the gas trap.

It appears also that the release mechanism is slower for systems with low surface tensions. The temperature

A preliminary estimation range for the value of Alpha_2, which may be suggested on the basis of the experimental results, is 50 to 80% according to the mud characteristics, the length of the flow-line and the flow-rate. Further study is required in order to verify validity of this suggestion.

Generally, the problem in micro bubbles in petroleum-related fluids requires further investigation. This investigation may be relevant to the GWD process, since, on the basis of the experiment carried out, it is likely that the gas in the mud is contained in the form of the bubbles.

The study of the transportation of bubbles in complex systems could give answers about the release mechanism and the amount of gas retained in the mud. Raman Spectrometry could also be used in order to quantify the relative amount of dissolved gas and bubble-gas.

6 Study of Alpha_2 – Field test with well P

6.1 Objectives

In the previous section the parameter Alpha_2 was investigated experimentally. It was shown that bubbles existed and a rough estimation for Alpha_2 was given. In order to evaluate the losses of hydrocarbons in more detail, to directly determine a value for Alpha_2 which could be used in the simulation, and to verify whether the model with the same Alpha_2 for all the hydrocarbon components is adequate, a test was carried out on-field. This test had a purpose to study the degassing of the drilling mud between two gas-traps installed at two points of a flow-line: in the middle of the flow-line and on its usual position.

The present chapter describes the experiment and attempts to analyse its results in terms of the loss coefficients for different hydrocarbon components.

The work was carried out with the collaboration of Eni E&P.

At first, the study concentrated on fitting Alpha_2 by simulating the whole GWD process with two gas-traps. Unfortunately, the information about the reservoir fluid could not be available at once as was expected.

Then a more general study of the variations of Alpha_2 was carried out emphasizing the aspects that could give a better knowledge of the degassing in the flow-line and of the behaviour of the parameter Alpha_2

6.2 Conditions of the test

The test consisted in installing two gas-traps at two different locations on the flow-line and monitoring the two GWD signals. The test was carried out at the on-shore drilling site of well P. One particularity of this drilling site was that the flow-line had an intermediate pit where an additional gas-trap could easily be placed.

Two similar gas detection systems (Reserval, containing a GZG gas-trap) were installed at the different positions along the flow-line. One system was connected to an ALS unit (Geoservices) as acquisition system while the other was connected to a Geonext unit. The two gas-traps were separated by 8 meters of flow-line, corresponding to an internal flow-line volume of 580 l. With a mud flow-rate of 700 l/min the transit time would thus be 50 s while for a flow-rate of 1000 l/min the transit time would be of 35s. The gas-trap located in the flow-line is referred as GZG1 and the gas-trap located at the shale-shaker as GZG2.

It should be pointed out that a lot of gas loss happened already before the first gas trap. Unfortunately, installation of the gas trap directly at the well head was impossible due to technical problems and safety regulations.

The test was carried out on a horizontal section in the interval 4000-5259 mTR (depth measured with the rotating table as reference). In this interval three different bit runs and two cores were carried out as described below:

- From 4000 to 4580 mRT, the section was drilled with a PDC bit 6" drill-bit and the mud flow-rate was 1000 l/min
- From 4580 to 4592 mRT, the first core was sampled and the mud flow-rate was 650 l/min
- From 4592 to 4574 mRT, the section was drilled with a PDC bit 6" drill-bit and the mud flow-rate was 1000 l/min
- From 4574 to 5259 mRT, the section was drilled with a PDC bit 6" drill-bit and the mud flow-rate was 1000 l/min
- From 5259 to 5270 mRT, the second core was sampled and the mud flow-rate was 700 l/min

The mud was a water-based mud of type FW-Polymer. It had a density of 1150 g/l and a viscosity of 18 cP at 49°C. The average temperature of the mud out of the well was 45°C.

A study carried by P. Ceragioli showed that the fluid composition from a neighbour well could not be used for the well P as intended beforehand.

No porosity-log was available for the horizontal Well P. A neutron porosity log was available for the vertical well from which the well P was deviated. Thus an indication of the porosity at the same depth in another well was at disposal. Knowledge of the porosity at the vicinity of Well P in the interval of interest can give an idea of the maximum of porosity that can correspond to the high values of gas shows. The porosity was very low. The mean value was 4% with some maximum values at 8%.

There was no direct indication of the water saturation, which is very difficult to measure for such low porosities. The default value of the water saturation was taken at 30% after discussion with C. Carugo.

6.3 Selection and definition of the peaks

Before performing any calculation, the representative peaks were identified by using the GWD™ procedure on the gas shows from the second gas-trap. Eleven peaks were then selected for having absolute values of C1 greater than 3000 ppm. The chosen peaks are listed in the table below and shown on Fig. 6.1. This definition is in accordance with the GWD procedure, where only the top of the peaks are used in the interpretation.

Fig. 6.1. Selected peaks for the study of Alpha_2

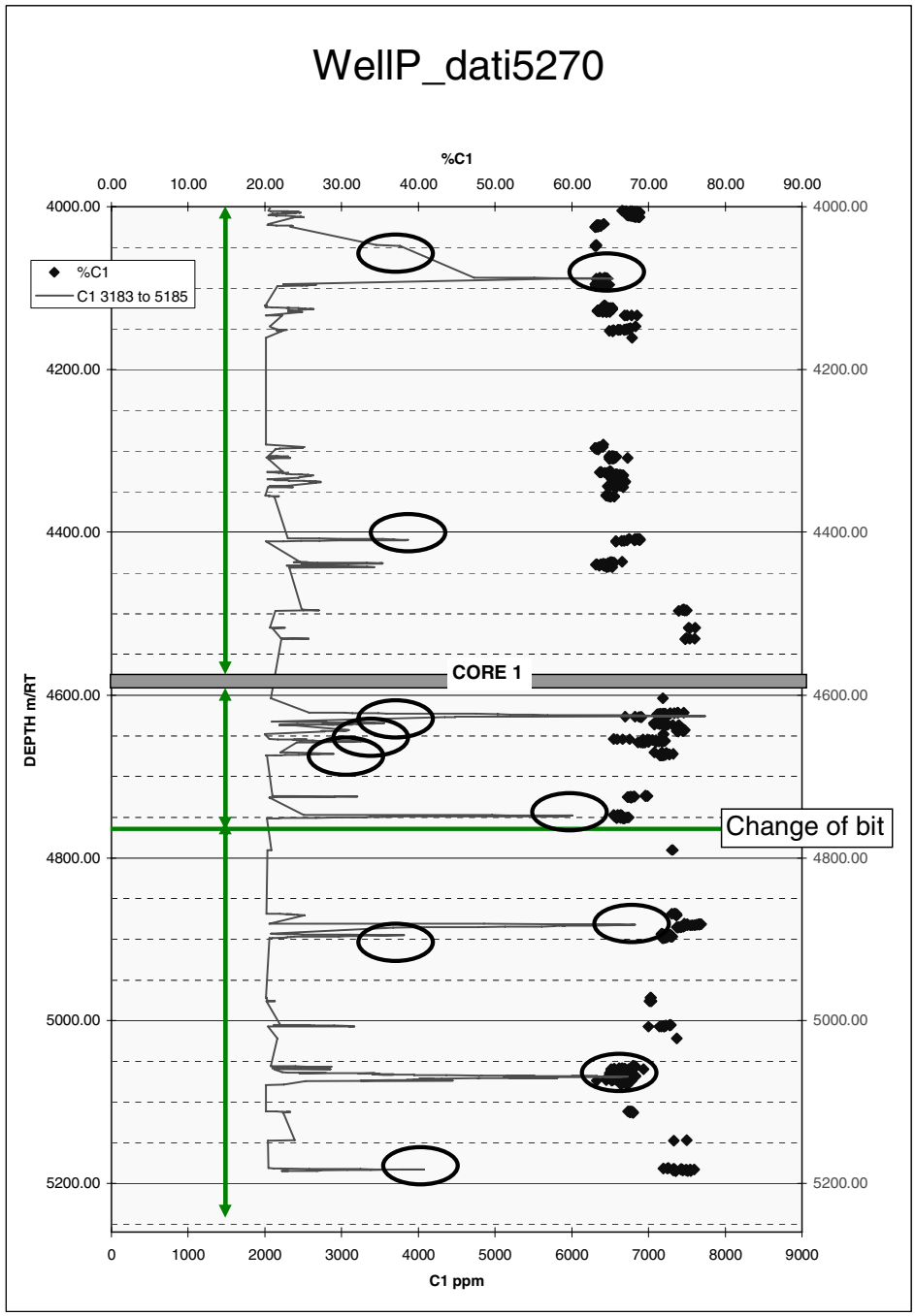

In Fig. 6.1 all the ellipses are shifted with respect to the diagram. In this figure, the "strange" slight increase of %C1 from about 4500 m MD should also be emphasized. This could be related to the configuration of the horizontal drain hole that facilitate the liberation from cuttings of C1 and C2 (increasing lag time, the hole irregularity and the sinusoidal well profile, the increasing mechanical action of the BHA components on the cuttings).

A large and connected pore network with good porosity and permeability generally allows a rapid liberation of C1 and C2 also from cuttings while the small pore size in a low porosity rock with high presence of bound water probably retard this liberation. As a matter of fact the Head Space samples result richer in heavy gas components indicating that generally the liberation of the heavy gas components from the cuttings pores at the gas trap is not complete

Table 6.1. Locations of the peaks selected for the study of alpha2 in terms of total depth, percentage of C1 in the gas show and absolute value of C1 measured at the shale-shaker

Depth	**%C1**	**C1 ppm at the shaker**
4048.2	63	3760
4087.9	63	6530
4409.4	67	3834
4438.4	65	3520
4442	65	3400
4657	69	3340
4748.4	66	5950
4882.2	74	6735
4895.2	71	3781
5069	66	6730
5183	74	4070

When looking closely at each peak, they appeared very different in terms of shape, more or less large, with a flat top or not. It also appeared that there is always a slight depth difference between the peak from the gas-trap located in the flow-line GZG1 and the corresponding peak at the second gas-trap GZG2. This difference is not the same from one show to another: sometimes the signal at the GZG1 is in advance compared to the corresponding signal at the GZG2 –which respects the succession of events- as shown of Fig. 6.2 and 6.3, but sometimes the opposite situation is observed as shown on Fig. 6.4 and 6.5.

It looks like different peaks travel with different velocities in the flow-line. This would not happen if the hydrocarbons would only be in dissolved state, since in this case their velocity would be the same as the velocity of the flow. However, this could happen if the hydrocarbons would move as a separate phase, for example, as ensembles of bubbles or as a surface film (which is less probable, due to the turbulent character of the flow in the flow-line). It is known that the particles/bubbles in the flow are non-uniformly distributed between the centre and the peripheral, so that their velocity does not coincide with the average velocity of the flow.

This is combined with the fact that the signals from the two gas-traps are recorded by two different logging units, so that the time scales are originally different for the two signals. These differences are then again modified when the data from the time-based log are converted into depth-based data. Indeed, these two units did not agree in the calculated depth for example.

Consequently, we needed first to have a better coincidence between the two peaks before performing any calculation. The maxima of the peaks were then used in the calculations. The peaks were matched as shown on Fig. 6.2 to 6.5. When the peaks have the same shape or present a single maximum point (Fig 6.2 and 6.3), then the peaks are matched easily. In the case shown on of Fig. 6.4 and 6.5, matching directly the maximum would mean that the two peaks are not centred together. This definition is accordance with the GWD procedure, where only the top of the peaks are used in the interpretation.

Fig. 6.2. Peaks at 4895 m (total depth) from the flow-line and the shaker

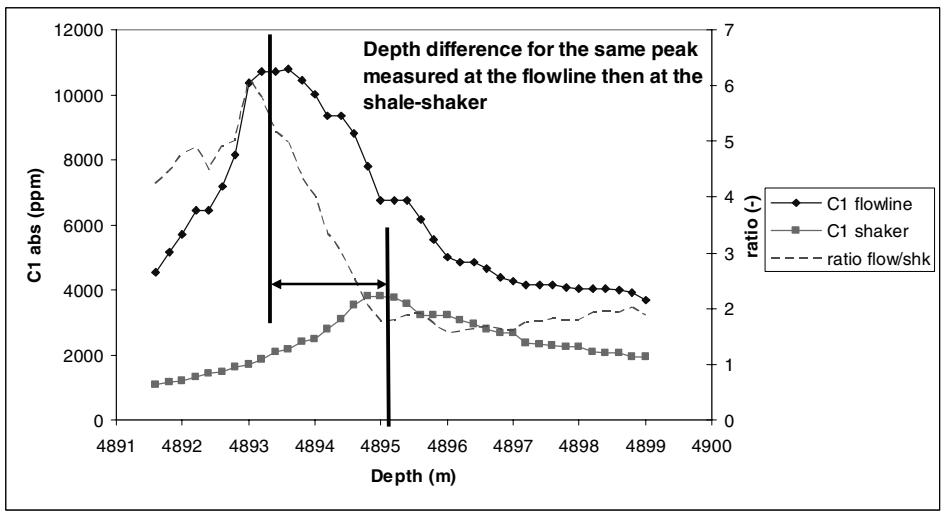

Fig. 6.3. Peaks at 4895 m (total depth) from the flow-line and the shaker after matching of the maxima; the calculated ratio is modified

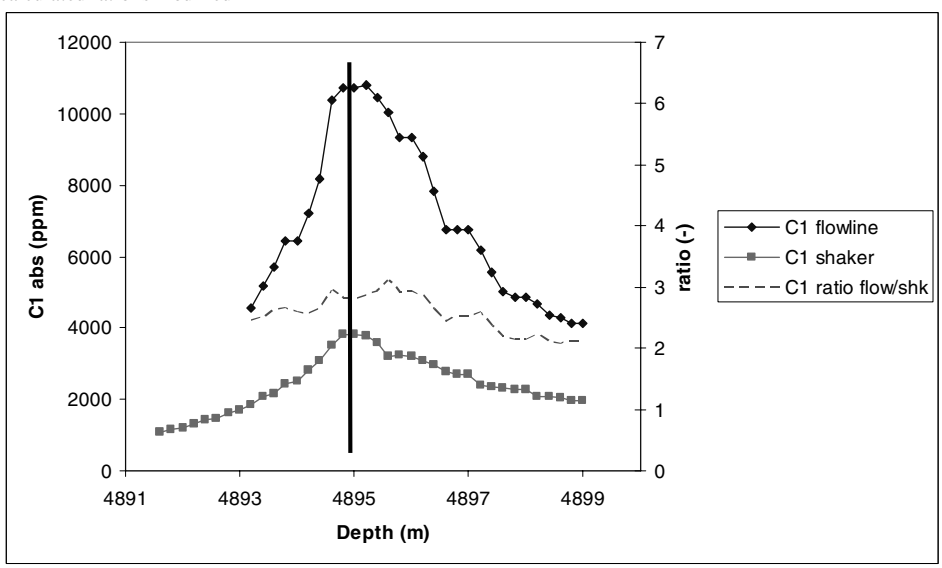

Fig. 6.4. Peaks at 4408 m (total depth) from the flow-line and the shaker. The peak from the shaker is slightly in advance compared to the peak of the flow-line. A different definition of the maximum is used in order to centre the two peaks.

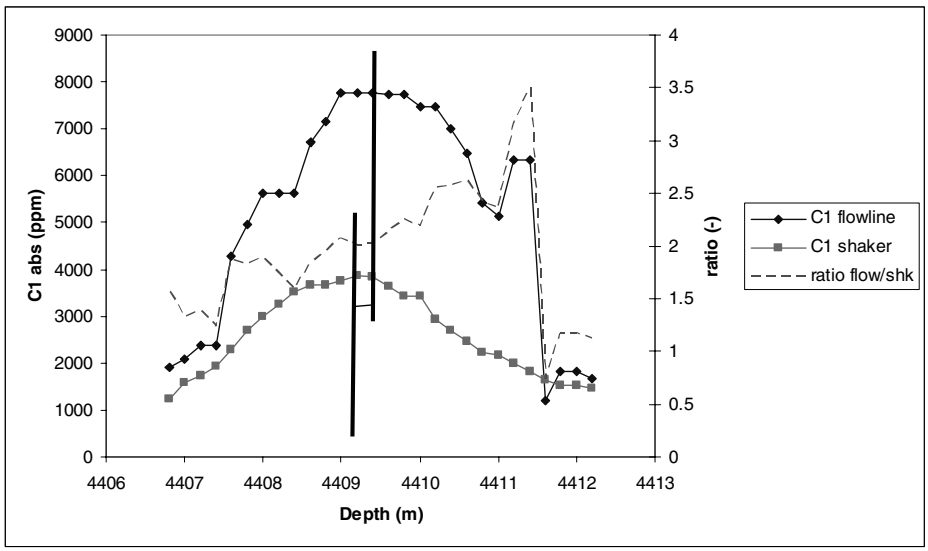

Fig. 6.5. Peaks at 4408 m (total depth) from the flow-line and the shaker after matching of the maxima; the calculated ratio is modified

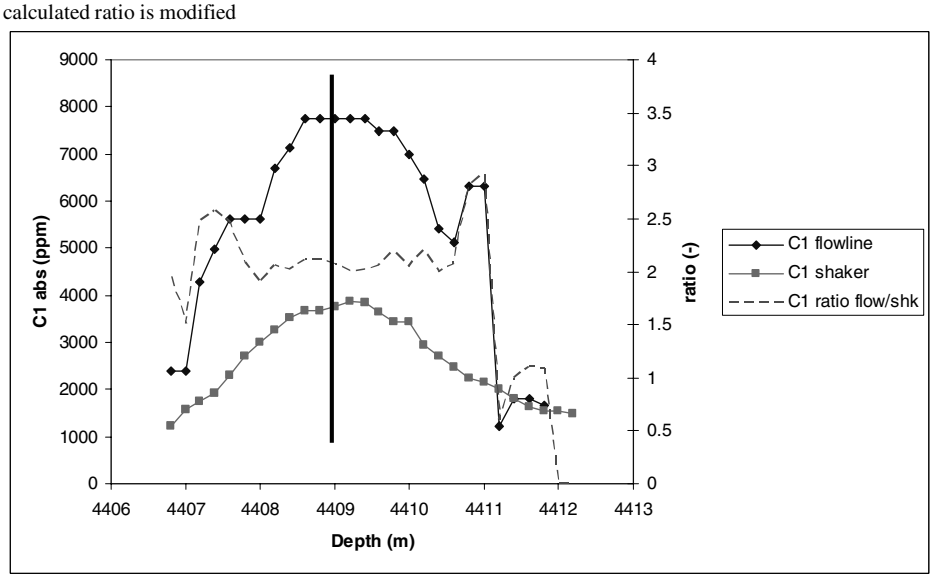

6.4 Analysis of the results - Discussion

The calculation of Alpha_2 based on the results of the two gas-traps would require a simulation with BEST since Alpha_2 corrects the amount of vapour formed from the hydrocarbons in the mud. From the gas-traps we obtain an amount of hydrocarbons that is related to the total amount from the mud and not solely to the vapour phase. Thus it was decided to study the ratio of Gas In Air from the gas-trap GZG1 over the Gas In Air from GZG2. This gives an indirect relation between the gas content in the mud at two different locations of the flow-line. As both amounts are corrected by the trap efficiency coefficient Alpha_3, the ratio is independent of this parameter.

The ratios defined previously were calculated using the maxima of each peak. Table 6.2 presents the different values at different depth for all the components, while Fig. 6.6 shows the evolution of the ratio as a function of depth.

In Table 6.2, it can be seen that the ratio different for each compound and is decreasing when the hydrocarbon becomes heavier. Moreover, the ratio has similar high values for methane and ethane, while the values for the heavier hydrocarbons are lower. This difference can be explained by the fact that the methane and ethane are mostly present as bubbles in the mud, thus highly affected by Alpha_2. On the contrary, as propane/butanes/pentanes are mostly present in the liquid hydrocarbon phase, these compounds are less affected.

It can also be seen that the ratio for C1 and C2 has a higher standard deviation and seems to reach two threshold values as seen on Fig. 6.6. This is still unexplained.

In Table 6.3, a total hydrocarbon loss factor was calculated as following:

$$Total\ loss\ for\ hydrocarbon\ C_i = \frac{(x_{C_i}\ at\ GZG1) - (x_{C_i}\ at\ GZG2)}{x_{C_i}\ at\ GZG1} \cdot 100 \qquad (6.1)$$

where x_{Ci} is in ppm. This factor is different of Alpha_2 as it is related to the total amount of hydrocarbon in the mud (may they be dissolved or as bubbles). Nevertheless, in the case of methane and ethane, the dissolved amount is very low compared to the amount present as bubbles and it can be assumed that the separation in the gas-trap is very good for these compounds. In this case, this calculated factor might approach Alpha_2 of methane and ethane. However the factor was calculated for all light hydrocarbons.

Table 6.2. Calculated ratios of the amount of gas detected at the flow-line over the amount detected at the shaker for each component. The maxima of each peak were used.

Tot Depth (m)	C1/C1 Flowline /shaker	C2/C2 Flowline /shaker	C3/C3 Flowline /shaker	iC4/iC4 Flowline /shaker	nC4/nC4 Flowline /shaker	iC5/iC5 Flowline /shaker	nC5/nC5 Flowline /shaker
4046.8	2.050	2.154	1.799	1.630	1.573	1.422	1.457
4086.6	2.011	2.028	1.713	1.595	1.458	1.405	1.437
4408	2.007	2.021	1.644	1.551	1.485	1.377	1.347
4437.6	2.072	2.111	1.723	1.587	1.503	1.391	1.394
4442.4	1.798	1.953	1.690	1.560	1.509	1.385	1.391
4656.4	2.522	2.550	2.044	1.968	1.864	1.694	1.804
4747.8	2.923	2.822	2.252	1.977	1.823	1.625	1.639
4881.8	2.969	2.862	2.217	1.963	1.841	1.610	1.545
4893.2	2.830	2.705	2.088	1.933	1.787	1.632	1.603
5068.4	2.763	2.709	2.214	1.947	1.780	1.570	1.510
5182.6	2.446	2.366	1.915	1.818	1.703	1.544	1.515
Mean Value	2.399	2.389	1.936	1.775	1.666	1.514	1.513
Standard Deviation	0.408	0.334	0.224	0.180	0.154	0.114	0.126

Fig. 6.6. Calculated ratios (gas at the flow-line over gas at the shaker) for each component vs. total depth.

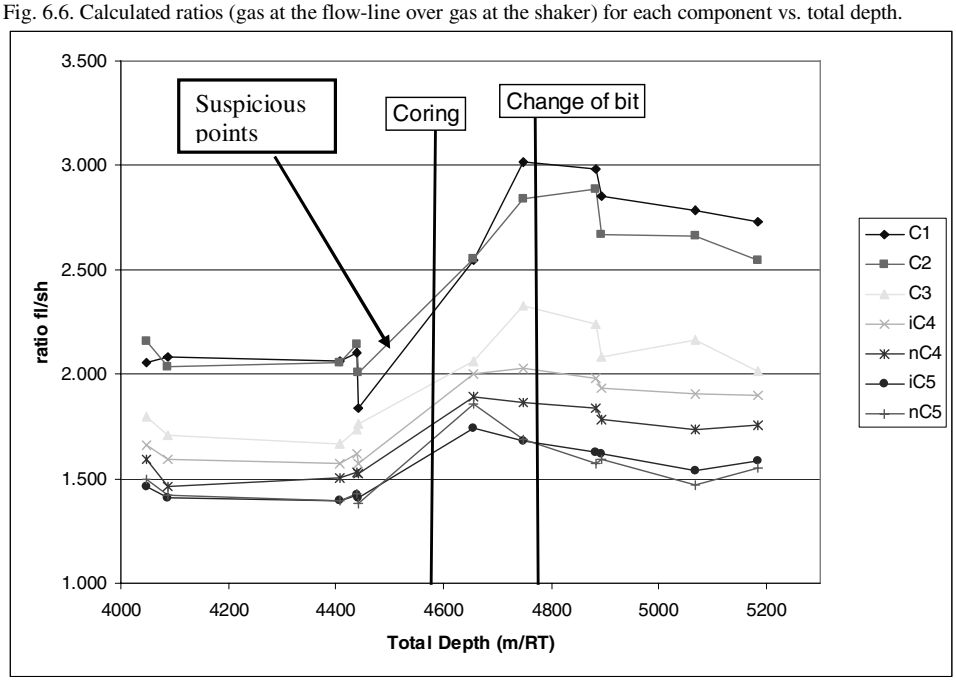

Table 6.3. Total loss of hydrocarbons between the two gas-traps in %. Only the loss for C1 and C2 might be close to Alpha_2

Tot Depth (m)	C1 (%)	C2 (%)	C3 (%)	iC4 (%)	nC4 (%)	iC5 (%)	nC5 (%)
4046.8	51	54	44	39	36	30	31
4086.6	50	51	42	37	31	29	30
4408	50	51	39	36	33	27	26
4437.6	52	53	42	37	33	28	28
4442.4	44	49	41	36	34	28	28
4656.4	60	61	51	49	46	41	45
4747.8	66	65	56	49	45	38	39
4881.8	66	65	55	49	46	38	35
4893.2	65	63	52	48	44	39	38
5068.4	64	63	55	49	44	36	34
5182.6	59	58	48	45	41	35	34
Mean Value	57	57	48	43	39	34	33
Standard Deviation	7	6	6	6	6	5	5

As can be seen in Table 6.3, the total loss for methane and ethane is 57%. As for these two compounds it might be assumed that they are almost only present in vapour state as bubbles, and then this loss might approach the value of Alpha_2. This value only covers the degassing of the mud between the middle of the flow-line to the shale-shaker since some previous degassing has surely occurred at the bell-nipple and at the intermediate pit where GZG1 is located.

6.5 Conclusions

A field test has been carried in order to quantify on-field the loss of hydrocarbons between two points of the mud circulating line. It does not take into account the prior degassing of the mud occurring between the well-head and the first gas-trap. Nevertheless, an important degassing could be measured.

It was shown that the peaks move with different velocities. This may come from the effect induced by the different transfer functions used by the logging company to generate a signal as a function of depth. But it could also mean that the hydrocarbons present in bubbles and dissolved travel at different velocities, thus modifying the shape and relative position between the peaks.

The maxima of each peak were used for the calculation as they correspond to the most representative part of the gas-show.

The degassing ratio for methane and ethane is different with the ratios for C3 to C5. This means that Alpha_2 affects greatly methane and ethane. For propane to pentane, Alpha_2 goes decreasing with the volatility of the compound.

The average Alpha_2 for methane and ethane between the middle of the flow-line and the shale-shaker is 57%.

Further analysis is required as far as the composition of the reservoir fluid will become available. It is especially needed in order to calculate Alpha_2 for heavier hydrocarbons propane to pentanes by simulating the dissolved amount in the mud.

7 Simulations with BEST

7.1 Introduction

The scheme of the simulation presented in Chapter 4 was implemented with Total's PVT software BEST. A Macro program in Visual Basic was developed in order to command the simulation and take care of the pre-processing and post-processing of the data and results.

Some field cases were provided by the companies during the project in order to improve the simulation scheme in a first time. After the three adjustment parameters were defined (cf. Chapter 4), the field cases were used to fit these parameters.

The objective was to obtain a quantitative simulation of the field cases reproducing the amounts of hydrocarbons in the gas shows and the gas ratios.

Three cases were simulated: the case A was first simulated in order to define the simulation scheme and identify key phenomena. The case B and C were later simulated in order to improve the degassing part of the simulator. Finally the case C was simulated using the additional input of the porosity and the water saturation.

7.2 Results

7.2.1 Field Case A

Case A was the very first studied case. This case presents five different hydrocarbon bearing layers: A1, A3, A7, A8 and T2. The respective depths, pressures, temperatures, porosities and water saturations of each layer are presented in Appendix 8. For this case, constant porosities and water saturations are used over each layer.

The characterization –i.e. the description of the composition of the crude oil based on laboratory analyses and PVT properties- is also presented in Appendix 8 for the reservoir fluid sampled in each layer.

Simulations for the five different layers are presented below from Fig 7.1 and 7.10. For each layer, two figures are associated: the first one presents the rate of penetration (ROP, in m/h) of the drilling bit and the mud flow-rate (Qmud, in l/min); the second one compares the simulated gas show for methane to the field values of the gas show for methane.

As shown on Fig. 7.2, the simulated signal does not reproduce well the GWD signal for methane. The simulated signal "integrates" the variations of both the ROP and the mud flow-rate, which vary as seen on Fig. 7.1. In the case of this first layer, the simulated signal presents values which are quite close to the field signal without using any correction parameter.

In the case of layer A3 (Fig 7.3 and 7.4), the mud flow-rate is almost constant, so that the simulated signals reflect the variations of the ROP. In this case, the simulated amount is always superior to the field signal.

In the case of layer A7 (Fig 7.5 and 7.6), it became necessary to use correction parameters as the amount of gas obtained after the gas-trap was too important. It has to be noted that the fluid from layer A7 contains more methane (49% mol C1) than for the fluids from layer A1 and A3 (38% mol). A degassing parameter Alpha_2 of 93% and trap efficiency Alpha_3 of 45% were used for the best fit of the methane signal.

In the case of the layer A8 (Fig 7.7 and 7.8), even more drastic correction parameters were used, as a degassing in the flow-line of 98% was used. The trap efficiency was set at 50%. In the case of layer A8, the fluid present was a gas condensate. In this case, the characterization of such a fluid is very difficult to obtain. Especially in our case, as the dew-point was fitted for this fluid, letting the GLR (Gas-Liquid Ratio) very badly reproduced.

Much attention was paid to the layer T2 (Fig 7.9 and 7.10), given the rather qualitative good match between the variations of the simulated signal and the field signal for methane on Fig 7.10. As for the layer A8, T2 is a gas condensate, and for the same reasons, high correction parameters had to be used. Anyway, three different GWD ratios were simulated in order to see if the judge the quality of the signal: C1/C2 on Fig 7.11, C2/C3 on Fig 7.12 and sum of C1 to C5 on Fig 7.13.

The general conclusions which could be drawn from the case A were that

- the ROP alone does not suffice to reproduce the variations of signal; porosity and water saturation data are needed to obtain good qualitative results;
- in some case, the ROP follows well the porosity changes and then enables to give a good qualitative trend;
- the quality of the characterization of the reservoir fluid is of prior importance; especially, the GOR or GLR must be well reproduced.

Fig 7.1. ROP (m/h) and mud flow-rate (l/min) versus depth for the layer A A1

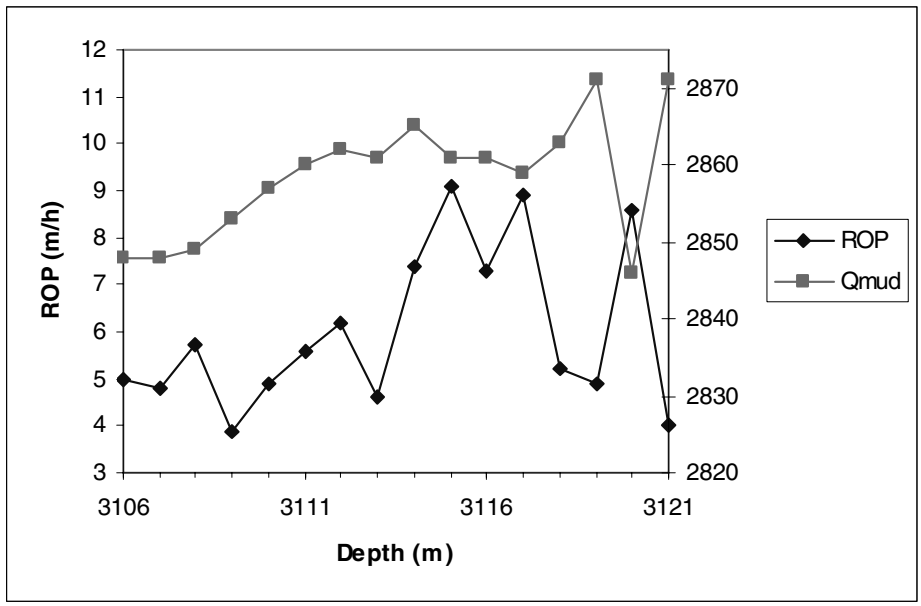

Fig 7.2. Simulated methane, with no Alpha, for the layer A A1

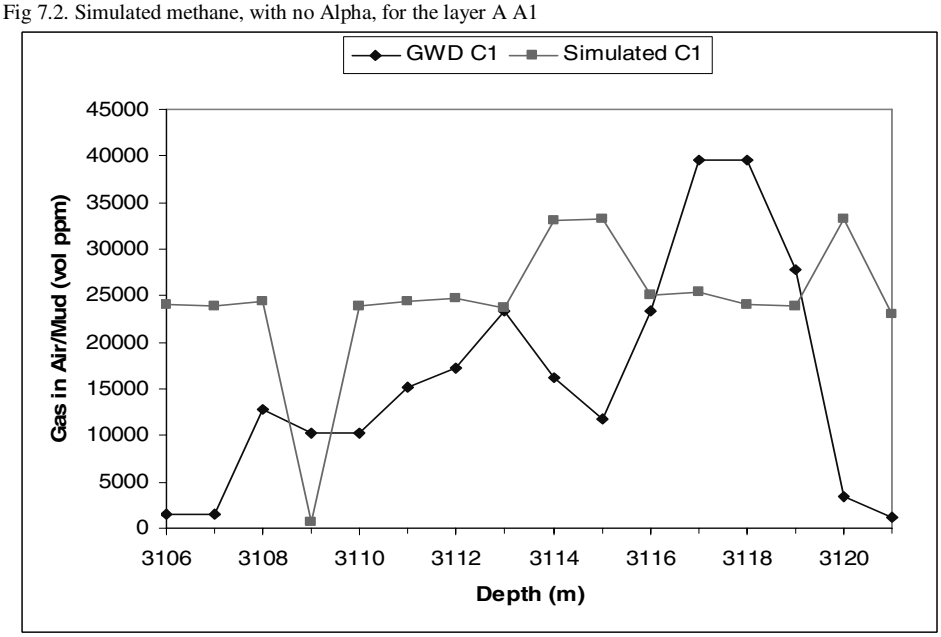

Fig 7.3. ROP (m/h) and mud flow-rate (l/min) versus depth for the layer A A3

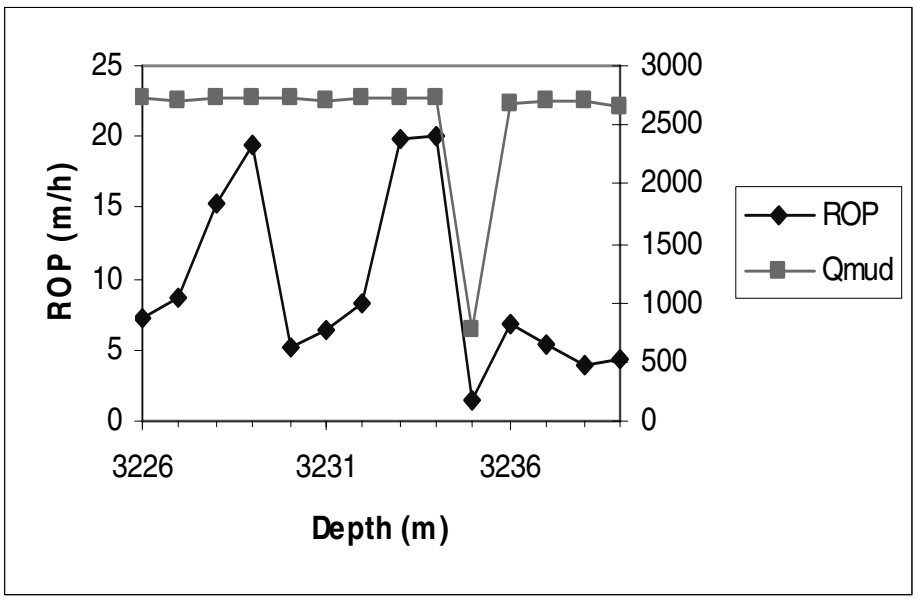

Fig 7.4. Simulated methane, with no Alpha, for the layer A A3

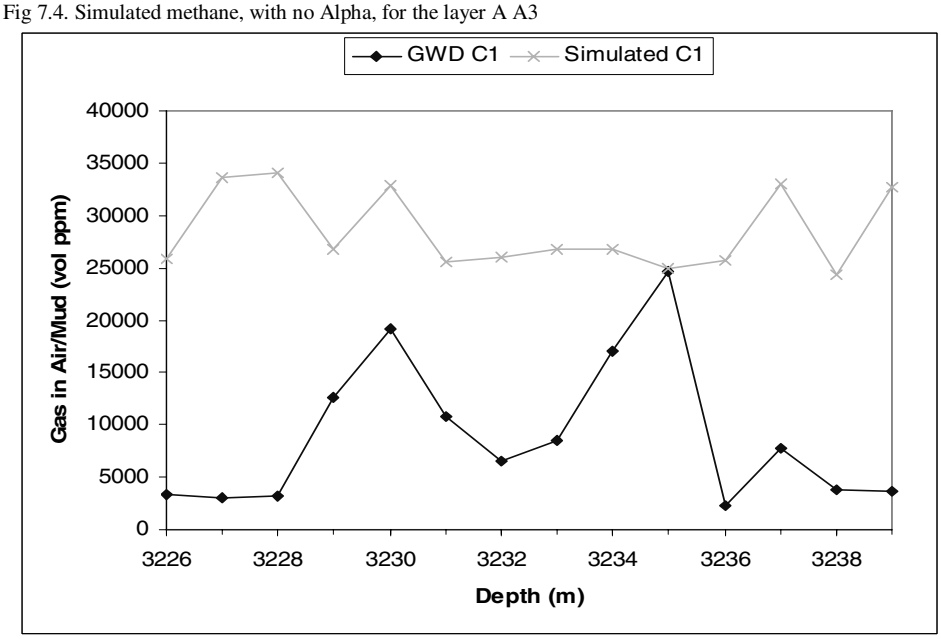

Fig 7.5. ROP (m/h) and mud flow-rate (l/min) versus depth for the layer A A7

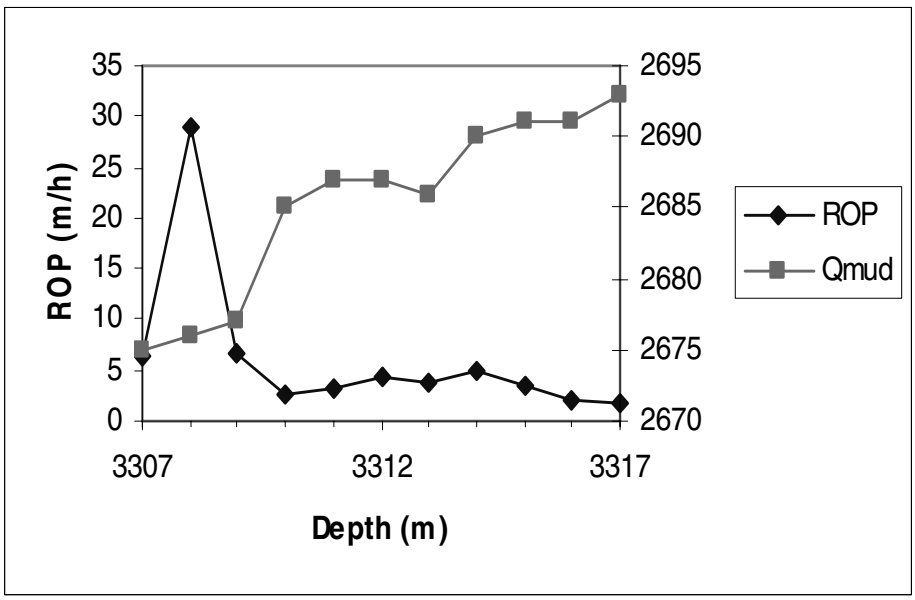

Fig 7.6. Simulated methane, with two different sets of Alpha_2, Alpha_3, for the layer A A7

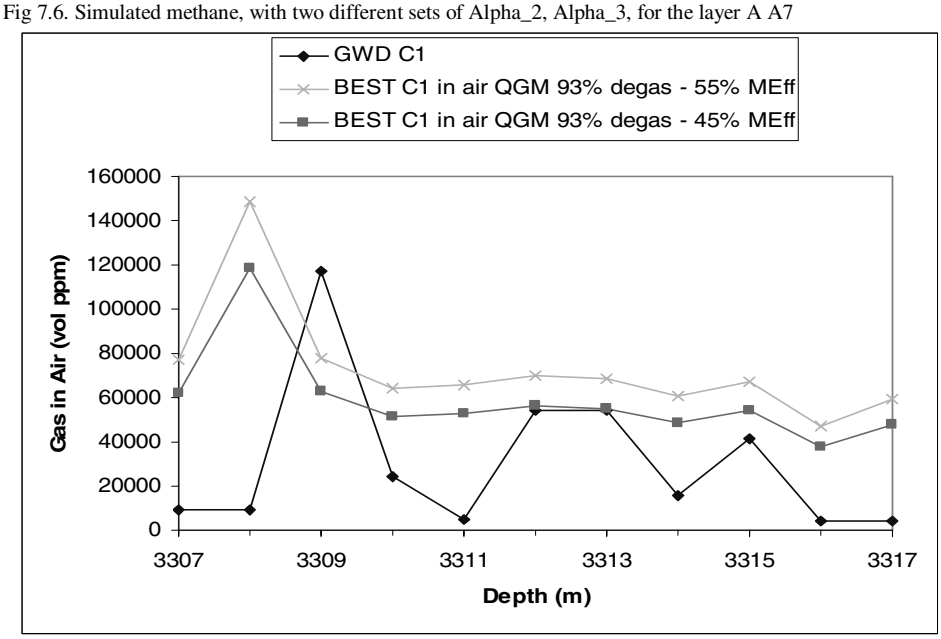

Fig 7.7. ROP (m/h) and mud flow-rate (l/min) versus depth for the layer A A8

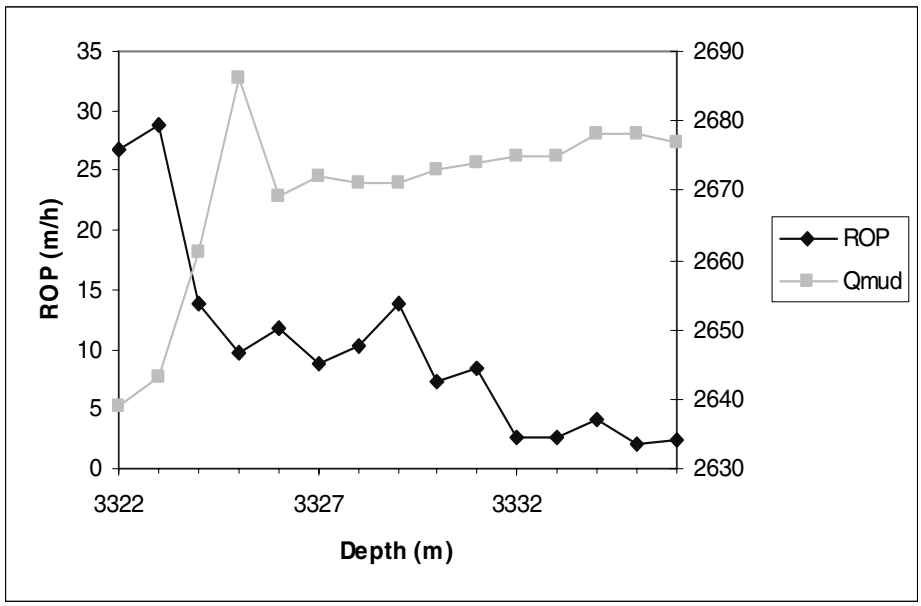

Fig 7.8. Simulated methane, with one set of Alpha_2 = 98%, Alpha_3 = 50%, for the layer A A8

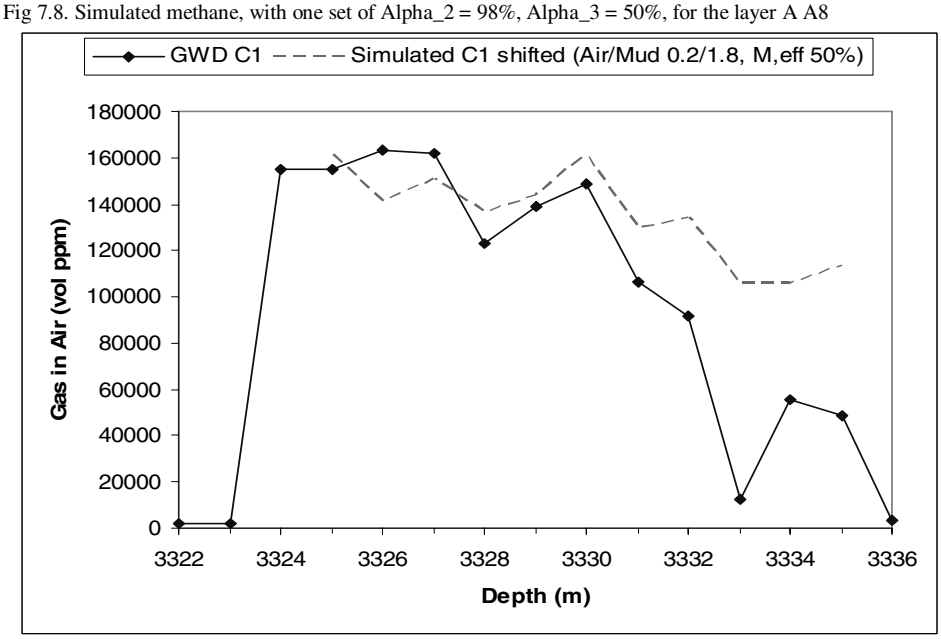

Fig 7.9. ROP (m/h) and mud flow-rate (l/min) versus depth for the layer T2

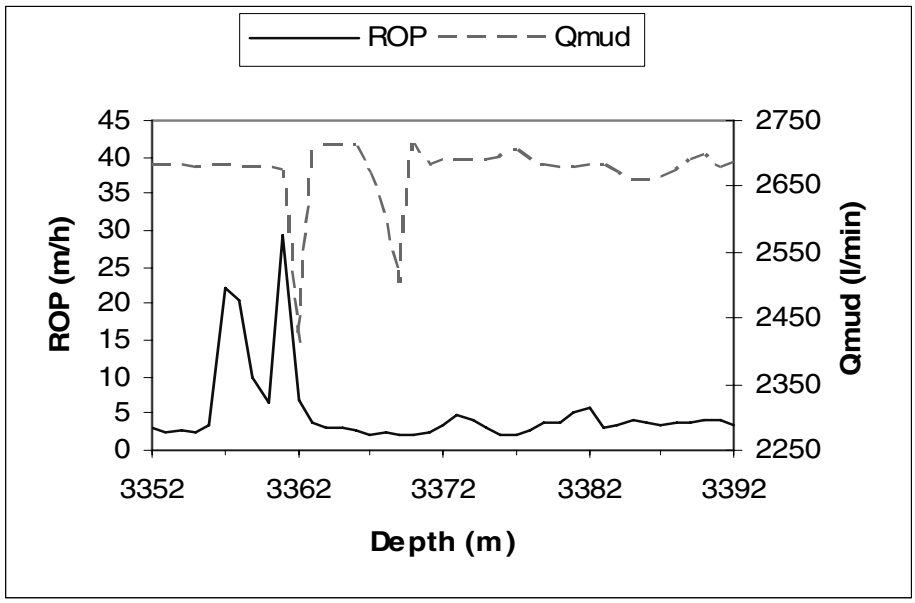

Fig 7.10. Simulated methane, with two different sets of Alpha_2, Alpha_3, for the layer A T2

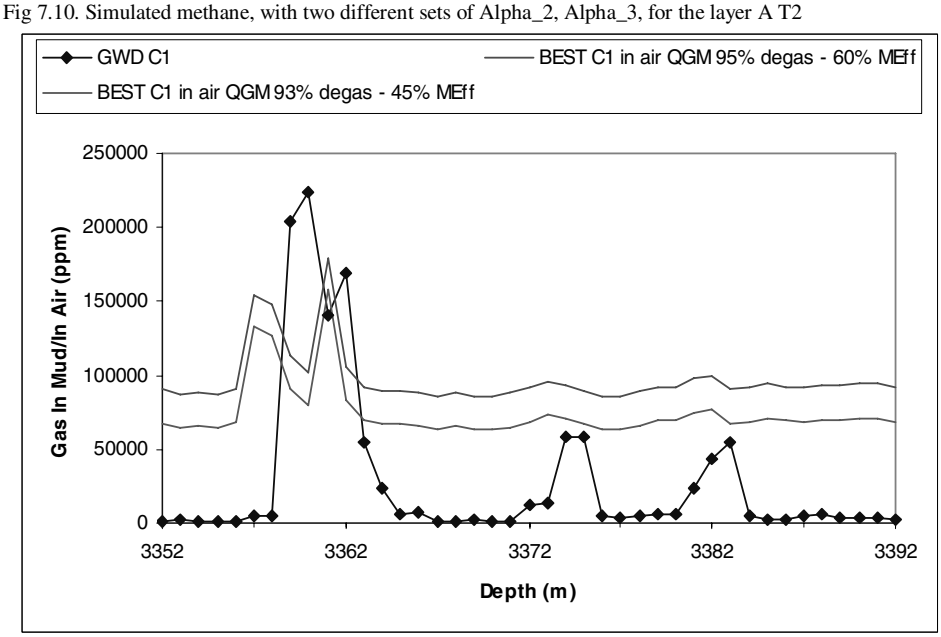

Fig 7.11. Simulated ratio C1/C2, with two different sets of Alpha_2, Alpha_3, for the layer A T2

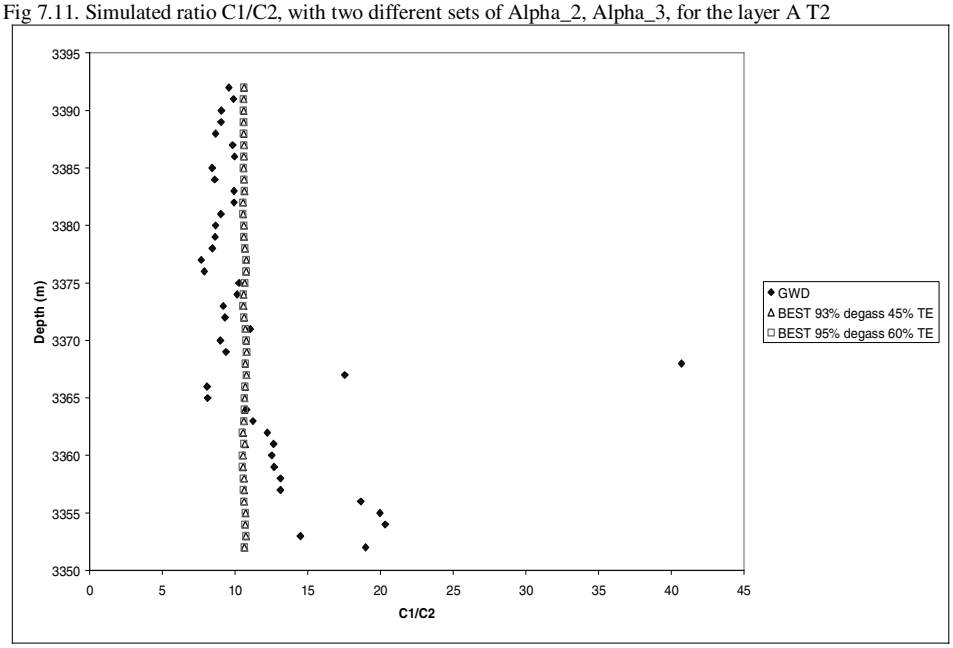

Fig 7.12. Simulated ratio C2/C3, with two different sets of Alpha_2, Alpha_3, for the layer A T2

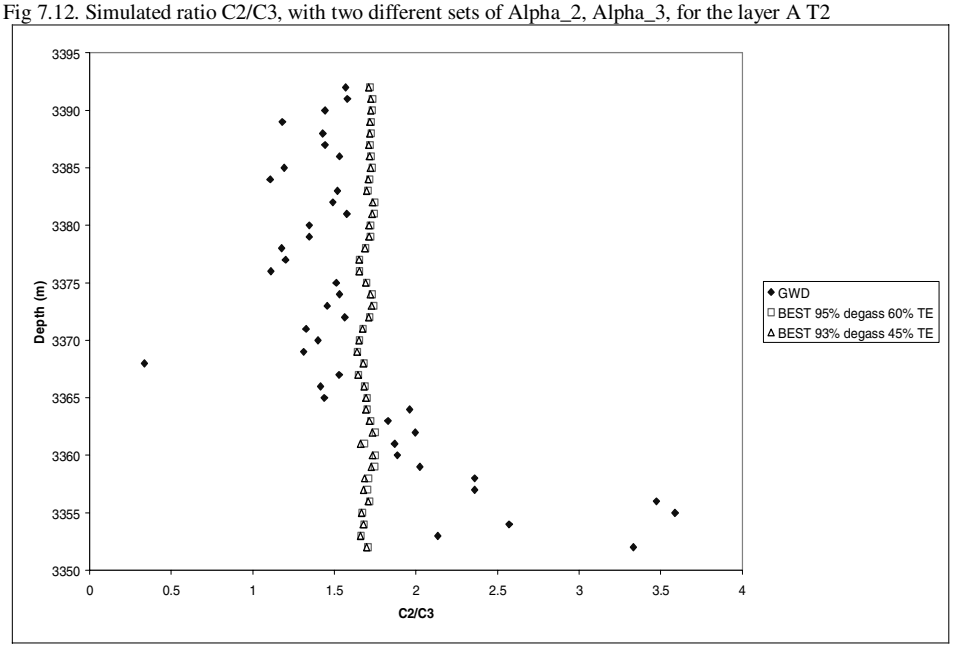

Fig 7.13. Simulated SumC1C5, with two different sets of Alpha_2, Alpha_3, for the layer A T2

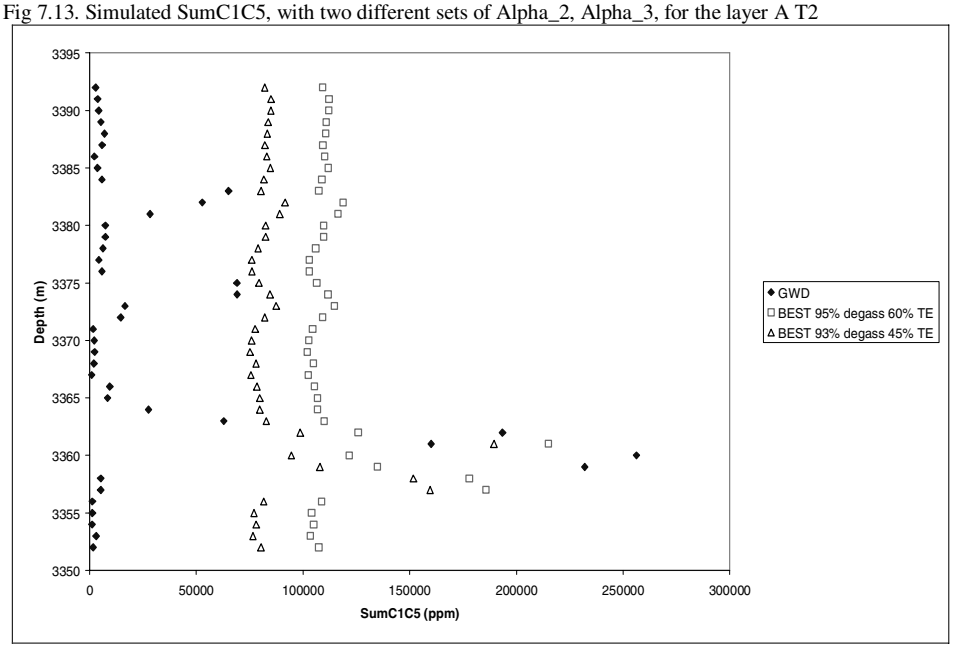

7.2.2 Field Case B

Field Case B presents a succession of layers containing hydrocarbons, as revealed by the methane gas show on Fig 7.14. The formation characteristics and the sampled reservoir fluid characterization results are shown in Appendix 9.

On fig. 7.15, the simulation fails to follow the trends set by the ROP (shown on Fig 7.14). In this case we can even say that there is no correspondence between the ROP and the GWD signal which, added to the lack of information about porosity and water saturation, makes doubtful any chance of successful simulation.

Moreover, a lot of simulation problems occurred for case B as seen Fig 7.15. The inverted peaks represent the points where the water phase is identified as vapour and is mostly lost in the flow-line: almost no hydrocarbon is thus detected in the gas-trap for numerical reasons. As a consequence, the right gas-show cannot be simulated (cf. Fig. 7.15).

Fig 7.14. ROP (in m/h) and methane gas show (ppm in air) versus depth for Field Case B.

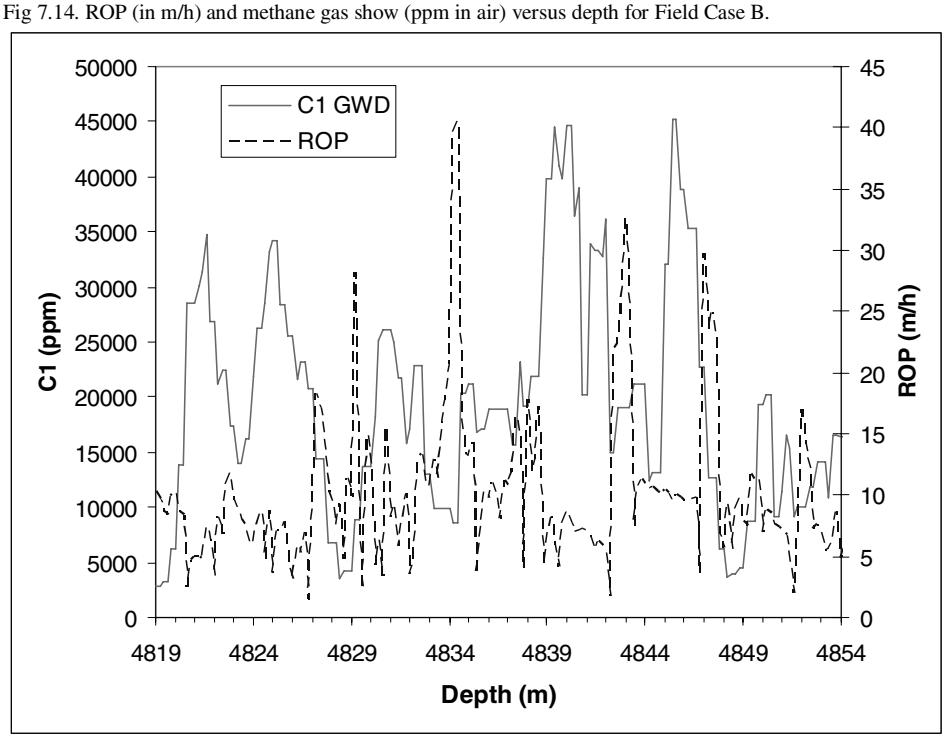

Fig 7.15. Simulation problems occurring while simulating with BEST for the case B: field and simulated methane (ppm in air) versus depth

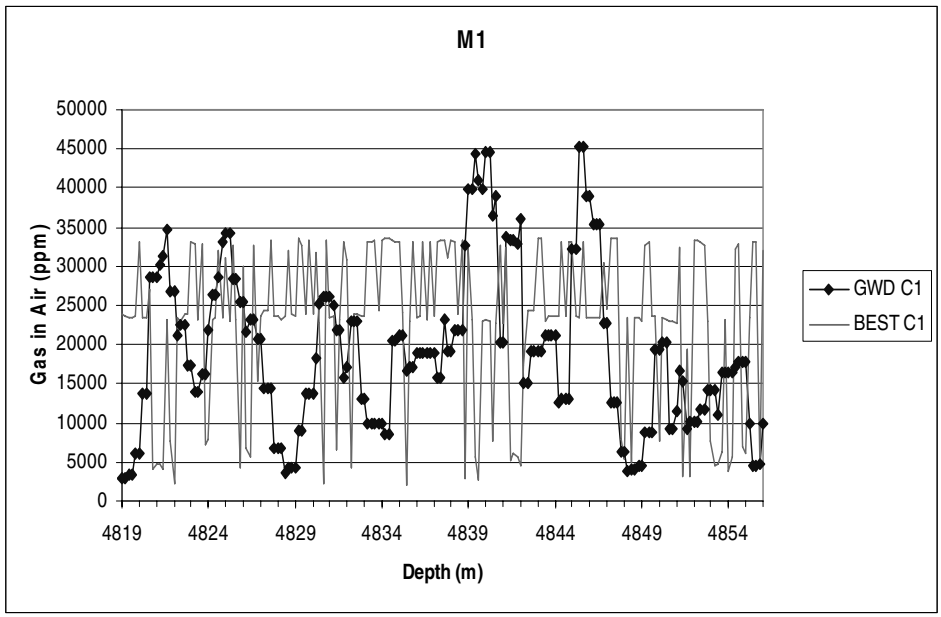

7.2.3 Field Case C

The field Case C presents three hydrocarbon bearing layers. Based on the limited results from the previous simulations, a case with more extensive data and information was provided by ENI E&P, especially porosity and water saturation data. Appendix 10 presents all this information, as well as the characterization results for the concerned reservoir fluids.

The results presented below concern only the hydrocarbon bearing layers 1 and 2, located respectively at 1104 m and 1114 m deep. The two layers are highlighted on Fig 7.16.

Based on the previous remarks, it was decided to use as new input the porosity and the water saturation as functions of depth instead of parameters kept constant.

The case C gave good qualitative results, but in this case too much hydrocarbons are present in the system even after a total degassing of the mud at the open-parts.

Two adjustment parameters were fitted during the simulations and are summarized in table 7.1 below.

Table 7.1. Parameters α_1, α_2 and α_3 used in the simulations, with regard to the layer simulated and the number of flashes used for the degassing part

	1st Layer (1104 m)			2nd Layer (1114 m)		
	1 flash	**2 flashes**	**3 flashes**	**1 flash**	**2 flashes**	**3 flashes**
α_1	50	50	50	50	50	50
α_2	80	60	50	90	80	70
α_3	30	60	70	20	35	50

The same parameters could not be used for the two layers. This can be understood when having a closer look to the operating conditions and the gas show for C1, as shown on Fig. 7.16: while the second layer has a higher porosity and higher ROP, and thus where we would expect a higher signal, the gas show is significantly lower than for the first layer.

The parameters in Table 7.1 were mainly fitted with regard to the level of C1. This leads to the fact that the gas levels for the heavier compounds are still not satisfactory (Fig. 7.16 to 7.26).

Moreover, for layer 1 (Fig. 7.18), we obtain a high level of gas around 1105 m deep, coming from a high ROP coupled with a high porosity and a low water saturation, while the measured signal seems to be attenuated. Our model does not take this fact into account. We can also see that using more than one flash for the degassing between the well head and the gas trap does not improve the results significantly: the first flash is the most effective of all three.

Fig. 7.16. Operation conditions for the 2 simulated layers

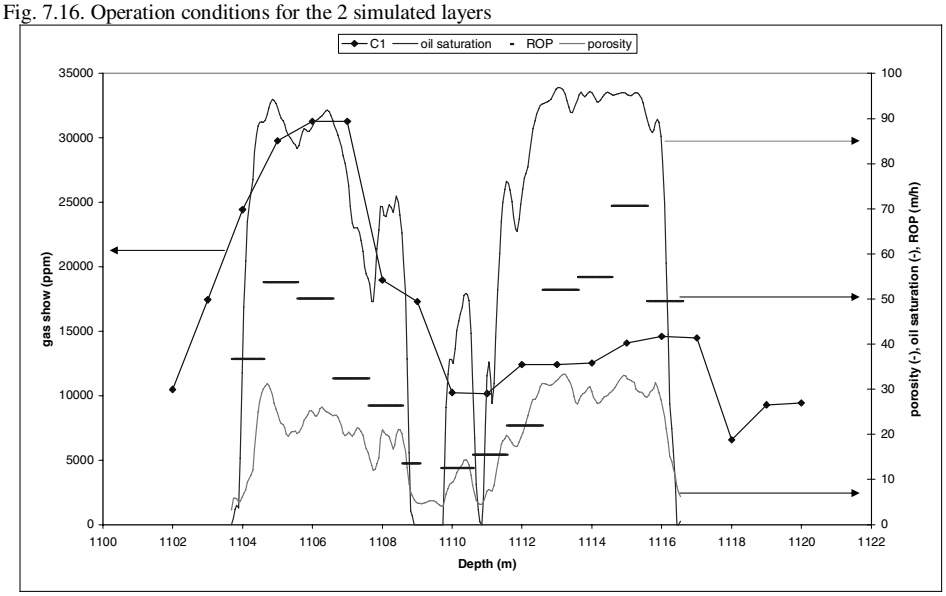

Fig. 7.17. Gas show for C1 as measured and simulated (The simulation parameters are reported in Table 17)

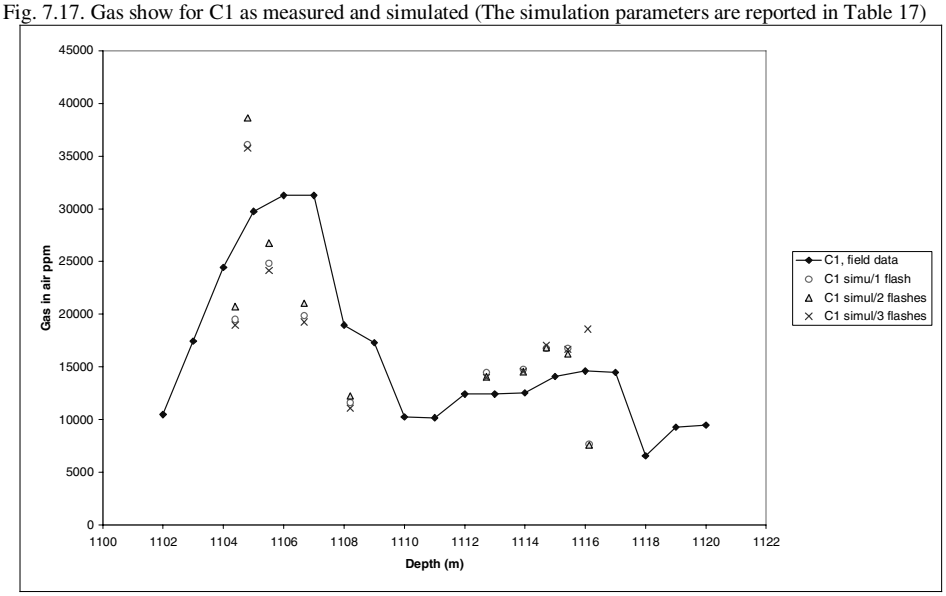

Fig. 7.18. Gas show for C2 as measured and simulated (The simulation parameters are reported in Table 17)

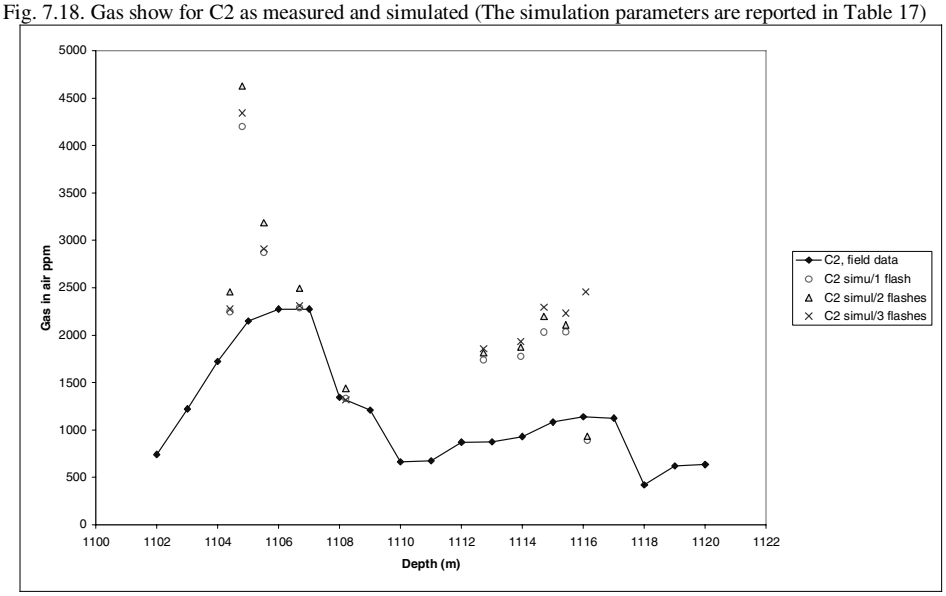

Fig. 7.19. Gas show for C3 as measured and simulated (The simulation parameters are reported in Table 17)

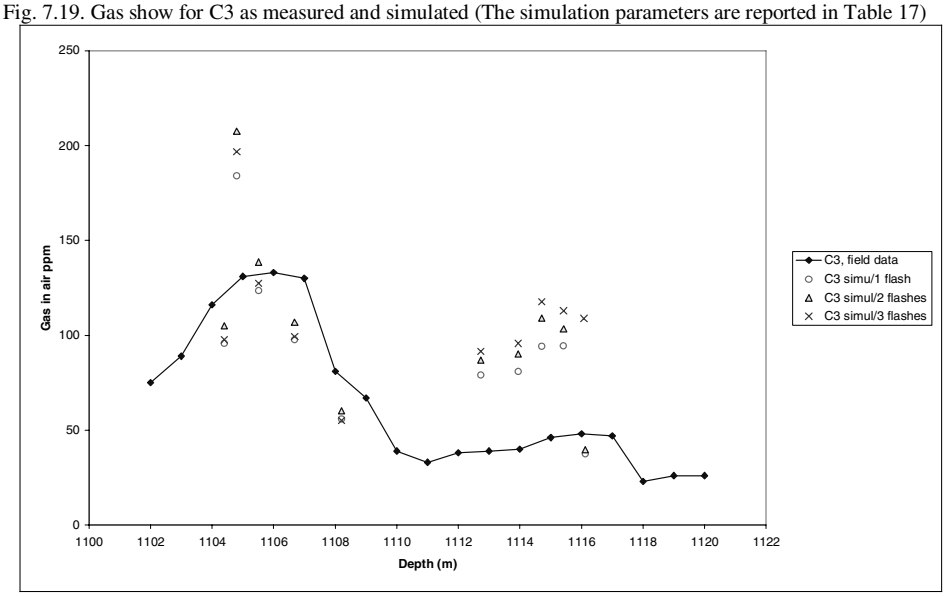

Fig. 7.20. Gas show for iC4 as measured and simulated (The simulation parameters are reported in Table 17)

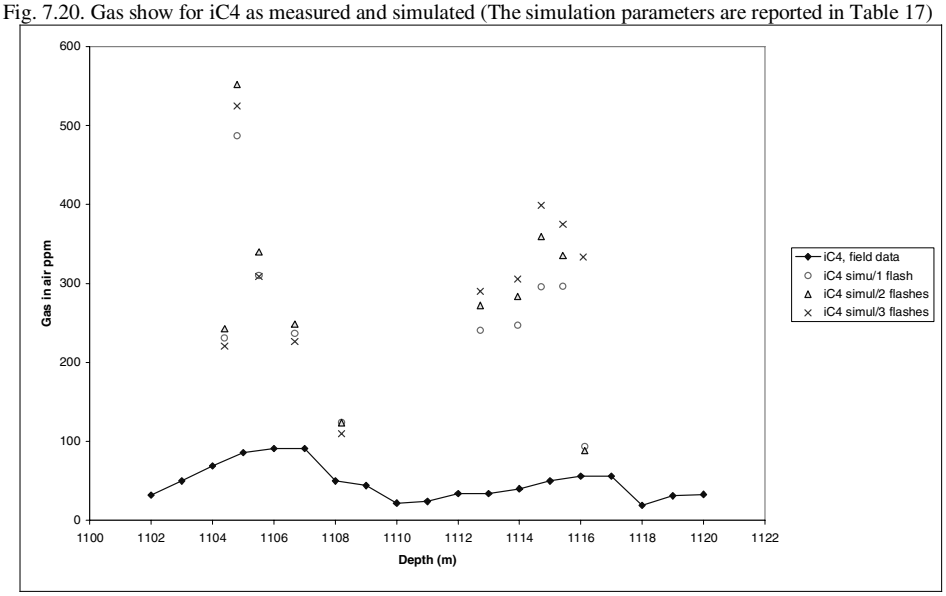

Fig. 7.21. Gas show for TG as measured and simulated (The simulation parameters are reported in Table 17)

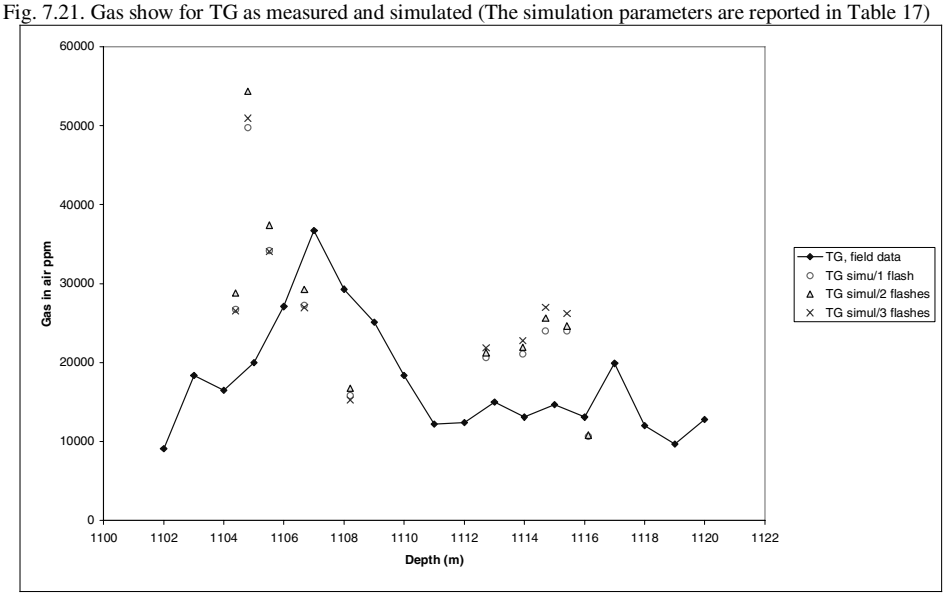

Fig. 7.22. Gas ratio C1/C2 as measured and simulated (The parameters are reported in the legend as α_1, α_2 and α_3)

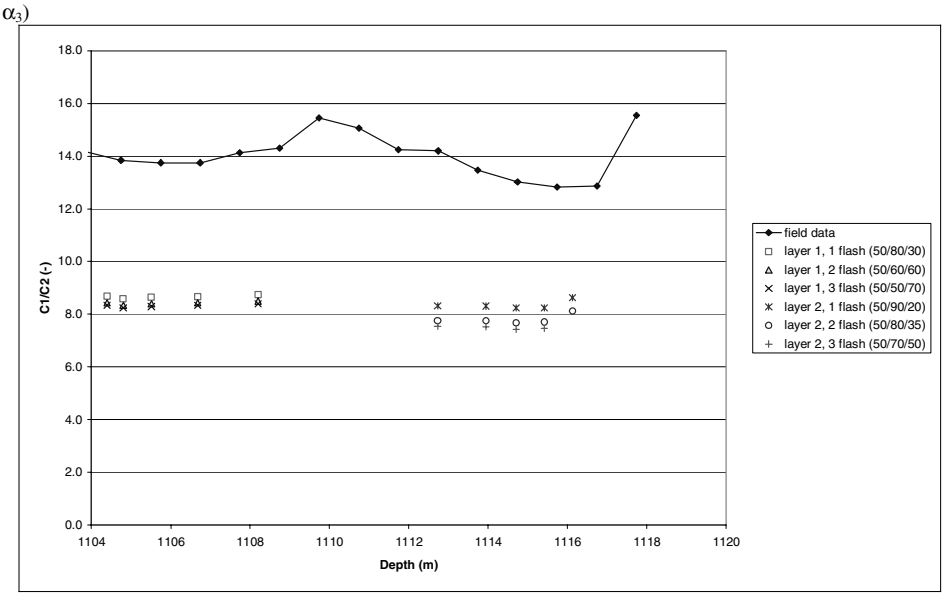

Fig. 7.23. Gas ratio C1/C3 as measured and simulated (The parameters are reported in the legend as α_1, α_2 and α_3)

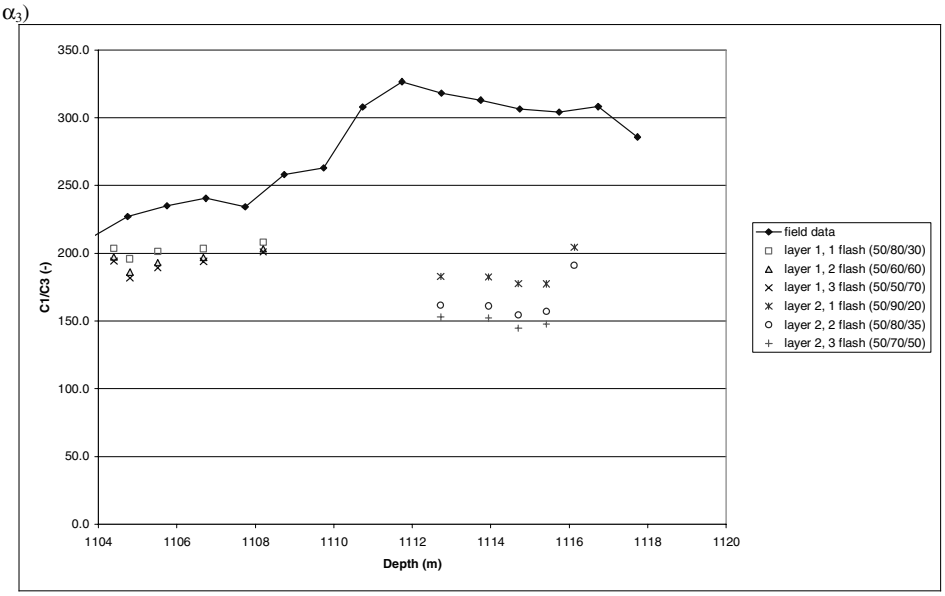

Fig. 7.24. Gas ratio C2/C3 as measured and simulated (The parameters are reported in the legend as α_1, α_2 and α_3)

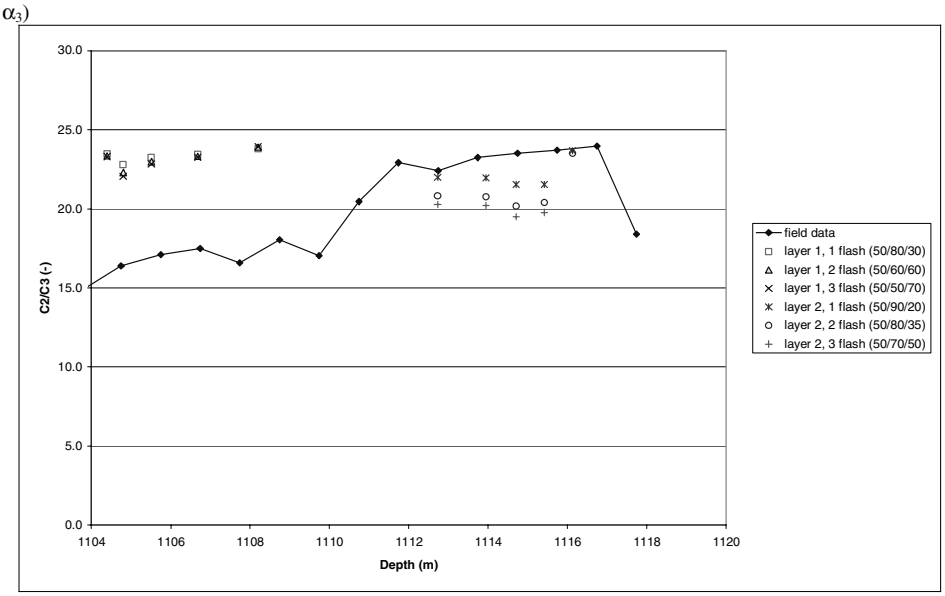

Fig. 7.25. Gas ratio iC5/nC5 as measured and simulated (The parameters are reported in the legend as α_1, α_2 and α_3)

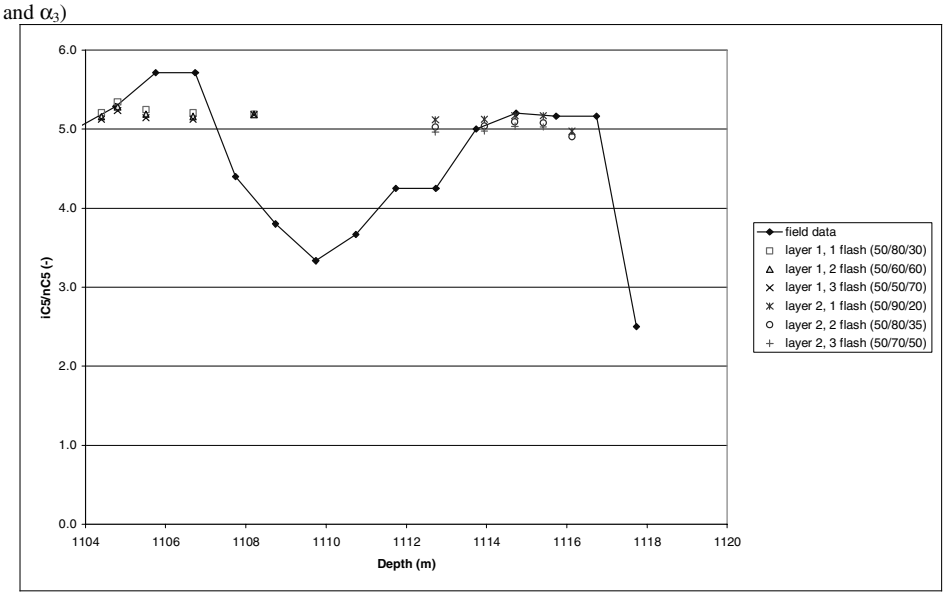

7.2.4 Conclusions

The simulations of case C are relatively successful in amount with a set of fitted parameters. But still the ratios are not well matched. Moreover, different sets of adjustments parameters were obtained for each field case.

The reasons for such results may be:

- low reservoir temperature and, as consequence low mud temperature in deep water wells, could be critical for ethane detection;
- the riser volumes produces attenuation (i.e. dilution) of the gas in mud peaks;
- the drilling mud differential pressure that increases with depth and the reservoir permeability variations would need a different Alpha_1 per each layer;
- based on the result of the study of the case Well P, different values of Alpha_2 should be used for different components;
- many other factors are taken into account in the model, which may be of more important than supposed at the start of the project. These factors are adsorption mechanisms, dynamics of the degassing and of bubble formation, …

Especially, it may be due to the presence of bubbles as shown in the experiment (cf. Chapter 5). One possible assumption is that the total amount of bubbles contains much more hydrocarbons than the solution. The bubbles are then in a different thermodynamic equilibrium than any other bulk phase. In the gas-trap, only part of these bubbles is released to the atmosphere. In this case the redistribution of components between air and mud is unpredictable. This might the subject of another study. In this case, the ratio of hydrocarbons in the bubbles could be studied and may correspond to the ratio of GWD.

8 Conclusions and recommendations for future work

The main goal of the thesis was to better understand the mechanisms, which govern the dilution and release of light hydrocarbons in the drilling mud from the bottom-hole to the gas-trap.

First, over 1000 data points of solubility between water and light hydrocarbons were collected. Some erroneous values were discarded. The study of the phase diagrams of water/light hydrocarbons enabled to clarify the definition of the solubility limit and help building solubility curves for methane to n-butane.

Three thermodynamic models based on cubic equations of state were studied to reproduce the behaviour of the system water/light hydrocarbons: the Peng-Robinson EOS modified by Søreide & Whitson (Søreide, 1992), Henry's law extension by Nghiem (Li, 1986), and the Soave-Redlich-Kwong EOS with the Original Huron-Vidal mixing rule (Huron, 1979). The models appeared to be accurate only at high pressures, as the parameters they use were fitted with high pressure data. The model of Søreide and Whitson appeared to be the most accurate at high pressures, while the model of Nghiem et *al.* appeared more reliable at lower pressures. However, fitting new parameters for one of these models was not in the scope of this project.

A thermodynamic model for the GWD process has then been developed. In a first time it enabled to conceptualise what is happening to the drilling mud and the reservoir fluid between the bottom-hole and the gas-trap. Three adjustment parameters were identified in this conceptualisation phase. The evaluation of Alpha_2, corresponding to the degassing of the mud between the well-head and the gas-trap, was the focus of our further work.

A model experiment has been carried out in order to determine whether the hydrocarbons are present in the mud in the form of solution, or may be contained in the form of micro bubbles. The experiment indicated that, given the conditions between the well head and the gas trap, there will definitely be gas in mud in the form of micro bubbles, which amount largely exceeds the amount of the dissolved gas. The full degassing, if possible at all, will proceed over much larger times than the travel time between the well head and the gas trap. A preliminary estimation range for the value of Alpha_2, was suggested based on the experimental results, to be 50 to 80% according to the mud characteristics, the length of the flow-line and the flow-rate. Further study is required in order to verify validity of this suggestion.

A field test has been carried in order to quantify on-field the loss of hydrocarbons between two points of the mud circulating line. It showed that the peaks move with different velocities. This may come from the effect induced by the different transfer functions used by the logging company to generate a signal as a function of depth. But it could also mean that the hydrocarbons present in bubbles and dissolved travel at different velocities, thus modifying the shape and relative between the peaks. The degassing ratio for methane and ethane appeared to be different with the ratios for C3 to C5. This means that Alpha_2 affects greatly methane and ethane. For propane to pentane, Alpha_2 goes decreasing with the volatility of the compound. The average Alpha_2 for methane and ethane between the middle of the flow-line and the shale-shaker is 57%.

Finally, the simulations are relatively successful in amount with a set of fitted parameters. The importance of field data such as porosity and water saturation was demonstrated. But still the ratios are not well matched. Moreover, different sets of adjustments parameters were obtained for each field case.

The basic interactions between drilling mud and the drilling mud are now understood. Still, the three adjustable parameters could not be satisfactorily estimated.

The estimation of Alpha_1 would require pressure data in the reservoir as well as calculating the pressure exerted by the mud on the walls of the well. The reservoir permeability would also have to be taken into account.

The study of the transportation of bubbles in complex systems could give answers about the release mechanism and the amount of gas retained in the mud, thus leading to better estimates of Alpha_2. Raman Spectrometry could also be used in order to quantify the relative amount of dissolved gas and bubble-gas.

Finally, the study of Alpha_3 would require knowing more characteristics of the gas-traps, in the case of the GZG and the extractor. The study of the trap-response could be undertaken by the service companies designing and operating these traps.

9 References

Amirijafari B., Campbell J.M., "Solubility of gaseous hydrocarbon mixtures in water" , SPE J. 12, 21-27 (1972)

Anthony, R. G.; McKetta, J. J., "Phase equilibrium in the ethylene-water system", J. Chem. Eng. Data 12, 17-20 (1967a)

Anthony, R. G.; McKetta, J. J., "Phase equilibrium in the ethylene-ethane-water system", J. Chem. Eng. Data 12-1, 21-28 (1967b)

Austin E.H., "Drilling Engineering Handbook", D. Reidel Publ. Comp., 1983.

Azarnoosh A., McKetta Jr. J.J., "The solubility of propane in water. (Experimental and smoothed data are given here for pressures from atmospheric to 500 psia and for temperatures from 60 to 280 F", Petrol. Ref. 37, 275-278 (1958)

Barone G., Crescenzi V., Pispisa B., Quadrifoglio F., J. Macromol. Chem. 1, 761-771 (1966)

Beda G., Quagliaroli R., Segalini G., Barraud B., Mitchell A., "Gas While Drilling : A real time geologic and reservoir interpretation tool", SPWLA Paper D, SPWLA Annual Conference, Oslo May, 31st to June, 3rd 1999.

Bizanti M.S., Bayyaa S. M., "Well-Bore Dynamic Density Model," Paper SPE 17093, 1988.

Black CH., Joris G.G., Taylor H.S., J. Chem. Phys. 16, 537 (1948)

Blanco S.T., Velasco I., Rauzy E., Otin S., "Water dew points of binary nitrogen+water and propane+water mixtures. Measurement and correlation", Fluid Phase Eq. 161, 107-117 (1999)

Bodwadkar S.V., Bayyaa S.M., "Diffusion of Gas in Oil Based Drilling Fluids," Paper SPE 37675 (1997)

Brumboiu A., Hawker D., Norquay D. A., Wolcott D. K., "Application of Semipermeable Membrane Technology in the Measurement of Hydrocarbon Gases in Drilling Fluids", SPE 62525 (2000)

Brunner E., "Fluid mixtures at high pressures: IX. Phase separation and critical phenomena in 23 (n-alkane + water) mixtures", J. Chem. Thermodyn. 22, 335 (1990)

Brunner G., Steffen A., Dohrn R., "High pressure liquid-liquid equilibria in ternary systems containing water, benzene, toluene, n-hexane and n-hexadecane", Fluid Phase Eq. 82, 165-172 (1993)

Burd S.D., Braun W.G., "Vapor-liquid equilibria of some C6 hydrocarbons with water", Proc. Div. Ref., Am. Pet. Inst. 48, 464-476 (1968)

Caenn R., Chillingar G.V., “Drilling fluids: State of the art”, Journal of Petroleum Science and Engineering, 14, pp 221-230, 1996.

Carroll J. J., Jou F. Y., Mather A. E., "Fluid phase equilibria in the system n-butane + water", Fluid Phase Eq. 140, 157-169 (1997)

Carroll J.J., Jou F.-Y., Mather A., Otto F.D., "The solubility of methane in aqueous solutions of monoethanolamine, diethanolamine and triethanolamine", Can. J. Chem. Eng. 76, 945-951 (1998)

Claussen W. F., Polglase M. F., "Solubilities and structures in aqueous aliphatic hydrocarbon solutions", J. Am. Chem. Soc. 74, 4817-4819 (1952)

Coan C.R., King A.D., "Solubility of water in compressed carbon dioxide, nitrous oxide, and ethane. Evidence for hydration of carbon dioxide and nitrous oxide in he gas phase", J. Am. Chem. Soc. 93, 1857-1862 (1971)

Connolly J.F., "Solubility of hydrocarbons in water near the critical solution temperatures", J. Chem. Eng. Data 11, 13 (1966)

Crovetto R., Fernandez-Prini R., Japas M.L., "Solubilities of inert gases and methane in H2O and in D2O in the temperature range of 300 to 600 K", J. Chem. Phys. 76, 1077-1086 (1982)

Culberson O.L., Horn A.B., McKetta Jr. J.J., "Phase equilibria in hydrocarbon-water systems: the solubility of ethane in water at pressures to 1200 pounds per square inch", J. Petrol. Tech. 2, or Petrol. Trans. AIME 189, 1-6 (1950)

Culberson O.L., McKetta Jr. J.J., "Phase equilibria in hydrocarbon-water systems. II - The solubility of ethane in water at pressures to 10,000 psia", Trans AIME, Pet. Div. 189, 319-322 (1950)

Culberson O.L., McKetta Jr. J.J., "Phase equilibrium in hydrocarbon-water systems. III. The solubility of methane in water at pressures to 10,000 psia", J. Petrol. Tech., vol. 3, or Petroleum Trans. AIME 192, 223-226 (1951a)

Culberson O.L., McKetta Jr. J.J., "Phase equilibria in hydrocarbon-water systems. IV - Vapor-liquid equilibrium constants in the methane-water and ethane-water systems", Trans AIME, Pet. Div. 192, 297-300 (1951b)

Danneil A., Toedheide K., Franck E. U., "Verdamfungsgleichgewichte und kritische kurven in den systemen äthane/wasser und n-butan/wasser bei hohen drücken", Chem.-Ing.-Tech. 39-13, 816-822 (1967)

Davis J.E., McKetta J.J., "Solubility of methane in water", Petroleum Refiner Vol. 39, 3, 205-206 (1960)

De Loos T.W., Wijen A.J.M., Diepen G.A.M., "Phase equilibria and critical phenomena in fluid (propane-water) at high pressures and temperatures", J. Chem. Thermodynamics 12, 193-204 (1980)
De Loos T.W., Penders W.G., Lichtenhaler R.N., "Phase equilibria and critical phenomena in fluid (n-hexane+water) at high pressures and temperatures", J. Chem. Thermodynamics 14, 83-91 (1982)

De Loos T.W., Van Dorp J.H., Lichtenthaler R.N., "Phase equilibria and critical phenomena in fluid (n-alkane + water) systems at high pressure and temperatures", Fluid Phase Eq. 10, 279-287 (1983)

Dhima A., De Hemptinne J.C. , Moracchini G., "Solubility of light hydrocarbons and their mixtures in pure water under high pressure", Fluid Phase Equilibria, 145, 129-150 (1998)

Duffy J.R., Smith N.O., Nagy B., "Solubility of natural gases in aqueous salt solutions - I. Liquidus surfaces in the system CH4-H2O-NaCl-CaCl2 at room temperatures and at pressures below 1000 psia", Geochem. Et Cosmochim. Acta, 24, 23-31 (1961)

Durand R., C. R. Hebd. Seances Acad. Sci. 226, 409 (1948)

Englin B.A. et al., Khim. Tekhnol. Topl. Masel. 9, 42 (1965)

Frederickson A.G. Bird R.B., “Non-Newtonian flow in annuli”, Industrial and Engineering Chemistry, Vol. 50, No. 3, pp 347-352, 1958.

Fuehner H., Ber. Dtscg. Chem. Ges. 57, 510 (1924)

Gillepsie P.C., Wilson G.M., "Vapor-liquid and liquid-liquid equilibria: water-methane, water-carbon dioxide, water-hydrogen sulfide, water-n-pentane, water-methane-n-pentane", Gas processors Association Research Report RR-48, Provo, Utah, April (1982)

Hanson S.A., “Integrating GGM™ with downhole data improves formation evaluation”, Gas TIPS (http://gastechnology.org/pub/content/feb/19990218/130735/gt0299c-toc.html) (1999)

Hayworth J.H., Sellens M.P., Gurvis R.L., “Reservoir characterization by analysis of light hydrocarbon shows”, SPE 12914 (1984)

Hemphill T., Campos W., Pilehvari A., “Yield-power law model more accurately predicts mud rheology”, Oil & Gas Journal, pp.45-50, August, 1993.

Huron M. J., Vidal J., ”New mixing rules in simple equations of state for representing vapour-liquid equilibria of strongly non-ideal mixtures”, Fluid Phase Eq. 3, 255-271 (1979)

Joffrion L. L., Eubank P. T., "P-V-T Data and Virial coefficients for gaseous methane-water mixtures with correction for adsorption effects", Fluid Phase Equilib. 43, 263-294 (1988)

Jönsson J.Aa., Vejrosta J., Novak J., "Air/water partition coefficients for normal alkanes (n-pentane to n-nonane)", Fluid Phase Eq. 9, 279-285 (1982)

Jou F.-Y., Mather A.E., "Vapor-liquid-liquid locus of the system pentane + water", J. Chem. Eng. Data 45, 728-729 (2000)

Kandel D., Quagliaroli R., Segalini G., Barraud B.: “Improved Integrated Reservoir Interpretation using the Gas While Drilling (GWD) data”, SPE 65176, presented at the SPE European Petroleum Conference (2000)

Kertes A.S. (ed.), IUPAC Solubility Data Series, Vol 9 (1982)

Kertes A.S. (ed.), IUPAC Solubility Data Series, Vol 27/28 (1987)

Kertes A.S. (ed.), IUPAC Solubility Data Series, Vol 24, 451 (1989a)

Kertes A.S. (ed.), IUPAC Solubility Data Series, Vol 37 (1989b)

Kobayashi R., Katz D. L., "Vapor-liquid equilibria for binary hydrocarbon-water systems", Ind. Eng. Chem. 45 No 2, 440-446 (1953)

Kudchadker A.P., McKetta J.J., "Solubility of hexane in water", Hydrocarbon Process., Pet. Ref., 40, 231-232 (1961)

Kyoo Y.S., Feneyrou G., Fleyel F., Martin R., Lievois J., Kobayashi R., "Further studies in the elucidation of the abnormal solubilities of the lower molecular weight gases in aqueous solutions near hydrate formation temperatures", J. of the Chin. I. Ch. E., 27-4, 328-335 (1996)

Lannung A., Gjaldbæk J.C. , Acta Chem. Scand. 14, 1124-1128 (1960)

Le Breton J.G., McKetta J.J., "Low pressure solubility of n-butane in water", Hydrocarbon Processing & Petroleum Refiner 43, 136-138 (1964)

Lebeau M.P., "Sur quelques propriétés physiques du propane", Bull. Soc. Chim. France, [3] 33, 1137-1139 (1905)

Lebeau M.P., "Uber einige physikalische Eigenschaften des Butans und Isobutans", Chem. Zentralbl., 79, II, 291-292 (1908)

Lekvam K., P. R. Bishnoi, "Dissolution of methane in water at low temperatures and intermediate pressures”, Fluid Phase Equilibria 131, 297-309 (1997)

Li Y.-K., Nghiem L. X., “Phase equilibria of oil, gas and water/brine mixtures from a cubic equation of state and Henry’s law”, Can. J. Chem. Eng. 64, 486-496 (1986)

McAuliffe C., "Solubility in water of C1-C9 hydrocarbons", Nature 200, 1092-1093 (1963)

McAuliffe C., "Solubility in water of paraffin, cycloparaffin, olefin, acetylene, cycloolefin, and aromatic hydrocarbons", J. Phys. Chem., 70 No 4, 1267-1275 (1966)

Michell S.J., “Fluid and Particle Mechanics”, Pergamon Press, 1970.

Michels A., Gerver J., Biji A., Physica 3, 797-808 (1936)

Moore P.L., “Drilling Practice Manual”, The Petroleum Publishing C., 1974.

Munson B.R., Young D.F., Okiishi T.H., “Fundamentals of fluid mechanics”, John Wiley & Sons, Inc, 1990.

Namiot A.Y., Bender S.Y., Khim. Tekhnol. Topl. Masel. 7, 52-55 (1960)

Namiot A.Y., Skripka V.G., Lottek Y.G., Zh. Fiz. Khim., 50, 2718-2719 (1976)

Nelson H.D., De Ligny C.L., "The determination of the solubilities of some n-alkanes in water at different temperatures, by means of gas chromatography", Recl. Trav. Chim. Pays-Bas 87, 528-544 (1968)

NIST Chemistry Webbook, http://webbook.nist.gov/chemistry/

Olds R.H., Sage B.H., Lacey W.N., "Phase equilibria in hydrocarbon systems. Composition of the dew-point gas of the methane-water system", Industrial and Engineering Chemistry, 34, 10, 1223-1227 (1942)

O'Sullivan T.D., Smith N.O., "The solubility and partial molar volume of nitrogen and methane in water and in aqueous sodium chloride from 50 to 125° and 100 to 600 atm", J. Phys. Chem., 74 (7), 1460-1466 (1970)

Peng D. Y., Robinson D. B., “A new two-constant equation of state”, Ind. Eng. Chem. Fundam. 15, 59-64 (1976)

Peters E.J., Chenevert M.E., Zhang C., “A model for predicting the density of oil-based muds at high pressures and temperatures”, SPE 18036 (1990)

Pierotti R.A., Liabastre A.A., "Structure and properties of water solutions", U.S. Nat. Tech. Inform. Serv., PB Rep., No 21163, 113 pp (1972)

Pixler B.O., “Mud analysis logging”, J. of Petr. Tech., April, 323-326 (1961)

Pixler B.O., “Formation evaluation by analysis of hydrocarbon ratio”, 43rd Annual Meeting SPE, Houston, SPE 2254 (1968)

Polak J., Lu B.C.-Y., "Mutual solubilities of hydrocarbons and water at 0 and 25°C", Can. J. Chem. 51, 4018-4023 (1973)

Price L.C., "Aqueous solubility of methane at elevated pressures and temperatures", Am. Assoc. Pet. Geol. Bull., 63, 1527-1533 (1979)

“QGM Quantitative Gas Measurement System, User’s Guide”, published by Gas Research Institute (Chicago, Illinois USA) and Texaco (Houston, Texas USA) (1998)

Rabia H., “Oilwell Drilling Engineering, Principles and Practice”, Graham & Trotman, 1985.

Reamer H.H., Olds R.H., Sage B.H., Lacey W.N., "Phase equilibria in hydrocarbon systems, composition of dew-points gas in ethane-water system", Ind. Eng. Chem. 35, 790-793 (1943)

Reamer H. H., Olds R. H., Sage B. H., Lacey W. N., "Phase equilibria in hydrocarbon systems. Compositions of the coexisting phases of n-butane-water system in the three-phase region", Ind. Eng. Chem. 36, 381-384 (1944)

Reamer H. H., Sage B. H., Lacey W. N., "Phase equilibria in hydrocarbon systems. N-butane-water system in the two-phase region", Ind. Eng. Chem. 44, No 3, 609-615 (1952)

Rebert C.J., Hayworth K.E., "The gas and liquid solubility relations in hydrocarbon-water systems", AIChE Journal 13-1, 118-121 (1967)

Roof J.G., "Three-phase critical point in hydrocarbon-water systems", J. Chem. Eng. Data 15-2, 301-303 (1970)

Scheffer F.E.C., "On the system hexane-water", Koninkl. Akad. Wetenschap. Amsterdam 16 Part 1, 404 (1913)

Soave G., "Equilibrium constants from a modified Redlich-Kwong equation of state", Chem. Eng. Sci. 27, 1197-1203 (1972)

Søreide I., Whitson C. H., "Peng-Robinson predictions for hydrocarbons, CO_2, N_2 and H_2S with pure water and NaCl brine", Fluid Phase Eq. 77, 217-240 (1992)

Stephen H., Stephen T., "Solubilities of inorganic and organic compounds", Pergamon Press, Oxford, 1963

Stoessel R.K., Byrne P.A., Clays Clay Miner, 30, 67-72 (1982a)

Stoessel R.K., Byrne P.A., "Salting-out of methane in single-salt solutions at 25°C and below 800 psia", Geochem. Cosmochim Acta, 46, 1327-1332 (1982b)

Sultanov R.C., Skripka V.C., Namiot A.Y., "Rastvorimost metana v vode pri novysjennykh temperaturakh i davlenijakh" (Solubility of methane in water at high temperatures and pressures), Gazova Promyshlennost, v. 17, May, 6-7 (1972a) (in russian)

Sultanov R.G, Skripka V.G., Namoit A.Y, Zh. Fiz. Khim., 46, 2160 (1972b)

Sultanov R.G., Skripka V.G., Zh. Fiz. Khim., 47, 1035 (1973)

Swanson B.W., Gilvary B., McEwan F., "Experimental measurement and modelling of gas solubility in invert emulsion drilling fluids explains surface observations during kicks", SPE 18371 (1988)

Thomas D.C., Lea Jr. J.F., Turek E.A., "Gas solubility in oil-based drilling fluids: effects on kick detection", paper SPE 11115 (1982)

Tsonopoulos C., Wilson G.M., "High-temperature mutual solubilities of hydrocarbons and water. Part I: Benzene, cyclohexane and n-hexane", AIChE J. 29, 990-999 (1983)

Van Konynenburg P.H., Scott R.L., “Critical lines and phase equilibria in binary Van der Waals mixtures”, Phil. Trans. Roy. Soc., A298, 495-540 (1980)

Wehe A.H., McKetta J.J., "Method for determining total hydrocarbons dissolved in water", Anal. Chem. 33, 291-293 (1961a)

Wehe A. H., McKetta J. J., "n-butane - 1-butene - water system in the three phase region", J. Chem. Eng. Data 6, 167-172 (1961b)

Wetlaufer D.B., Malik S.K., Stoller L., Coffin R.L., "Nonpolar group participation in the denaturation of proteins by urea and guanadium salts. Model compound studies", J. Am. Chem. Soc., 86, 508-514 (1964)

Winkler, Z. Physik. Chem. 9, 171 (1899)

Winkler L.W., "Die Löslichkeit der Gase in Wasser", Berliner Berichte, 34, 1408-1422 (1901)

“World Oil’s Fluids ‘97”, World Oil, 82-116 (1997)

Yamamoto S., Alcauskas J.B., Crozier T.E., "Solubility of methane in distilled water and seawater", J. Chem. Eng. Data 21 1, 78-80 (1976)

Yang S.O., Cho S.H., Lee H., Lee C.S., "Measurement and prediction of phase equilibria for water + methane in hydrate forming conditions", Fluid Phase Eq. 185, 53-63 (2001)

Yarym-Agaev, N. L.; Sinyavskaya, R. P.; Koliushko, I. I.; Levinton, L. Ya. Zh. Prikl. Khim. (Leningrad) 58, 165 (1985)

Yiling T., Michelberger T., Franck E. U., "High pressure phase equilibria and critical curves of (water + n-butane) and (water + n-hexane) at temperatures to 700 K and pressures to 300 MPa", J. Chem. Thermodyn. 23, 105-112 (1991)

Appendix 1. Bibliographic study of the mud systems and their hydrodynamics

1. Drilling mud

1.1. General definition

A drilling fluid is a complex mixture of different liquids and of various solid materials, which are added to impart or control the necessary properties of the mixture. The composition of a drilling mud will then be imposed by the desired properties, or, in other words, the functions that we want it to fulfil.

The primary functions of drilling fluids are the following (Austin, 1983; Moore, 1974):

- To remove the rock cuttings from the bottom of the hole so that the bit can drill on a fresh rock surface, thereby increasing the efficiency of the drilling operation.
- To transport the cuttings to the surface where they can be removed from the drilling fluid.
- To suspend the cuttings in the hole whenever mud circulating is stopped.
- To cool and lubricate the bit and clean its cutting surface.
- To cool and lubricate the drill string.
- To exert sufficient hydrostatic pressure to exclude formation fluids from the hole.
- To maintain a stable, lubricated well bore that can be re-entered at any time during the drilling operation.

A drilling fluid will be classified according to its continuous fluid phase, which can be made of water, oil or air. Most of the world's drilling operations use water-based muds. Only 5 to 10% of the wells drilled use oil muds and a much smaller percentage use air (Caenn, 1996).

Table A1.1. (Moore, 1974) shows the possible components of drilling fluids with a liquid fluid phase.

Table A1.1. Liquid and solid components of drilling muds (Moore, 1974)

Liquid	Solids
1. Fresh water	1. Low gravity (Specific gravity = 2.5)
2. Salt water	a. Non-reactive: sand, chert, limestone, shale
3. Oil	b. Reactive solids: clays
4. Mixtures of these fluids	2. High gravity
	a. Barite (Specific gravity = 4.2)
	b. Iron Ore and Lead Sulfide (Specific gravity = 7.0)

1.2. Properties of mud

The principle measurable properties of a drilling fluid are its density, viscosity, water loss, gel strength, pH, resistivity and abrasiveness. In fact, most of these properties can be attached to a function of the mud, and the change in a given property will change the behaviour of the mud.

Among the properties of mud, the viscosity and the density are particularly important. The viscosity plays an important role in the lifting capacity of the mud, which enables it to remove the drill cuttings. The density of mud is important for the control of the subsurface pressure.

Different muds will be used depending on the depth, the difficulties encountered, and the geological characteristics of the drilled formation. As an illustration, the following table gives some recommendation for a drilling program (Austin, 1983):

Table A1.2. Example of drilling muds and their characteristics according to the range depth (Austin, 1983):

Depth Interval (m)	Mud wt. (g/cc)	Water Loss (ml)	System
0 - 308	1.01 – 1.05	N.C.	Water
308 - 2130	1.01 – 1.13	20	Brine
2130 - 3600	1.13 – 1.74	6	Brine
3600 - 4938	1.13 – 1.37	4	Brine

The water loss is the measure of the volume of fluid lost through filter media (usually, filter paper) when drilling fluid is subjected to a differential pressure.

1.2.1. Solid content of mud

- **Low gravity, non-reactive solids: sand, chert, limestone, shale**

By the API definition, sand is defined as any solid particle with a size greater than 74 µm. But the non-reactive solid may contain smaller particles and those when larger than 15 µm, may create an erosive environment, which is detrimental to circulating equipment. Commonly, an average density of 2.5 g/cc is taken for the low gravity solids, when no other information is available (Moore, 1974; Rabia, 1985).

- **Low gravity, reactive solids: clays**

Clay can be defined by many ways: a solid particle with an equivalent diameter of less than 2 microns, as a particle with an electrical charge and capable of adsorbing water or also as a material that gives the appearance of swelling when water is adsorbed on it.

Clays are used to influence the viscosity of the drilling mud. The properties of clays in regard to viscosity are linked to the internal structure of the clay particles and the electrostatic forces, which act to hold them together when they are dispersed in water. Two

types of clay are usually used in drilling muds: bentonite (sodium montmorillonite) and attapulgite, commonly called salt gel.

Bentonite, which is the most commonly used, is hydrated by water when used in a drilling mud. This adsorption goes with a swelling and an increase of the thickness of the mixture. Bentonite cannot be used in saltwater, because the clay adsorbs the salt ions, and no properties are added to the water. More precisely, bentonite has a layer structure, and between each layer (or plate) some exchangeable ions Na+, Ca++, or K+ are adsorbed. Then when in presence of water, a layer of water replaces the exchangeable ions. Water is also adsorbed on the external surfaces. Swelling of the clay is caused when four or more layers of water molecules are occupying a space that previously only contained one layer of sodium or calcium atoms (Rabia, 1985).

Clays do not hydrate or swell in oil. Formation clay can also get mixed in the mud: it could be lime or calcium chloride systems. Generally, as seen previously for low gravity solids, the density of clays is taken at 2.5 g/cc.

Hereafter two examples of clays are given with the size-repartition of solid particles they contain (Moore, 1974):

Table A1.3. Size repartition of solid particles in a bentonitic clay and another clay (Moore, 1974)

Size Range (µm)	Average diameter (µm)	Bentonite Weight Percentage	Clay Weight Percentage
0 – 2	1	87.4	71
2 – 3.3	2.65	1.6	6
3.3 – 5	4.15	1.1	4
5 – 8	6.5	1.3	3.9
8 – 12	10	1.4	1.3
12 – 18	15	1.6	0.5
18 – 30	24	1.4	1.3
30 – 44	37	1.1	3.5
44 – 74	59	1.8	5.5
74 – 110	192	1.3	1.3
110 – 165	137.5	0	0.1
165 – 250	207.5	0	0.1
250 - 400	650	0	1.5

- **High gravity solids**

High gravity non-reactive solids are used to increase the mud weight. Barite, primarily barium sulfate ($BaSO_4$), is the most commonly used one. The API specifications for barite give a minimum density of 4.3 g/cc. By API specification, a barite should contain at least 5% of particles bigger than 44 µm and no more than 3% of particles bigger than 74 µm.

Four examples of barite are given in Table A1.4. (Moore, 1974), displaying the size distribution of the solid particles.

Table A1.4. Four examples of barite composition in term of particle size distribution (Moore, 1974)

		Barite A	Barite B	Barite C	Barite D
Size Range (μm)	Average Diameter (μm)	Weight Percentage	Weight Percentage	Weight Percentage	Weight Percentage
0 – 2	1	7	13	10.8	13
2 – 3.3	2.65	2.5	5	3.6	3.4
3.3 – 5	4.15	2.7	5	3.9	3.3
5 – 8	6.5	7	8	8.5	8
	Sub total	**19.2**	**31.0**	**26.8**	**27.7**
8 – 12	10	7.8	11	13.5	7.2
12 – 18	15	15	12.5	17	16.5
18 – 30	24	23	17.5	18.5	21
30 – 44	37	18	13.5	13.2	16.5
44 – 74	59	13	12	10	8.1
74 – 110	192	3	2	0.5	1
110 – 165	137.5	1	0.5	0.5	2
165 – 250	207.5	0	0	0	0
250 - 400	650	0	0	0	0

Lead sulphides (as galena for example) can also be used as high gravity solids. They have a specific gravity of 6.5-7. Iron ores can also be used (Specific gravity > 5).

1.2.2. Water-based mud

Different kinds of water muds are encountered, like for example, low solid system (fresh water and bentonite) or also saltwater muds and attapulgite.

A water-based mud is composed of the following different components (Rabia, 1985):

- Water
- Solid part
    - Reactive fraction, which role is to change the viscosity of the mud. This reactive fraction is always composed of low gravity solids, clays.
    - Inert fraction, to affect the density of the mud. It can be composed of low or high-density compounds, like sand, barite, limestone or chert.
    - Chemical additives, to control mud properties.

We can find below two example of the composition of water-based muds:

Table A1.5. Composition of two water-based muds

Source	**Bizanti *et al.*, 1988**	**Swanson *et al.*, 1988**
Density	1600 kg/m^3	1190 kg/m^3
Oil	0.0 % vol	0.0 % vol
Solids	23 % vol	6 % vol
Water	77 % vol	*Non available*
Salinity (Brine = CaCl2)	*Non available*	75 g/l

1.2.3. Oil-based mud

In oil-based muds, oil makes up to 60 to 98% of the liquids. Diesel fuel is commonly used as the continuous phase, although some crude oils are satisfactory.

Water is the dispersed or emulsified phase and is present in amounts of 2 to 40% by volume, but the range 15-30% by volume is rather normal for invert-emulsion muds. Water gives the emulsion the required properties of gel strength and barite suspension. As for water-based mud, the addition of barite or limestone in oil-base mud increases the density.

In addition to that, an oil-based drilling mud will be used specifically when the following tasks are required (Austin, 1983):

- To prevent damage to the productive formation by the drilling fluid.
- To drill or core evaporates.
- To drill troublesome shales.
- To overcome wall sticking of a drill pipe.
- To release stuck pipe.
- To drill under extreme temperatures conditions, high temperatures (T > 180°C) in very deep holes, or low temperatures in permafrost and cold climates.
- To place in the tubing-casing annulus and the casing-hole annulus to facilitate recovery of pipe.
- To drill formations containing corrosive fluids, such as hydrogen sulfide.

A few examples of oil-based muds and their composition are displayed below:

Table A1.6. Three examples of oil-based muds and their compositions

Source	**Bodwadkar *et al.*, 1997**	**Peters *et al.*, 1990**	**Thomas *et al.*, 1982**
Density	2.02 g/cc	1.31 g/cc	1.67 g/cc
Type of oil	Diesel oil	Diesel oil	Diesel oil
Oil phase	194.7 cm^3	231.5 cm^3	52 %vol
Organophilic Clay	3.00 g	6.45 g	*non available*
Emulsifier	2.00 g	2.00 g	*non available*
Emulsifier, Wetting Agent	2.00 g	2.00 g	*non available*
Lime	2.00 g	2.00 g	*non available*
Water	25.30 cm^3	63.2 g	22.3 %vol
CaCl2, 96% purity	8.93 g	22.3 g	*non available*
Barite	504.50 g	167.3 g	*non available*
Solids	*non available*	*non available*	25.7 %vol

1.2.4. Gas (Air) Drilling Fluid

This class of drilling fluids ranges from dry gas, through mist, foam, "stiff foam", to aerated mud. The principal benefit derived from air and aerated drilling fluids is the gain in penetration rate resulting from the lowered differential pressure.

As gas drilling fluids are of marginal use (Caenn *et al.* 1996), they will not be investigated any longer. On the contrary, the study will focus on water-based and oil-based drilling fluids.

2. Hydrodynamics

2.1. Classification of flow types

The type of flow for Newtonian fluids can be decided by the value of the Reynolds number (Re). For annular flows, we have the following classification according to Rabia (1985):

- $Re \leq 2000$, laminar flow
- $2000 \leq Re \leq 3000$, transitional flow (fluid often described as plug flow)
- $3000 \leq Re$, turbulent flow

Turbulent flow is to be avoided in the annulus, because it can cause severe hole erosion (Rabia, 1985). But turbulent flow on the other hand enables a better transport of the drilling cuttings to the surface.

2.2. Hydrodynamic behaviour of a particle

- **Terminal Settling Velocity**

The terminal settling velocity is defined as the constant velocity at which a particle falls in a stationary fluid.

More precisely, a spherical particle of diameter D_p moving at a velocity V through a stationary fluid of density ρ experiences various fluid forces, which result in a force, called *drag force*. The drag force (D) has then for expression:

$$D = C_D \,.\, 1/8 \,.\, \rho \,.\, V^2 \,.\, \pi \,.\, D_p^{\,2} \qquad \text{(A1.1)}$$

where C_D is a dimensionless factor called drag coefficient.

The force balance of a particle between the drag force, the weight of the sphere and the buoyant force, once a constant velocity has been reached, yields the expression for the terminal settling velocity V_T:

$$V_T = [4.g.D_p.(\rho_p/\rho_{fl} - 1) / (3.C_D)] \qquad \text{(A1.2)}$$

where V_T in m/s, D_p in m, ρ_p and ρ_{fl} respectively the density of the solid particle and the density of the fluid in kg/m^3 and g the gravitational constant in m/s^2.

Depending on the nature of flow (reflected by the particle Reynolds Number, Re_p), the drag coefficient takes different values, as presented in Table A1.7 below. The values were established for limestone and shale cuttings from field drilling operation in a mixture of water and glycerine (Moore, 1974).

Table A1.7. Drag coefficient formula and nature of flow according to the Reynold's number.

Reynolds Number Re_p	Nature of flow	Drag Coefficient CD
$Re_p \leq 1.0$	Laminar	$C_D = 40 / Re_p$
$10 \leq Re_p \leq 100$	Laminar	$C_D = 22 / Re_p^{0.5}$
$2000 \leq Re_p$	Turbulent	$C_D = 1.50$

- **Velocity of the particle**

The behaviour of a particle in a fluid in movement depends on the relative values of the terminal settling velocity of the particle and the fluid velocity.

In the case we are interested in the fluid is moving upwards. Four cases can be distinguished (Michell, 1970):

- If the fluid velocity is equal to zero, then the particle is simply moving downwards with a velocity equal to its terminal settling velocity.
- If the fluid velocity is lower than the terminal settling velocity of the particle, then the particle is moving downwards at a velocity equal to the difference of the terminal settling velocity and the fluid velocity.
- If the fluid velocity is equal to the terminal settling velocity, then the particle is suspended in the fluid.
- If the fluid velocity is greater than the terminal settling velocity, then the particle is moving upwards at a velocity equal to the difference of the fluid velocity and the terminal settling velocity.

These relations enable us to obtain the average velocity of a solid particle, based on the average velocity of the fluid in the annulus.

Nevertheless, the velocity of the fluid in the annulus changes with the radius: close to the walls of the annulus, the fluid velocity is less than V_T the terminal settling velocity of the particle, while in the central part of the annulus the velocity of the fluid is greater than V_T. Thus, in the middle of the stream, the recovery of solids may be faster than anticipated and next to the pipe walls some particles may never reach the surface (Moore, 1974).

2.3. Viscosity of drilling muds

The term viscosity was first introduced to represent the thickness of a Newtonian fluid in a laminar flow. Later the concept of thickness and viscosity became synonymous for drilling fluids regardless of flow pattern and it has become common practice to refer to mud thickness as viscosity (Rabia, 1985). The relation between the shear stress τ and its shear strain γ is different according to the model used, as shown below for three of them.

♦ For the Bingham plastic model, two parameters, the plastic viscosity (PV) and the yield point (YP) are used:

$$\tau = YP + PV \cdot \gamma \qquad \text{(A1.3)}$$

This model represents fairly well the behaviour of bentonite slurries (Hemphill, 1993).

♦ For the power-law model, two parameters n and K are used:

$$\tau = K.(\gamma)^n \qquad \text{(A1.4)}$$

This model fits better the behaviour of polymer-based fluids than the Bingham plastic model (Hemphill, 1993).

The power-Law is more accurate than Bingham for quantitative calculation (Moore, 1974)

♦ For the yield power-law (Herschel-Bulkley) model, three parameters τ_0, n and K define the relation:

$$\tau = \tau_0 + K.(\gamma)^n \qquad \text{(A1.5)}$$

2.4. Velocity profiles of fluids

In order to fully understand the behaviour of the particles in the annulus, the velocity profile has to be known. Hereafter, the equations governing the velocity of two kinds of fluids have been reported. Further developments will present the equations for the Bingham-plastic model.

- **Newtonian fluid**

A Newtonian fluid is defined as a fluid for which the shear stress is proportional to the shear strain. The proportional factor is defined as the viscosity μ of the fluid. Drilling muds do not have the behaviour of Newtonian fluids, nevertheless, the Newtonian case can always be taken as a limit case and also bring useful information.

Solving the momentum balance in an annulus of internal radius R_1 and external radius R_2 yields the following results (Munson *et al.*, 1990):

- A radius R_m, at which the velocity is at a maximum in the annulus

$$R_m = \sqrt{\left(R_2^{\,2} - R_1^{\,2}\right) / \left(2\ln\left(\frac{R_2}{R_1}\right)\right)} \qquad \text{(A1.6)}$$

- Velocity of the fluid, at a radius r, depending on the volume flow rate of the fluid Q, and the two radii R_1 and R_2:

$$v(r) = \frac{2Q}{\pi} \cdot \frac{R_2^{\,2} - r^2 - \left(R_2^{\,2} - R_1^{\,2}\right) \cdot \ln\left(\frac{r}{R_2}\right) / \ln\left(\frac{R_1}{R_2}\right)}{R_2^{\,4} - r^4 - \left(R_2^{\,2} - R_1^{\,2}\right)^2 / \ln\left(\frac{R_1}{R_2}\right)} \qquad \text{(A1.7)}$$

- **Power-law fluid**

For a power-law fluid in an annulus of internal radius R_1 and external radius R_2, the momentum balance yields (Frederickson, 1958):

- Dimensionless radius λ (R_m/R_2), at which the velocity is at a maximum in the annulus, is solution of the following equation

$$\int_{\kappa}^{\lambda} \left(\frac{\lambda^2}{\phi} - \phi\right)^{1/n} d\phi = \int_{\lambda}^{1} \left(\phi - \frac{\lambda^2}{\phi}\right)^{1/n} d\phi \qquad \text{(A1.8)}$$

where $\kappa = R_1/R_2$ and ϕ is the dimensionless radius appearing in the integrals.

- The pressure-drop term ΔP is then given by solving:

$$Q = \pi R_2^3 \left(\frac{\Delta P \cdot R_2}{2K}\right)^{1/n} \cdot \int_{\kappa}^{1} \phi^{-1/n} \left|\lambda^2 - \phi^2\right|^{1+1/n} d\phi \quad \text{(A1.9)}$$

where $\Delta P = \dfrac{P_L - P_0}{L} - \rho g$

Q, is the volume flow rate of the fluid, P_L the pressure at the bottom of the annulus,
P_0 the pressure at the top of the annulus and L the length of the annulus,
ρ the density of the fluid and g, the gravitational constant,
ϕ is the dimensionless radius appearing in the integral.

- Finally, the velocity is given by the following expressions

when $R_1 \leq r \leq R_m$

$$v(r) = R_2 \left(\frac{\Delta P \cdot R_2}{2K}\right)^{1/n} \cdot \int_{\kappa}^{r/R_2} \left(\frac{\lambda^2}{\phi} - \phi\right)^{1/n} d\phi \qquad \text{(A1.10)}$$

when $R_m \leq r \leq R_2$

$$v(r) = R_2 \left(\frac{\Delta P \cdot R_2}{2K}\right)^{1/n} \cdot \int_{r/R_2}^{1} \left(\phi - \frac{\lambda^2}{\phi}\right)^{1/n} d\phi \qquad \text{(A1.11)}$$

with ϕ is the dimensionless radius appearing in the integrals.

Appendix 2. Solubility data for methane

All experimental data are reported with their original unit and converted when needed into K for temperature, bar for pressure and molar ppm for the composition. For the composition, the index 1 refers to hydrocarbon in the binary mixture with water. The letter x refers to the molar fraction of a component in an aqueous liquid phase, the letter x' refers to composition of a hydrocarbon liquid phase and the letter y to a vapour/gas phase.

Amirijafari B., Campbell J.M., "Solubility of gaseous hydrocarbon mixtures in water", SPE J., 12, 21-27 (1972)

P	P	T	T	x[1]	x[1]
psia	bar	°F	K	mol frac	ppm
600	41.37	100	310.9	0.000759	759
600	41.37	160	344.3	0.000602	602
2000	137.90	100	310.9	0.001956	1956
2000	137.90	160	344.3	0.001612	1612
3000	206.84	100	310.9	0.002519	2519
3000	206.84	160	344.3	0.00215	2150
5000	344.74	100	310.9	0.00335	3350
5000	344.74	160	344.3	0.0028	2800

Claussen W. F., M. F. Polglase, "Solubilities and structures in aqueous aliphatic hydrocarbon solutions", J. Am. Chem. Soc. 74, 4817-4819 (1952)

P	T	T	x[1]	x[1]
bar	deg C	K	Bunsen	ppm
1.01325	1.6	274.8	0.0547	44.33
1.01325	2.0	275.2	0.0538	43.67
1.01325	10.5	283.7	0.0428	35.81
1.01325	19.8	293.0	0.0351	30.38
1.01325	30.4	303.6	0.0289	25.99
1.01325	39.6	312.8	0.0255	23.70

Crovetto R., Fernandez-Prini R., Japas M.L., "Solubilities of inert gases and methane in H2O and in D2O in the temperature range of 300 to 600 K",J. Chem. Phys. 76, 1077-1086 (1982)

P	P	T	x[1]	x[1]	y[1]	y[1]
MPa	bar	K	mol frac * 1e4	ppm	mol. frac.	ppm
1.861	18.61	297.5	4.351	435.1	0.9983	998300
1.327	13.27	333.7	2.124	212.4	0.9840	984000
2.092	20.92	385.3	2.985	298.5	0.9226	922600
2.156	21.56	388.4	3.085	308.5	0.9166	916600
2.131	21.31	430.6	3.025	302.5	0.7147	714700
3.21	32.1	473.2	4.146	414.6	0.4873	487300
6.451	64.51	518.3	10.337	1033.7	0.3875	387500

Culberson O.L., Horn A.B., McKetta Jr. J.J., "Phase equilibria in hydrocarbon-water systems: the solubility of ethane in water at pressures to 1200 pounds per square inch", J. Petrol. Tech. 2, or Petrol. Trans. AIME 189, 1-6 (1950)

P	P	T	T	n(C1)/n(H2O)	x[1]	x[1]
psia	bar	°F	K			ppm
525	36.20	77	298.15	0.00077	0.000769408	769.4
1000	68.95	77	298.15	0.00110	0.001098791	1098.8
1450	99.97	77	298.15	0.00180	0.001796766	1796.8
1845	127.21	77	298.15	0.00202	0.002015928	2015.9
1930	133.07	77	298.15	0.00227	0.002264859	2264.9
2535	174.78	77	298.15	0.00231	0.002304676	2304.7
3615	249.25	77	298.15	0.00288	0.002871729	2871.7
4435	305.78	77	298.15	0.00328	0.003269277	3269.3
6342	437.27	77	298.15	0.00407	0.004053502	4053.5
7935	547.10	77	298.15	0.00391	0.003894771	3894.8
9680	667.41	77	298.15	0.00451	0.004489751	4489.8

Culberson O.L., McKetta Jr. J.J., "Phase equilibria in hydrocarbon-water systems. IV - Vapor-liquid equilibrium constants in the methane-water and ethane-water systems", Trans AIME, Pet. Div. 192, 297-300 (1951)

P	P	T	T	y[2]	y[1]
psia	bar	°F	K	mol frac *1000	(ppm)
758	52.26	100	310.93	1.770	998230
1600	110.32	100	310.93	0.762	999238
2375	163.75	100	310.93	0.745	999255
3615	249.25	100	310.93	0.483	999517
5185	357.49	100	310.93	0.502	999498

Davis J.E., McKetta J.J., "Solubility of methane in water", Petroleum Refiner Vol. 39, 3, 205-206 (1960)

P	P	T	T	x[1]	x[1]
psia	bar	deg F	K	mol. frac. * 1e4	ppm
50	3.45	100	310.9	0.70	70.0
50	3.45	130	327.6	0.53	53.0
50	3.45	160	344.3	0.46	46.0
50	3.45	190	360.9	0.44	44.0
50	3.45	220	377.6	0.39	39.0
50	3.45	250	394.3	0.24	24.0
100	6.89	100	310.9	1.39	139.0
100	6.89	130	327.6	1.08	108.0
100	6.89	160	344.3	0.98	98.0
100	6.89	190	360.9	0.99	99.0
100	6.89	220	377.6	0.98	98.0
100	6.89	250	394.3	0.85	85.0
150	10.34	100	310.9	2.09	209.0
150	10.34	130	327.6	1.63	163.0
150	10.34	160	344.3	1.49	149.0
150	10.34	190	360.9	1.53	153.0
150	10.34	220	377.6	1.57	157.0
150	10.34	250	394.3	1.46	146.0
200	13.79	100	310.9	2.79	279.0
200	13.79	130	327.6	2.19	219.0
200	13.79	160	344.3	2.01	201.0
200	13.79	190	360.9	2.09	209.0
200	13.79	220	377.6	2.16	216.0
200	13.79	250	394.3	2.07	207.0
250	17.24	100	310.9	3.49	349.0
250	17.24	130	327.6	2.74	274.0
250	17.24	160	344.3	2.53	253.0
250	17.24	190	360.9	2.64	264.0
250	17.24	220	377.6	2.75	275.0
250	17.24	250	394.3	2.68	268.0
300	20.68	100	310.9	4.18	418.0
300	20.68	130	327.6	3.29	329.0
300	20.68	160	344.3	3.04	304.0
300	20.68	190	360.9	3.19	319.0
300	20.68	220	377.6	3.34	334.0
350	24.13	100	310.9	4.88	488.0
350	24.13	130	327.6	3.87	387.0
350	24.13	160	344.3	3.56	356.0
350	24.13	190	360.9	3.74	374.0
350	24.13	220	377.6	3.93	393.0
400	27.58	100	310.9	5.58	558.0
400	27.58	130	327.6	4.40	440.0
400	27.58	190	360.9	4.29	429.0

Dhima A., De Hemptinne J.C., Moracchini G., "Solubility of light hydrocarbons and their mixtures in pure water under high pressure", Fluid Phase Equilibria, 145, 129-150 (1998)

P	P	T	T	x[1]	x[1]
Mpa	bar	deg C	K	% mol.	ppm
20	200	71	344.15	0.2183	2183
50	500	71	344.15	0.3723	3723
75	750	71	344.15	0.466	4660
100	1000	71	344.15	0.5085	5085

Duffy J.R., Smith N.O., Nagy B., "Solubility of natural gases in aqueous salt solutions - I. Liquidus surfaces in the system CH4-H2O-NaCl-CaCl2 at room temperatures and at pressures below 1000 psia", Geochem. Et Cosmochim. Acta, 24, 23-31 (1961)

P	T	x[1]	x[1]
(bar)	(K)	(mol frac)	(ppm)
3.17	303.15	6.00E-05	60
5.57	303.15	1.15E-04	115
7.93	303.15	1.84E-04	184
9.38	303.15	2.32E-04	232
11.03	298.15	2.14E-04	214
14.82	298.15	2.73E-04	273
15.86	298.15	3.76E-04	376
19.72	303.15	4.90E-04	490
20.48	303.15	4.93E-04	493
27.44	303.15	6.12E-04	612
29.65	298.15	7.08E-04	708
30.68	298.15	7.03E-04	703
35.44	298.15	8.00E-04	800
36.06	303.15	7.64E-04	764
40.33	298.15	9.39E-04	939
46.88	298.15	9.79E-04	979
51.71	298.15	1.13E-03	1130

Gillepsie P.C., Wilson G.M., "Vapor-liquid and liquid-liquid equilibria: water-methane, water-carbon dioxide, water-hydrogen sulfide, water-n-pentane, water-methane-n-pentane", Gas processors Association Research Report RR-48, Provo, Utah, April (1982)

P	P	T	T	x[1]	x[1]	y[1]	y[1]
psia	bar	deg F	K	mol. frac.	ppm	mol. frac.	ppm
200	13.79	122	323.2	0.000222	222.00	0.99036	990360
200	13.79	167	348.2	0.000188	188.00	0.97065	970650
200	13.79	302	423.2	0.000173	173.00	0.64540	645400
900	62.05	122	323.2	0.000945	945.00	0.99755	997550
900	62.05	167	348.2	0.000842	842.00	0.99290	992900
900	62.05	302	423.2	0.001000	1000.00	0.91500	915000
900	62.05	400	477.6	0.001260	1260.00	0.69640	696400
1500	103.42	400	477.6	0.002330	2330.00	0.79950	799500
1500	103.42	500	533.2	0.002840	2840.00	0.49040	490400
2000	137.90	122	323.2	0.001770	1770.00	0.99864	998640
2000	137.90	167	348.2	0.001640	1640.00	0.99634	996340
2000	137.90	302	423.2	0.002090	2090.00	0.95700	957000
2000	137.90	400	477.6	0.003170	3170.00	0.83900	839000
2000	137.90	500	533.2	0.004450	4450.00	0.59790	597900
2000	137.90	600	588.7	0.003370	3370.00	0.16780	167800
2450	168.92	600	588.7	0.006760	6760.00	0.25400	254000

Kertes A.S. (ed.), IUPAC Solubility Data Series, Vol 27/28 (1987)

P	T	x[1]	x[1]
bar	K	mol. frac	ppm
1.01325	273.15	4.6666E-05	46.67
1.01325	278.15	4.0221E-05	40.22
1.01325	283.15	3.5192E-05	35.19
1.01325	288.15	3.1224E-05	31.22
1.01325	293.15	2.8062E-05	28.06
1.01325	298.15	2.5523E-05	25.52
1.01325	303.15	2.3469E-05	23.47
1.01325	308.15	2.1802E-05	21.80
1.01325	313.15	2.0445E-05	20.45
1.01325	318.15	1.9340E-05	19.34
1.01325	323.15	1.8442E-05	18.44
1.01325	328.15	1.7717E-05	17.72
1.01325	333.15	1.7138E-05	17.14
1.01325	338.15	1.6683E-05	16.68
1.01325	343.15	1.6336E-05	16.34
1.01325	348.15	1.6082E-05	16.08
1.01325	353.15	1.5911E-05	15.91
1.01325	358.15	1.5815E-05	15.82
1.01325	363.15	1.5785E-05	15.79
1.01325	368.15	1.5817E-05	15.82
1.01325	373.15	1.5905E-05	15.91

Kertes, (1987) continuing

P	T	x[1]	x[1]
bar	K	mol. frac	ppm
5	300	1.6910E-04	169.10
5	325	1.3010E-04	130.10
5	350	1.1640E-04	116.40
5	375	1.1660E-04	116.60
5	400	1.2740E-04	127.40
5	425	1.4860E-04	148.60
10	300	2.8500E-04	285.00
10	325	2.1920E-04	219.20
10	350	1.9620E-04	196.20
10	375	1.9660E-04	196.60
10	400	2.1470E-04	214.70
10	425	2.5040E-04	250.40
10	450	3.0720E-04	307.20
100	300	1.6140E-03	1614.00
100	325	1.2420E-03	1242.00
100	350	1.1110E-03	1111.00
100	375	1.1140E-03	1114.00
100	400	1.2160E-03	1216.00
100	425	1.4180E-03	1418.00
100	450	1.7400E-03	1740.00
100	475	2.2200E-03	2220.00
100	500	2.9180E-03	2918.00
100	525	3.9250E-03	3925.00
100	550	5.3760E-03	5376.00
100	575	7.4630E-03	7463.00
500	300	5.4300E-03	5430.00
500	325	4.1700E-03	4170.00
500	350	3.7300E-03	3730.00
500	375	3.7400E-03	3740.00
500	400	4.0900E-03	4090.00
500	425	4.7700E-03	4770.00
500	450	5.8500E-03	5850.00
500	475	7.4600E-03	7460.00
500	500	9.8100E-03	9810.00
500	525	1.3190E-02	13190.00
500	550	1.8070E-02	18070.00
500	575	2.5080E-02	25080.00
500	600	3.5170E-02	35170.00
500	625	4.9690E-02	49690.00

Joffrion L. L., Eubank P. T., "P-V-T Data and Virial coefficients for gaseous methane-water mixtures with correction for adsorption effects", Fluid Phase Equilib. 43, 263-294 (1988)

P	P	T	y[2]	y[1]
Mpa	bar	K	mol. frac.	ppm
4.0323	40.323	481.85	0.5	500000
2.6676	26.676	463.18	0.5	500000
1.7608	17.608	445.65	0.5	500000
1.1625	11.625	429.52	0.5	500000
0.7654	7.654	414.28	0.5	500000
0.5044	5.044	400.23	0.5	500000
0.3321	3.321	387.22	0.5	500000
0.2188	2.188	375.01	0.5	500000
0.1437	1.437	362.51	0.5	500000
0.095	0.95	353.17	0.5	500000
0.0627	0.627	343.26	0.5	500000
8.2641	82.641	478.25	0.25	750000
5.4345	54.345	461.02	0.25	750000
3.5727	35.727	444.18	0.25	750000
2.3505	23.505	428.4	0.25	750000
1.546	15.46	413.53	0.25	750000
1.0172	10.172	399.63	0.25	750000
0.667	6.67	386.38	0.25	750000
0.4411	4.411	374.66	0.25	750000
0.2907	2.907	363.5	0.25	750000
0.1913	1.913	352.45	0.25	750000
10.6243	106.243	447.58	0.1	900000
6.9542	69.542	432.35	0.1	900000
4.5735	45.735	418.05	0.1	900000
3.0116	30.116	404.41	0.1	900000
1.9849	19.849	391.56	0.1	900000
1.3085	13.085	379.59	0.1	900000
0.8617	8.617	367.65	0.1	900000
0.5686	5.686	356.85	0.1	900000

Lannung A., Gjaldbæk J.C., Acta Chem. Scand. 14, 1124-1128 (1960)

P	T	T	x[1]	x[1]
bar	deg C	K	Bunsen	ppm
1.01325	18.0	291.2	0.0352	30.27
1.01325	25	298.2	0.0313	27.60
1.01325	37	310.2	0.026	23.94

Lekvam K., P. R. Bishnoi, "Dissolution of methane in water at low temperatures and intermediate pressures", Fluid Phase Equilibria 131, 297-309 (1997)

P	T	x[1]	x[1]
bar	K	mol. frac.	ppm
5.67	274.4	0.000258	258
10.05	274.48	0.000399	399
15.05	274.48	0.000592	592
17.65	274.28	0.000735	735
17.65	283.37	0.000562	562
23.31	285.67	0.000656	656
24.81	274.19	0.000966	966
25.15	274.29	0.000978	978
25.32	274.29	0.00096	960
27.98	285.65	0.000778	778
27.99	283.37	0.000832	832
28.06	274.38	0.001142	1142
45.99	283.37	0.001123	1123
46.3	279.38	0.001378	1378
70.46	283.37	0.001851	1851
70.58	285.37	0.001639	1639
87.89	285.67	0.001881	1881
90.82	285.68	0.002002	2002

McAuliffe C., "Solubility in water of paraffin, cycloparaffin, olefin, acetylene, cycloolefin, and aromatic hydrocarbons", J. Phys. Chem., 70 No 4, 1267-1275 (1966)

P	T	T	x[1]	x[1]
bar	deg C	K	g HC / 10e6 g H2O	ppm
1.01325	25.0	298.2	24.4	27.40

Michels A., Gerver J., Biji A., Physica 3, 797-808 (1936)

P	T	x[1]	x[1]
bar	K	mol frac	ppm
40.60	298.15	0.00081	810
44.30	348.15	0.00061	610
46.00	298.15	0.00090	900
47.10	423.15	0.00062	620
49.00	373.15	0.00066	660
49.00	398.15	0.00064	640
49.60	323.15	0.00072	720
79.20	348.15	0.00101	1010
81.30	298.15	0.00128	1280
81.70	423.15	0.00093	930
82.10	398.15	0.00098	980
82.20	373.15	0.00101	1010
82.30	323.15	0.00112	1120
110.80	423.15	0.00119	1190
112.00	298.15	0.00158	1580
113.00	373.15	0.00127	1270
113.00	398.15	0.00124	1240
113.10	323.15	0.00142	1420
114.50	348.15	0.00133	1330
145.40	423.15	0.00142	1420
145.60	323.15	0.00169	1690
145.90	298.15	0.00187	1870
148.10	348.15	0.00157	1570
148.30	373.15	0.00152	1520
150.00	398.15	0.00150	1500
176.20	348.15	0.00174	1740
176.50	298.15	0.00210	2100
176.50	323.15	0.00190	1900
177.80	423.15	0.00160	1600
180.50	373.15	0.00171	1710
181.10	398.15	0.00166	1660
204.90	298.15	0.00228	2280
206.10	423.15	0.00173	1730
208.00	348.15	0.00193	1930
208.20	323.15	0.00207	2070
209.20	373.15	0.00184	1840
212.30	398.15	0.00179	1790
330.80	298.15	0.00268	2680
469.10	298.15	0.00297	2970

Olds R.H., Sage B.H., Lacey W.N., "Phase equilibria in Hydrocarbon systems. Composition of the dew-point gas of the methane-water system", Industrial and Engineering Chemistry, 34, 10, 1223-1227 (1942)

P	P	T	T	y[2]	y[1]
psia	bar	deg F	K	mol. frac. * 1000	ppm
1205.4	83.11	100	310.93	1.278	998722
1249.6	86.16	100	310.93	1.467	998533
1955.9	134.85	100	310.93	0.671	999329
1989.3	137.16	100	310.93	0.671	999329
3019.4	208.18	100	310.93	0.645	999355
3025.8	208.62	100	310.93	0.630	999370
4049.1	279.18	100	310.93	0.423	999577
5027.7	346.65	100	310.93	0.506	999494
6049.8	417.12	100	310.93	0.484	999516
7037.5	485.22	100	310.93	0.423	999577
8029.7	553.63	100	310.93	0.427	999573
9042.4	623.45	100	310.93	0.408	999592
387.6	26.72	160	344.26	13.350	986650
912.2	62.89	160	344.26	6.417	993583
1398.9	96.45	160	344.26	4.503	995497
2088.4	143.99	160	344.26	3.394	996606
3055.0	210.63	160	344.26	2.721	997279
4090.8	282.05	160	344.26	2.301	997699
5098.4	351.52	160	344.26	2.128	997872
6061.7	417.94	160	344.26	1.890	998110
9885.0	681.55	160	344.26	1.692	998308
433.2	29.87	220	377.59	42.810	957190
955.9	65.91	220	377.59	20.690	979310
1351.1	93.16	220	377.59	15.450	984550
2003.0	138.10	220	377.59	11.200	988800
3034.6	209.23	220	377.59	8.459	991541
4046.7	279.01	220	377.59	7.123	992877
5136.0	354.11	220	377.59	6.253	993747
6059.9	417.82	220	377.59	5.788	994212
6999.6	482.61	220	377.59	5.336	994664
7937.2	547.25	220	377.59	5.238	994762
8104.7	558.80	220	377.59	4.943	995057
9029.2	622.54	220	377.59	4.882	995118
9040.4	623.31	220	377.59	4.620	995380
9918.8	683.88	220	377.59	4.722	995278
494.0	34.06	280	410.93	12.06	987940
949.4	65.46	280	410.93	12.53	987470
1431.5	98.70	280	410.93	13.45	986550
2040.1	140.66	280	410.93	14.37	985630
4084.5	281.62	280	410.93	15.45	984550
5161.4	355.87	280	410.93	16.71	983290
6107.1	421.07	280	410.93	18.98	981020
7010.4	483.35	280	410.93	31.52	968480

Olds (1942), continuing

P	P	T	T	y[2]	y[1]
psia	bar	deg F	K	mol. frac. * 1000	ppm
8043.8	554.60	280	410.93	41.45	958550
9022.0	622.04	280	410.93	58.99	941010
9987.4	688.61	280	410.93	110.83	889170
499.2	34.42	340	444.26	253.34	746660
1268.3	87.45	340	444.26	109.35	890650
2064.9	142.37	340	444.26	71.06	928940
3072.0	211.81	340	444.26	53.62	946380
4084.2	281.60	340	444.26	43.84	956160
5015.1	345.78	340	444.26	38.35	961650
6073.0	418.72	340	444.26	34.57	965430
7072.7	487.65	340	444.26	31.54	968460
8086.9	557.57	340	444.26	29.71	970290
9057.4	624.49	340	444.26	27.65	972350
9989.5	688.75	340	444.26	26.16	973840
487.8	33.63	400	477.59	555.57	444430
930.2	64.14	400	477.59	302.67	697330
1280.1	88.26	400	477.59	228.27	771730
2037.1	140.45	400	477.59	154.18	845820
3015.5	207.91	400	477.59	113.60	886400
5047.5	348.01	400	477.59	79.61	920390
6009.2	414.32	400	477.59	70.24	929760
7038.1	485.26	400	477.59	65.19	934810
8074.9	556.74	400	477.59	60.82	939180
9076.5	625.80	400	477.59	56.30	943700
9969.0	687.34	400	477.59	53.28	946720
771.3	53.18	460	510.93	654.59	345410
1379.3	95.10	460	510.93	400.33	599670
2094.2	144.39	460	510.93	285.10	714900
3046.7	210.06	460	510.93	212.87	787130
4015.4	276.85	460	510.93	175.66	824340
5163.8	356.03	460	510.93	148.39	851610
6047.1	416.93	460	510.93	133.88	866120
7039.0	485.32	460	510.93	123.91	876090
7823.8	539.43	460	510.93	111.89	888110
9064.8	625.00	460	510.93	106.41	893590

O'Sullivan T.D., Smith N.O., "The solubility and partial molar volume of nitrogen and methane in water and in aqueous sodium chloride from 50 to 125° and 100 to 600 atm", J. Phys. Chem., 74 (7), 1460-1466 (1970)

P	P	T	T	x[1]	x[1]
atm	bar	°C	K	mol frac * 1e4	ppm
100	101.33	51.5	324.65	14.27	1427
101	102.34	102.5	375.65	13.55	1355
103	104.36	125	398.15	14.34	1434
200	202.65	51.5	324.65	22.79	2279
201	203.66	102.5	375.65	22.05	2205
204	206.70	125	398.15	23.21	2321
300	303.98	51.5	324.65	28.70	2870
302	306.00	102.5	375.65	28.70	2870
305	309.04	125	398.15	29.60	2960
400	405.30	51.5	324.65	33.40	3340
403	408.34	102.5	375.65	33.30	3330
405	410.37	125	398.15	34.30	3430
500	506.63	51.5	324.65	37.30	3730
503	509.66	102.5	375.65	38.50	3850
507	513.72	125	398.15	39.60	3960
600	607.95	51.5	324.65	40.90	4090
604	612.00	102.5	375.65	41.90	4190
608	616.06	125	398.15	43.00	4300

Price L.C., "Aqueous solubility of methane at elevated pressures and temperatures", Am. Assoc. Pet. Geol. Bull., 63, 1527-1533 (1979)

P	P	t	T	x[1]	x[1]
psi	bar	°C	K	SCF/bbl	ppm
514	35.4	154	427.15	5.65	740.7
2205	152.0	154	427.15	21.81	2859.3
4645	320.3	154	427.15	34.43	4513.8
6790	468.2	154	427.15	42.03	5510.1
9760	672.9	154	427.15	46.72	6125.0
12670	873.6	154	427.15	49.78	6526.2
15260	1052.1	154	427.15	58.76	7703.4
18260	1259.0	154	427.15	67.37	8832.2
23780	1639.6	154	427.15	78.76	10325.4
750	51.7	206	479.15	9.51	1246.8
2323	160.2	206	479.15	30.82	4040.5
4270	294.4	206	479.15	48.12	6308.5
7923	546.3	206	479.15	72.36	9486.4
13759	948.6	206	479.15	98.11	12862.2
18906	1303.5	206	479.15	116.50	15273.2
23652	1630.7	206	479.15	127.00	16649.7
27915	1924.7	206	479.15	143.50	18812.9
583	40.2	221	494.15	9.73	1275.6
5331	367.6	221	494.15	62.87	8242.3

Price, (1979), continuing

P	P	t	T	x[1]	x[1]
psi	bar	°C	K	SCF/bbl	ppm
9109	628.0	221	494.15	101.7	13332.9
12670	873.6	221	494.15	116.4	15260.0
15020	1035.6	221	494.15	131.4	17226.5
17940	1236.9	221	494.15	135.3	17737.8
20530	1415.5	221	494.15	139.4	18275.3
1176	81.1	234	507.15	19.92	2611.5
2160	148.9	234	507.15	34.91	4576.7
3014	207.8	234	507.15	54.75	7177.7
4027	277.7	234	507.15	63.97	8386.5
6836	471.3	234	507.15	108.2	14185.0
8658	596.9	234	507.15	117.3	15378.0
11330	781.2	234	507.15	140	18354.0
13540	933.6	234	507.15	150.8	19769.9
15690	1081.8	234	507.15	161.9	21225.1
15770	1087.3	234	507.15	159.2	20871.1
19230	1325.9	234	507.15	169.3	22195.2
21340	1471.3	234	507.15	172.1	22562.3
23830	1643.0	234	507.15	181	23729.1
2866	197.6	280	553.15	65	8521.5
4616	318.3	280	553.15	101.6	13319.8
6953	479.4	280	553.15	160	20976.0
10170	701.2	280	553.15	206.3	27045.9
14490	999.1	280	553.15	252.3	33076.5
18330	1263.8	280	553.15	264.9	34728.4
22020	1518.2	280	553.15	282.8	37075.1
23120	1594.1	280	553.15	292.5	38346.8
27400	1889.2	280	553.15	308.4	40431.2
1566	108.0	292	565.15	22.59	2961.5
2770	191.0	292	565.15	67.26	8817.8
4337	299.0	292	565.15	115.2	15102.7
13130	905.3	292	565.15	278.3	36485.1
15940	1099.0	292	565.15	293.9	38530.3
22050	1520.3	292	565.15	336.1	44062.7
24500	1689.2	292	565.15	349.9	45871.9
1632	112.5	316	589.15	11.2	1468.3
3631	250.3	316	589.15	132.2	17331.4
7747	534.1	316	589.15	321.2	42109.3
10440	719.8	316	589.15	377.9	49542.7
13390	923.2	316	589.15	421.1	55206.2
17010	1172.8	316	589.15	474	62141.4
23990	1654.1	316	589.15	509.1	66743.0
27750	1913.3	316	589.15	527.6	69168.4
2837	195.6	354	627.15	46.79	6134.2
3631	250.3	354	627.15	134.7	17659.2
4689	323.3	354	627.15	268.5	35200.4
6174	425.7	354	627.15	422.1	55337.3

Price, (1979), continuing

P	P	t	T	x[1]	x[1]
psi	bar	°C	K	SCF/bbl	ppm
7688	530.1	354	627.15	488.7	64068.6
15820	1090.8	354	627.15	669.7	87797.7
18460	1272.8	354	627.15	700.3	91809.3
24650	1699.6	354	627.15	775.9	101720.5
26940	1857.4	354	627.15	803	105273.3
28610	1972.6	354	627.15	828.8	108655.7

Stoessel R.K., Byrne P.A., Clays Clay Miner, 30, 67-72 (1982a)

P	P	T	x[1]	x[1]
psia	bar	K	molality	ppm
350	24.13	298.15	0.0318	573
550	37.92	298.15	0.0473	851
750	51.71	298.15	0.0623	1121

Stoessel R.K., Byrne P.A.,"Salting-out of methane in single-salt solutions at 25°C and below 800 psia", Geochem. Cosmochim Acta, 46, 1327-1332 (1982b)

P	T	x[1]
bar	K	ppm
24.13	298.15	574
37.92	298.15	869
51.71	298.15	1110

Sultanov R.C., Skripka V.C., Namiot A.Y., "Rastvorimost metana v vode pri novysjennykh temperaturakh i davlenijakh" (Solubility of methane in water at high temperatures and pressures), Gazova Promyshlennost, v. 17, May, 6-7 (1972a) (in russian)

P	P	T	T	x[1]	x[1]
psia	bar	°C	K	SCF/bbl	ppm
711	49.0	150	423.15	6.13	803.6
711	49.0	200	473.15	7.6	996.4
1422	98.0	150	423.15	11.4	1494.5
1422	98.0	200	473.15	16.8	2202.5
1422	98.0	250	523.15	19.8	2595.8
1422	98.0	300	573.15	9.14	1198.3
2133	147.1	150	423.15	17.5	2294.3
2133	147.1	200	473.15	26.7	3500.4
2133	147.1	250	523.15	35.1	4601.6
2133	147.1	300	573.15	45.9	6017.5
2133	147.1	330	603.15	18	2359.8
2845	196.2	150	423.15	22.9	3002.2
2845	196.2	200	473.15	35.2	4614.7
2845	196.2	250	523.15	50.5	6620.6
2845	196.2	300	573.15	79.95	10481.4
2845	196.2	330	603.15	69.1	9059.0
2845	196.2	350	623.15	52.8	6922.1
3556	245.2	150	423.15	25.9	3395.5
3556	245.2	200	473.15	43.6	5716.0
3556	245.2	250	523.15	61.56	8070.5
3556	245.2	300	573.15	112.7	14775.0
3556	245.2	330	603.15	119	15600.9
3556	245.2	350	623.15	130.8	17147.9
3556	245.2	360	633.15	126.9	16636.6
4267	294.2	150	423.15	29	3801.9
4267	294.2	200	473.15	49.8	6528.8
4267	294.2	250	523.15	79.22	10385.7
4267	294.2	300	573.15	141.8	18590.0
4267	294.2	330	603.15	168.8	22129.7
4267	294.2	350	623.15	199.9	26206.9
4267	294.2	360	633.15	217.6	28527.4
5689	392.2	150	423.15	35.9	4706.5
5689	392.2	200	473.15	61.37	8045.6
5689	392.2	250	523.15	101.8	13346.0
5689	392.2	300	573.15	193.5	25367.9
5689	392.2	330	603.15	269.5	35331.5
5689	*392.2*	*350*	*623.15*	*329.5*	*43197.5*
5689	*392.2*	*360*	*633.15*	*403*	*52833.3*
7112	490.4	150	423.15	41.3	5414.4
7112	490.4	200	473.15	68.3	8954.1
7112	490.4	250	523.15	120.6	15810.7
7112	490.4	300	573.15	233.7	30638.1
7112	490.4	330	603.15	349.5	45819.5

Sultanov (1972a) continuing

P	P	T	T	x[1]	x[1]
psia	bar	°C	K	SCF/bbl	ppm
7112	490.4	350	623.15	478.2	62692.0
7112	490.4	360	633.15	596.6	78214.3
8534	588.4	150	423.15	45.9	6017.5
8534	588.4	200	473.15	76.09	9975.4
8534	588.4	250	523.15	135.6	17777.2
8534	588.4	300	573.15	264.9	34728.4
8534	588.4	330	603.15	416.9	54655.6
8534	588.4	350	623.15	613.12	80380.0
8534	588.4	360	633.15	833.2	109232.5
11380	784.6	150	423.15	55.2	7236.7
11380	784.6	200	473.15	91.66	12016.6
11380	784.6	250	523.15	161.7	21198.9
11380	784.6	300	573.15	321.2	42109.3
11380	784.6	330	603.15	561.3	73586.4
11380	784.6	350	623.15	815.45	106905.5
11380	784.6	360	633.15	1117	146438.7
14220	980.4	150	423.15	61.4	8049.5
14220	980.4	200	473.15	101.8	13346.0
14220	980.4	250	523.15	180.7	23689.8
14220	980.4	300	573.15	361.9	47445.1
14220	980.4	330	603.15	639.3	83812.2
14220	980.4	350	623.15	1062.3	139267.5
15645	1078.7	150	423.15	62.1	8141.3
15645	1078.7	200	473.15	105.7	13857.3
15645	1078.7	250	523.15	185.5	24319.1
15645	1078.7	300	573.15	374.4	49083.8
15645	1078.7	330	603.15	664.38	87100.2
15645	1078.7	350	623.15	1181.5	154894.7

Sultanov R.G, Skripka V.G., Namoit A.Y, Zh. Fiz. Khim., 46, 2160 (1972b)

P	T	x[1]	x[1]	y[1]	y[1]
bar	K	mol frac	ppm	mol frac	ppm
98.068	423.2	1.00E-03	1000	9.40E-01	940000
196.140	423.2	1.80E-03	1800	9.63E-01	963000
392.270	423.2	3.00E-03	3000	9.78E-01	978000
588.410	423.2	4.60E-03	4600	9.83E-01	983000
784.540	423.2	5.60E-03	5600	9.84E-01	983500
980.680	423.2	5.60E-03	5600	9.85E-01	985000
98.068	473.2	2.00E-03	2000	8.10E-01	810000
196.140	473.2	3.80E-03	3800	8.92E-01	891500
392.270	473.2	6.70E-03	6700	9.35E-01	935000
588.410	473.2	8.70E-03	8700	9.48E-01	948000
784.540	473.2	1.00E-02	10000	9.55E-01	954500
980.680	473.2	1.04E-02	10400	9.63E-01	963000
98.068	523.2	2.50E-03	2500	5.30E-01	530000
196.140	523.2	6.30E-03	6300	7.33E-01	733000
392.270	523.2	1.17E-02	11700	8.33E-01	832500
588.410	523.2	1.40E-02	14000	8.72E-01	872000
784.540	523.2	1.46E-02	14600	8.98E-01	898000
980.680	523.2	1.51E-02	15100	9.10E-01	910000
98.068	573.2	1.50E-03	1500	9.50E-02	95000
196.140	573.2	7.80E-03	7800	4.36E-01	436000
392.270	573.2	1.85E-02	18500	6.26E-01	626000
588.410	573.2	2.65E-02	26500	6.79E-01	679000
784.540	573.2	3.40E-02	34000	7.15E-01	715000
980.680	573.2	4.07E-02	40700	7.50E-01	750000
196.140	603.2	1.00E-02	10000	1.95E-01	195000
392.270	603.2	3.25E-02	32500	4.17E-01	417000
588.410	603.2	4.64E-02	46400	5.04E-01	504000
784.540	603.2	5.72E-02	57200	5.54E-01	554000
980.680	603.2	6.35E-02	63500	5.85E-01	585000
196.140	623.2	5.30E-03	5300	8.00E-02	80000
392.270	623.2	4.14E-02	41400	2.35E-01	235000
588.410	623.2	7.07E-02	70700	2.98E-01	298000
784.540	623.2	9.55E-02	95500	3.15E-01	315000
980.680	623.2	1.23E-01	123000	3.35E-01	335000
245.170	625.2	1.35E-02	13500	1.39E-01	139000
294.200	625.2	2.30E-02	23000	1.85E-01	185000
392.270	625.2	4.10E-02	41000	2.28E-01	228000
490.340	625.2	5.50E-02	55000	2.49E-01	249000
588.410	625.2	6.60E-02	66000	2.66E-01	266000
686.480	625.2	8.00E-02	80000	2.78E-01	278000
784.540	625.2	1.05E-01	105000	2.75E-01	275000
882.610	625.2	1.25E-01	125000	2.31E-01	231000
916.940	625.2	1.80E-01	180000	1.80E-01	180000
972.840	625.2	1.73E-01	173000	1.73E-01	173000
980.680	625.2	1.25E-01	125000	2.00E-01	200000

Sultanov (1972b) continuing

P	T	x[1]	x[1]	y[1]	y[1]
bar	K	mol frac	ppm	mol frac	ppm
1029.700	625.2	8.20E-02	82000	2.40E-01	240000
1078.700	625.2	6.80E-02	68000	2.47E-01	247000
245.170	628.2	1.65E-02	16500	1.05E-01	105000
294.200	628.2	2.75E-02	27500	1.53E-01	153000
392.270	628.2	5.40E-02	54000	2.05E-01	205000
490.340	628.2	8.30E-02	83000	2.15E-01	215000
588.410	628.2	1.20E-01	120000	1.24E-01	124000
637.440	628.2	1.43E-01	143000	2.04E-01	204000
666.860	628.2	1.72E-01	172000	1.72E-01	172000
245.170	633.2	1.60E-02	16000	8.20E-02	82000
294.200	633.2	2.60E-02	26000	1.19E-01	119000
392.270	633.2	5.00E-02	50000	1.59E-01	159000
490.340	633.2	7.00E-02	70000	1.71E-01	171000
588.410	633.2	9.60E-02	96000	1.57E-01	157000
608.020	633.2	1.28E-01	128000	1.28E-01	128000

Wetlaufer D.B., Malik S.K., Stoller L., Coffin R.L., "Nonpolar group participation in the denaturation of proteins by urea and guanadium salts", J. Am. Chem. Soc., 86, 508-514 (1964)

P	T	T	x[1]	x[1]
bar	deg C	K	(mol HC / l H2O)*1000	ppm
1.01325	5	278.2	2.19	39.45
1.01325	25	298.2	1.41	25.47
1.01325	45	318.2	1.07	19.47

Winkler, Z. Physik. Chem. 9, 171 (1899)

P	P	T	T	x[1]	x[1]
psia	bar	°F	K	mol. frac.	ppm
14.7	1.0135	77	298.2	0.000019	18.6
14.7	1.0135	100	310.9	0.000001	1.0

Winkler L.W., "Die Löslichkeit der Gase in Wasser", Berliner Berichte, 34, 1408-1422 (1901)

P	T	T	x[1]	x[1]
bar	deg C	K	Bunsen	ppm
1.01325	1.6	274.8	0.05307	43.01
1.01325	2.0	275.2	0.05244	42.56
1.01325	10.5	283.7	0.04124	34.51
1.01325	19.8	293.0	0.03322	28.75
1.01325	30.4	303.6	0.02753	24.76
1.01325	39.6	312.8	0.02383	22.15

Yarym-Agaev, N. L.; Sinyavskaya, R. P.; Koliushko, I. I.; Levinton, L. Ya. Zh. Prikl. Khim. (Leningrad) 58, 165 (1985)

P	T	x[1]	x[1]	y[1]	y[1]
bar	K	mol. frac.	ppm	mol. frac.	ppm
25	298.15	0.000599	599	0.99746	997460
25	313.15	0.00049	490	0.99697	996970
25	338.15	0.000405	405	0.99017	990170
50	298.15	0.00112	1120	0.99854	998540
50	313.15	0.000929	929	0.99813	998130
50	338.15	0.000771	771	0.99391	993910
75	298.15	0.00146	1460	0.999066	999066
75	313.15	0.00127	1270	0.99866	998660
75	338.15	0.0011	1100	0.99552	995520
100	298.15	0.0019	1900	0.99918	999180
100	313.15	0.00164	1640	0.99888	998880
100	338.15	0.00136	1360	0.99652	996520
125	298.15	0.00221	2210	0.999416	999416
125	313.15	0.00187	1870	0.999074	999074
125	338.15	0.00162	1620	0.99702	997020

The value reported at 50 bars and 313.15 K was 9290 ppm. It was changed to 920 ppm for a better consistency.

Yang S.O., Cho S.H., Lee H., Lee C.S., "Measurement and prediction of phase equilibria for water + methane in hydrate forming conditions", Fluid Phase Eq. 185, 53-63 (2001)

P	P	T	x[1]	x[1]
MPa	bar	K	mol frac *1000	ppm
2.33	23.3	298.1	0.684	684
4.11	41.1	298.1	0.894	894
4.40	44.0	298.1	1.160	1160
4.88	48.8	298.1	0.988	988
5.65	56.5	298.1	1.300	1300
6.01	60.1	298.1	1.260	1260
6.61	66.1	298.1	1.460	1460
6.72	67.2	298.1	1.310	1310
7.39	73.9	298.1	1.430	1430
7.67	76.7	298.1	1.620	1620
7.82	78.2	298.1	1.490	1490
8.00	80.0	298.1	1.660	1660
8.18	81.8	298.1	1.450	1450
8.40	84.0	298.1	1.740	1740
8.75	87.5	298.1	1.530	1530
9.56	95.6	298.1	1.930	1930
11.68	116.8	298.1	2.100	2100
11.84	118.4	298.1	2.030	2030
12.68	126.8	298.1	2.060	2060

Appendix 3. Solubility data for ethane

Anthony, R. G.; McKetta, J. J., "Phase equilibrium in the ethylene-water system", J. Chem. Eng. Data 12, 17-20 (1967)

P	P	T	T	x[1]	x[1]	y[2]	y[1]
psia	bar	°F	K	mol frac*1000	ppm	mol frac	ppm
372.1	25.7	100	310.9	***	***	0.00267	997330
434.2	29.9	160.1	344.3	***	***	0.01134	988660
1458.2	100.5	220.2	377.7	***	***	0.01322	986780
1566.2	108.0	279.9	410.9	***	***	0.0367	963300
504.7	34.8	160.1	344.3	0.407	407	***	***
2940.7	202.8	160	344.3	0.837	837	***	***
4004.7	276.1	160.2	344.4	1.028	1028	***	***
4085.7	281.7	220.1	377.7	1.153	1153	***	***
3774.7	260.3	220.1	377.7	1.18	1180	***	***

Claussen W. F., Polglase M. F., "Solubilities and structures in aqueous aliphatic hydrocarbon solutions", J. Am. Chem. Soc. 74, 4817-4819 (1952)

P	T	T	x[1]	x[1]
bar	deg C	K	Bunsen	ppm
1.01325	1.5	274.7	0.0937	76.51
1.01325	10.5	283.7	0.0655	55.25
1.01325	17.5	290.7	0.0527	45.59
1.01325	19.8	293.0	0.0496	43.27
1.01325	29.8	303.0	0.0375	33.92
1.01325	39.7	312.9	0.0307	28.77

Coan C.R., King A.D., "Solubility of water in compressed carbon dioxid, nitrous oxide, and ethane. Evidence for hydration of carbon dioxide and nitrous oxide in he gas phase", J. Am. Chem. Soc. 93, 1857-1862 (1971)

P	P	T	T	y[2]	y[1]
atm	bar	°C	K	mol frac	ppm
24.10	24.42	25	298.15	0.00142	998580
29.30	29.69	25	298.15	0.00111	998890
35.50	35.97	25	298.15	0.0009	999100
35.60	36.07	25	298.15	0.00093	999070
22.50	22.80	50	323.15	0.00563	994370
29.30	29.69	50	323.15	0.00432	995680
29.30	29.69	50	323.15	0.00432	995680
29.30	29.69	50	323.15	0.00437	995630
35.30	35.77	50	323.15	0.00354	996460
35.80	36.27	50	323.15	0.00354	996460
23.00	23.30	75	348.15	0.0175	982500
23.40	23.71	75	348.15	0.0169	983100

Coan (1971) continuing

P	P	T	T	y[2]	y[1]
atm	bar	°C	K	mol frac	ppm
29.90	30.30	75	348.15	0.0132	986800
35.80	36.27	75	348.15	0.0109	989100
25.60	25.94	100	373.15	0.0414	958600
28.90	29.28	100	373.15	0.0367	963300
29.50	29.89	100	373.15	0.036	964000
35.90	36.38	100	373.15	0.0296	970400

Culberson O.L., Horn A.B., McKetta Jr. J.J., "Phase equilibria in hydrocarbon-water systems: the solubility of ethane in water at pressures to 1200 pounds per square inch", J. Petrol. Tech. 2, or Petrol. Trans. AIME 189, 1-6 (1950a)

P	P	T	T	x[1]	x[1]
psia	bar	deg F	K	mol. frac. *10000	ppm
59	4.07	100	310.9	0.893	89.3
110	7.58	100	310.9	2.04	204.0
200	13.79	100	310.9	3.11	311.0
340	23.44	100	310.9	5.21	521.0
568	39.16	100	310.9	6.47	647.0
767	52.88	100	310.9	7.09	709.0
1080	74.46	100	310.9	8.01	801.0
113	7.79	160	344.3	0.812	81.2
196	13.51	160	344.3	1.54	154.0
315	21.72	160	344.3	3.09	309.0
512	35.30	160	344.3	4.17	417.0
785	54.12	160	344.3	5.7	570.0
1215	83.77	160	344.3	6.79	679.0
123	8.48	220	377.6	0.698	69.8
212	14.62	220	377.6	1.3	130.0
322	22.20	220	377.6	2.56	256.0
548	37.78	220	377.6	3.91	391.0
752	51.85	220	377.6	5.6	560.0
1120	77.22	220	377.6	6.61	661.0
113	7.79	280	410.9	0.475	47.5
210	14.48	280	410.9	1.58	158.0
320	22.06	280	410.9	2.72	272.0
557	38.40	280	410.9	4.64	464.0
785	54.12	280	410.9	6	600.0
1215	83.77	280	410.9	8.65	865.0
226	15.58	340	444.3	1.4	140.0
334	23.03	340	444.3	2.61	261.0
529	36.47	340	444.3	5.03	503.0
742	51.16	340	444.3	6.71	671.0
1140	78.60	340	444.3	9.7	970.0

Culberson O.L., McKetta Jr. J.J., "Phase equilibria in hydrocarbon-water systems. II - The solubility of ethane in water at pressures to 10,000 psia", Trans AIME, Pet. Div. 189, 319-322 (1950b)

P	P	T	T	x[1]	x[1]
psia	bar	°F	K	mol. frac.	ppm
1925	132.72	100	310.9	0.0008210	821
3115	214.77	100	310.9	0.0008900	890
5035	347.15	100	310.9	0.0010180	1018
5800	399.90	100	310.9	0.0010660	1066
6330	436.44	100	310.9	0.0011050	1105
7605	524.35	100	310.9	0.0010600	1060
9455	651.90	100	310.9	0.0011300	1130
1985	136.86	160	344.3	0.0007880	788
3275	225.80	160	344.3	0.0008950	895
4885	336.81	160	344.3	0.0010110	1011
6485	447.12	160	344.3	0.0010780	1078
7350	506.76	160	344.3	0.0011000	1100
8330	574.33	160	344.3	0.0011780	1178
9650	665.34	160	344.3	0.0011660	1166
1965	135.48	220	377.6	0.0009440	944
2030	139.96	220	377.6	0.0009640	964
2535	174.78	220	377.6	0.0010420	1042
3455	238.21	220	377.6	0.0011320	1132
5320	366.80	220	377.6	0.0012490	1249
7010	483.32	220	377.6	0.0013290	1329
8480	584.68	220	377.6	0.0014340	1434
9935	684.99	220	377.6	0.0015140	1514
979	67.50	280	410.9	0.0008030	803
1470	101.35	280	410.9	0.0010650	1065
2105	145.13	280	410.9	0.0012080	1208
2680	184.78	280	410.9	0.0013840	1384
3585	247.18	280	410.9	0.0015300	1530
5045	347.84	280	410.9	0.0017030	1703
6465	445.75	280	410.9	0.0018670	1867
8055	555.37	280	410.9	0.0019010	1901
9775	673.96	280	410.9	0.0020050	2005
737	50.81	340	444.3	0.000770	770
992	68.40	340	444.3	0.001039	1039
1370	94.46	340	444.3	0.001311	1311
1985	136.86	340	444.3	0.001671	1671
2605	179.61	340	444.3	0.001970	1970
3640	250.97	340	444.3	0.002325	2325
4285	295.44	340	444.3	0.002480	2480
5035	347.15	340	444.3	0.002515	2515
5250	361.97	340	444.3	0.002635	2635
6630	457.12	340	444.3	0.002790	2790
8320	573.64	340	444.3	0.003060	3060
9335	643.63	340	444.3	0.003200	3200
9835	678.10	340	444.3	0.003300	3300

Danneil A., Toedheide K., Franck E. U., "Verdamfungsgleichgewichte und kritische kurven in den systemen äthane/wasser und n-butan/wasser bei hohen drücken", Chem.-Ing.-Tech. 39-13, 816-822 (1967)

P	T	T	x[1]	x[1]	y[1]	y[1]
bar	°C	K	mol. %	ppm	mol. %	ppm
200	200	473.15	0.5	5000	88	880000
500	200	473.15	0.5	5000	93	930000
1000	200	473.15	0.5	5000	93	930000
1500	200	473.15	0.5	5000	93	930000
2000	200	473.15	0.5	5000	93	930000
2500	200	473.15	0.5	5000	93	930000
3000	200	473.15	0.5	5000	93	930000
3500	200	473.15	0.5	5000	93	930000
200	250	523.15	0.7	7000	69	690000
500	250	523.15	1	10000	78.1	781000
1000	250	523.15	1.25	12500	85	850000
1500	250	523.15	1.5	15000	88.5	885000
2000	250	523.15	1.75	17500	90.2	902000
2500	250	523.15	2	20000	90.2	902000
3000	250	523.15	2.25	22500	90.2	902000
3500	250	523.15	2.5	25000	90.2	902000
200	300	573.15	1	10000	45.4	454000
500	300	573.15	2	20000	58.7	587000
1000	300	573.15	2.4	24000	73.4	734000
1500	300	573.15	2.8	28000	82.8	828000
2000	300	573.15	3.2	32000	85.5	855000
2500	300	573.15	3.5	35000	85.5	855000
3000	300	573.15	3.8	38000	85.5	855000
3500	300	573.15	4.1	41000	85.5	855000
200	350	623.15	0.9	9000	15	150000
300	350	623.15	3.5	35000	23	230000
400	350	623.15	6.5	65000	27.5	275000
500	350	623.15	9.9	99000	30.2	302000
600	350	623.15	14.3	143000	30.5	305000
680	350	623.15	22.5	225000	22.5	225000
760	350	623.15	24	240000	24	240000
800	350	623.15	12.5	125000	32	320000
900	350	623.15	9.7	97000	42.3	423000
1000	350	623.15	8.5	85000	48.9	489000
1500	350	623.15	7.5	75000	67.8	678000
2000	350	623.15	7.3	73000	73.8	738000
2500	350	623.15	7.2	72000	75.6	756000
3000	350	623.15	7.1	71000	76	760000
3500	350	623.15	7	70000	76	760000
200	356	629.15	0.9	9000	13.5	135000
300	356	629.15	3.7	37000	21	210000
400	356	629.15	8	80000	22.7	227000
500	356	629.15	17.5	175000	17.5	175000

Danneil (1967) continuing

P	T	T	x[1]	x[1]	y[1]	y[1]
bar	°C	K	mol. %	ppm	mol. %	ppm
1205	356	629.15	29.5	295000	29.5	295000
1300	356	629.15	11.7	117000	54.2	542000
1400	356	629.15	10.6	106000	59.2	592000
1500	356	629.15	10.4	104000	62.5	625000
2000	356	629.15	9.7	97000	70.4	704000
2500	356	629.15	9	90000	73	730000
3000	356	629.15	8.7	87000	74	740000
3500	356	629.15	8.3	83000	74	740000
1680	370	643.15	31.5	315000	31.5	315000
1700	370	643.15	21.1	211000	36.7	367000
1800	370	643.15	13.5	135000	53.7	537000
1900	370	643.15	12.3	123000	58.9	589000
2000	370	643.15	11.4	114000	61.9	619000
2500	370	643.15	9.6	96000	68.4	684000
3000	370	643.15	9.3	93000	71.2	712000
3500	370	643.15	9	90000	72.2	722000
1990	378	651.15	32	320000	32	320000
2000	378	651.15	21.4	214000	36.1	361000
2100	378	651.15	13.7	137000	51.6	516000
2200	378	651.15	11.8	118000	57.4	574000
2500	378	651.15	10.2	102000	65.3	653000
3000	378	651.15	9.9	99000	69	690000
3500	378	651.15	9.6	96000	69.2	692000
2190	385	658.15	32.5	325000	32.5	325000
2200	385	658.15	20.2	202000	41.1	411000
2300	385	658.15	16.7	167000	53.2	532000
2400	385	658.15	15.8	158000	57.5	575000
2500	385	658.15	15.2	152000	60.3	603000
3000	385	658.15	13.3	133000	65.4	654000
3500	385	658.15	12	120000	65.5	655000
3215	400	673.15	34	340000	34	340000
3300	400	673.15	14.5	145000	56.1	561000
3400	400	673.15	13.8	138000	59.1	591000
3500	400	673.15	13.5	135000	59.5	595000
3700	400	673.15	13.2	132000	60.1	601000

Dhima A., De Hemptinne J.C., Moracchini G., "Solubility of light hydrocarbons and their mixtures in pure water under high pressure", Fluid Phase Equilibria, 145, 129-150 (1998)

P	P	T	T	x[1]	x[1]
MPa	bar	deg C	K	% mol.	ppm
20	200	71	344.15	0.0926	926
50	500	71	344.15	0.1146	1146
75	750	71	344.15	0.1284	1284
100	1000	71	344.15	0.1398	1398

Kertes A.S. (ed.), IUPAC Solubility Data Series, Vol 9 (1982)

P	T	x[1]
bar	K	ppm
1.01325	273.15	79.90
1.01325	278.15	65.10
1.01325	283.15	54.00
1.01325	288.15	45.56
1.01325	293.15	39.07
1.01325	298.15	34.01
1.01325	303.15	30.02
1.01325	308.15	26.86
1.01325	313.15	24.34
1.01325	318.15	22.32
1.01325	323.15	20.69

McAuliffe C., "Solubility in water of paraffin, cycloparaffin, olefin, acetylene, cycloolefin, and aromatic hydrocarbons", J. Phys. Chem., 70 No 4, 1267-1275 (1966)

P	T	T	x[1]	x[1]
bar	deg C	K	g HC / g H2O	ppm
1.01325	25.0	298.2	60.4	36.18

Reamer H.H., Olds R.H., Sage B.H., Lacey W.N., "Phase equilibria in hydrocarbon systems, composition of dew-points gas in ethane-water system", Ind. Eng. Chem. 35, 790-793 (1943)

P	P	T	T	y[2]	y[1]
psia	bar	°F	K	mol frac * 1000	ppm
926.3	63.87	100	310.93	1.33	998670
1977.3	136.33	100	310.93	0.802	999198
3091	213.12	100	310.93	0.723	999277
5172.4	356.62	100	310.93	0.623	999377
6982.9	481.45	100	310.93	0.62	999380
8010	552.27	100	310.93	0.656	999344
9010.2	621.23	100	310.93	0.647	999353
320.8	22.12	160	344.26	15.57	984430
6017.4	414.89	160	344.26	2.034	997966
7001.2	482.72	160	344.26	2.19	997810
8992	619.98	160	344.26	1.96	998040
536.6	37.00	220	377.59	33.362	966638
4117.4	283.88	220	377.59	7.224	992776
6106.6	421.04	220	377.59	6.346	993654
7084.8	488.48	220	377.59	5.639	994361
1033.7	71.27	280	410.93	51.982	948018
3049.8	210.28	280	410.93	21.8	978200
5047	347.98	280	410.93	16.235	983765
6096.8	420.36	280	410.93	16.006	983994
7138.7	492.20	280	410.93	14.99	985010
8123.6	560.10	280	410.93	14.404	985596

Reamer (1943) continuing

P	P	T	T	y[2]	y[1]
psia	bar	°F	K	mol frac * 1000	ppm
8985.1	619.50	280	410.93	13.196	986804
9892.1	682.04	280	410.93	12.68	987320
1150.1	79.30	340	444.26	115.76	884240
2998.5	206.74	340	444.26	52.81	947190
4046.8	279.02	340	444.26	43.62	956380
5097.8	351.48	340	444.26	39.17	960830
9003.1	620.74	340	444.26	29.63	970370
9896.3	682.33	340	444.26	27.96	972040
3989.2	275.05	400	477.59	93.73	906270
4945.8	341.00	400	477.59	81.84	918160
5982.1	412.45	400	477.59	74.48	925520
6855.6	472.68	400	477.59	69.11	930890
7979.5	550.17	400	477.59	64.26	935740
9042.9	623.49	400	477.59	59.85	940150
9843.6	678.69	400	477.59	56.26	943740
3983.6	274.66	460	510.93	179.95	820050
5502.8	379.40	460	510.93	148.71	851290
7006.8	483.10	460	510.93	131.81	868190
8503.8	586.32	460	510.93	117.71	882290
9652.7	665.53	460	510.93	110.79	889210

The reported value at 536.6 psia and 220°F is 3.362. It was corrected into 33,362 as the reported value is too low and does not fit with the value showed on Fig 1inthe article.

Wetlaufer D.B., Malik S.K., Stoller L., Coffin R.L., "Nonpolar group participation in the denaturation of proteins by urea and guanadium salts", J. Am. Chem. Soc., 86, 508-514 (1964)

P	T	T	x[1]	x[1]
bar	deg C	K	(mol HC / l H2O)*1000	ppm
1.01325	5	278.2	3.61	65.03
1.01325	25	298.2	1.86	33.60
1.01325	45	318.2	1.25	22.74

Winkler L.W., "Die Löslichkeit der Gase in Wasser", Berliner Berichte, 34, 1408-1422 (1901)

P	T	T	x[1]	x[1]
bar	deg C	K	Bunsen	ppm
1.01325	1.5	274.7	0.0928	75.81
1.01325	10.5	283.7	0.0644	54.35
1.01325	17.5	290.7	0.0508	43.96
1.01325	19.8	293.0	0.0475	41.45
1.01325	29.8	303.0	0.0364	32.93
1.01325	39.7	312.9	0.0293	27.50

Appendix 4. Solubility data for propane

Azarnoosh A., McKetta Jr. J.J., "The solubility of propane in water. (Experimental and smoothed data are given here for pressures from atmospheric to 500 psia and for temperatures from 60 to 280 F", Petrol. Ref. 37, 275-278 (1958)

P	P	T	T	x[1]	x[1]
psia	bar	deg F	K	mo. frac. *1e5	ppm
14.7	1.014	60	288.7	5.89	58.9
20.2	1.39	60	288.7	7.70	77.0
49.8	3.43	60	288.7	19.05	190.5
62.7	4.32	60	288.7	22.44	224.4
84.3	5.81	60	288.7	24.96	249.6
100.5	6.93	60	288.7	25.98	259.8
21.7	1.50	100	310.9	2.34	23.4
33.7	2.32	100	310.9	3.88	38.8
52.5	3.62	100	310.9	6.23	62.3
70.5	4.86	100	310.9	7.70	77.0
84.2	5.81	100	310.9	10.26	102.6
96.7	6.67	100	310.9	10.50	105.0
114.7	7.91	100	310.9	12.44	124.4
116.7	8.05	100	310.9	12.56	125.6
120.2	8.29	100	310.9	13.62	136.2
122.0	8.41	100	310.9	14.04	140.4
131.7	9.08	100	310.9	14.30	143.0
131.7	9.08	100	310.9	14.76	147.6
139.7	9.63	100	310.9	15.03	150.3
140.2	9.67	100	310.9	15.41	154.1
142.7	9.84	100	310.9	15.67	156.7
151.7	10.46	100	310.9	16.87	168.7
160.2	11.05	100	310.9	16.91	169.1
30.7	2.12	160	344.3	1.75	17.5
39.2	2.70	160	344.3	2.25	22.5
40.2	2.77	160	344.3	2.50	25.0
55.2	3.81	160	344.3	3.48	34.8
60.2	4.15	160	344.3	4.02	40.2
80.7	5.56	160	344.3	5.20	52.0
107.7	7.43	160	344.3	7.42	74.2
122.7	8.46	160	344.3	8.12	81.2
144.7	9.98	160	344.3	9.05	90.5
167.7	11.56	160	344.3	10.65	106.5
186.7	12.87	160	344.3	12.10	121.0
200.7	13.84	160	344.3	12.96	129.6
232.7	16.04	160	344.3	14.17	141.7
242.2	16.70	160	344.3	15.06	150.6
244.0	16.82	160	344.3	15.00	150.0
244.7	16.87	160	344.3	15.07	150.7

Azarnoosh (1958) continuing

P	P	T	T	x[1]	x[1]
psia	bar	deg F	K	mol. frac. *1e5	ppm
270.7	18.66	160	344.3	16.08	160.8
283.7	19.56	160	344.3	17.30	173.0
305.7	21.08	160	344.3	18.45	184.5
344.7	23.77	160	344.3	20.00	200.0
370.4	25.54	160	344.3	21.04	210.4
385.2	26.56	160	344.3	21.50	215.0
37.2	2.56	220	377.6	1.20	12.0
75.2	5.18	220	377.6	4.00	40.0
131.7	9.08	220	377.6	7.61	76.1
131.7	9.08	220	377.6	7.55	75.5
181.2	12.49	220	377.6	11.00	110.0
195.7	13.49	220	377.6	11.69	116.9
217.2	14.98	220	377.6	13.10	131.0
258.7	17.84	220	377.6	15.12	151.2
273.7	18.87	220	377.6	16.80	168.0
290.7	20.04	220	377.6	16.02	160.2
305.7	21.08	220	377.6	17.75	177.5
310.7	21.42	220	377.6	17.66	176.6
314.0	21.65	220	377.6	18.00	180.0
355.7	24.52	220	377.6	20.38	203.8
408.7	28.18	220	377.6	21.95	219.5
425.7	29.35	220	377.6	23.85	238.5
447.2	30.83	220	377.6	24.06	240.6
497.2	34.28	220	377.6	26.50	265.0
511.7	35.28	220	377.6	27.00	270.0
75.3	5.19	280	410.9	2.72	27.2
125.4	8.65	280	410.9	6.04	60.4
315.6	21.76	280	410.9	19.65	196.5
390.2	26.90	280	410.9	23.60	236.0
431.0	29.72	280	410.9	27.24	272.4
487.3	33.60	280	410.9	29.20	292.0
498.7	34.38	280	410.9	31.30	313.0

Claussen W. F., Polglase M. F., "Solubilities and structures in aqueous aliphatic hydrocarbon solutions", J. Am. Chem. Soc. 74, 4817-4819 (1952)

P	T	T	x[1]	x[1]
bar	deg C	K	Bunsen	ppm
1.01325	19.8	293.0	0.0394	34.81
1.01325	29.8	303.0	0.0288	26.38

Kertes A.S. (ed.), IUPAC Solubility Data Series, Vol 24, 451 (1989a)

P	T	x[1]
bar	K	ppm
1.014	288.7	57
1.014	310.9	15
1.014	344.3	8
1.379	377.6	3
2.758	288.7	150
2.758	310.9	45
2.758	344.3	26
2.758	377.6	18
4.137	410.9	12
5.516	288.7	245
5.516	310.9	92
5.516	344.3	54
5.516	377.6	45
6.895	288.7	259
6.895	310.9	115
6.895	344.3	68
6.895	377.6	58
6.895	410.9	45
10.342	310.9	156
10.342	344.3	100
10.342	377.6	89
10.342	410.9	80
13.789	344.3	130
13.789	377.6	120
13.789	410.9	118
17.237	344.3	157
17.237	377.6	149
17.237	410.9	154
20.684	344.3	180
20.684	377.6	174
20.684	410.9	186
24.132	344.3	200
24.132	377.6	197
24.132	410.9	214
27.579	377.6	219
27.579	410.9	247
31.026	377.6	240
31.026	410.9	274
34.474	377.6	260
34.474	410.9	312

Kobayashi R., Katz D. L., "Vapor-liquid equilibria for binary hydrocarbon-water systems", Ind. Eng. Chem. 45 2, 440-446 (1953)

Two-phase region, water-rich liquid

P	P	T	T	x[1]	x[1]
psia	bar	°F	K	mol. frac.	ppm
617	42.54	54	285.37	0.0002963	296.3
617	42.54	54	285.37	0.0003029	302.9
1222	84.25	54	285.37	0.0002906	290.6
1988	137.07	54	285.37	0.0002948	294.8
72	4.96	100	310.93	0.0000863	86.3
117	8.07	100	310.93	0.0001552	155.2
428	29.51	100	310.93	0.0002046	204.6
622	42.89	100	310.93	0.0002175	217.5
1531	105.56	100	310.93	0.0002151	215.1
2012	138.72	100	310.93	0.0002239	223.9
2687	185.26	100	310.93	0.0002304	230.4
188	12.96	133	329.26	0.0001499	149.9
1199	82.67	133	329.26	0.0002249	224.9
1810	124.80	133	329.26	0.0002267	226.7
2787	192.16	133	329.26	0.0002364	236.4
181	12.48	170	349.82	0.0001146	114.6
307	21.17	170	349.82	0.0001763	176.3
131	9.03	190	360.93	0.0000796	79.6
224	15.44	190	360.93	0.0001330	133.0
359	24.75	190	360.93	0.0001960	196.0
990	68.26	190	360.93	0.0002580	258.0
1523	105.01	190	360.93	0.0002703	270.3
2012	138.72	190	360.93	0.0002745	274.5
2787	192.16	190	360.93	0.0002880	288.0
230	15.86	205.7	369.65	0.0001261	126.1
400	27.58	205.7	369.65	0.0002162	216.2
478	32.96	205.7	369.65	0.0002449	244.9
910	62.74	205.7	369.65	0.0002842	284.2
1810	124.80	205.7	369.65	0.0003008	300.8
2787	192.16	205.7	369.65	0.0003134	313.4
222	15.31	230	383.15	0.0001301	130.1
504	34.75	230	383.15	0.0002633	263.3
810	55.85	230	383.15	0.0003243	324.3
1128	77.77	230	383.15	0.0003414	341.4
1810	124.80	230	383.15	0.0003542	354.2
2787	192.16	230	383.15	0.0003765	376.5
170	11.72	260	399.82	0.0001001	100.1
332	22.89	260	399.82	0.0001964	196.4
511	35.23	260	399.82	0.0002892	289.2
751	51.78	260	399.82	0.0003665	366.5
1232	84.94	260	399.82	0.0004197	419.7
1810	124.80	260	399.82	0.0004393	439.3
2787	192.16	260	399.82	0.0004766	476.6

Kobayashi (1953) continuing

P	P	T	T	x[1]	x[1]
psia	bar	°F	K	mol. frac.	ppm
265	18.27	300	422.04	0.0001666	166.6
471	32.47	300	422.04	0.0003031	303.1
694	47.85	300	422.04	0.0004130	413.0
987	68.05	300	422.04	0.0004876	487.6
1565	107.90	300	422.04	0.0005801	580.1
1810	124.80	300	422.04	0.0006078	607.8
2787	192.16	300	422.04	0.0006861	686.1

Kobayashi (1953) continuing
Two-phase region, propane-rich liquid

P	P	T	T	x'[2]	x'[1]
psia	bar	°F	K	mol frac	ppm
102	7.03	100	310.93	0.009540	990460
141	9.72	100	310.93	0.006960	993040
533	36.75	100	310.93	0.004920	995080
818	56.40	100	310.93	0.000587	999413
1015	69.98	100	310.93	0.000673	999327
2018	139.14	100	310.93	0.000540	999460
2023	139.48	100	310.93	0.000643	999357
2798	192.91	100	310.93	0.000591	999409
2798	192.91	100	310.93	0.000623	999377
146	10.07	150	338.71	0.026490	973510
217	14.96	150	338.71	0.017020	982980
289	19.93	150	338.71	0.012000	988000
856	59.02	150	338.71	0.002328	997672
1564	107.83	150	338.71	0.002224	997776
2484	171.26	150	338.71	0.002060	997940
2803	193.26	150	338.71	0.002046	997954
190	13.10	190	360.93	0.049670	950330
309	21.30	190	360.93	0.029100	970900
465	32.06	190	360.93	0.017220	982780
1342	92.53	190	360.93	0.005020	994980
2003	138.10	190	360.93	0.004750	995250
2803	193.26	190	360.93	0.004630	995370
207	14.27	205.7	369.65	0.063700	936300
445	30.68	205.7	369.65	0.026390	973610
603	41.58	205.7	369.65	0.015680	984320
637	43.92	205.7	369.65	0.009980	990020
696	47.99	205.7	369.65	0.008130	991870
755	52.05	205.7	369.65	0.007790	992210
1217	83.91	205.7	369.65	0.007260	992740
2023	139.48	205.7	369.65	0.006740	993260
2803	193.26	205.7	369.65	0.006400	993600
252	17.37	230	383.15	0.080940	919060
446	30.75	230	383.15	0.043250	956750

Kobayashi (1953) continuing

P	P	T	T	x'[2]	x'[1]
psia	bar	°F	K	mol frac	ppm
630	43.44	230	383.15	0.026590	973410
718	49.50	230	383.15	0.020280	979720
823	56.74	230	383.15	0.013660	986340
1530	105.49	230	383.15	0.013300	986700
2023	139.48	230	383.15	0.009590	990410
2704	186.43	230	383.15	0.009190	990810
439	30.27	260	399.82	0.078560	921440
675	46.54	260	399.82	0.046600	953400
812	55.98	260	399.82	0.035990	964010
996	68.67	260	399.82	0.024990	975010
1411	97.28	260	399.82	0.018430	981570
2023	139.48	260	399.82	0.016460	983540
2023	139.48	260	399.82	0.016490	983510
2755	189.95	260	399.82	0.014900	985100
622	42.89	300	422.04	0.101460	898540
928	63.98	300	422.04	0.063500	936500
1217	83.91	300	422.04	0.044960	955040
1441	99.35	300	422.04	0.038750	961250
2023	139.48	300	422.04	0.031050	968950
2803	193.26	300	422.04	0.026840	973160

Kobayashi (1953) continuing
Three-phase region, water-rich liquid

P	P	T	T	x[1]	x[1]
psia	bar	°F	K	mol frac	ppm
82.2	5.67	42.3	278.87	0.0003660	366.0
101	6.96	53.9	285.32	0.0002913	291.3
142	9.79	78.1	298.76	0.0002208	220.8
143	9.86	79.1	299.32	0.0002208	220.8
191	13.17	100.2	311.04	0.0002045	204.5
191	13.17	100.6	311.26	0.0002001	200.1
284	19.58	132.9	329.21	0.0002046	204.6
300	20.68	137.7	331.87	0.0002003	200.3
366	25.23	154.2	341.04	0.0002063	206.3
391	26.96	160.3	344.43	0.0002107	210.7
446	30.75	172.2	351.04	0.0002298	229.8
482	33.23	179.7	355.21	0.0002360	236.0
538	37.09	189.6	360.71	0.0002495	249.5
543	37.44	191.1	361.54	0.0002489	248.9
608	41.92	201.7	367.43	0.0002638	263.8
632	43.57	205.4	369.48	0.0002726	272.6

Kobayashi (1953) continuing
Three-phase region, vapour phase

P	P	T	T	y[2]	y[1]
psia	bar	°F	K	mol frac	ppm
113.8	7.85	63	290.37	0.002322	997678
114.6	7.90	64.1	290.98	0.002370	997630
151.8	10.47	83.1	301.54	0.003582	996418
159.7	11.01	87	303.71	0.003708	996292
195	13.44	102.5	312.32	0.004855	995145
220	15.17	111.6	317.37	0.005520	994480
220	15.17	111.8	317.48	0.005490	994510
270	18.62	127.7	326.32	0.006960	993040
271	18.68	128.2	326.59	0.006960	993040
328	22.61	144.1	335.43	0.008540	991460
328	22.61	144.1	335.43	0.008630	991370
437	30.13	170	349.82	0.010970	989030
488	33.65	179	354.82	0.011750	988250
487	33.58	179.2	354.93	0.011770	988230
529	36.47	187.6	359.59	0.012630	987370
535	36.89	188.6	360.15	0.012780	987220
540	37.23	190.3	361.09	0.012820	987180
561	38.68	192.8	362.48	0.012820	987180
562	38.75	193	362.59	0.012700	987300
613	42.26	201.6	367.37	0.012120	987880
612	42.20	201.7	367.43	0.012080	987920

Three-phase region, propane-rich liquid

P	P	T	T	x[2]	x[1]
psia	bar	°F	K	mol frac	ppm
107.1	7.38	58.4	287.82	0.0001368	999863
142.5	9.83	78.5	298.98	0.0003340	999666
142.5	9.83	78.7	299.09	0.0003403	999660
195	13.44	101.9	311.98	0.0006140	999386
195.6	13.49	101.9	311.98	0.0006260	999374
272	18.75	128.5	326.76	0.0013680	998632
271	18.68	128.8	326.93	0.0013780	998622
330	22.75	144.6	335.71	0.0019950	998005
438	30.20	170	349.82	0.0035550	996445
443	30.54	171	350.37	0.0036820	996318
535	36.89	188.6	360.15	0.0054200	994580
551	37.99	191.4	361.71	0.0060500	993950
549	37.85	191.6	361.82	0.0054400	994560
572	39.44	195.6	364.04	0.0065900	993410
611	42.13	201.7	367.43	0.0076400	992360
612	42.20	202.1	367.65	0.0076900	992310
633	43.64	205.4	369.48	0.0100100	989990
638	43.99	206.1	369.87	0.0099500	990050

Lebeau M.P., "Sur quelques propriétés physiques du propane", Bull. Soc. Chim. France, [3] 33, 1137-1139 (1905)

P	T	T	x[1]	x[1]
bar	deg C	K	Bunsen	ppm
1.01325	17.0	290.2	0.0650	56.85

McAuliffe C., "Solubility in water of paraffin, cycloparaffin, olefin, acetylene, cycloolefin, and aromatic hydrocarbons", J. Phys. Chem., 70 No 4, 1267-1275 (1966)

P	T	T	x[1]	x[1]
bar	deg C	K	g HC / g H2O	ppm
1.01325	25.0	298.2	62.4	25.49

Wehe A.H., McKetta J.J., "Method for determining total hydrocarbons dissolved in water", Anal. Chem. 33, 291-293 (1961)

P	P	T	T	x[1]	x[1]
psia	bar	deg F	K	mol. frac. * 1e5	ppm
74.6	5.14	160	344.3	5.49	54.9
112.2	7.74	160	344.3	8.06	80.6
120.3	8.29	160	344.3	8.2	82
128.8	8.88	160	344.3	8.69	86.9
136.7	9.43	160	344.3	9.69	96.9
148.9	10.27	160	344.3	10.1	101
165.0	11.38	160	344.3	11.1	111
180.9	12.47	160	344.3	12.3	123

Wetlaufer D.B., Malik S.K., Stoller L., Coffin R.L., "Nonpolar group participation in the denaturation of proteins by urea and guanadium salts", J. Am. Chem. Soc., 86, 508-514 (1964)

P	T	T	x[1]	x[1]
bar	deg C	K	(mol HC / l H2O)*1000	ppm
1.01325	5	278.2	3.14000	56.56
1.01325	25	298.2	1.47000	26.56
1.01325	45	318.2	0.95000	17.28

Blanco S.T., Velasco I., Rauzy E., Otin S., "Water dew points of binary nitrogen+water and propane+water mixtures. Measurement and correlation", Fluid Phase Eq. 161, 107-117 (1999)

P	T	y[2]	y[1]
bar	K	mol frac	ppm
1.01	256.21	0.00127	998730
1.21	258.05	0.00127	998730
1.41	259.66	0.00127	998730
1.61	261.10	0.00127	998730
1.81	262.40	0.00127	998730
2.01	263.50	0.00127	998730
2.41	265.61	0.00127	998730
2.61	266.52	0.00127	998730
2.80	267.33	0.00127	998730
3.00	268.12	0.00127	998730
3.21	268.89	0.00127	998730
3.40	269.57	0.00127	998730
3.61	270.26	0.00127	998730
3.80	270.88	0.00127	998730
4.00	271.31	0.00127	998730
4.20	272.07	0.00127	998730
4.40	272.70	0.00127	998730
4.60	273.33	0.00127	998730
4.66	273.63	0.00127	998730
1.01	257.45	0.00147	998530
1.19	259.22	0.00147	998530
1.41	260.90	0.00147	998530
1.61	262.46	0.00147	998530
1.80	263.78	0.00147	998530
2.01	264.99	0.00147	998530
2.21	265.99	0.00147	998530
2.41	266.99	0.00147	998530
2.60	267.95	0.00147	998530
2.81	268.82	0.00147	998530
3.01	269.62	0.00147	998530
3.21	270.53	0.00147	998530
3.61	271.74	0.00147	998530
3.80	272.44	0.00147	998530
4.01	273.22	0.00147	998530
4.21	273.94	0.00147	998530
4.41	274.61	0.00147	998530
4.60	275.22	0.00147	998530
4.68	275.45	0.00147	998530
1.04	257.54	0.00178	998220
1.15	258.63	0.00178	998220
1.36	260.71	0.00178	998220
1.57	262.43	0.00178	998220
1.78	263.96	0.00178	998220
2.01	265.43	0.00178	998220

Blanco (1999) continuing

P	T	y[2]	y[1]
bar	K	mol frac	ppm
2.16	266.45	0.00178	998220
2.56	268.65	0.00178	998220
2.77	269.62	0.00178	998220
2.96	270.57	0.00178	998220
3.16	271.49	0.00178	998220
3.39	272.43	0.00178	998220
3.58	273.35	0.00178	998220
3.80	274.14	0.00178	998220
4.00	274.91	0.00178	998220
4.20	275.52	0.00178	998220
4.40	276.26	0.00178	998220
4.60	276.90	0.00178	998220
4.80	277.53	0.00178	998220
4.99	278.12	0.00178	998220
1.02	259.91	0.00215	997850
1.21	261.91	0.00215	997850
1.40	263.72	0.00215	997850
1.60	265.34	0.00215	997850
1.80	266.82	0.00215	997850
2.00	268.16	0.00215	997850
2.20	269.44	0.00215	997850
2.40	270.60	0.00215	997850
2.60	271.72	0.00215	997850
2.80	272.72	0.00215	997850
3.00	273.67	0.00215	997850
3.20	274.59	0.00215	997850
3.40	275.38	0.00215	997850
3.60	276.23	0.00215	997850
3.81	277.02	0.00215	997850
4.00	277.69	0.00215	997850
4.21	278.49	0.00215	997850
4.40	279.06	0.00215	997850
4.60	279.71	0.00215	997850
4.80	280.46	0.00215	997850
4.99	280.87	0.00215	997850
1.01	262.29	0.00278	997220
1.21	264.44	0.00278	997220
1.40	266.30	0.00278	997220
1.60	268.07	0.00278	997220
1.81	269.61	0.00278	997220
2.00	271.05	0.00278	997220
2.21	272.29	0.00278	997220
2.40	273.40	0.00278	997220
2.61	274.68	0.00278	997220
2.80	275.65	0.00278	997220
3.00	276.65	0.00278	997220

Blanco (1999) continuing

P	T	y[2]	y[1]
bar	K	mol frac	ppm
3.20	277.48	0.00278	997220
3.40	278.43	0.00278	997220
3.61	279.19	0.00278	997220
3.81	280.06	0.00278	997220
4.01	280.84	0.00278	997220
4.20	281.47	0.00278	997220
4.41	282.16	0.00278	997220
4.61	282.83	0.00278	997220
4.81	283.55	0.00278	997220
4.93	283.84	0.00278	997220

Appendix 5. Solubility data for n-butane

Carroll J. J., Jou F. Y., Mather A. E., "Fluid phase equilibria in the system n-butane + water", Fluid Phase Eq. 140, 157-169 (1997)

P	P	T	T	x[1]	x[1]
kPa	bar	°C	K	mol. frac. * 1e5	ppm
104.3	1.04	25	298.15	2.12	21.2
140	1.40	25	298.15	2.61	26.1
190	1.90	25	298.15	3.74	37.4
245	2.45	25	298.15	4.8	48
108.7	1.09	40	313.15	1.6	16
200	2.00	40	313.15	3.15	31.5
300	3.00	40	313.15	4.4	44
382	3.82	40	313.15	5.77	57.7
132.5	1.33	70	343.15	1.28	12.8
270	2.70	70	343.15	2.68	26.8
530	5.30	70	343.15	5.18	51.8
840	8.40	70	343.15	7.8	78
202.6	2.03	100	373.15	1.11	11.1
410	4.10	100	373.15	2.83	28.3
500	5.00	100	373.15	3.58	35.8
830	8.30	100	373.15	6.17	61.7
1610	16.10	100	373.15	13.2	132
338	3.38	125	398.15	1.21	12.1
530	5.30	125	398.15	2.82	28.2
1230	12.30	125	398.15	8.4	84
2650	26.50	125	398.15	18.6	186
578	5.78	150	423.15	1.4	14
860	8.60	150	423.15	4.5	45
1200	12.00	150	423.15	7.86	78.6
2200	22.00	150	423.15	17.2	172
4130	41.30	150	423.15	30	300

Claussen W. F., Polglase M. F., "Solubilities and structures in aqueous aliphatic hydrocarbon solutions", J. Am. Chem. Soc. 74, 4817-4819 (1952)

P	T	T	x[1]	x[1]
bar	deg C	K	Bunsen	ppm
1.01325	19.8	293.0	0.0327	29.48
1.01325	29.8	303.0	0.0233	21.78

Danneil A., Toedheide K., Franck E. U., "Verdamfungsgleichgewichte und kritische kurven in den systemen äthane/wasser und n-butan/wasser bei hohen drücken", Chem.-Ing.-Tech. 39-13, 816-822 (1967)

P	P	T	x[1]	x[1]	y[1]	y[1]
kPa	bar	K	mol. frac.	ppm	mol. frac.	ppm
25500	255.00	628.15	0.025	25000	0.124	124000
29500	295.00	628.15	0.048	48000	0.105	105000
51000	510.00	628.15	0.055	55000	***	***
52000	520.00	628.15	***	***	0.188	188000
59000	590.00	628.15	0.043	43000	0.287	287000
69000	690.00	637.15	0.077	77000	0.256	256000
72500	725.00	628.15	0.036	36000	***	***
73500	735.00	628.15	***	***	0.356	356000
83000	830.00	637.15	0.041	41000	0.318	318000
109000	1090.00	637.15	***	***	0.417	417000
112500	1125.00	637.15	0.041	41000	***	***

Dhima A., De Hemptinne J.C., Moracchini G., "Solubility of light hydrocarbons and their mixtures in pure water under high pressure", Fluid Phase Equilibria, 145, 129-150 (1998)

P	P	T	x[1]	x[1]
MPa	bar	K	% mol.	ppm
10	100	344.15	0.0095	95
20	200	344.15	0.0093	93
50	500	344.15	0.0092	92
75	750	344.15	0.0103	103
100	1000	344.15	0.0098	98

Kertes A.S. (ed.), IUPAC Solubility Data Series, **Vol 24**, 451 (1989)

The values reported by Kertes are the same as the values from Le Breton (1964).

Le Breton J.G., McKetta J.J., "Low pressure solubility of n-butane in water", Hydrocarbon Processing & Petroleum Refiner 43, 136-138 (1964)

P	P	T	T	x[1]	x[1]
psia	bar	deg F	K	mol. frac. * 1e5	ppm
52.2	3.60	100.00	310.9	4.42	44.2
52.2	3.60	100.00	310.9	4.96	49.6
52.2	3.60	100.00	310.9	4.83	48.3
212.7	14.67	100.00	310.9	4.52	45.2
608.7	41.97	100.00	310.9	4.51	45.1
52.2	3.60	100.00	310.9	4.48	44.8
19.7	1.36	100.00	310.9	1.73	17.3
23.7	1.63	100.00	310.9	1.92	19.2
29.7	2.05	100.00	310.9	2.78	27.8
34.7	2.39	100.00	310.9	2.92	29.2

Le Breton (1964) continuing

P	P	T	T	x[1]	x[1]
psia	bar	deg F	K	mol. frac. * 1e5	ppm
41.2	2.84	100.00	310.9	3.76	37.6
52.2	3.60	100.00	310.9	4.36	43.6
310.7	21.42	100.00	310.9	4.43	44.3
806.7	55.62	100.00	310.9	4.44	44.4
459.7	31.70	100.00	310.9	4.33	43.3
708.7	48.86	100.00	310.9	4.44	44.4
856.7	59.07	100.00	310.9	4.68	46.8
125.2	8.63	160.00	344.3	5.54	55.4
125.2	8.63	160.00	344.3	5.67	56.7
125.2	8.63	160.00	344.3	5.464	54.64
125.2	8.63	160.00	344.3	5.473	54.73
880.7	60.72	160.00	344.3	5.82	58.2
658.7	45.42	160.00	344.3	5.69	56.9
558.7	38.52	160.00	344.3	5.67	56.7
454.7	31.35	160.00	344.3	5.8	58
261.7	18.04	160.00	344.3	5.75	57.5
321.7	22.18	160.00	344.3	5.63	56.3
187.7	12.94	160.00	344.3	5.6	56
201.7	13.91	160.00	344.3	5.46	54.6
38.7	2.67	160.00	344.3	1.6	16
44.7	3.08	160.00	344.3	1.89	18.9
47.7	3.29	160.00	344.3	2	20
58.7	4.05	160.00	344.3	2.58	25.8
73.7	5.08	160.00	344.3	3.21	32.1
85.7	5.91	160.00	344.3	3.86	38.6
96.7	6.67	160.00	344.3	4.23	42.3
108.7	7.49	160.00	344.3	4.93	49.3
125.2	8.63	160.00	344.3	5.28	52.8
766.7	52.86	160.00	344.3	5.54	55.4
182.7	12.60	160.00	344.3	5.44	54.4
222.7	15.35	160.00	344.3	5.43	54.3
756.7	52.17	160.00	344.3	5.75	57.5
125.2	8.63	160.00	344.3	5.49	54.9
125.2	8.63	160.00	344.3	5.54	55.4
125.2	8.63	160.00	344.3	5.46	54.6
386.7	26.66	160.00	344.3	5.46	54.6
212.7	14.67	160.00	344.3	5.45	54.5
459.7	31.70	160.00	344.3	5.49	54.9
934.7	64.45	160.00	344.3	5.52	55.2
259.7	17.91	220.00	377.6	8.59	85.9
259.7	17.91	220.00	377.6	8.24	82.4
259.7	17.91	220.00	377.6	8.67	86.7
259.7	17.91	220.00	377.6	9.21	92.1
259.7	17.91	220.00	377.6	9.07	90.7
68.7	4.74	220.00	377.6	2.24	22.4
82.7	5.70	220.00	377.6	2.81	28.1

Le Breton (1964) continuing

P	P	T	T	x[1]	x[1]
psia	bar	deg F	K	mol. frac. * 1e5	ppm
102.7	7.08	220.00	377.6	3.84	38.4
119.7	8.25	220.00	377.6	4.49	44.9
126.7	8.74	220.00	377.6	4.84	48.4
140.7	9.70	220.00	377.6	5.39	53.9
147.7	10.18	220.00	377.6	6.32	63.2
180.7	12.46	220.00	377.6	7.24	72.4
212.7	14.67	220.00	377.6	8.02	80.2
227.7	15.70	220.00	377.6	8.26	82.6
259.7	17.91	220.00	377.6	9.1	91
259.7	17.91	220.00	377.6	8.55	85.5
259.7	17.91	220.00	377.6	8.61	86.1
805.7	55.55	220.00	377.6	9.23	92.3
756.7	52.17	220.00	377.6	9.23	92.3
707.7	48.79	220.00	377.6	9.04	90.4
608.7	41.97	220.00	377.6	8.97	89.7
509.7	35.14	220.00	377.6	8.75	87.5
411.7	28.39	220.00	377.6	9.12	91.2
312.7	21.56	220.00	377.6	9.35	93.5
421.7	29.08	220.00	377.6	9.24	92.4
509.7	35.14	220.00	377.6	9.19	91.9
322.7	22.25	220.00	377.6	9.34	93.4
490.7	33.83	280.00	410.9	17.64	176.4
490.7	33.83	280.00	410.9	17.85	178.5
490.7	33.83	280.00	410.9	17.5	175
89.7	6.18	280.00	410.9	2.19	21.9
129.7	8.94	280.00	410.9	4.23	42.3
164.7	11.36	280.00	410.9	6.29	62.9
194.7	13.42	280.00	410.9	7.64	76.4
226.7	15.63	280.00	410.9	9.17	91.7
264.7	18.25	280.00	410.9	11.01	110.1
299.7	20.66	280.00	410.9	12.26	122.6
329.7	22.73	280.00	410.9	13.31	133.1
360.7	24.87	280.00	410.9	14.4	144
401.7	27.70	280.00	410.9	15.7	157
430.7	29.70	280.00	410.9	16.415	164.15
450.7	31.07	280.00	410.9	16.86	168.6
490.7	33.83	280.00	410.9	17.77	177.7
490.7	33.83	280.00	410.9	17.54	175.4
954.7	65.82	280.00	410.9	17.6	176
845.7	58.31	280.00	410.9	17.88	178.8
746.7	51.48	280.00	410.9	18	180
668.7	46.11	280.00	410.9	17.97	179.7
598.7	41.28	280.00	410.9	17.64	176.4
554.7	38.25	280.00	410.9	17.66	176.6
954.7	65.82	280.00	410.9	17.98	179.8
756.7	52.17	280.00	410.9	18.15	181.5

Le Breton (1964) continuing

P	P	T	T	x[1]	x[1]
psia	bar	deg F	K	mol. frac. * 1e5	ppm
658.7	45.42	280.00	410.9	17.57	175.7
608.7	41.97	280.00	410.9	18.1	181
490.7	33.83	280.00	410.9	18.03	180.3
490.7	33.83	280.00	410.9	17.66	176.6
578.7	39.90	280.00	410.9	18.11	181.1

Lebeau M.P., "Uber einige physikalische Eigenschaften des Butans und Isobutans", Chem. Zentralbl., 79, II, 291-292 (1908)

P	T	T	x[1]	x[1]
bar	deg C	K	Bunsen	ppm
1.01325	17.0	290.2	0.1500	133.87

McAuliffe C., "Solubility in water of paraffin, cycloparaffin, olefin, acetylene, cycloolefin, and aromatic hydrocarbons", J. Phys. Chem., 70 No 4, 1267-1275 (1966)

P	T	T	x[1]	x[1]
bar	deg C	K	g HC / g H2O	ppm
1.01325	25.0	298.2	61.4	19.03

Reamer H. H., Olds R. H., Sage B. H., Lacey W. N., "Phase equilibria in hydrocarbon systems. Compositions of the coexisting phases of n-butane-water system in the three-phase region", Ind. Eng. Chem. 36, 381-384 (1944)

P	P	T	T	x'[2]	x'[1]	y[2]	y[1]
psia	bar	°F	K	mol. Frac.	ppm	mol. frac.	ppm
52.45	3.62	100	310.93	0.0005	999500	0.01670	983300
82.80	5.71	130	327.59	0.001	999000	0.02450	975500
125.40	8.65	160	344.26	0.0021	997900	0.03380	966200
182.80	12.60	190	360.93	0.0043	995700	0.04390	956100
259.30	17.88	220	377.59	0.0085	991500	0.05410	945900
360.00	24.82	250	394.26	0.0157	984300	0.06390	936100
490.90	33.85	280	410.93	0.0268	973200	0.07080	929200
542.40	37.40	290	416.48	0.0317	968300	0.06980	930200
600.50	41.40	300	422.04	0.0379	962100	0.06250	937500
637.50	43.95	305.6	425.15	0.0483	951700	0.04830	951700
60	4.14	108.6	315.71	0.0006	999400	0.0187	981300
80	5.52	127.6	326.26	0.0009	999100	0.0238	976200
100	6.89	143.3	334.98	0.0014	998600	0.0285	971500
125	8.62	159.8	344.15	0.0021	997900	0.0338	966200
150	10.34	173.9	351.98	0.0030	997000	0.0385	961500
175	12.07	186.4	358.93	0.0040	996000	0.0427	957300
200	13.79	197.6	365.15	0.0052	994800	0.0465	953500
250	17.24	216.8	375.82	0.0080	992000	0.0531	946900
300	20.68	233.2	384.93	0.0113	988700	0.0585	941500
350	24.13	247.4	392.82	0.0150	985000	0.0631	936900

Reamer (1944) continuing

P	P	T	T	x'[2]	x'[1]	y[2]	y[1]
psia	bar	°F	K	mol. Frac.	ppm	mol. frac.	ppm
400	27.58	260.1	399.87	0.0189	981100	0.067	933000
450	31.03	271.5	406.21	0.0231	976900	0.0698	930200
500	34.47	281.8	411.93	0.0276	972400	0.0708	929200
550	37.92	291.3	417.21	0.0324	967600	0.0693	930700
600	41.37	299.9	421.98	0.0379	962100	0.0626	937400
625	43.09	303.7	424.09	0.0420	958000	0.0555	944500

Reamer H. H., Sage B. H., Lacey W. N., "Phase equilibria in hydrocarbon systems. N-butane-water system in the two-phase region", Ind. Eng. Chem. 44, 609-615 (1952)

P	P	T	T	x[1]	x[1]	x'[2]	x'[1]
psia	bar	deg F	K	mol. frac. *1000	ppm	mol. frac. *1000	ppm
20	1.38	100.00	310.9	0.024	24	46.5	953500
20	1.38	160.00	344.3	0.012	12	235	765000
20	1.38	220.00	377.6	0.002	2	858	142000
40	2.76	100.00	310.9	0.048	48	22.8	977200
40	2.76	160.00	344.3	0.029	29	115	885000
40	2.76	220.00	377.6	0.017	17	427	573000
60	4.14	100.00	310.9	0.062	62	0.5	999500
60	4.14	160.00	344.3	0.044	44	75.7	924300
60	4.14	220.00	377.6	0.03	30	282	718000
60	4.14	280.00	410.9	0.008	8	820	180000
80	5.52	100.00	310.9	0.062	62	0.5	999500
80	5.52	160.00	344.3	0.058	58	55.7	944300
80	5.52	220.00	377.6	0.044	44	209	791000
80	5.52	280.00	410.9	0.021	21	614	386000
100	6.89	100.00	310.9	0.062	62	0.5	999500
100	6.89	160.00	344.3	0.071	71	43.8	956200
100	6.89	220.00	377.6	0.057	57	166	834000
100	6.89	280.00	410.9	0.035	35	491	509000
200	13.79	100.00	310.9	0.062	62	0.5	999500
200	13.79	160.00	344.3	0.088	88	2	998000
200	13.79	220.00	377.6	0.113	113	75.6	924400
200	13.79	280.00	410.9	0.096	96	239	761000
200	13.79	340.00	444.3	0.074	74	594	406000
300	20.68	100.00	310.9	0.063	63	0.5	999500
300	20.68	160.00	344.3	0.088	88	2	998000
300	20.68	220.00	377.6	0.14	140	8.2	991800
300	20.68	280.00	410.9	0.148	148	148	852000
300	20.68	340.00	444.3	0.151	151	391	609000
300	20.68	400.00	477.6	0.065	65	831	169000
400	27.58	100.00	310.9	0.063	63	0.5	999500
400	27.58	160.00	344.3	0.088	88	2	998000
400	27.58	220.00	377.6	0.14	140	8	992000
400	27.58	280.00	410.9	0.191	191	99.1	900900

Reamer (1952) continuing

P	P	T	T	x[1]	x[1]	x'[2]	x'[1]
psia	bar	deg F	K	mol. frac. *1000	ppm	mol. frac. *1000	ppm
400	27.58	340.00	444.3	0.219	219	275	725000
400	27.58	400.00	477.6	0.175	175	635	365000
500	34.47	100.00	310.9	0.063	63	0.5	999500
500	34.47	160.00	344.3	0.089	89	2	998000
500	34.47	220.00	377.6	0.141	141	7.8	992200
500	34.47	280.00	410.9	0.22	220	26.8	973200
500	34.47	340.00	444.3	0.279	279	198	802000
500	34.47	400.00	477.6	0.27	270	512	488000
500	34.47	460.00	510.9	0.078	78	944	56000
600	41.37	100.00	310.9	0.064	64	0.5	999500
600	41.37	160.00	344.3	0.089	89	2	998000
600	41.37	220.00	377.6	0.142	142	7.6	992400
600	41.37	280.00	410.9	0.22	220	26.2	973800
600	41.37	340.00	444.3	0.322	322	142	858000
600	41.37	400.00	477.6	0.355	355	423	577000
600	41.37	460.00	510.9	0.288	288	811	189000
800	55.16	100.00	310.9	0.064	64	0.5	999500
800	55.16	160.00	344.3	0.089	89	2	998000
800	55.16	220.00	377.6	0.143	143	7.4	992600
800	55.16	280.00	410.9	0.221	221	24.4	975600
800	55.16	340.00	444.3	0.368	368	81.6	918400
800	55.16	400.00	477.6	0.488	488	303	697000
800	55.16	460.00	510.9	0.6	600	623	377000
1000	68.95	100.00	310.9	0.065	65	0.5	999500
1000	68.95	160.00	344.3	0.09	90	2	998000
1000	68.95	220.00	377.6	0.143	143	7.3	992700
1000	68.95	280.00	410.9	0.222	222	22.6	977400
1000	68.95	340.00	444.3	0.386	386	61.8	938200
1000	68.95	400.00	477.6	0.569	569	225	775000
1000	68.95	460.00	510.9	0.792	792	493	507000
1250	86.18	220.00	377.6	0.143	143	7.1	992900
1250	86.18	280.00	410.9	0.224	224	20.9	979100
1250	86.18	340.00	444.3	0.4	400	54.5	945500
1250	86.18	400.00	477.6	0.637	637	168	832000
1250	86.18	460.00	510.9	0.973	973	382	618000
1500	103.42	100.00	310.9	0.066	66	0.5	999500
1500	103.42	160.00	344.3	0.091	91	2	998000
1500	103.42	220.00	377.6	0.144	144	6.9	993100
1500	103.42	280.00	410.9	0.226	226	19.6	980400
1500	103.42	340.00	444.3	0.409	409	49.7	950300
1500	103.42	400.00	477.6	0.677	677	140	860000
1500	103.42	460.00	510.9	1.089	1089	311	689000
1750	120.66	220.00	377.6	0.144	144	6.7	993300
1750	120.66	280.00	410.9	0.228	228	18.4	981600
1750	120.66	340.00	444.3	0.417	417	46.1	953900

Reamer (1952) continuing

P	P	T	T	x[1]	x[1]	x'[2]	x'[1]
psia	bar	deg F	K	mol. frac. *1000	ppm	mol. frac. *1000	ppm
1750	120.66	400.00	477.6	0.709	709	123	877000
1750	120.66	460.00	510.9	1.15	1150	268	732000
2000	137.90	100.00	310.9	0.068	68	0.5	999500
2000	137.90	160.00	344.3	0.092	92	2	998000
2000	137.90	220.00	377.6	0.145	145	6.5	993500
2000	137.90	280.00	410.9	0.23	230	17.5	982500
2000	137.90	340.00	444.3	0.423	423	43.3	956700
2000	137.90	400.00	477.6	0.736	736	110	890000
2000	137.90	460.00	510.9	1.195	1195	238	762000
2500	172.37	220.00	377.6	0.146	146	6.1	993900
2500	172.37	280.00	410.9	0.235	235	16.3	983700
2500	172.37	340.00	444.3	0.434	434	39.7	960300
2500	172.37	400.00	477.6	0.777	777	94.8	905200
2500	172.37	460.00	510.9	1.265	1265	202	798000
3000	206.84	100.00	310.9	0.071	71	0.5	999500
3000	206.84	160.00	344.3	0.094	94	2	998000
3000	206.84	220.00	377.6	0.148	148	5.8	994200
3000	206.84	280.00	410.9	0.24	240	15.4	984600
3000	206.84	340.00	444.3	0.443	443	36.9	963100
3000	206.84	400.00	477.6	0.81	810	85	915000
3000	206.84	460.00	510.9	1.325	1325	179	821000
4000	275.79	100.00	310.9	0.073	73	0.5	999500
4000	275.79	160.00	344.3	0.096	96	2	998000
4000	275.79	220.00	377.6	0.15	150	5.2	994800
4000	275.79	280.00	410.9	0.25	250	13.9	986100
4000	275.79	340.00	444.3	0.463	463	33.3	966700
4000	275.79	400.00	477.6	0.855	855	73.6	926400
4000	275.79	460.00	510.9	1.42	1420	150	850000
5000	344.74	100.00	310.9	0.075	75	0.5	999500
5000	344.74	160.00	344.3	0.098	98	2	998000
5000	344.74	220.00	377.6	0.153	153	4.8	995200
5000	344.74	280.00	410.9	0.258	258	13	987000
5000	344.74	340.00	444.3	0.476	476	30.9	969100
5000	344.74	400.00	477.6	0.891	891	66.5	933500
5000	344.74	460.00	510.9	1.498	1498	135	865000
6000	413.69	100.00	310.9	0.076	76	0.5	999500
6000	413.69	160.00	344.3	0.099	99	2	998000
6000	413.69	220.00	377.6	0.155	155	4.5	995500
6000	413.69	280.00	410.9	0.265	265	12.1	987900
6000	413.69	340.00	444.3	0.487	487	28.7	971300
6000	413.69	400.00	477.6	0.92	920	61	939000
6000	413.69	460.00	510.9	1.556	1556	126	874000
7000	482.63	220.00	377.6	0.158	158	4.3	995700
7000	482.63	280.00	410.9	0.271	271	11.3	988700
7000	482.63	340.00	444.3	0.499	499	26.6	973400

Reamer (1952) continuing

P	P	T	T	x[1]	x[1]	x'[2]	x'[1]
psia	bar	deg F	K	mol. frac. *1000	ppm	mol. frac. *1000	ppm
7000	482.63	400.00	477.6	0.946	946	57.9	942100
7000	482.63	460.00	510.9	1.603	1603	120	880000
8000	551.58	100.00	310.9	0.078	78	0.5	999500
8000	551.58	160.00	344.3	0.101	101	2	998000
8000	551.58	220.00	377.6	0.161	161	4.2	995800
8000	551.58	280.00	410.9	0.277	277	10.6	989400
8000	551.58	340.00	444.3	0.509	509	24.8	975200
8000	551.58	400.00	477.6	0.966	966	54.7	945300
8000	551.58	460.00	510.9	1.643	1643	115	885000
9000	620.53	220.00	377.6	0.163	163	4	996000
9000	620.53	280.00	410.9	0.281	281	10	990000
9000	620.53	340.00	444.3	0.518	518	23.3	976700
9000	620.53	400.00	477.6	0.985	985	51.9	948100
9000	620.53	460.00	510.9	1.679	1679	111	889000
10000	689.48	100.00	310.9	0.08	80	0.5	999500
10000	689.48	160.00	344.3	0.103	103	2	998000
10000	689.48	220.00	377.6	0.165	165	3.9	996100
10000	689.48	280.00	410.9	0.285	285	9.5	990500
10000	689.48	340.00	444.3	0.528	528	22.1	977900
10000	689.48	400.00	477.6	1.002	1002	49.7	950300
10000	689.48	460.00	510.9	1.711	1711	108	892000

Wehe A. H., McKetta J. J., "n-butane - 1-butene - water system in the three phase region", J. Chem. Eng. Data 6, 167-172 (1961)

P	P	T	T	x[1]	x[1]	x'[2]	x'[1]	y[2]	y[1]
psia	bar	°F	K	mol. frac.*1e5	ppm	mol. frac.*1000	ppm	mol. frac.*1000	ppm
52.2	3.60	100.2	311.0	4.37	43.7	0.91	999090	14.3	985700
52.1	3.59	99.9	310.9	4.84	48.4	0.83	999170	15.7	984300
124.9	8.61	159.9	344.2	5.89	58.9	3.38	996620	35.1	964900
260.1	17.93	220.2	377.7	***	***	10.00	990000	55.6	944400
260.9	17.99	220.3	377.8	10.50	105.0	9.25	990750	53.0	947000
491.6	33.89	280	410.9	18.60	186.0	28.00	972000	75.1	924900
491.5	33.89	280	410.9	21.50	215.0	27.80	972200	74.6	925400

Wetlaufer D.B., Malik S.K., Stoller L., Coffin R.L., "Nonpolar group participation in the denaturation of proteins by urea and guanadium salts", J. Am. Chem. Soc., 86, 508-514 (1964)

P	T	T	x[1]	x[1]	y[1]
bar	deg C	K	(mol HC / l H2O)*1000	ppm	ppm
1.01325	5	278.2	2.85	51.34	***
1.01325	25	298.2	1.16	20.96	***
1.01325	45	318.2	0.69	12.55	***

Yiling T., Michelberger T., Franck E. U., "High pressure phase equilibria and critical curves of (water + n-butane) and (water + n-hexane) at temperatures to 700 K and pressures to 300 MPa", J. Chem. Thermodyn. 23, 105-112 (1991)

P	P	T	x[2]	x[1]
kPa	bar	K	mol. frac.	ppm
18800	188	496	0.1	900000
20500	205	502	0.1	900000
27600	276	509	0.1	900000
9000	90	502	0.2	800000
15100	151	519	0.2	800000
32000	320	543	0.2	800000
41700	417	551	0.2	800000
11100	111	519	0.3	700000
22700	227	547	0.3	700000
25700	257	553	0.3	700000
32800	328	563	0.3	700000
35000	350	563	0.3	700000
69700	697	588	0.3	700000
87700	877	597	0.3	700000
9400	94	525	0.4	600000
14500	145	549	0.4	600000
21300	213	560	0.4	600000
23700	237	562	0.4	600000
61900	619	589	0.4	600000
87800	878	605	0.4	600000
12100	121	550	0.5	500000
24900	249	567	0.5	500000
33000	330	575	0.5	500000
42500	425	589	0.5	500000
52800	528	594	0.5	500000
55400	554	595	0.5	500000
84700	847	611	0.5	500000
107000	1070	625	0.5	500000
11700	117	554	0.6	400000
19000	190	576	0.6	400000
32700	327	590	0.6	400000
34500	345	595	0.6	400000
39800	398	600	0.6	400000
49300	493	604	0.6	400000
66800	668	617	0.6	400000
80200	802	625	0.6	400000
83200	832	628	0.6	400000
182000	1820	668	0.6	400000
204000	2040	674	0.6	400000
16500	165	580	0.7	300000
26400	264	596	0.7	300000
27800	278	603	0.7	300000
47700	477	618	0.7	300000
49200	492	620	0.7	300000

Yiling (1991) continuing

P	P	T	x[2]	x[1]
kPa	bar	K	mol. frac.	ppm
59000	590	626	0.7	300000
78000	780	634	0.7	300000
101100	1011	643	0.7	300000
142400	1424	659	0.7	300000
148700	1487	664	0.7	300000
165900	1659	667	0.7	300000
234300	2343	689	0.7	300000
270200	2702	700	0.7	300000
16600	166	590	0.8	200000
19700	197	600	0.8	200000
23400	234	613	0.8	200000
26200	262	617	0.8	200000
49100	491	625	0.8	200000
89100	891	641	0.8	200000
92900	929	644	0.8	200000
133200	1332	659	0.8	200000
270500	2705	703	0.8	200000
310100	3101	707	0.8	200000
37400	246	626	0.9	100000
24600	277	629	0.9	100000
27700	374	624	0.9	100000
58300	583	629	0.9	100000
83100	831	639	0.9	100000
22000	220	616	0.925	75000
47400	268	629	0.925	75000
31400	314	628	0.925	75000
26800	474	618	0.925	75000
41900	419	618	0.95	50000
20500	205	627	0.95	50000

Appendix 6. Typical Px and Tx projections

1. Px projections for water/methane.

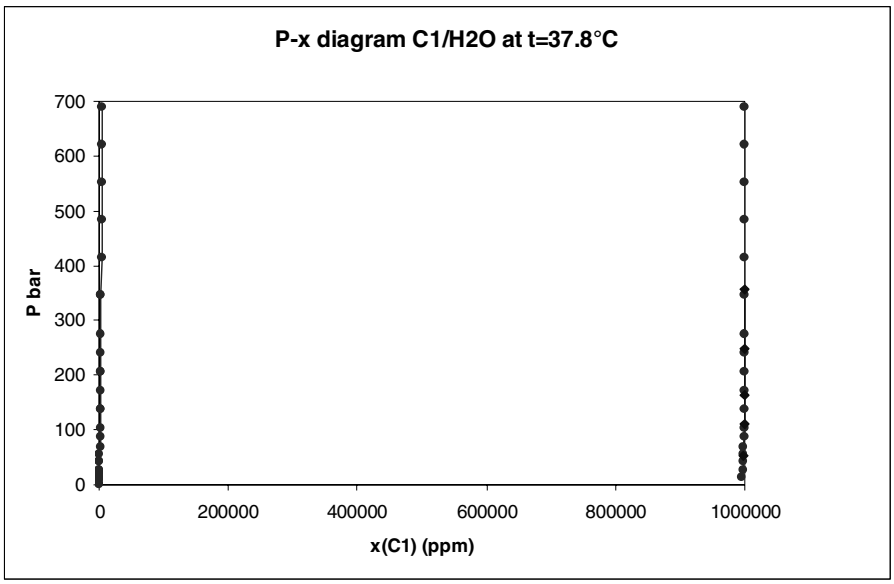

Data from Davis, 1960; Culberson, 1951a; Amirijafari 1972; Olds, 1942.

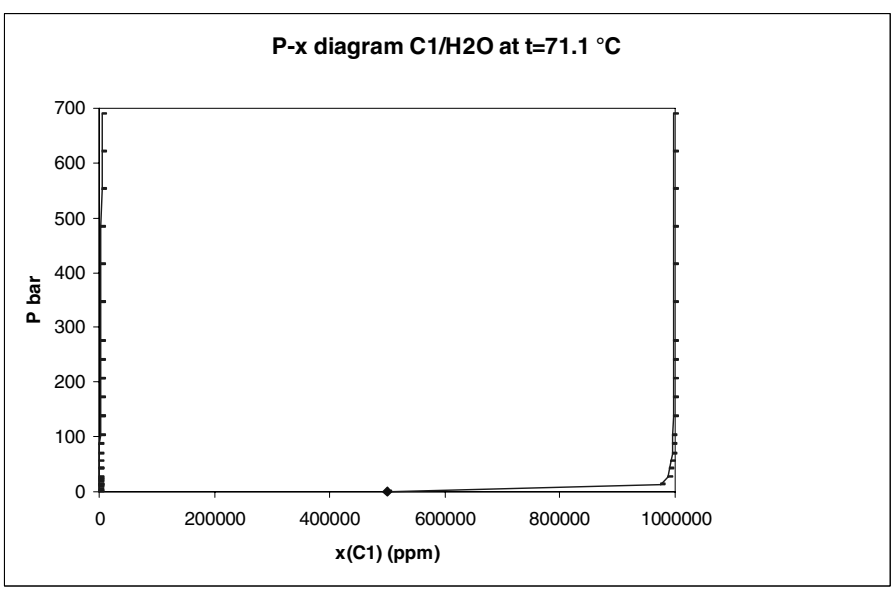

Data from Davis, 1960; Culberson, 1951a; Amirijafari 1972; Olds, 1942; Joffrion 1988.

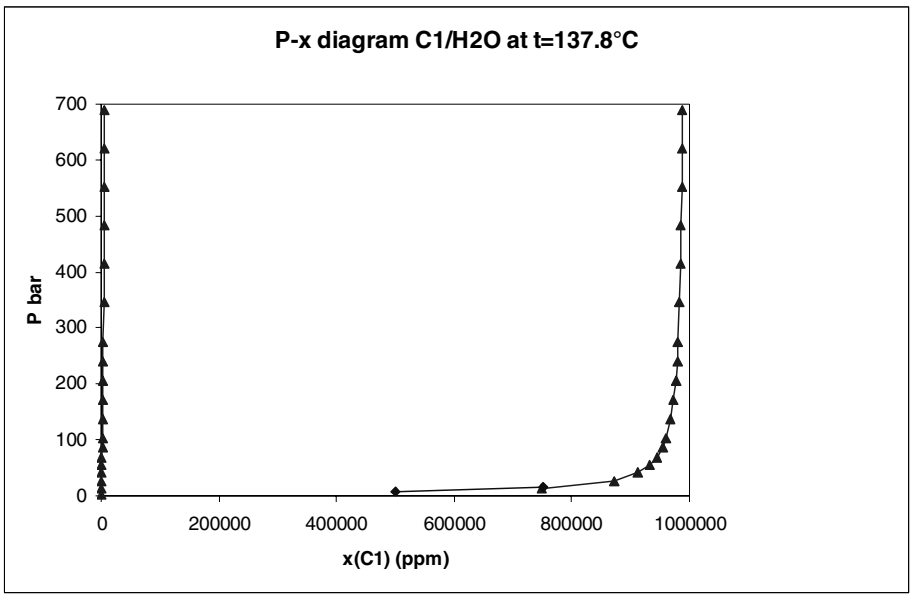

Data from Culberson, 1951a; Olds, 1942; Joffrion 1988.

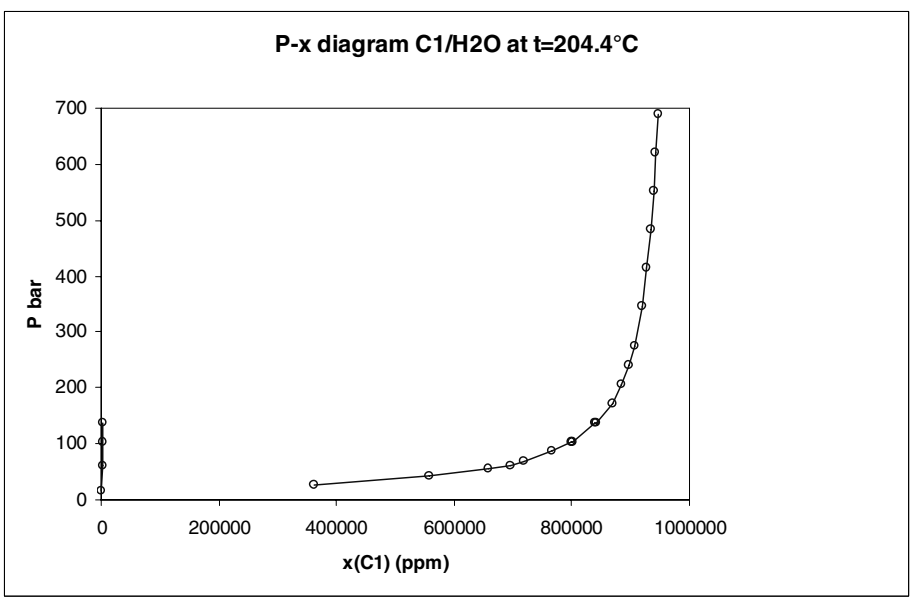

Data from Gillepsie, 1982; Olds, 1942.

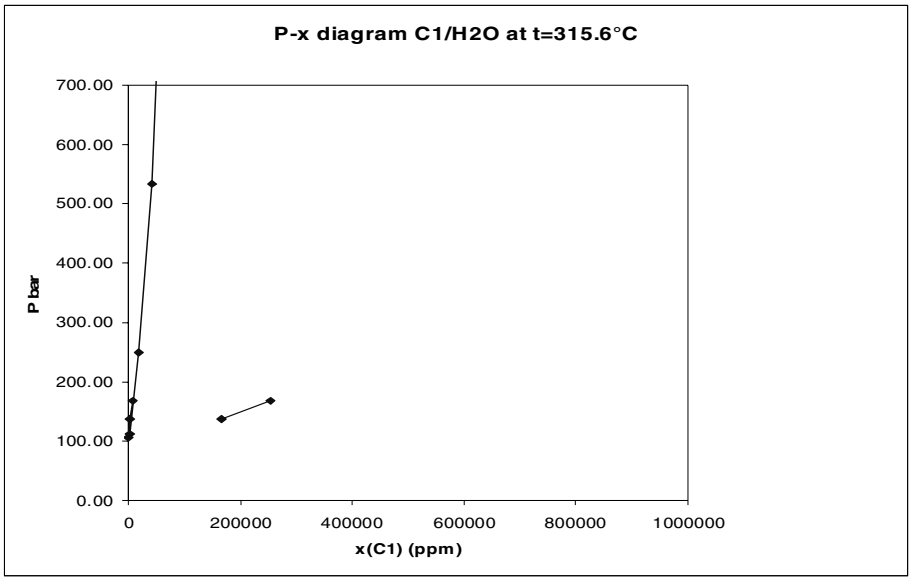

Data from Gillepsie, 1982; Price, 1979.

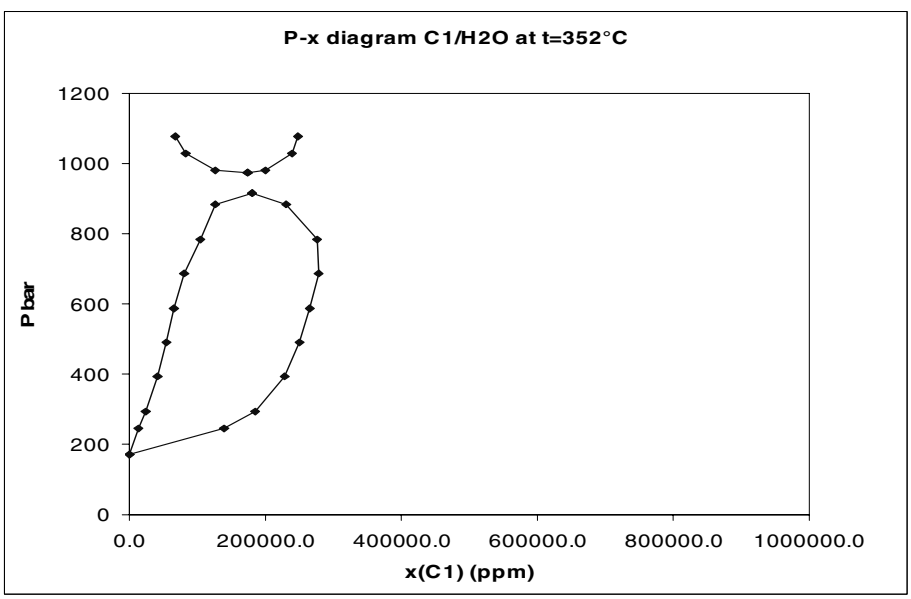

Data from Sultanov, 1972b.

2. Px projections for n-butane/water

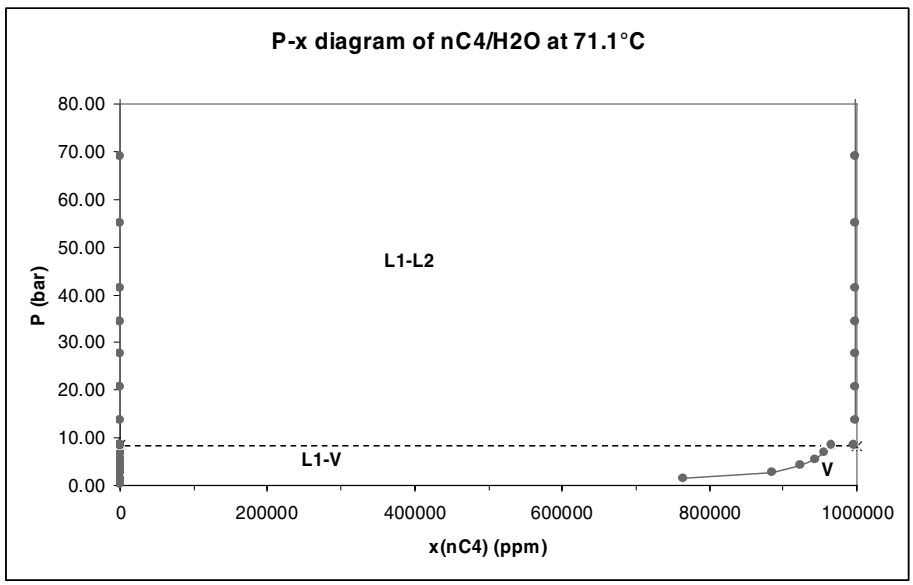

Data from Reamer, 1952; Le Breton, 1964; Wehe, 1961b; Carroll, 1997; Dhima, 1998.

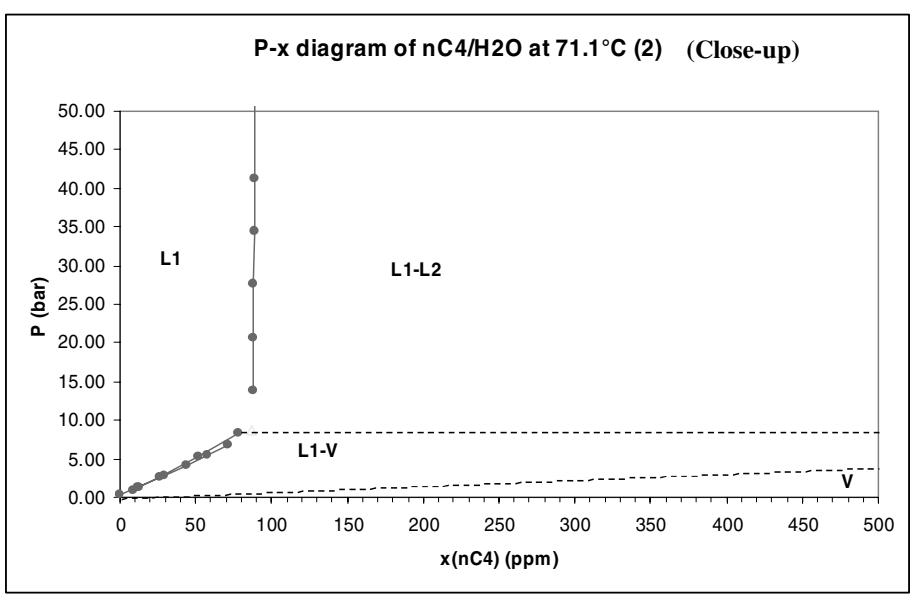

Data from Reamer, 1952; Le Breton, 1964; Wehe, 1961b; Carroll, 1997; Dhima, 1998.

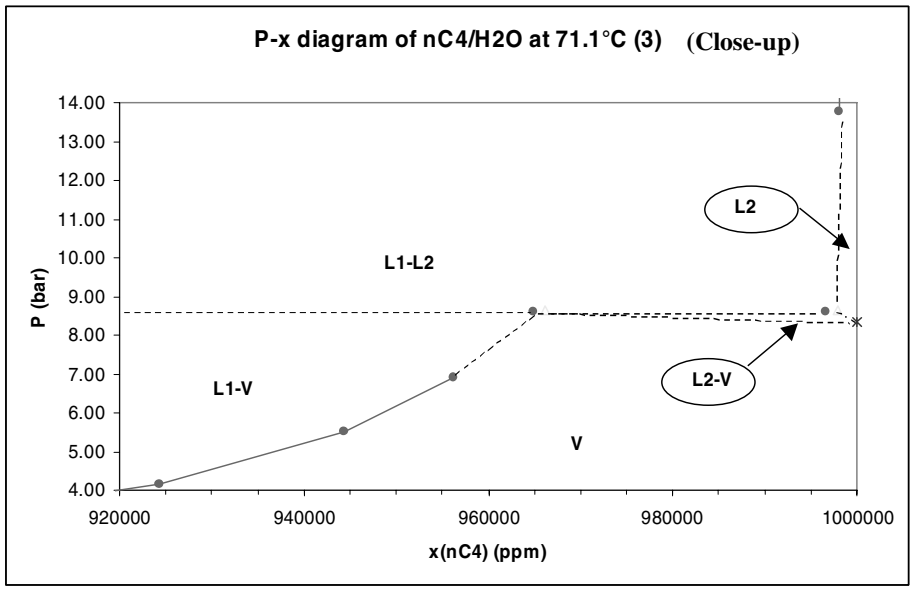

Data from Reamer, 1952; Le Breton, 1964; Wehe, 1961b; Carroll, 1997; Dhima, 1998.

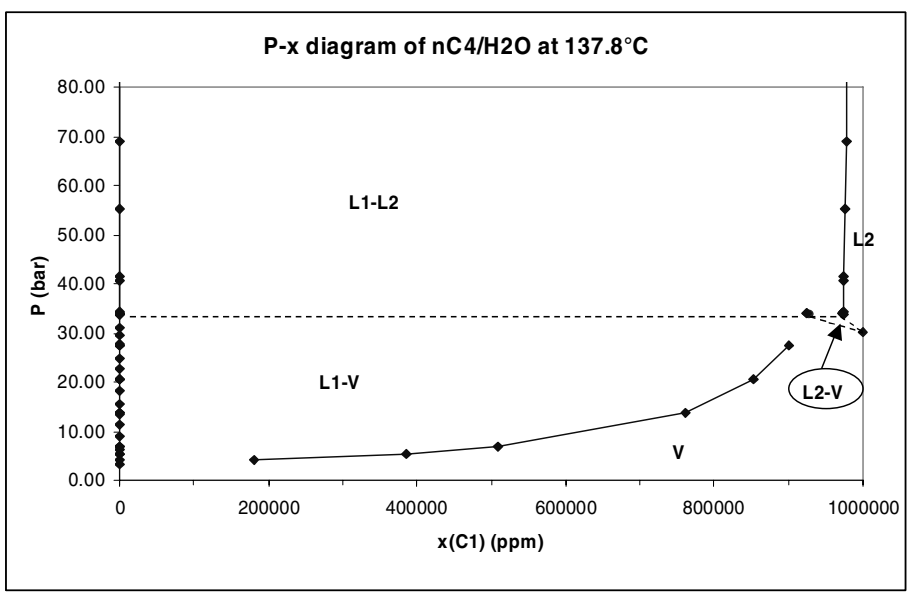

Data from Reamer, 1952; Le Breton, 1964; Wehe, 1961b; Reamer, 1944.

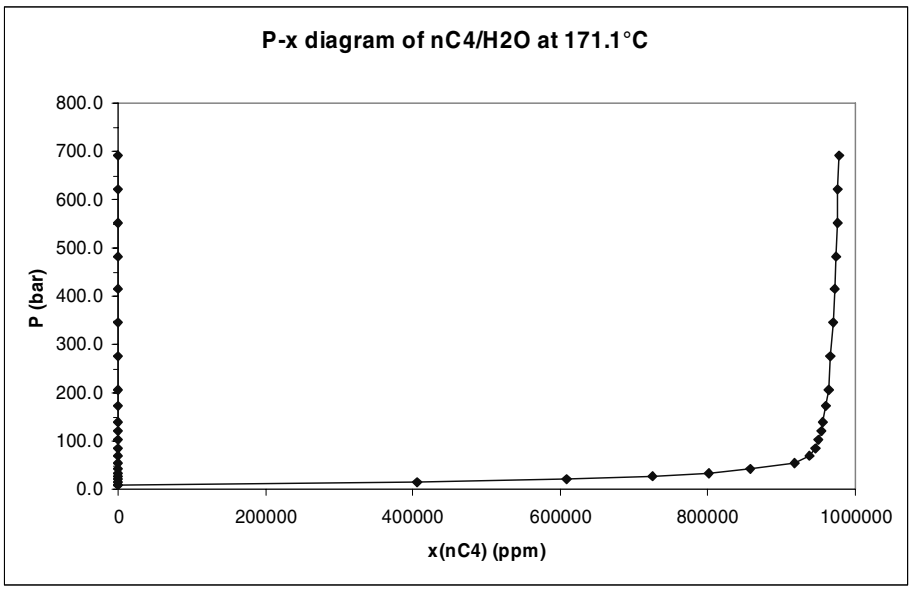

Data from Reamer, 1952.

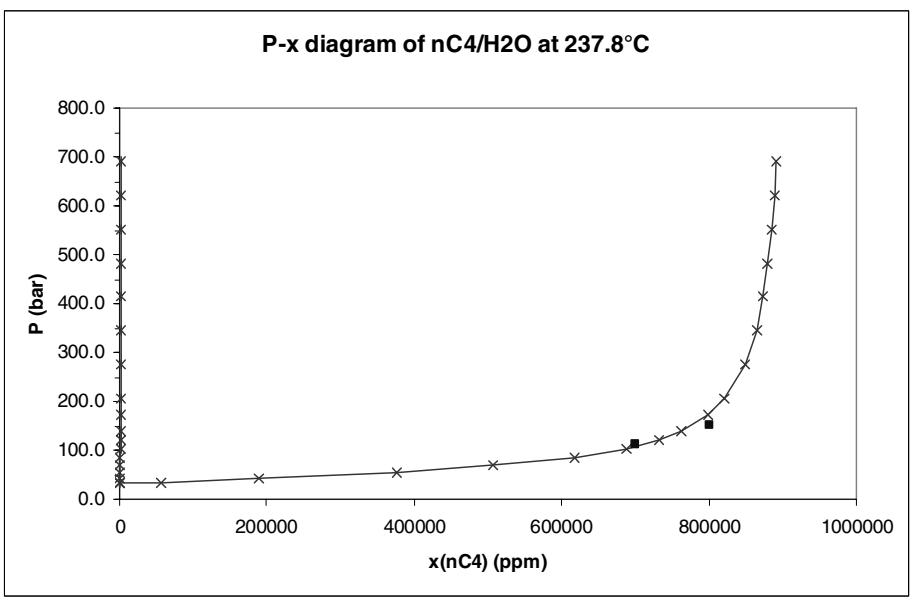

Data from Reamer, 1952; Yiling, 1991.

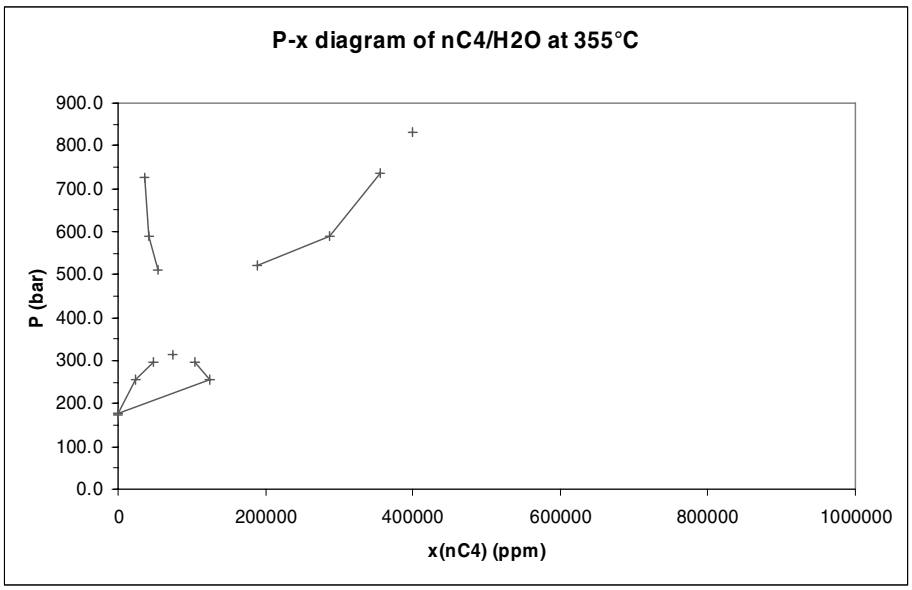

Data from Yiling, 1991; Danneil, 1967.

3. **Tx projections for n-butane/water**

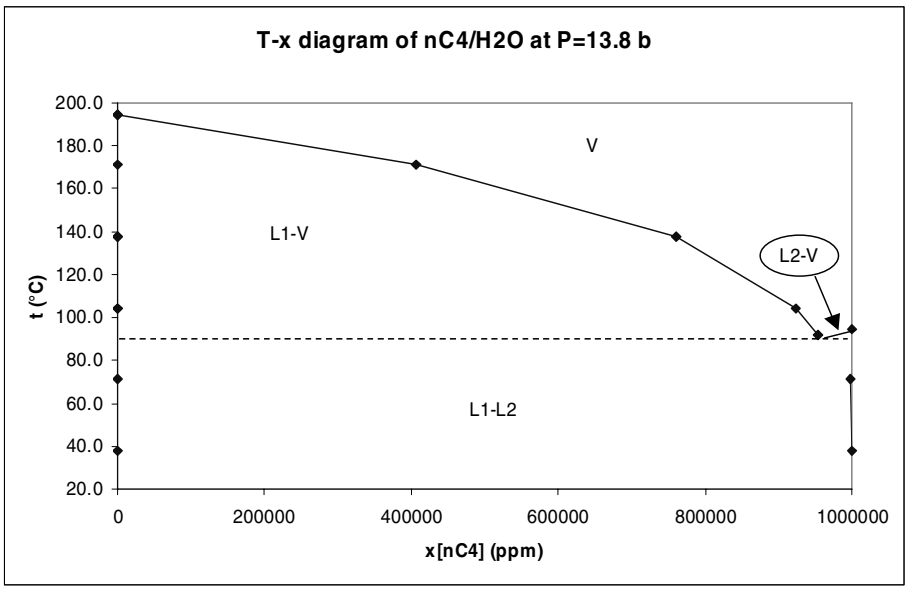

Data from Reamer, 1952; Le Breton, 1964; Reamer, 1944.

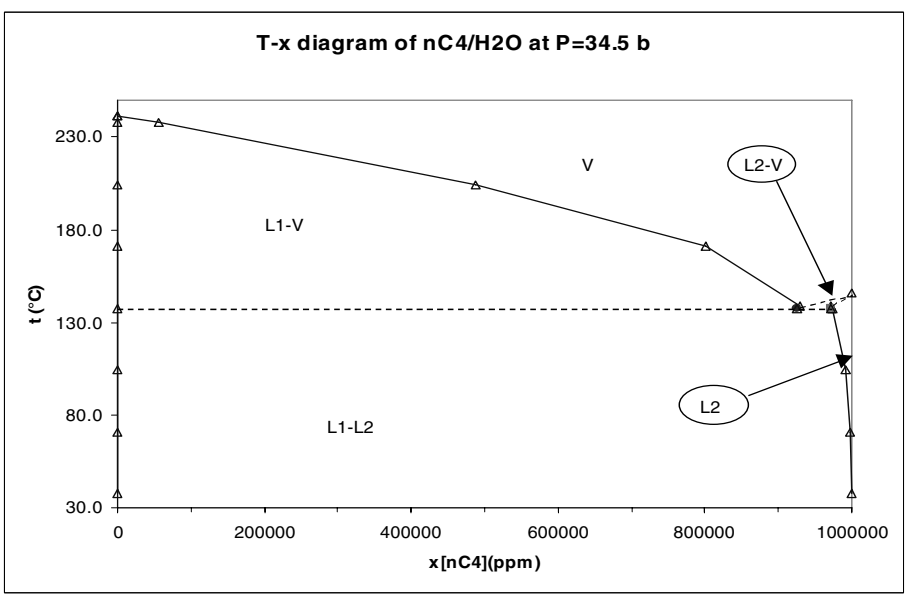

Data from Reamer, 1952; Reamer, 1944; Wehe, 1961b.

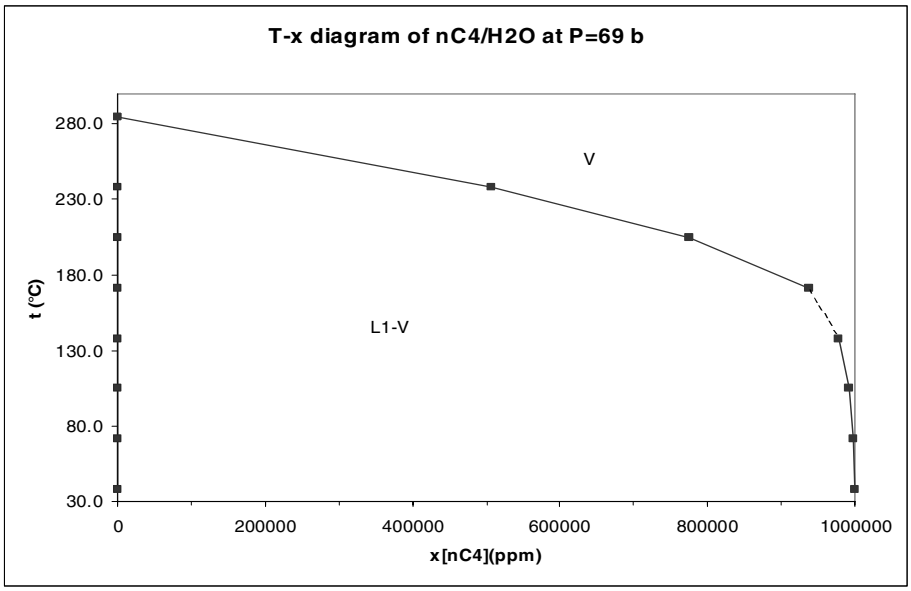

Data from Reamer, 1952.

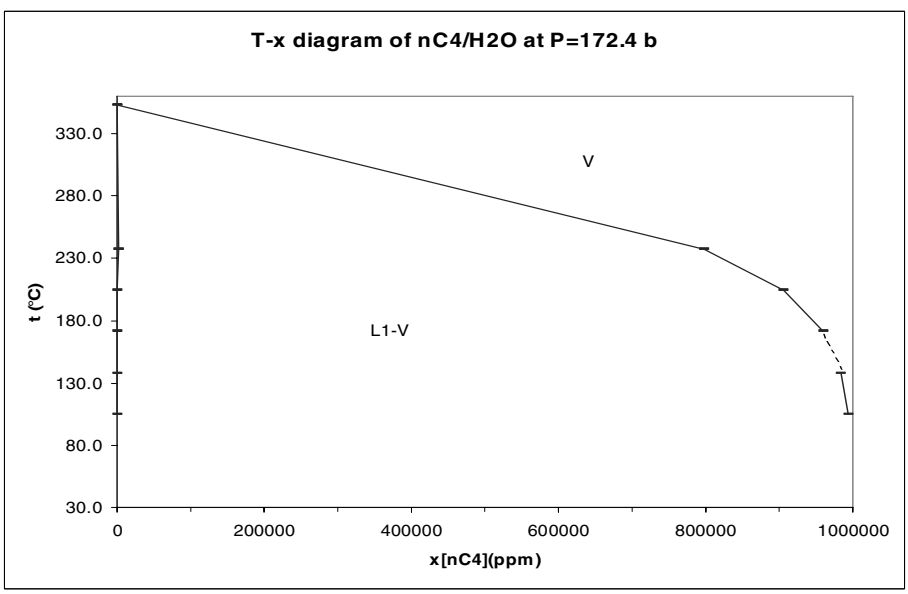

Data from Reamer, 1952.

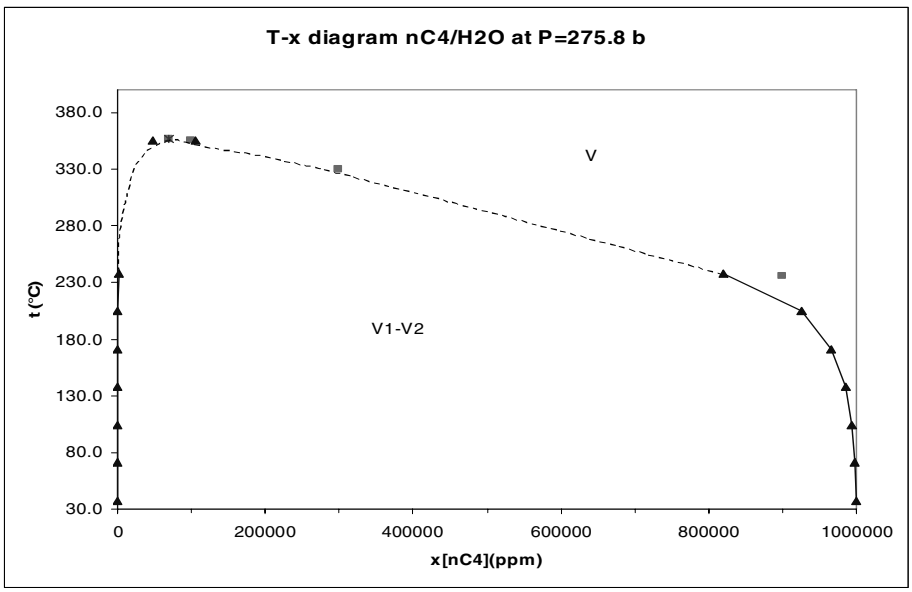

Data from Reamer, 1952; Yiling, 1991; Danneil, 1967.

Appendix 7. Presentation of the experiment

1. Equipment

The experimental set-up of the experiment is composed of the following items:

- an autoclave
- a thermostatic bath
- an agitator
- a manometer
- a thermocouple
- a pressure transducer
- a temperature transducer

The experimental setup is presented on Fig A7.1.

The analytical part of the experimental setup consists of a high precision mass-balance, a gas-chromatograph (GC) equipped with the adequate column to detect Argon and a tensiometer to measure the surface tension of the mud.

Pressurized samples are taken by means of 10cc glass syringes of gas-tight type. Atmospheric samples are taken by mean of 10cc plastic syringes. The plastic syringes are closed by a plastic cap before any transfer another container.

The samples are then transferred to 20cc crimp-top vials, in which vacuum was created.

The autoclave is shown on Fig. A7.2. It has the following characteristics:
Volume: 1 L
Internal diameter: 82 mm
Height: 18.93 cm
Features of the autoclave

- External jacket for thermostatic bath
- Sampling outlet at the bottom of the autoclave
- Outlet on top used as injection entry for the Nitrogen
- Security outlet on top (in case of overpressure)
- Outlet on top for the agitator

Fig A7.1. Experimental set-up ; [1] Autoclave, [2] Thermostatic bath, [3] Sampling port, [4] Protection glass, [5] Security outlet, [6] Agitator engine/regulator, [7] Nitrogen inlet, [8] Thermostatic bath circulation inlet and outlet, [9] Thermocouple and [10] Sampling syringes

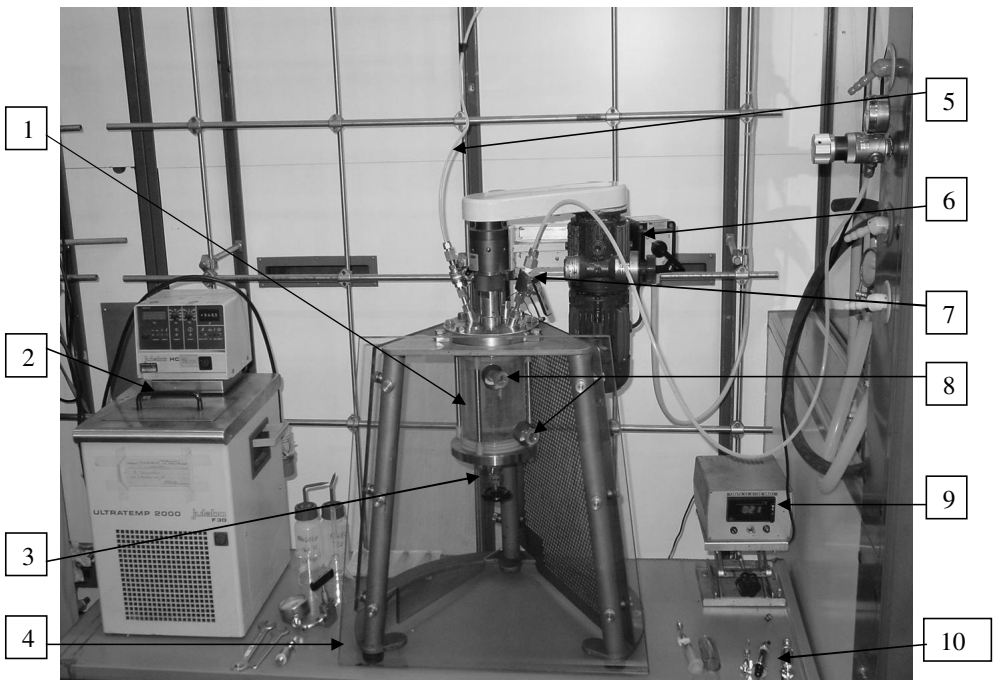

Fig A7.2. Autoclave close-up; [1] Volume graduation, [2] Sampling port

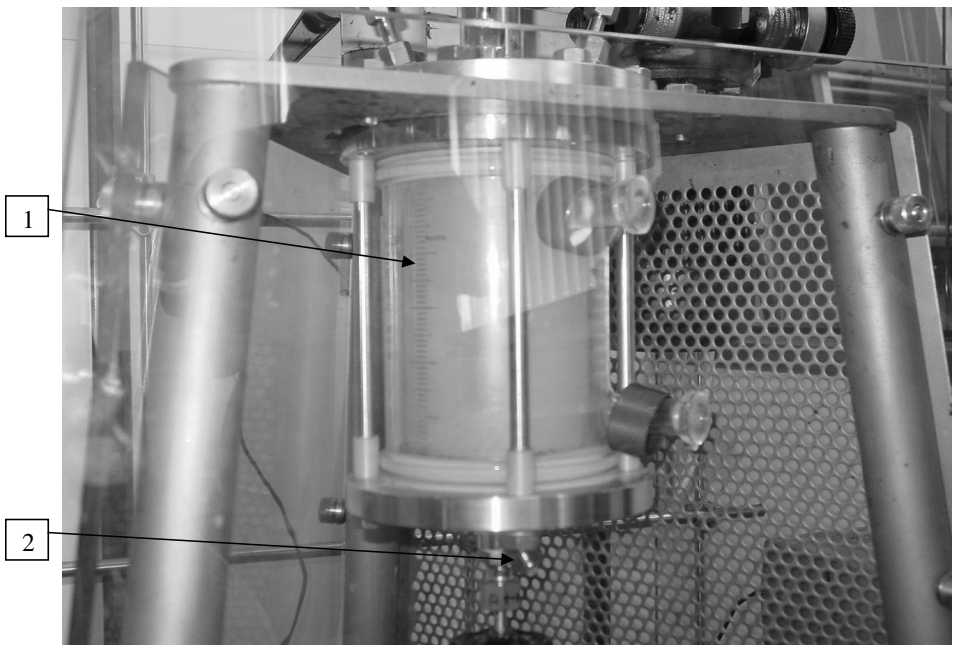

The equipment was prepared before any measurement, as follows:

- Preparation of the 20 ml vial: each vial was weighted and the measured tar was written on the vial. Each vial was calibrated by measuring its volume. Vacuum was created in each vial

- Preparation of the syringes: each syringe was marked with the corresponding sampling number (-1, 0, 1, etc.).

- Gas chromatograph was calibrated by measuring the peaks' area of known amounts of Argon.

- Preparation of the samples in the 20cc vials before the GC-analysis: each vial was inserted into the gas chromatograph apparatus. Each sample was brought to a temperature T= 70°C so as to make gas releasing easier without any risk of vaporising water too (aqueous vapour could damage the gas chromatograph). Then each vial was agitated in the apparatus at a fixed speed and for a fixed time. This enabled for a standard repeatable procedure which could be applied to all the samples so that the gas extraction procedure was well defined and the gas detected by all samples could possibly be affected by the same "loss" of extracted gas.

- Preparation of the mud: each mud was prepared in the laboratory of EniTecnologie. The mud compositions are reported in Table 5.2. A sample of each mud was saved in order to measure its density before any treatment in the autoclave. The interfacial tension between each mud sample and Argon was also measured by a tensiometer. The values of the surface tensions are shown in Table 5.3.

- It can be added also that a sealing capacity test was carried out in order to check that the vials were tight enough and that no Argon could escape.

2. Scheme of the experiment

The procedure of the experiment is explained below. First the mud is prepared in the autoclave in order to reach the right temperature, pressure and initial level of the dissolved Argon. Then the samples are taken.

The further procedure is as follows:

- Inject 500 ml of mud in the autoclave through the Argon inlet-port.
- Start heating of the mud.
  - Switch on the thermostatic bath and the circulation of water.
  - The thermostat is set to 60°C, and the mud is heated until it reaches 40°C; then the temperature of the thermostat is set to 40°C and remains constant.
- Remove the air dissolved in the mud by creating a depression with the help of a water-pump.
  - Plug the water-pump line on the Argon inlet-port and create a depression that will degas the mud.
  - Maintain the void while agitating at 500 rpm during 30 minutes.
  - End with a high agitation speed to homogenise the system.
  - Unplug the water-pump, and plug the Argon instead.
- Inject some Argon from the top of the autoclave until P= 1 bar.
- First sample, “sample –1”

No argon is yet dissolved in it.

  - With the first plastic syringe, take 2 ml of mud.
  - Each syringe is sealed with a plastic cap/valve.
- Inject Argon from the top until the pressure P=6 bar (or 5 bar rel.). is reached.
- Agitate at 1200 rpm during 40 minutes.
- Lower the pressure down to 2.5 bar by releasing some Argon. The pressurised sample will be taken at this pressure
- Slow down agitation to 50 rpm.
- “Sample 0”
  - With the glass syringe, take 2 ml of mud.
- Lower the pressure to P=1 bar.

This moment marks the time t=0, which is the reference time for all the following samplings. The agitation is still at 50 rpm.

- "Sample 1"
  - At t=10 seconds, take 2 ml of mud with a plastic or glass syringe.
- "Sample 2"
  - At t=1 minute , take 2 ml of mud with a plastic or glass syringe
- "Sample 3"
  - At t=2 minutes, take 2 ml of mud with a plastic or glass syringe
- "Sample 4"
  - At t=3 minutes, take 2 ml of mud with a plastic or glass syringe
- "Sample 5"
  - At t=5 minutes, take 2 ml of mud with a plastic or glass syringe
- "Sample 6"
  - At t=2 hours, take 2 ml of mud with a plastic or glass syringe
- "Sample 7"
  - At t=between 12 or 18 hours, take 2 ml of mud with a plastic syringe

Once the samples are ready and stored in the different syringes, the measurement phase can start.

Density measurements

- Take the syringe and inject 2 ml in the of the 20 ml vial tarred beforehand for the density measurement.
- Weight the vial.
- Report the measured weight, the tar weight of the vial and calculate by difference the mass of the 2cc sample.

Compositional analysis

- The vials are disposed on the tray for the automatic analysis sequence of the GC. Each sample is heated to 70°C and shaken as explained in the previous section.
- Analyse the gas.
- Report the composition of the gas, the sample number and the volume of the vial.

Appendix 8. Field Case A

The Well A T2 contains five hydrocarbon bearing layers

Table A8.1. Different hydrocarbon bearing layers if the well A, with their respective depths, reservoir pressures, reservoir temperatures, porosities and water saturations

Layer	Depth (mTVD)	Reservoir Pressure (bar)	Reservoir Temperature (°C)	Porosity (%)	Water saturation (%)
A1	3108-3119	309.9	85	18	35
A3	3225-3237	323.3	86	19	28
A7	3309-3315	327.4	87	25	40
A8	3324-3335	332.4	87	24	30
T2	3358-3383	336.7	86.2	20	40

Table A8.2. Different hydrocarbon present in the 5 layers of the well A; fluid type, dew point or bubble point, density of Stock Tank Oil.

Layer	Fluid type	Dew Point (bar)	Bubble Point (bar)	Density of STO (°API)
A1	Oil	-	173.6	n.a.
A3	Oil	-	173.9	41
A7	Oil	-	260.6	40
A8	Gas condensate	300.6	-	61
T2	Gas condensate	294.1	-	61

Characterization of layer A T2

Table A8.3. PVT data of the fluid from the layer A T2

Component		Reservoir Fluid
		Mole %
Hydrogen sulphide		0.00
Carbon dioxide		0.50
Nitrogen		1.15
Methane		74.58
Ethane		6.84
Propane		4.30
i-Butane		0.71
n-Butane		1.91
i-Pentane		0.85
n-Pentane		0.94
Hexanes		1.30
Heptanes		1.50
Octanes		1.43
Nonanes		0.94
Decanes		0.73
Undecanes		0.53
Dodecanes plus		1.80
Totals		**100.00**

Table A8.4. Calculated Properties for A T2

		Reservoir Fluid
C12 plus	Mole %	1.80
	Molecular Weight (g mol-1)	221.36
	Density at 15.0°C (kg m-3)	838
Atmospheric Flash GLR (m3/m3)		1062.5

Table A8.5. Composition and properties of the components of the modelled fluid A T2

	Mole (%)	Mw (g/mol)	Tc (°C)	Pc (bar)	Omega (-)
N2	1.15	28.01	-146.95	33.944	0.04
CO2	0.5	44.01	31.05	73.765	0.225
H2S	0	34.08	100.05	89.369	0.1
C1	74.57	16.04	-82.55	46.002	0.0115
C2	6.84	30.07	32.25	48.839	0.0908
C3	4.3	44.1	96.65	42.455	0.1454
IC4	0.71	58.12	134.95	36.477	0.176
NC4	1.91	58.12	152.05	37.997	0.1928
IC5	0.85	72.15	187.61	33.932	0.2268
NC5	0.94	72.15	196.45	33.741	0.2273
C6	1.3	85.93	242.13	32.57	0.2637
C7	1.5	92.03	300.9794	42.814	0.2576
C8	1.43	105.78	313.5548	38.235	0.3117
C9	0.94	117.83	325.8909	35.503	0.3582
C10	0.73	135.07	337.9653	30.163	0.4219
C11	0.53	146.99	349.4931	28.534	0.4654
C12	0.87	175.9777	374.0866	24.693	0.5685
C15	0.54	223.2289	411.4511	21.040	0.7212
C19	0.39	320	485.5173	17.614	0.9917

Table A8.6. Comparison between the modelled and sampled fluid A T2

C12+	Calculated	PVT	Error (%)
MW	221.36	**221.36**	0.00
Density	0.838	**0.838**	0.01
Dew Point	294.36	**294.1**	-0.09
°API	20	**61**	**66.9**
GLR	2242.5	**1062.5**	**-111.1**

Characterization of layer A A8

Table A8.7. PVT data of the fluid from the layer A A8

Component		Reservoir Fluid
		Mole %
Hydrogen sulphide		0.00
Carbon dioxide		0.47
Nitrogen		1.62
Methane		72.37
Ethane		8.81
Propane		6.03
i-Butane		0.74
n-Butane		2.13
i-Pentane		0.66
n-Pentane		0.75
Hexanes		1.02
Heptanes		1.18
Octanes		1.07
Nonanes		0.69
Decanes		0.54
Undecanes		0.39
Dodecanes plus		1.56
Totals		**100.00**

Table A8.8. Calculated Properties for A A8

		Reservoir Fluid
C12 plus	Mole %	1.56
	Molecular Weight (g mol-1)	232.48
	Density at 15.0°C (kg m-3)	831
Atmospheric Flash GLR (m3/m3)		1187.6

Table A8.9. Composition and properties of the components of the modelled fluid A A8

	Mole	Mw	Tc	Pc	Omega
	(%)	(g/mol)	(°C)	(bar)	(-)
N2	1.62	28.01	-146.95	33.94	0.0400
CO2	0.47	44.01	31.05	73.77	0.2250
H2S	0	34.08	100.05	89.37	0.1000
C1	72.37	16.04	-82.55	46.00	0.0115
C2	8.81	30.07	32.25	48.84	0.0908
C3	6.03	44.1	96.65	42.46	0.1454
IC4	0.74	58.12	134.95	36.48	0.1760
NC4	2.13	58.12	152.05	38.00	0.1928
IC5	0.66	72.15	187.61	33.93	0.2268
NC5	0.75	72.15	196.45	33.74	0.2273
C6	1.02	86.18	242.13	32.57	0.2637
C7	1.18	92.78	300.94	42.13	0.2605
C8	1.07	106.01	313.43	37.99	0.3125
C9	0.69	118.35	325.69	35.05	0.3600
C10	0.54	135.56	337.89	29.86	0.4236
C11	0.39	148.39	349.64	27.91	0.4703
C12	1.05	191.56	386.46	22.79	0.6254
C18	0.51	316.48	483.18	17.00	0.9877

Table A8.10. Comparison between the modelled and sampled fluid A A8

C12+	Calculated	PVT	Error (%)
MW	232.40	**232.48**	0.03
Density	0.831	**0.831**	0.01
Dew Point	300.74	**300.6**	-0.05
°API	19	**61**	**68.3**
GLR	3237.4	**1187.6**	**-172.6**

Characterization of layer A A7

Table A8.11. PVT data of the fluid from the layer A A7

Component		Reservoir Fluid
		Mole %
Hydrogen sulphide		0.00
Carbon dioxide		0.35
Nitrogen		0.99
Methane		49.01
Ethane		8.41
Propane		7.69
i-Butane		1.07
n-Butane		3.45
i-Pentane		1.39
n-Pentane		1.75
Hexanes		2.39
Heptanes		3.03
Octanes		3.09
Nonanes		2.19
Decanes		1.93
Undecanes		1.52
Dodecanes plus		11.74
Totals		**100.00**

Table A8.12. Calculated Properties for A A7

		Reservoir Fluid
C12 plus	Mole %	11.74
	Molecular Weight (g mol-1)	312.74
	Density at 15.0°C (kg m-3)	870
Atmospheric Flash GOR (m3/m3)		191.1

Table A8.13. Composition and properties of the components of the modelled fluid A A7

	Mole	Mw	Tc	Pc	Omega
	(%)	(g/mol)	(°C)	(bar)	(-)
N2	0.99	28.01	-146.95	33.944	0.0400
CO2	0.35	44.01	31.05	73.765	0.2250
H2S	0	34.08	100.05	89.369	0.1000
C1	49.01	16.04	-82.55	46.002	0.0115
C2	8.41	30.07	32.25	48.839	0.0908
C3	7.69	44.10	96.65	42.455	0.1454
IC4	1.07	58.12	134.95	36.477	0.1760
NC4	3.45	58.12	152.05	37.997	0.1928
IC5	1.39	72.15	187.61	33.932	0.2268
NC5	1.75	72.15	196.45	33.741	0.2273
C6	2.39	86.15	242.13	32.570	0.2637
C7	3.03	92.87	300.86	42.004	0.2608
C8	3.09	105.69	313.34	38.195	0.3113
C9	2.19	118.27	325.63	35.074	0.3597
C10	1.93	133.62	337.48	30.772	0.4167
C11	1.52	148.67	349.40	27.683	0.4712
C12	5.98	206.53	398.85	21.509	0.6782
C20	3.79	338.47	491.14	16.352	1.0314
C32	1.97	585.88	647.32	14.013	1.3062

Table A8.14. Comparison between the modelled and sampled fluid A A7

C12+	Calculated	PVT	Error (%)
MW	312.78	**312.74**	-0.01
Density	0.87	**0.87**	0.00
Bubble Point	261.7	**260.6**	-0.42
°API	8	**40**	**79.6**
GOR	330.1	**191.1**	**-72.8**

Characterization of layer A A3

Table A8.15. PVT data of the fluid from the layer A A3

Component		Reservoir Fluid
		Mole %
Hydrogen sulphide		0.00
Carbon dioxide		0.32
Nitrogen		0.85
Methane		37.84
Ethane		8.10
Propane		10.40
i-Butane		1.68
n-Butane		5.34
i-Pentane		2.03
n-Pentane		2.38
Hexanes		3.14
Heptanes		4.21
Octanes		2.92
Nonanes		2.34
Decanes		2.27
Undecanes		1.83
Dodecanes plus		1.55
Tridecanes		1.5
Tetradecanes		1.2
Pentadecanes		1.11
Hexadecanes		0.92
Heptadecanes		0.81
Octadecanes		0.74
Nonadecanes		0.68
Eicosanes plus		5.91
Totals		**100.00**

Table A8.16. Calculated Properties for A A3

		Reservoir Fluid
C20 plus	Mole %	5.91
	Molecular Weight (g mol-1)	388
	Density at 15.0°C (kg m-3)	903
Atmospheric Flash GOR (m3/m3)		206

Table A8.17. Composition and properties of the components of the modelled fluid A A3

	Mole	Mw	Tc	Pc	Omega
	(%)	(g/mol)	(°C)	(bar)	(-)
N2	0.85	28.01	-146.95	33.94	0.0400
CO2	0.32	44.01	31.05	73.77	0.2250
H2S	0.00	34.08	100.05	89.37	0.1000
C1	37.84	16.04	-82.55	46.00	0.0115
C2	8.10	30.07	32.25	48.84	0.0908
C3	10.40	44.10	96.65	42.46	0.1454
IC4	1.68	58.12	134.95	36.48	0.1760
NC4	5.34	58.12	152.05	38.00	0.1928
IC5	2.03	72.15	187.61	33.93	0.2268
NC5	2.38	72.15	196.45	33.74	0.2273
C6	3.14	84.00	242.13	32.57	0.2637
C7	4.21	96.00	304.15	41.17	0.2733
C8	2.92	107.00	315.48	38.29	0.3165
C9	2.34	121.00	328.69	34.67	0.3702
C10	2.27	134.00	340.39	31.79	0.4186
C11	1.83	147.00	351.55	29.34	0.4659
C12	1.55	161.00	363.28	27.19	0.5154
C13	1.5	175.00	374.84	25.48	0.5636
C14	1.2	190.00	386.91	23.99	0.6137
C15	1.11	206.00	399.31	22.64	0.6654
C16	0.92	222.00	411.05	21.44	0.7153
C17	0.81	237.00	422.07	20.56	0.7605
C18	0.74	251.00	431.84	19.79	0.8012
C19	0.68	263.00	440.21	19.24	0.8350
C20	2.62	300.74	466.32	17.85	0.9369
C25	2.00	386.52	520.92	15.89	1.1270
C33	1.29	568.23	633.524	14.12	1.3197

Table A8.18. Comparison between the modelled and sampled fluid A A3

C12+	Calculated	PVT	Error (%)
MW	388	**388**	-0.04
Density	0.903	**0.903**	0.00
Bubble Point	174.1	**173.9**	-0.11
°API	10	**41**	**74.7**
GOR	274	**206**	**-33.1**

Characterization of layer A A1

Table A8.19. PVT data of the fluid from the layer A A1

Component		Reservoir Fluid
		Mole %
Hydrogen sulphide		0.00
Carbon dioxide		0.32
Nitrogen		0.85
Methane		37.17
Ethane		7.96
Propane		10.23
i-Butane		1.66
n-Butane		5.31
i-Pentane		2.04
n-Pentane		2.40
Hexanes		3.29
Heptanes		4.42
Octanes		3.04
Nonanes		2.40
Decanes		2.33
Undecanes		1.87
Dodecanes plus		1.58
Tridecanes		1.47
Tetradecanes		1.20
Pentadecanes		1.12
Hexadecanes		0.92
Heptadecanes		0.82
Octadecanes		0.75
Nonadecanes		0.68
Eicosanes plus		6.17
Totals		**100.00**

Table A8.20. Calculated Properties for A A1

		Reservoir Fluid
C20 plus	Mole %	6.17
	Molecular Weight (g mol-1)	384
	Density at 15.0°C (kg m-3)	902
Atmospheric Flash GOR (m3/m3)		202

Table A8.21. Composition and properties of the components of the modelled fluid A A1

	Mole	Mw	Tc	Pc	Omega
	(%)	(g/mol)	(°C)	(bar)	(-)
N2	0.85	28.01	-146.95	33.94	0.0400
CO2	0.32	44.01	31.05	73.77	0.2250
H2S	0.00	34.08	100.05	89.37	0.1000
C1	37.17	16.04	-82.55	46.00	0.0115
C2	7.96	30.07	32.25	48.84	0.0908
C3	10.23	44.10	96.65	42.46	0.1454
IC4	1.66	58.12	134.95	36.48	0.1760
NC4	5.31	58.12	152.05	38.00	0.1928
IC5	2.04	72.15	187.61	33.93	0.2268
NC5	2.40	72.15	196.45	33.74	0.2273
C6	3.29	84.00	242.13	32.57	0.2637
C7	4.42	96.00	304.15	41.17	0.2733
C8	3.04	107.00	315.48	38.29	0.3165
C9	2.40	121.00	328.69	34.67	0.3702
C10	2.33	134.00	340.39	31.79	0.4186
C11	1.87	147.00	351.55	29.34	0.4659
C12	1.58	161.00	363.28	27.19	0.5154
C13	1.47	175.00	374.84	25.48	0.5636
C14	1.20	190.00	386.91	23.99	0.6137
C15	1.12	206.00	399.31	22.64	0.6654
C16	0.92	222.00	411.05	21.44	0.7153
C17	0.82	237.00	422.07	20.56	0.7605
C18	0.75	251.00	431.84	19.79	0.8012
C19	0.68	263.00	440.21	19.24	0.8350
C20	2.81	300.62	466.25	17.86	0.9366
C25	2.09	386.22	520.76	15.90	1.1265
C33	1.27	564.53	631.09	14.14	1.3201

Table A8.22. Comparison between the modelled and sampled fluid A A1

C12+	Calculated	PVT	Error (%)
MW	384	**384**	0.02
Density	0.902	**0.902**	0.01
Bubble Point	174.1	**173.6**	-0.27
GOR	249	**202**	**-23.4**

Appendix 9. Field Case B

The well B presents some gas shows in the interval 4770-4970 m.

The available porosities are taken from a porosity log:
4777 - 4820 = 3 - 5 %
4820 - 4840 = 7 -20 % (average 15-16%)
4840 - 4900 = 6 -7%

The average water saturation is 15-20%.

Fig A9.1 shows the operating conditions in terms of ROP and flow rate. Fig A9.2 shows the gas shows for methane.

Fig A9.1. ROP and mud flow rate for well B

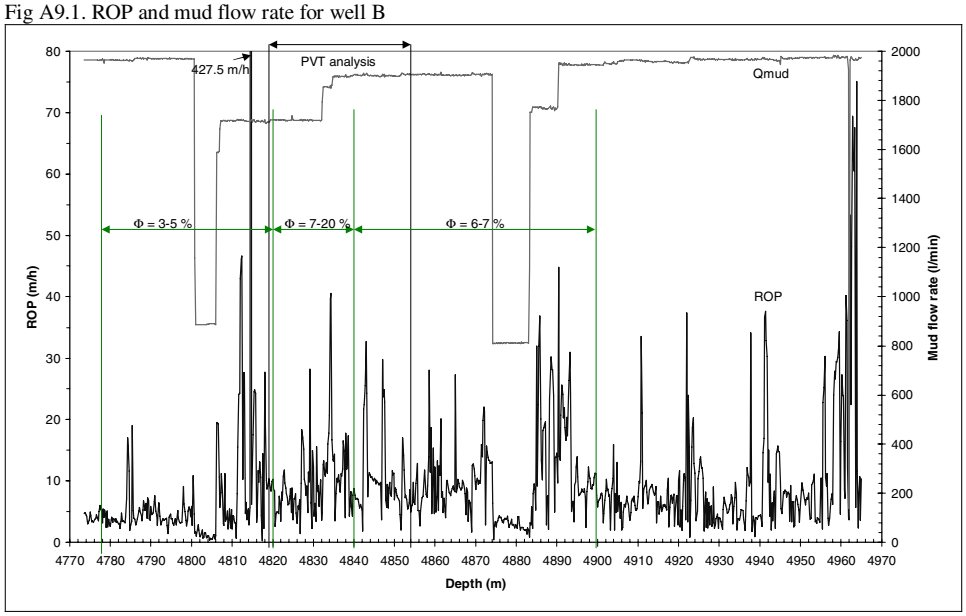

Fig A9.2. ROP, Qmud and methane gas-show for well B in the interval of interest.

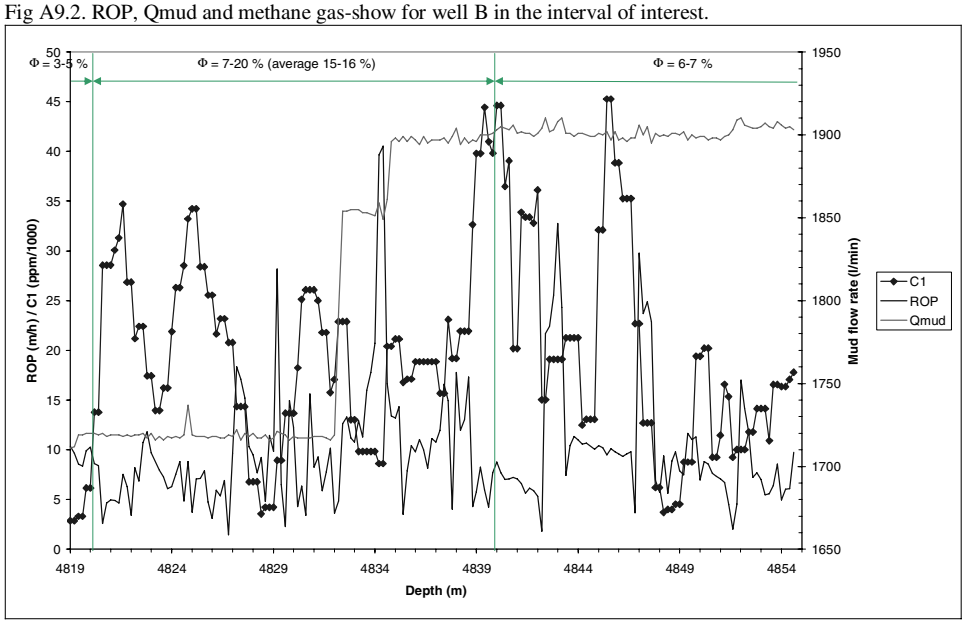

Characterisation of the oil B

Table A9.1. PVT data of the fluid from the layer B

		Reservoir Fluid
	Mole	Weight
Component	%	%
Hydrogen sulphide	3.26	1.539
Carbon dioxide	2.95	1.800
Nitrogen	0.91	0.353
Methane	37.72	8.390
Ethane	11.44	4.770
Propane	6.93	4.234
i-Butane	1.38	1.114
n-Butane	3.53	2.847
i-Pentane	1.72	1.723
n-Pentane	2.08	2.084
Hexanes	3.61	4.308
Heptanes	3.35	4.465
Octanes	2.44	3.620
Nonanes	2.62	4.398
Decanes	2.27	4.217
Undecanes	1.77	3.614
Dodecanes	1.39	3.107
Tridecanes	1.16	2.813
Tetradecanes	1.00	2.631
Pentadecanes	0.90	2.563
Hexadecanes	0.76	2.327
Heptadecanes	0.59	1.929
Octadecanes	0.50	1.723
Nonadecanes	0.48	1.764
Eicosanes	0.46	1.735
C21	0.41	1.642
C22	0.36	1.483
C23	0.31	1.347
C24	0.26	1.183
C25	0.25	1.147
C26	0.22	1.044
C27	0.22	1.116
C28	0.21	1.060
C29	0.19	0.999
C30	0.19	1.033
C31	0.19	1.043
C32	0.15	0.840
C33	0.13	0.748
C34	0.11	0.694
C35	0.10	0.632
C36+	1.50	9.919
	_____	_____
Totals	100.02	99.998

Table A9.2. Calculated Properties for B

Physical Properties at 15°C and 1 bar				
Molecular weight	72.1	g/mol		
GOR	300.6	Nm3/m3		
Pres	477.3	bar		
Tres	110.7	°C		
Density at Pres	635	kg/m3		
C36+				
Molecular Weight	476	g/mol		
Density	21.1	°API	0.927	g/cm3
Normal Boiling Point	511.8	°C		

Table A9.3. Composition and properties of the components of the modelled fluid B

	Mole (%)	Mw (g/mol)	Tc (°C)	Pc (bar)	Omega (-)
N2	0.91	28.010	-146.95	33.944	0.0400
CO2	2.95	44.010	31.05	73.77	0.2250
H2S	3.26	34.080	100.05	89.37	0.1000
C1	37.72	16.040	-82.55	46.00	0.0115
C2	11.44	30.070	32.25	48.84	0.0908
C3	6.93	44.100	96.65	42.46	0.1454
IC4	1.38	58.120	134.95	36.48	0.1760
NC4	3.53	58.120	152.05	38.00	0.1928
IC5	1.72	72.128	187.61	33.93	0.2268
NC5	2.08	72.150	196.45	33.74	0.2273
C6	3.61	84.000	239.39	33.55	0.2504
C7	3.35	96.000	274.96	31.43	0.2848
C8	2.44	107.000	303.18	29.68	0.3155
C9	2.62	121.000	331.81	27.58	0.3535
C10	2.27	134.000	356.73	25.95	0.3877
CN1	4.32	159.023	397.93	23.43	0.4504
CN2	2.66	204.556	454.72	19.81	0.5555
CN3	1.57	249.408	498.98	17.28	0.6470
CN4	1.80	297.094	544.84	15.44	0.7294
CN5	1.09	358.651	600.16	13.73	0.8188
CN6	0.87	415.885	621.46	12.56	0.8802
CN7	1.50	480.000	694.02	11.60	0.9246

Table A9.4. Comparison between the modelled and sampled fluid B

Res Fluid	Calculated	PVT	Error (%)
MW	72.1	72.1	-0.01
GOR	294.4	300.60	2.06
Density	650	635	-2.29
Flashed gas			
MW	30.4	30.6	0.72
Density	1.230	1.305	5.76
Viscosity	0.0105	0.0068	-54.24
MW C7+	102	107	4.49

Appendix 10. Field case C

1. Presentation of the reservoir

Hydrocarbon bearing layers	3 layers centred at 1106, 1114 and 1141 m (TVD)	(Cf Figure A10.2)
Temperature at 1106 m (TVD)	29.6°C	
Pressure at 1105.8 m (TVD)	120.5 bar	(Cf Figure A10.1)
Porosity *	≈ 26-32%	(Cf Figure A10.2)
Water saturation *	≈ 20%	(Cf Figure A10.2)
Permeability *	≈ 1900 – 2500 mD	(Cf Figure A10.3)

(*: average values in the hydrocarbon bearing layers)

Pressure profiles

The Table and Figure below show:

- the formation pressure as measured in the well in the depth-interval of interest
- the Equivalent Circulating Density (ECD)

Table A10.1. Formation pressure and Equivalent Circulating Density, expressed in Bar.

TVD (m)	Test (-)	Formation Pressure (Bar)	Estimated Equivalent Circulating Density (Bar)
1105.80	2	120.47	155.12
1112.57	3	120.99	157.28
1113.76	4	121.08	157.44
1114.75	5	121.16	157.58
1123.26	6	121.83	158.79
1130.25	7	122.38	159.77
1133.76	8	122.65	160.27
1140.24	9	123.15	161.19
1145.26	10	123.53	161.90
1150.24	11	124.05	162.60

Fig. A10.1. Pressure profile in the reservoir between 1105 and 1150 m (TVD)

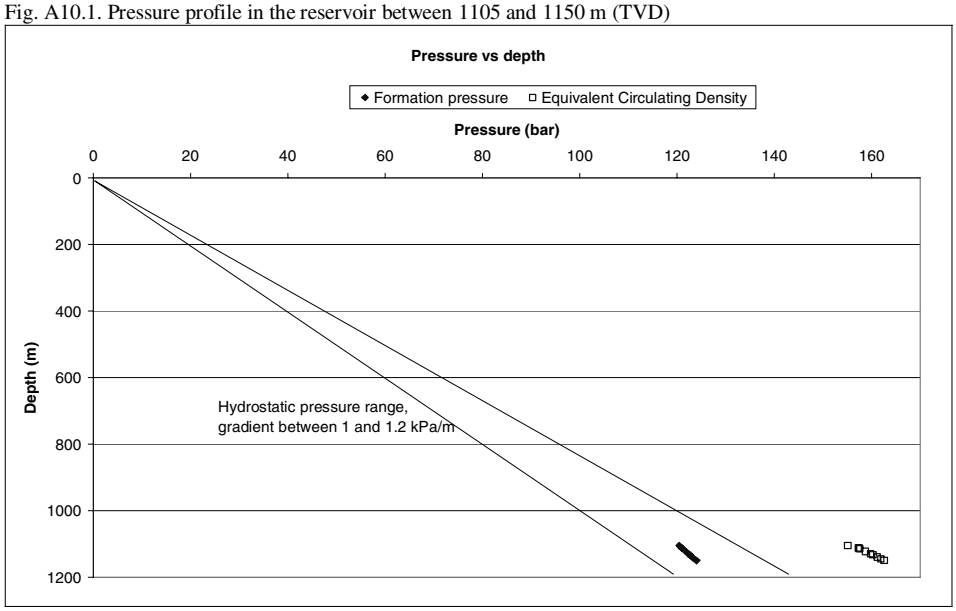

The ECD always exceeds the formation pressure by more than 35 bar, the latter being defined as the maximum pressure difference allowed before invasion: in this case, we can think that some drilling fluid invaded the reservoir.

Temperature

The reservoir temperature at 1106 m (TVD) deep is 29.6°C. If we use a geothermal gradient of 0.029 K/m (Archer p13), we find that at 1140 m (TVD) the temperature would have increased of 1°C. Hence, we consider the temperature constant on the interval of interest, 1104-1140 m.

Porosity, oil saturation, permeability

The porosity and oil saturation profiles are presented below in Figure A10.2, showing clearly the hydrocarbon bearing layers. The 3 layers (at 1105, 1114 and 1140 m TVD) for which the PVT data are available are also referenced on Figure A10.2.

The permeability data are presented in Figure A10.3, (as well as the porosity).

Fig. A10.2. Porosity and oil saturation profiles in the reservoir between 1105 and 1150 m (TVD)

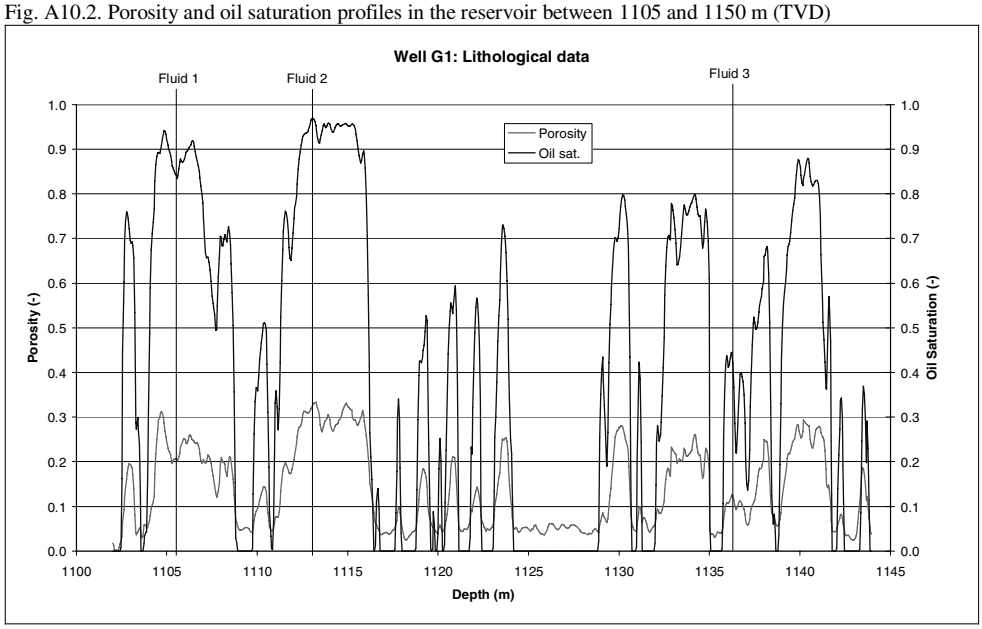

Fig. A10.3. Porosity and permeability profiles in the reservoir between 1105 and 1150 m (TVD)

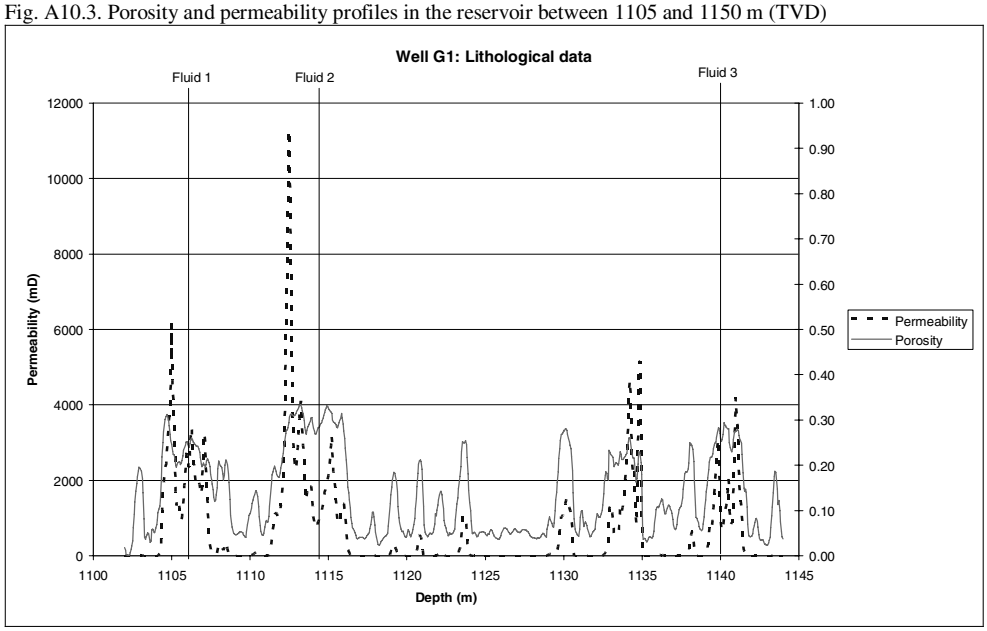

2. Operating conditions

Rate of penetration, mud flow rate

Table A10.2. Average and maximum ROP and mud flow rates.

	ROP (m/h)		Mud flow rate (l/min)	
	Average	**Max**	**Average**	**Max**
Layer 1104 m	35	53	2322	2362
Layer 1114 m	43	70	2246	2325
Layer 1140 m	8	14	649	650

Fig. A10.4. Rate of penetration and mud flow rate for the well C.

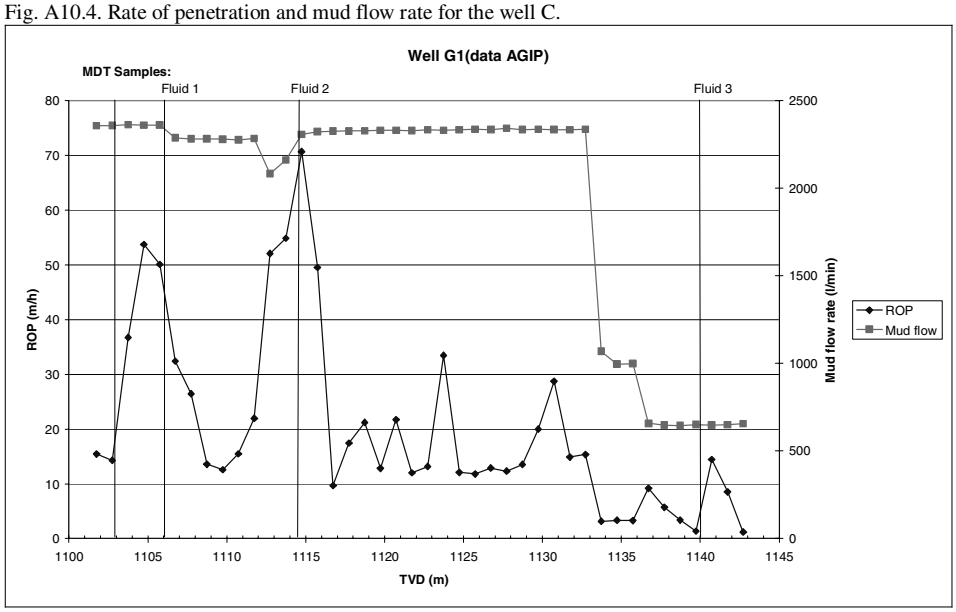

Mud properties

The mud properties are presented in Table A10.3 below

Table A10.3. Mud properties.

Mud type	WBM	Format/Polymer
Density	1.3 kg/l	
Marsh Viscosity	50 s	

Coring intervals

The well C was cored in the interval 1133-1178 m (TR). Three cores were cut as following (cf Figure A10.5), first coring at 1133-1136, second coring at 1136-1151 and third coring at 1151-1178.

Besides, the coring operation perturbed the quality of the gas shows. The mud flow is different. More precisely, the third layer belongs to the first coring interval.

Fig. A10.5. Coring intervals, influence on the drilling conditions and position of the reservoir fluid at 1140 m.

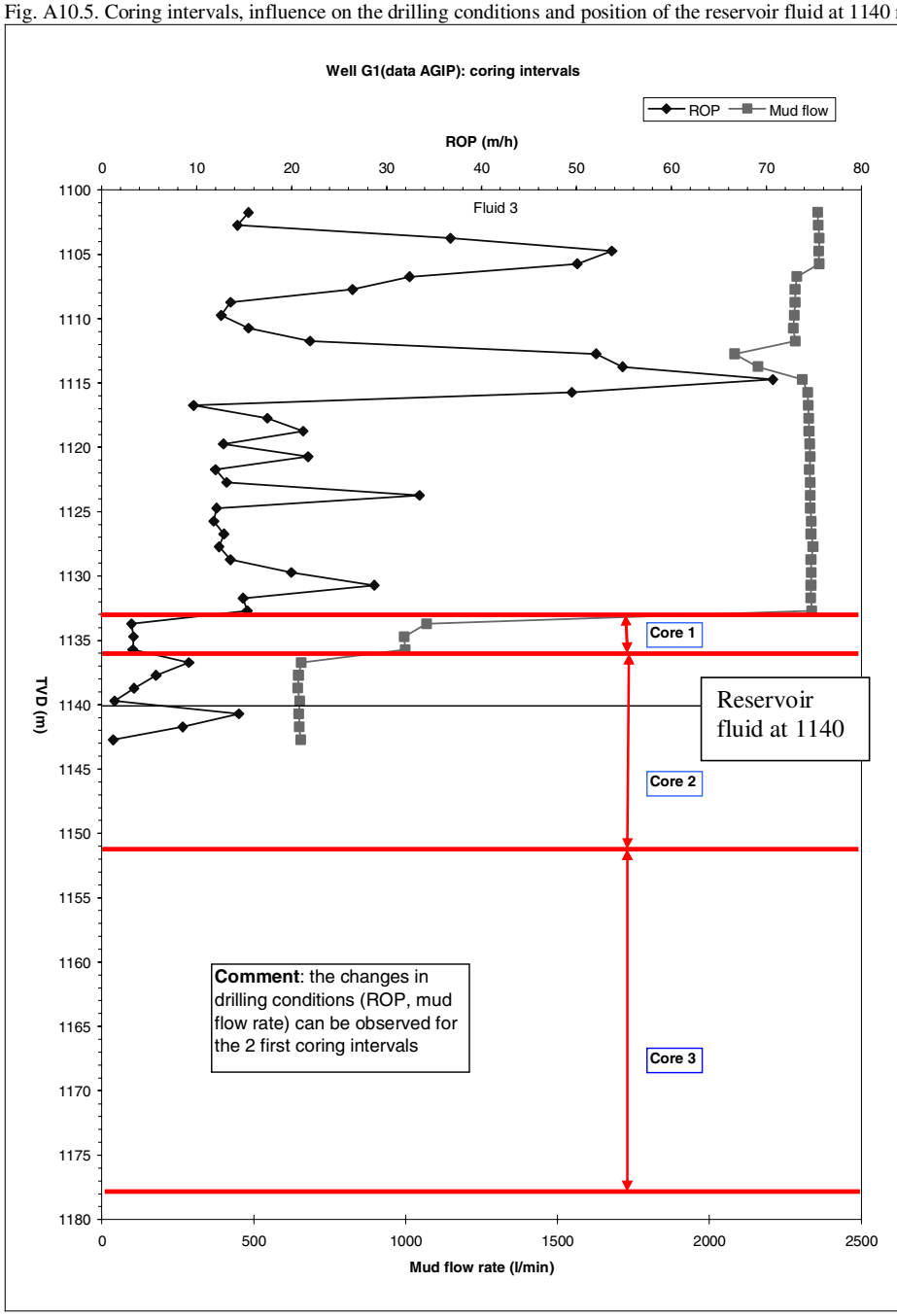

3. Fluids in the hydrocarbon bearing layers

First layer, layer 1106 m (TVD)

PVT data

The first layer is centred at the depth 1106.0 m, where the reservoir temperature is 29.6°C. The Bubble point at reservoir temperature was measured at 10.13 MPa. Moreover, at reservoir conditions, the fluid density is 814.2 kg/m3.

The laboratory analysis of the fluid at this depth is presented in Tables A10.4-5:

Table A10.4.Hydrocarbon Analysis of Reservoir Fluid from Atmospheric Flash at 15.0°C - Depth 1106.0m

Component		Flashed Liquid		Flashed Gas		Reservoir Fluid	
		Mole %	Weight %	Mole %		Mole %	Weight %
Hydrogen		0.00	0.00	0.00		0.00	0.00
Hydrogen sulphide		0.00	0.00	0.00		0.00	0.00
Carbon dioxide		0.00	0.00	16.33		6.29	1.94
Nitrogen		0.00	0.00	0.23		0.09	0.02
Methane		0.01	0.00	73.00		28.09	3.17
Ethane		0.09	0.01	7.85		3.08	0.65
Propane		0.03	0.01	0.30		0.13	0.04
i-Butane		0.16	0.04	0.63		0.34	0.14
n-Butane		0.04	0.01	0.10		0.09	0.04
neo-Pentane		0.02	0.01	0.03		0.00	0.00
i-Pentane		0.28	0.09	0.23		0.26	0.13
n-Pentane		0.07	0.02	0.03		0.05	0.03
Hexanes		0.91	0.36	0.28		0.66	0.40
Heptanes		7.21	2.97	0.60		4.66	2.92
Octanes		12.05	5.68	0.32		7.52	5.42
Nonanes		7.79	4.16	0.05		4.80	3.91
Decanes		6.25	4.00	0.02		3.85	3.75
Undecanes		4.88	3.31	0.00		3.00	3.10
Dodecanes		4.51	3.35	0.00		2.78	3.14
Tridecanes		5.07	4.10	0.00		3.12	3.84
Tetradecanes		5.10	4.47	0.00		3.14	4.19
Pentadecanes		5.77	5.48	0.00		3.55	5.14
Hexadecanes		4.57	4.68	0.00		2.81	4.38
Heptadecanes		3.93	4.30	0.00		2.42	4.03
Octadecanes		3.93	4.55	0.00		2.42	4.27
Nonadecanes		3.41	4.14	0.00		2.10	3.88
Eicosanes plus		23.92	44.26	0.00		14.75	41.47
Totals		**100.00**	**100.00**	**100.00**		**100.00**	**100.00**

Table A10.5. Calculated Properties

		Flashed Liquid	Flashed Gas	Reservoir Fluid
C7 plus	Mole %	98.39	0.99	60.92
	Molecular Weight (g mol-1)	219	94	218
	Density at 15.0°C (kg m-3)	846.8	766.5	860.9
C11 plus	Mole %	65.09		40.09
	Molecular Weight (g mol-1)	275		275
	Density at 15.0°C (kg m-3)	866.1		884.3
C20 plus	Mole %	23.92		14.75
	Molecular Weight (g mol-1)	401		401
	Density at 15.0°C (kg m-3)	900.9		938.4
Atmospheric Flash GOR (1) (Flash at 15.0°C)				58.42

(1) Cubic meters of gas at 0.1016 MPa abs and 15.0°C per cubic meter of residual oil at 15.0°C.

Characterization

The reservoir fluid has been modelled with a special care regarding the GOR and the density at reservoir conditions. Table A10.6 shows the relative errors between the modelled and the sampled fluid. Table 8 shows the modelled fluid along with the different thermodynamic properties (Molecular weight in g/mol, critical temperature in °C, critical pressure in bar, and acentric factor).

Table A10.6. Comparison between the modelled and sampled fluid at 1104 m.

	PVT data	Simulated BEST	Error %
GOR	58.42	58.02	0.69
Density at reservoir conditions	814.20	815.06	-0.11
Bubble Pt	101.30	101.07	0.22

Table A10.7. Composition and properties of the components of the modelled fluid at 1104 m.

Coupe	Mole	Mw	Tc	Pc	Omega
N2	0.09	28.01	-146.95	33.94	0.0400
CO2	6.29	44.01	31.05	73.76	0.2250
H2S	0	34.08	100.05	89.369	0.1000
C1	28.09	16.04	-82.55	46.00	0.0115
C2	3.08	30.07	32.25	48.84	0.0908
C3	0.13	44.10	96.65	42.46	0.1454
IC4	0.34	58.12	134.95	36.48	0.1760
NC4	0.09	58.12	152.05	38.00	0.1928
IP05	0	72.15	433.8	32	0.197
IC5	0.26	72.01	190.27	34.48	0.2247
NC5	0.05	72.15	196.45	33.74	0.2273
C6	0.66	84	239.4	33.5	0.2504
C7	4.66	96	275.0	31.4	0.2848
C8	7.52	107	303.2	29.7	0.3155
C9	4.8	121	331.8	27.6	0.3535
C10	3.85	134	356.7	26.0	0.3877
C11	3	147	380.3	24.6	0.4210
C12	2.78	161	401.7	23.2	0.4556
C13	3.12	175	420.4	22.0	0.4891
C14	3.14	190	438.7	20.8	0.5237
C15	3.55	206	456.7	19.7	0.5591
C16	2.81	222	473.5	18.7	0.5929
C17	2.42	237	488.4	17.9	0.6233
C18	2.42	251	499.8	17.2	0.6504
C19	2.1	263	511.0	16.6	0.6727
C20	14.75	401	635.69370	13.934	0.866934

Second hydrocarbon bearing layer, C_1114

PVT data

The second layer is centred at the depth 1114.0 m, where the reservoir temperature is 29.6°C. Data are not available, but we can assume the same reservoir temperature and the same density. Especially, we have the fluid composition, so we can see that this fluid is not from another origin and rather close to the fluid present in the other layers.

We took the same reservoir density, 814.1 kg/m^3 as in the previous layer. For the Bubble point at reservoir temperature, we took an average of the two saturation pressures at 1106 and 1140 m deep: P_sat(calculated for 1114.4 m)= 10.45 MPa.

The laboratory analysis of the fluid at this depth is the following:

Table A10.8. Hydrocarbon Analysis of Reservoir Fluid from Atmospheric Flash at 15.0°C - Depth 1114.0m

Component		Flashed Liquid		Flashed Gas		Reservoir Fluid	
		Mole %	Weight %	Mole %		Mole %	Weight %
Hydrogen		0.00	0.00	0.00		0.00	0.00
Hydrogen sulphide		0.00	0.00	0.00		0.00	0.00
Carbon dioxide		0.00	0.00	16.83		6.74	2.13
Nitrogen		0.00	0.00	0.17		0.07	0.01
Methane		0.03	0.00	72.60		29.09	3.34
Ethane		0.11	0.02	7.58		3.11	0.67
Propane		0.03	0.01	0.29		0.13	0.04
i-Butane		0.17	0.04	0.70		0.38	0.16
n-Butane		0.04	0.01	0.11		0.07	0.03
neo-Pentane		0.02	0.01	0.03		0.02	0.10
i-Pentane		0.32	0.11	0.28		0.30	0.16
n-Pentane		0.07	0.02	0.04		0.06	0.03
Hexanes		0.92	0.37	0.33		0.68	0.42
Heptanes		7.07	2.93	0.64		4.50	2.89
Octanes		12.08	5.73	0.34		7.37	5.44
Nonanes		7.83	4.18	0.05		4.72	3.93
Decanes		6.33	4.04	0.01		3.80	3.77
Undecanes		4.90	3.32	0.00		2.94	3.10
Dodecanes		4.50	3.34	0.00		2.70	3.11
Tridecanes		5.07	4.09	0.00		3.04	3.81
Tetradecanes		5.09	4.45	0.00		3.05	4.15
Pentadecanes		5.78	5.48	0.00		3.46	5.11
Hexadecanes		4.54	4.65	0.00		2.72	4.33
Heptadecanes		3.90	4.26	0.00		2.34	3.97
Octadecanes		3.91	4.52	0.00		2.35	4.22
Nonadecanes		3.39	4.11	0.00		2.03	3.83
Eicosanes plus		23.90	44.31	0.00		14.33	41.34
Totals		**100.00**	**100.00**	**100.00**		**100.00**	**100.09**

Table A10.9. Calculated Properties of the reservoir fluid at 1114 m.

		Flashed Liquid	**Flashed Gas**	**Reservoir Fluid**
C7 plus	Mole %	98.29	1.04	59.35
	Molecular Weight (g mol-1)	220	94	219
	Density at 15.0°C (kg m-3)	846.5	767.3	846.2
C11 plus	Mole %	64.98		38.96
	Molecular Weight (g mol-1)	276		276
	Density at 15.0°C (kg m-3)	866.4		866.4
C20 plus	Mole %	23.90		14.33
	Molecular Weight (g mol-1)	403		403
	Density at 15.0°C (kg m-3)	901.3		901.3
Atmospheric Flash GOR (1) (Flash at 15.0°C)				62.25

(1) Cubic meters of gas at 0.1016 MPa abs and 15.0°C per cubic meter of residual oil at 15.0°C

Characterization

Table A10.10. Comparison between the modelled and sampled fluid at 1114 m.

	PVT data	Simulated BEST	Error %
GOR	62.25	61.97	0.45
Density at reservoir conditions	814.10	818.03	-0.48
Bubble Pt	104.50	104.39	0.11

Table A10.11. Composition and properties of the components of the modelled fluid at 1114 m.

Coupe	Mole	Mw	Tc	Pc	Omega
N2	0.09	28.01	-146.95	33.94	0.0400
CO2	6.29	44.01	31.05	73.76	0.2250
H2S	0	34.08	100.05	89.369	0.1000
C1	28.09	16.04	-82.55	46.00	0.0115
C2	3.08	30.07	32.25	48.84	0.0908
C3	0.13	44.10	96.65	42.46	0.1454
IC4	0.34	58.12	134.95	36.48	0.1760
NC4	0.09	58.12	152.05	38.00	0.1928
IP05	0	72.15	433.8	32	0.197
IC5	0.26	72.01	190.27	34.48	0.2247
NC5	0.05	72.15	196.45	33.74	0.2273
C6	0.66	84	239.4	33.5	0.2504
C7	4.66	96	275.0	31.4	0.2848
C8	7.52	107	303.2	29.7	0.3155
C9	4.8	121	331.8	27.6	0.3535
C10	3.85	134	356.7	26.0	0.3877
C11	3	147	380.3	24.6	0.4210
C12	2.78	161	401.7	23.2	0.4556
C13	3.12	175	420.4	22.0	0.4891
C14	3.14	190	438.7	20.8	0.5237
C15	3.55	206	456.7	19.7	0.5591
C16	2.81	222	473.5	18.7	0.5929
C17	2.42	237	488.4	17.9	0.6233
C18	2.42	251	499.8	17.2	0.6504
C19	2.1	263	511.0	16.6	0.6727
C20	14.75	401	635.69370	13.934	0.866934

Third hydrocarbon bearing layer, C_1140

PVT data

The third layer is centred at the depth 1140.0 m, where the reservoir temperature is 29.6°C. The Bubble point at reservoir temperature was measured at 11.43 MPa. Moreover, at reservoir conditions, the fluid density is 814.1 kg/m3.

The laboratory analysis of the fluid at this depth is the following:

Table A10.12. Hydrocarbon Analysis of Reservoir Fluid from Atmospheric Flash at 15.0°C - Depth 1140.0m

Component		Flashed Liquid		Flashed Gas		Reservoir Fluid	
		Mole %	Weight %	Mole %		Mole %	Weight %
Hydrogen		0.00	0.00	0.00		0.00	0.00
Hydrogen sulphide		0.00	0.00	0.00		0.00	0.00
Carbon dioxide		0.00	0.00	21.03		8.90	2.81
Nitrogen		0.00	0.00	0.16		0.07	0.01
Methane		0.02	0.00	70.35		29.76	3.43
Ethane		0.08	0.01	6.48		2.79	0.60
Propane		0.01	0.00	0.16		0.08	0.02
i-Butane		0.08	0.02	0.33		0.18	0.08
n-Butane		0.03	0.01	0.04		0.05	0.02
neo-Pentane		0.01	0.00	0.03		0.09	0.05
i-Pentane		0.09	0.03	0.09		0.00	0.00
n-Pentane		0.02	0.01	0.01		0.02	0.01
Hexanes		0.64	0.25	0.26		0.47	0.29
Heptanes		6.53	2.61	0.63		4.04	2.60
Octanes		11.91	5.45	0.36		7.02	5.16
Nonanes		7.31	3.80	0.06		4.24	3.54
Decanes		6.10	3.78	0.01		3.52	3.50
Undecanes		4.73	3.11	0.00		2.73	2.88
Dodecanes		4.50	3.23	0.00		2.59	3.00
Tridecanes		5.09	3.98	0.00		2.94	3.69
Tetradecanes		5.18	4.40	0.00		2.99	4.08
Pentadecanes		5.94	5.47	0.00		3.43	5.07
Hexadecanes		4.71	4.67	0.00		2.72	4.33
Heptadecanes		4.03	4.26	0.00		2.32	3.95
Octadecanes		4.05	4.54	0.00		2.34	4.21
Nonadecanes		3.50	4.11	0.00		2.02	3.81
Eicosanes plus		25.44	46.26	0.00		14.69	42.86
Totals		**100.00**	**100.00**	**100.00**		**100.00**	**100.00**

Table A10.13. Calculated Properties of the reservoir fluid at 1140 m.

			Flashed Liquid	Flashed Gas	Reservoir Fluid
C7 plus	Mole %		99.02	1.06	57.59
	Molecular Weight (g mol-1)		225	94	225
	Density at 15.0°C (kg m-3)		849.3	765.4	862.1
C11 plus	Mole %		67.17		38.77
	Molecular Weight (g mol-1)		280		280
	Density at 15.0°C (kg m-3)		868.1		884.5
C20 plus	Mole %		25.44		14.69
	Molecular Weight (g mol-1)		407		407
	Density at 15.0°C (kg m-3)		902.4		935.1
Atmospheric Flash GOR (1) (Flash at 15.0°C)					66.47

(1) Cubic meters of gas at 0.1016 MPa abs and 15.0°C per cubic meter of residual oil at 15.0°C.

Characterization

Table A10.14. Comparison between the modelled and sampled fluid at 1140 m.

	PVT data	Simulated BEST	Error %
GOR	66.47	66.48	-0.01
Density at reservoir conditions	814.10	814.20	-0.01
Bubble Pt	114.30	114.13	0.15

Table A10.15. Composition and properties of the components of the modelled fluid at 1140 m.

Coupe	Mole	Mw	Tc	Pc	Omega
N2	0.07	28.01	-146.95	33.94	0.0400
CO2	6.74	44.01	31.05	73.76	0.2250
H2S	0	34.08	100.05	89.369	0.1000
C1	29.09	16.04	-82.55	46.00	0.0115
C2	3.11	30.07	32.25	48.84	0.0908
C3	0.13	44.10	96.65	42.46	0.1454
IC4	0.38	58.12	134.95	36.48	0.1760
NC4	0.07	58.12	152.05	38.00	0.1928
IP05	0.02	72.15	433.8	32	0.197
IC5	0.3	72.01	190.27	34.48	0.2247
NC5	0.06	72.15	196.45	33.74	0.2273
C6	0.68	84	239.4	33.5	0.2504
C7	4.5	96	275.0	31.4	0.2848
C8	7.37	107	303.2	29.7	0.3155
C9	4.72	121	331.8	27.6	0.3535
C10	3.8	134	356.7	26.0	0.3877
C11	2.94	147	380.3	24.6	0.4210
C12	2.7	161	401.7	23.2	0.4556
C13	3.04	175	420.4	22.0	0.4891
C14	3.05	190	438.7	20.8	0.5237
C15	3.46	206	456.7	19.7	0.5591
C16	2.72	222	473.5	18.7	0.5929
C17	2.34	237	488.4	17.9	0.6233
C18	2.35	251	499.8	17.2	0.6504
C19	2.03	263	511.0	16.6	0.6727
C20	14.33	403	637.55531	13.943636	0.868946

4. Gas-trap and GWD data

The data acquisition system is Reserval, which contains a volumetric GZG gas-trap and a high speed/high resolution Gas Chromatograph.

The levels of gas are different from one layer to another as seen on the Figure A10.6:

- Layer 1106: 35000 ppm of Total Gas (equivalent C1), and 30000 ppm of C1
- Layer 1114: 20000 ppm of Total Gas (equivalent C1), and 15000 ppm of C1
- Layer 1140: 10000 ppm of Total Gas (equivalent C1), and 7000 ppm of C1

If we compare the operating conditions, we should expect a higher signal for the second layer, where the drilled volume and the mud flow rate are respectively higher and less than for the layer 1104.

Fig. A10.6. Gas shows (Total Gas, C1, and C2) for the well C